THE ORIGIN OF BARITE AND RELATED VEINS ON THE AVALON PENINSULA OF NEWFOUNDLAND

JAMES ANDREW MALONEY, B.Sc.

NOTICE

The quality of this microform is heavily dependent upon the quality of the original thesis submitted for microfilming. Every effort has been made to ensure the highest quality of reproduction possible.

If pages are missing, contact the university which granted the degree.

Some pages may have indistinct print especially if the original pages were typed with a poor typewriter ribbon or if the university sent us an inferior photocopy.

Reproduction in full or in part of this microform is governed by the Canadian Copyright Act, R.S.C. 1970, c. C-30, and subsequent amendments.

AVIS

La qualité de cette microforme dépend grandement de la qualité de la thèse soumise au microfilmage. Nous avons tout fait pour assurer une qualité supérieure de reproduction.

S'il manque des pages, veuillez communiquer avec l'université qui a conféré le grade.

La qualité d'impression de certaines pages peut laisser à désirer, surtout si les pages originales ont été dactylographiées à l'aide d'un ruban usé ou si l'université nous a fait parvenir une photocopie de qualité inférieure.

La reproduction, même partielle, de cette microforme est soumise à la Loi canadienne sur le droit d'auteur, SRC 1970, c. C-30, et ses amendements subséquents.

THE ORIGIN OF BARITE AND RELATED VEINS ON THE AVALON PENINSULA OF NEWFOUNDLAND

BY

James Andrew Maloney, B.Sc.

A thesis submitted to the School of Graduate Studies in partial fulfillment of the requirements for the degree of Master of Science

Department of Earth Sciences
Memorial University of Newfoundland

November 1990

St. John's Newfoundland

ISBN 0-315-65349-3

ABSTRACT

Hydrothermal barite ± calcite ± sulphide mineral veins occur in Newfoundland on the Isthmus of Avalon and along the west, southern and south-eastern coasts of the Cape St. Mary's area of the Avalon Peninsula. Earlier formed quartz-dominated veins are the most abundant vein type in this area and occur over a much larger area. The data collected in this study (field relationships, paragenetic data, fluid inclusion data, carbon, oxygen and sulphur isotope data, REE data) allow for the following conclusions:

1) The early quartz ± chlorite veins were formed during a regional deformational and low-grade metamorphic event, by precipitation in fracture sets developed during this deformation.

2) During this deformational event a hot pulse of hydrothermal fluid moved through the same fracture set in more localized areas. This later fluid pulse deposited sulphide-mineral-dominated veins where it was hottest and presumably closest to its source. Further from the source, where the fluid was cooler, calcite- and barite-dominated veins were precipitated.

3) The proximity of the "hottest" sulphide-dominated veins to known syndeformational granitic intrusions, combined with the geochemical evidence, strongly suggest

that the hot fluid pulse was sourced by fluid exsolved during crystallization of these granitic magmas. Carbon, oxygen, sulphur and rare earth elements were all likely sourced from these granitic melts as well. In some of the veins studied, there is evidence that elemental and isotopic exchange took place between this magmatic fluid and either the surrounding country rock or meteoric waters.

ACKNOWLEDGEMENTS

I would like to thank my thesis advisor Dr. Dave Strong for sharing with me his inspiring enthusiasm for research; for his open door approach to his graduate students and for his understanding of my personal situation during the completion of this thesis.

My wife, Laurie Dodds, suffered the most in support of my initiating and finishing a quest for an M.Sc. degree, by giving up an attractive career opportunity, by not complaining too much about the long hours of work and by spending long hours herself typing draft copies of this thesis. Thank-you for your support.

I would also like to thank Dr. Ian Gibson, of the University of Waterloo, for providing the rare earth element analysis and the carbon and oxygen isotope analysis of calcites, used in this study.

Next I would like to thank Ambrose Howse and Cel Collins of the Newfoundland Department of Mines and Energy, who provided an abundance of information cn the occurrence of barite on the Avalon Peninsula and who both aided me in my field work. Also I would like to thank Cyril O'Driscoll of the Newfoundland Department of Mines and Energy, for providing the samples of granite from Red Island and Fox Island for analysis.

Finally I wish to express my gratitude to a bunch of graduate students who really knew how to make graduate work a rewarding culinary experience. Special thanks to a good friend Dave Gower, for many hours of thoughtful discussion and for your easy going practical approach to problems. I would also like to thank both Pat O'Neil and Paul Barrette for good advice and for good friendship.

This study was funded by Dr. Strong's Natural Sciences and Engineering Research Council of Canada grant A7975 and by a Memorial University Fellowship.

Table of Contents

List of Tables

List of Figures

CHAPTER 1. GEOLOGY OF THE FIELD AREA

1.1. Introduction

Hydrothermal barite ± calcite ± sulphide mineral veins (BCS veins) occur in an area of eastern Newfoundland which includes the Isthmus of Avalon and the west, southern and the south-eastern coast of the Cape St. Mary's area of the Avalon Peninsula (Fig. 1). Barite-dominated veins occur in rocks of variable lithology, including subaerial volcanic rocks, marine sedimentary rocks and redbeds, which range in age from late Haydrinian to Middle Cambrian. Earlier-formed quartz-dominated veins are the most abundant vein type in this area and occur over a much larger area. The formation of these early quartz-dominated veins is closely linked to the formation of the barite-dominated veins.

Sulphide minerals exist in minor amounts in a number of barite veins, and comprise the dominant components of several veins, two of which have been mined for their metal content (the Silver Cliff and La Manche veins). Howley and Murray (1918) and Chute (1939) suggested that the barite veins and the sulphide-rich veins are related in their origin, due to the presence of barite as a late stage gangue mineral in the sulphide-rich veins.

The origin of the BCS veins has not been studied in any detail. Green (1981) studied the galena-bearing calcite vein at La Manche (Fig. 4, Chap. 2), but was not conclusive

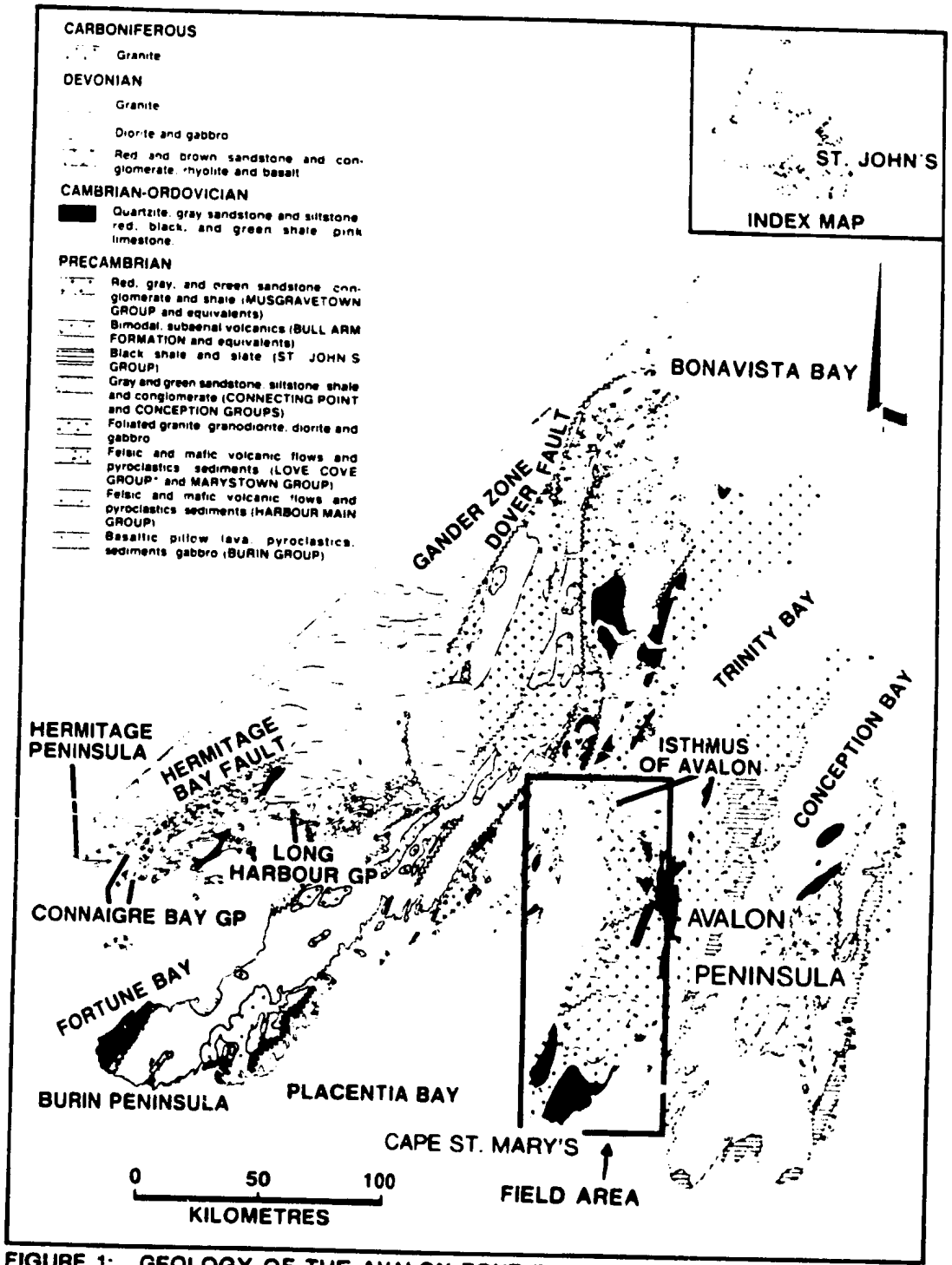

FIGURE 1: GEOLOGY OF THE AVALON ZONE IN NEWFOUNDLAND AFTER DALLMEYER et al(1983). STUDY AREA IS ENCLOSED BY RECTANGLE (SHOWN IN FIGURE 4).

as to its origin. He did suggest that magmatic processes were probably involved in the vein formation. This thesis will demonstrate that the barite-dominated veins of the study area were formed slightly later than, but very close to the time of formation of the more abundant quartz-dominated veins. Vein formation took place during the Devonian Acadian Orogeny, which resulted in folding, faulting and metamorphism of Avalon Zone strata and the emplacement of syntectonic granitic magmas.

1.2. Geology of the Avalon Zone

The area of eastern Newfoundland which hosts the BCS veins, is geologically within the tectono-stratigraphic subdivision of the Appalachian Orogen, designated as the Avalon Zone (Williams 1976; 1978; 1979) (Fig. 1), previously called the Avalon Platform (Kay and Colbert 1965; Kay 1967).

In Newfoundland, rocks of the Avalon Zone, which in no place exceed greenschist grade metamorphism, have been juxtaposed next to crystalline metamorphic rocks of the Gander Zone (Williams *et al*. 1974). These two contrasting terranes are separated by the Dover Fault in northeastern Newfoundland (Blackwood and Kennedy 1975) and by the Hermitage Bay Fault in the south (Blackwood and O'Driscoll 1976) (Fig. 1). Avalon Zone rocks continue northwards and eastwards offshore of the Avalon Peninsula, possibly for an additional 250 km, as suggested by geophysical (Miller 1977;

Haworth and Lefort 1979, Miller et al. 1985) and marine geological studies (Lilly 1966; Pelletier 1971). Miller (1987) has also modelled the presence of Avalon type rocks offshore in St. Mary's Bay and Placentia Bay in the southern region of the Avalon Peninsula.

The stratigraphy of the Avalon Zone in Newfoundland can be generally described as a sequence of late Precambrian volcanic flows, pyroclastic rocks and volcanogenic sediments, locally overlain by lower Paleozoic sedimentary rocks. Proterozoic to Carboniferous plutonic rocks intrude into the various sequences of strata (Strong et al. 1978). Figure 1 shows the geology of the Avalon Zone.

O'Brien et al. (1983) subdivided the rocks of the Avalon Zone on the basis of age and lithology. The following description of Avalon Zone geology uses their format for subdividing the various units and refers to the geological map shown in Figure 1 and the stratigraphic relationships shown in Figure 2.

1.3. Upper Proterozoic Magmatism

The oldest rocks recognized in the Newfoundland Avalon Zone are mafic volcanic rocks of the Burin Peninsula called the Burin Group (Strong et al. 1976). These are interpreted as oceanic tholeiitic volcanic rocks, formed during a period of rifting that resulted in the formation of a small ocean basin during the late Precambrian (Strong et al. 1978).

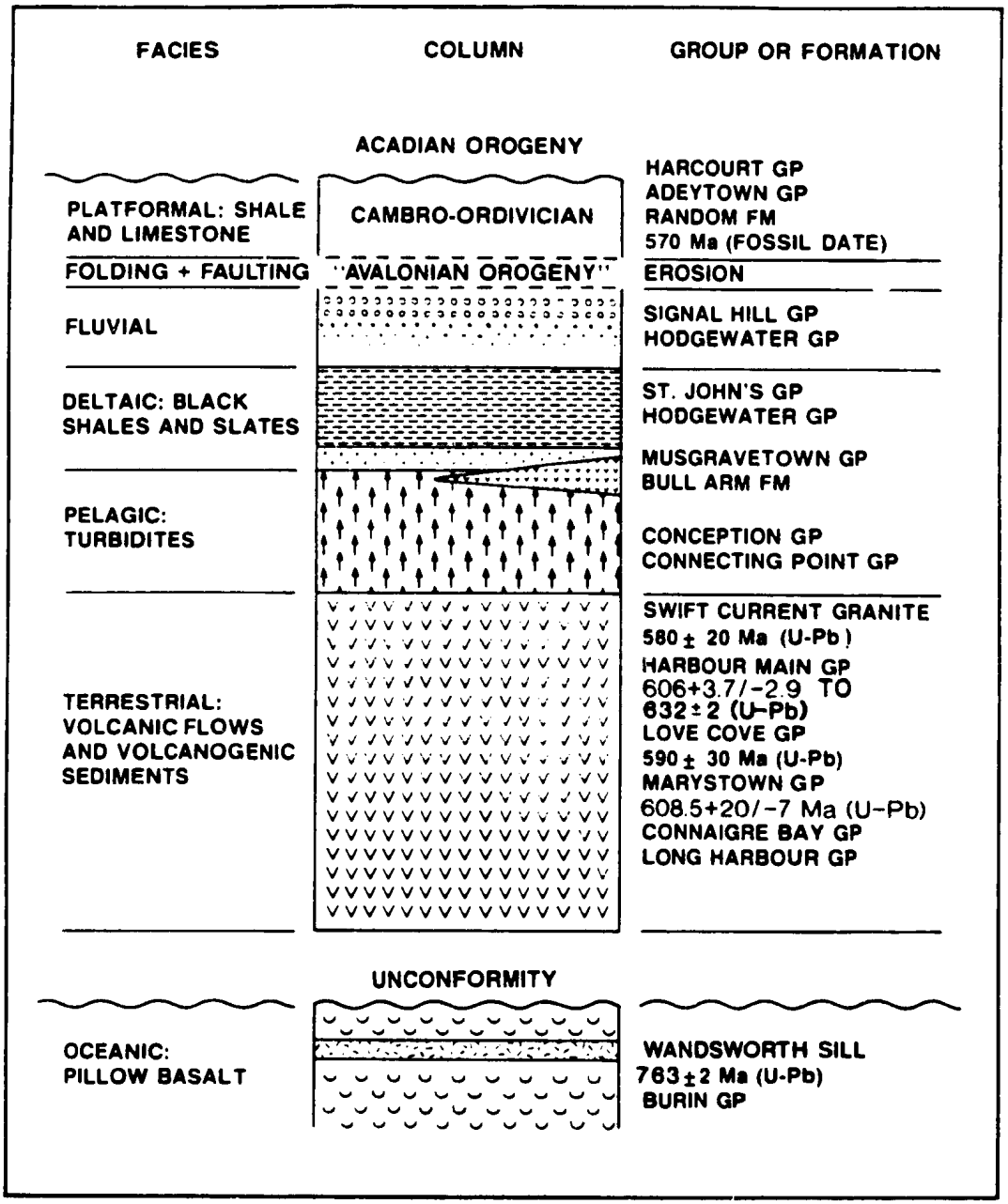

FIGURE 2: MAJOR FACIES AND GROUPS OF THE AVALON ZONE IN NEWFOUNDLAND. PRECISE STRATIGRAPHIC RELATIONSHIPS ARE NOT IMPLIED. TAKEN FROM O'BRIEN et al (1983). VARIOUS SOURCES OF DATA REFERENCED IN TEXT

The Wandsworth Sill, a pematitic gabbro that intruded into the Burin Group has been dated at 763 ± 2 Ma (U-Pb in zircon) (Krogh et al. 1988). This unit was previously dated at 762 ± 2 Ma (U-Pb in zircon) by Krogh et al. (1983). Strong et al. (1976), Taylor (1976) and Strong et al. (1978) interpret this gabbroic sill as being co-magmatic with the Burin Group volcanic rocks.

Late Proterozoic volcanic rocks, separated from the underlying Burin Group by a presumed unconformity (Strong et al. 1978), occur in four geographically distinct belts. The belts are bounded by faults which developed during the Acadian (Devonian) deformation (O'Brien et al. 1983).

Furthest west, occurring on the Hermitage Peninsula north of Fortune Bay, are the strongly bimodal calc-alkaline volcanic rocks of the Connaigre Bay and Long Harbour Groups. These rocks were interpreted by O'Driscoll and Strong (1979) to be transitional between orogenic (Cascades) and non-orogenic (Basin and Range) environments.

East of the Connaigre Bay and Long Harbour Groups, upper Proterozoic subaerial volcanic rocks of the Marystown Group dominate the geology of the Burin Peninsula (O'Brien, 1979). These volcanic rocks are bimodal, and are dominated by silicic compositions.

Subaerial, bimodal volcanic rocks of the Love Cove Group (Jenness 1957) occur north of the Marystown Group (O'Brien et al. 1983). The Love Cove and Marystown Groups

are typically alkaline volcanic rocks, although both groups contain stratigraphically low mafic to intermediate rocks of mildly tholeiitic affinities (O'Brien 1979; Hussey 1980). The Marystown Group has been dated at 608.5 +20/-7 Ma (U-Pb in zircon) by Krogh et al. (1988). This unit was previously dated at 608 ± 8 Ma (U-Pb in zircon) by Krogh et al. (1983). The Love Cove Group has been dated at 590 ± 30 Ma (U-Pb in zircon) by Dallmeyer et al. (1981a).

Further east is another belt of dominantly subaerial, bimodal volcanic rocks which belong to the Bull Arm Formation of the Musgravetown Group (McCartney 1967; Malpas 1971). In the only area where it has been studied in any detail, original chemical characteristics of the Bull Arm Formation have been masked by intense sodium metasomatism (Hughes and Malpas 1971).

Bimodal volcanic rocks of the Harbour Main Group (Rose 1952; Papezik 1970) comprise the most easterly belt of volcanic rocks on the Avalon Peninsula. Papezik (1970) described these rocks as being weakly alkalic and occurring in a continental extensional environment similar to the Basin and Range province. Various units within the Harbour Main Group have been dated at ages ranging from 606 +3.7/-2.9 Ma to 632 ± 2 Ma (Krogh et al. 1988, U-Pb in zircon). Rocks of the Harbour Main Group have been intruded by the Holyrood Granite which has been dated at 620.5 ± 2 Ma (Krogh

et al. 1988, U-Pb in zircon). This unit was previously dated at 607 ± 11 Ma (McCartney et al. 1967).

In the eastern half of the Avalon Peninsula, pink medium grained equigranular biotite granite of the Holyrood pluton (Rose 1952; McCartney 1969) intrudes into Harbour Main volcanic rocks and intercalated sediments (Conception Group). Hughes and Bruckner (1971) suggested that the Holyrood Granite represents a high-level subvolcanic intrusion, contemporaneous with the extrusion of Harbour Main volcanic rocks. Strong and Minatidis (1975) demonstrated that the Holyrood plutonic rocks were chemically dissimilar to the Harbour Main volcanic rocks and were therefore not a co-magmatic suite. Hughes (1973) suggested that the chemical differences were due to metasomatism of the Harbour Main volcanic rocks.

The Swift Current Granite in the western Avalon Zone, dated at 580 ± 20 Ma (U-Pb in zircon, Dallmeyer et al. 1981a), intrudes and is gradational into mafic and silicic flows and pyroclastic rocks of the Love Cove Group (590 ± 30 Ma, U-Pb in zircon), and is interpreted as co-magmatic with the Love Cove Group (Dallmeyer et al. 1981a). Based on geological relationships and geochemistry, several other possible co-magmatic volcanic-intrusive suites have been identified (Strong et al. 1978; O'Driscoll and Strong 1979; Hussey 1980), but are yet to be confirmed by age dating.

The interpretation of the tectonic environment into which Upper Proterozoic magmas were emplaced in the Avalon Zone of Newfoundland is enigmatic. There is an abundant volume of magmas with alkalic and tholeiitic affinities and a strong bimodal compositional nature, typical of magmas genrated during extensional tectonism. However there is also a significant proportion of calc alkalic igneous rocks (O'Driscoll & Strong 1979; O'Brien 1979) which is typically indicative of magmatism associated with compressional tectonism.

1.4. Upper Proterozoic Sedimentation

Upper Proterozoic marine sediments of the Conception Group conformably overlie the Harbour Main Group volcanics in the extreme east of the Avalon Peninsula, and overlie Harbour Main volcanic rocks with local angular unconformity further west (Williams and King 1979). McCartney (1969) had previously described this contact as an unconformity.

The Conception Group is a 3 to 5 km thick sequence of dominantly greenish-grey, but locally red, siliceous siltstones and shales, with varying amounts of turbiditic greywacke and chert beds (King et al. 1974). These beds all consist of dominantly felsic volcanic debris with a few layers of airfall tuff (King et al. 1974). Lateral interfingering of Conception Group sediments with Harbour Main Group volcanic rocks is observed in several locations,

and indicates the contemporaneous nature of the upper units of the Harbour Main Group with the lower units of the Conception Group (King et al. 1974).

The Conception Group is overlain conformably, with some local disconformity, by the 8 km thick Hodgewater Group in the central Avalon Peninsula area, and by the 8 to 9 km thick St. John's and Signal Hill Groups to the east (Rose 1952; McCartney 1967; Bruckner 1969; King et al. 1974).

The Hodgewater Group is very similar to the St. John's and overlying Signal Hill Groups. Dark grey to black shales of the Hodgewater and St. John's Group conformably and gradationally overly the youngest Conception Group strata (King et al. 1974). In both areas, the sequence coarsens upwards to sandstone-dominated rocks. In the east, the Signal Hill Group is topped by red sandstones and conglomerates (Bruckner 1969). Red beds also occur in a restricted area at the top of the Hodgewater Group, but generally the sequence is thinner and finer grained, consisting of greenish-grey strata with some interbedded red strata (King et al. 1974).

The Conception Group and overlying Hodgewater, St. John's and Signal Hill Groups, have been interpreted by King (1979) as being the result of early turbidite sedimentation, followed by shoaling of a marine basin and southward progradation of a delta front, followed by alluvial plain conditions. The source material for the infilling of this

basin is believed to be an active volcanic edifice in the Harbour Main Group (King 1979).

Conception Group sediments on the Avalon Peninsula have been correlated with similar appearing sediments of the Connecting Point Group (Buddington 1919; Hayes 1948; McCartney 1967). Rocks of the Connecting Point Group outcrop in the western half of the Avalon Zone along a belt which trends southward from Bonavista Bay, along the southwest shore of the Isthmus of Avalon, and onto Long Island in Placentia Bay (Fig. 1).

In the Bonavista Bay area, Jenness (1963) described 5200 metres of Connecting Point Group sediments, for which neither the base nor the top is exposed, as consisting predominantly of sandy and silty greywackes, black and grey slates with only minor conglomerates, pyroclastic rocks, lavas and cherty quartzites. On the Isthmus of Avalon, McCartney (1967) described about 2700 metres of Connecting Point Group strata, where again the base is not exposed, as consisting of predominantly dark grey and green siltstone, slate, argillite and greywacke. King et al. (1974) feel that Connecting Point Group strata closely resembles Conception Group strata, both of which consist of volcanic debris. However none of the formations established in the Conception Group (Williams and King 1979) have been recognized in the Connecting Point Group and at present it is not possible to make a direct correlation between the two

Groups (Hoffman et al. 1979). O'Driscoll and Muggeridge (1979) interpreted the strata of the Connecting Point Group in the Placentia Bay area as representing the infilling of a marine basin by an overall shallowing upward sequence.

Both McCartney (1967) and Jenness (1963) describe the occurrence of volcanic rocks near the top of the Connecting Point Group. McCartney (1967) suggested that these volcanic rocks are related to the overlying Musgravetown Group rocks and that the contact between the two groups is conformable. King et al. (1974) describe this contact as conformable and gradational in the isthmus area.

In the Bonavista Bay area, the Musgravetown Group lies with pronounced angular unconformity upon the Connecting Point Group (Jenness 1963). West of Trinity Bay, rocks of the Musgravetown Group occur in three belts which trend in a north-northeast direction. The easternmost of these belts continues onto the Isthmus of Avalon and down to the southwest area of the Avalon Peninsula.

The bimodal volcanic rocks of the Bull Arm Formation occur at the base of the Musgravetown Group (Jenness 1963; McCartney 1967; Malpas 1971). These rocks are overlain by a sequence of interbedded grey-green siltstone, argillite, arkose and red conglomerate (McCartney 1967; Jenness 1963). The upper sedimentary rock units of the Musgravetown Group have been correlated with similar rock units of the Hodgewater Group to the east (Jenness 1963; McCartney 1967;

King et al. 1974). Correlated units at the top of both the Hodgewater and Musgravetown Groups are overlain by a thin quartzite unit, the Random Formation, which underlies fossiliferous Cambrian strata (McCartney 1967). The Random Formation quartzite has been shown by Anderson (1981) and Bengston and Fletcher (1983) to be diachronous over a restricted range of time in the early Cambrian.

1.5. Cambrian and Ordovician Stratigraphy

Paleozoic rocks are preserved "only as isolated relics in the cores of several synclines in western Avalon, and within some down-faulted blocks in the southern half of the Conception Bay area in eastern Avalon" (King et al. 1974). In the western area, the Random Formation quartzite occurs at the probable base of the Paleozoic sequence with fossiliferous Cambrian strata overlying (Anderson 1981). The Random Formation is bounded by disconformities over most of its extent (Hiscott 1982). Previously a disconformity was interpreded to exist at the top of the Random Formation throughout the Avalon Zone (Jenness 1963; McCartney 1967). A disconformity was also interpreted to exist at the base, except westward from Placentia Bay where the Random Formation conformably overlies the Early Cambrian fossil-bearing strata of the Chapel Island Formation (Greene and Williams 1974). In the Conception Bay area no Random Formation equivalents are known (King et al. 1974). The

Random Formation is interpreted as having been deposited along a shoreline during a marine transgression during Early Cambrian time (Hiscott 1982).

Above the Random Formation in the west and above Precambrian strata in the Conception Bay area, is a sequence of strata which ranges in age from Early Cambrian to Early Ordovician (McCartney 1967; King et al. 1974). In total, these strata are in the order of 2 km in thickness. The Early Cambrian Adeytown Group, the lowest unit in the sequence, consists of red, green and grey silty mudstones and nodular limestone. Conformably above the Adeytown Group is the Late Cambrian Harcourt Group, which consists of dark laminated shales with interbeds of fine-grained sandstone which increase in abundance upwards. Conformably above this are the Ordovician-aged, shale- to sandstone-dominated, Bell Island and Wabana Groups, both occurring on islands in Conception Bay. The Cambrian and Ordovician sequence of rocks found above the Random Formation is thought to have formed in an epicontinental marine environment as sub-littoral and intertidal deposits (King et al. 1974).

1.6. Mid-Paleozoic Magmatism

Mid-Paleozoic granitoids in the Newfoundland Avalon Zone are generally restricted to its western regions. The Ackley batholith, which intruded across the boundary of the Gander and Avalon Zone (Fig. 1), is the largest such

granitoid body occupying an area of approximately 6500 square kilometres. It is composed predominantly of coarse-grained biotite granite (Strong et al. 1974; Dickson et al. 1980). Kontak et al. (1988) have demonstrated that three distinct episodes of magmatic activity were involved in the formation of the Ackley Granite. Total-fusion $^{40}Ar/^{39}Ar$ dating of biotites, muscovites and one hornblende have provided age dates which range from $\geq$ 410.4 $\pm$ 4.4 Ma to 352.0 $\pm$ 5.0 Ma. The Ackley Granite had been previously dated at 345 $\pm$ 5 Ma (Rb-Sr) by Bell et al. (1977).

The St. Lawrence pluton, located near the southern tip of the Burin Peninsula, intrudes Precambrian to Cambrian sedimentary and volcanic rocks, as well as its own volcanic carapace (Strong et al. 1978). It is composed of alkaline to peralkaline alaskite and granite and has been dated at 328 $\pm$ 5 Ma (Rb-Sr, Bell and Blenkinsop 1977).

Medium to coarse-grained K-feldspar-biotite granite (Red Island Granite) has intruded into fossiliferous Cambrian sediments on Red Island in Placentia Bay. Although this granite has not been dated radiometrically, it is definitely post-Cambrian and likely has formed in either Devonian or Carboniferous time, related to the Acadian Orogeny or the "Hercynian megashear" (Strong 1980). The Fox Island Granite which occurs closer to the Avalon Peninsula (Fig. 4) has not been studied in any detail but is thought to have a similar origin to the Red Island Granite.

1.7. Summary of Structural Features of the Avalon Zone

Structrual features resulting from two periods of deformation are recognized in the Avalon Zone of Newfoundland. The first period, during which only minor deformation took place, occurred at the end of the Precambrian and was called the "Avalonian Orogeny" by Lilly (1966). The second period of more extensive and intense deformation is of Devonian age and was related to the Acadian Orogeny (Dallmeyer et al. 1981).

There is limited local, but strong, evidence for the event called the "Avalonian Orogeny." The angular unconformity beneath the Random Formation indicates an uplift event which possibly occurred due to compressional stress (King et al. 1974). Hughes and Bruckner (1971) interpret this unconformity as a local phenomenon, rather than the result of "an important period of folding."

At Red Head, in the Flat Rock area north of St. John's, strongly deformed Conception Group sediments have been thrust over younger St. John's Group strata. Also, undeformed Signal Hill Group sediments unconformably overly strongly deformed Conception Group rocks (King et al. 1974; Anderson et al. 1975). Significant deformation due to compressional stress must have taken place at Red Head during late Precambrian time Anderson et al. 1975). At Bacon Cove in Conception Bay, horizontal Cambrian strata

unconformably overly Conception Group strata which dip from 45° to 90°, due to a period of deformation which occurred after deposition of the Conception Group (McCartney 1969).

Rast (1979) and Keppie (1979) describe the development of penetrative deformation in the Avalon Zone of New Brunswick and Nova Scotia as Cadomian in age (late Precambrian). Evidence from local areas indicates that a period of late Precambrian deformation in the Avalon Zone of Newfoundland may be related to more intense deformation of the same age in the Avalon Zone of both New Brunswick and Nova Scotia.

The most widespread deformation of Newfoundland Avalon Zone rocks occurred after the deposition of Cambrian and Ordovician strata. West of the Paradise Sound Fault (Fig. 3) rocks of the Love Cove Group and portions of the Marystown Group are deformed into tight to isoclinal folds with attendant development of a generally penetrative axial planar foliation (Jenness 1963; Hussey 1980; Dallmeyer et al. 1983). In the northwestern Avalon Zone, northeast trending folds have affected Proterozoic, Cambrian and Ordovician rocks alike (Hayes 1948; Jenness 1963). Strong et al. (1978) describe rocks of both late Precambrian and Paleozoic age on the Burin Peninsula to be asymmetrically folded and thrust towards the southeast. East of the

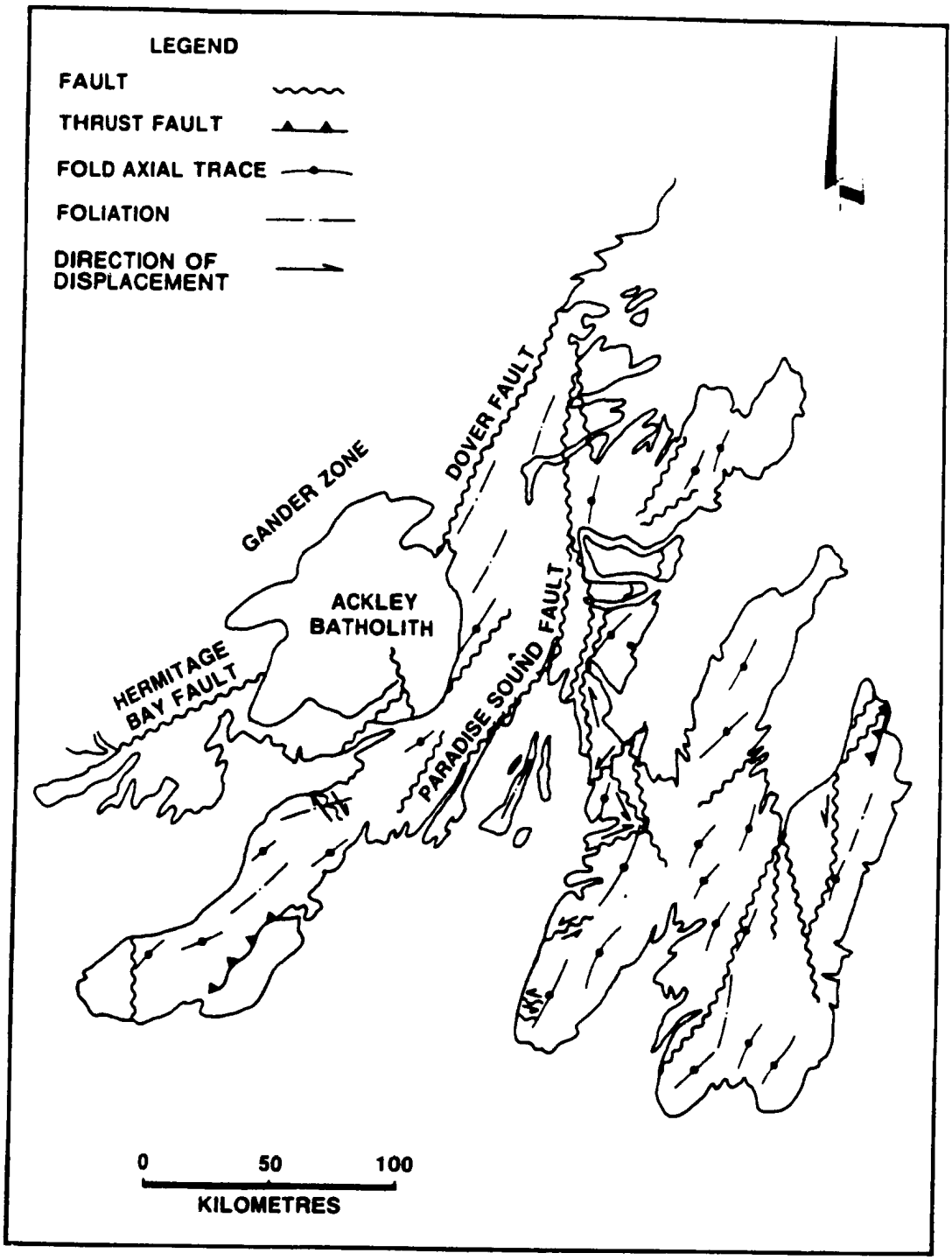

FIGURE 3: STRUCTURAL FEATURES OF THE AVALON ZONE. AFTER WILLIAMS et al. (1982) AND McCARTNEY (1969).

Paradise Sound Fault, Musgravetown Group sedimentary rocks and overlying Cambrian rocks are affected by moderately open folds with variable development of an axial planar foliation (Rose 1952; McCartney 1967; Williams and King 1979).

The metamorphic grade of Avalon Zone rocks ranges from unmetamorphosed areas in the east to mid-greenschist metamorphism (biotite grade) in rocks found next to the Dover Fault (McCartney 1969; Dallmeyer et al. 1983). Blackwood and Kennedy (1975) have shown that deformation of the Love Cove Group was concomitant with movement on the Dover Fault. The Ackley Granite intruded deformed and metamorphosed rocks of both the Gander and Avalon Zone, and has transected the Dover Fault (Dickson et al. 1980). This places a time constraint on the age of the last movement along the Dover Fault to be at least older than the youngest aged granite dated in the batholith (352 $\pm$ 5.0 Ma, age dating discussed above) and younger than the oldest aged granite ($\geq$ 410.4 $\pm$ 4.4 Ma). Movement on the Dover Fault is therefore likely of Devonian age, but may be Early Carboniferous. Elias and Strong (1982a) have shown that deformation of the Indian Point Granite and Hardy's Cove Granite, previously grouped together as the Straddling Granite, place an upper age limit of Early Carboniferous for final movement on the Hermitage Fault.

Dallmeyer et al. (1983) dated metamorphic recrystallization of the Love Cove Group as ranging from 370

to 390 Ma ($^{40}Ar/^{39}Ar$) for the metamorphic recrystallization of these rocks. The age dates for movement on the Dover Fault and for deformation and metamorphism of the western Avalon Zone correspond to the Acadian phase of Appalachian orogenesis which took place during the Devonian. Due to the similar nature of deformation in the western Avalon Zone to that of the Avalon Peninsula in the east (i.e., large scale north-northeast trending open folds with axial planar foliation) it is likely that the widespread post-Cambrian-Ordovician deformation seen across the Avalon Zone is of Acadian age (Williams et al. 1974).

Several workers have described faults of both Precambrian and post-Ordovician age on the Avalon Peninsula (Rose 1952; McCartney 1967, 1969; Bruckner 1969). McCartney (1969) described Precambrian faults as "high-angle, north-trending faults with stratigraphic displacement commonly in the order of several thousand feet." Such faults are most abundant south and east of Conception Bay, but also control the distribution of Connecting Point Group strata on the Isthmus of Avalon and just west of Trinity Bay (Fig. 3), through the presence of a number of horst and graben structures. Relatively minor post-Cambrian movements displace Cambrian beds in the opposite direction to the major Precambrian movement (McCartney 1969).

Faults which were initiated in post-Ordovician time form a "complimentary system" of strike-slip faults which

offset the fold axis of Paleozoic and older strata (McCartney 1969). On the isthmus and just east of the isthmus, strike slip faults with sinistral displacement vary in strike from 130° Az to 170° Az. Faults with dextral displacement vary in strike from 035° Az to 065° Az (McCartney 1967). Since folding of lower Paleozoic strata is of Devonian age, these faults are Devonian or younger, and likely developed during Acadian deformation. Thrust faults, some of which cut Cambrian strata, have also been recognized on the Avalon Peninsula (Rose 1952; McCartney 1967).

Jenness (1963) describes faults in the Terra Nova and Bonavista Bay areas which range in age from post-Early Ordovician to between Middle Ordovician and Late Devonian. These faults are also of Devonian age or younger, as they displace folds developed during Acadian orogenesis.

Southeastward-directed thrust faults on the southern Burin Peninsula produce the dominant structural style (Strong et al. 1978). Large areas of the Marystown and Inlet Groups are relatively undeformed, apart from minor open folding which can be timed between the Middle Cambrian and intrusion of the St. Lawrence Granite (334 ± 5 Ma, Bell et al. 1977; Rb-Sr) and is interpreted as being of Acadian age (Strong et al. 1978).

1.8. Summary

Late Precambrian volcanic rocks and volcanogenic sediments are the oldest and the most prevalent lithologies found in the Avalon Zone. Detrital marine sediment deposition predominates in Early Paleozoic time, with marine shoreline sediments and epicontinental marine sediments forming the most abundant deposits. In Devonian and Carboniferous time, igneous rocks are again most prevalent, due to the crystallization of syntectonic granites.

Although some of the structural elements of the Avalon Zone developed during late Precambrian time, most of the deformation took place during the Acadian Orogeny. The formation of BCS veins in Avalon Zone rocks is shown in Chapter 2 to be concurrent with the development of structural elements during Acadian orogeny.

CHAPTER 2. GEOLOGY OF BARITE AND ASSOCIATED VEINS

2.1. Occurrence of Barite and Associated Veins

In the study area (Fig. 4) quartz-dominated veins are by far the most abundant vein type, followed by barite, then calcite and sulphide mineral-dominated veins. Veins with a major proportion of one or two of these mineral phases have been found in several locations in the field area. Evidence to be presented indicates that the formation of these mineralogically different vein types are essentially contemporaneous on a geological time scale, and can be related to the Acadian deformational event which affected the study area. The orientation data for all veins analyzed in this study are tabulated in Appendix A.

In the area of study, BCS veins are exposed throughout a section of rocks which ranges in age from late Haydrinian through to Middle Cambrian (see Fig. 4 for a general location map of the veins). The stratigraphically lowest rock unit which hosts BCS veins is the Connecting Point Group, which occurs only on the Isthmus of Avalon in the field area. This group of sedimentary rocks continues northward off of the isthmus, but the occurrence of BCS veins apparently diminishes off the isthmus. The La Manche calcite-galena vein (BV12), once mined for its lead content (Chute 1939), occurs along the south shore of the isthmus (Fig. 5), also in rocks of the Connecting Point Group.

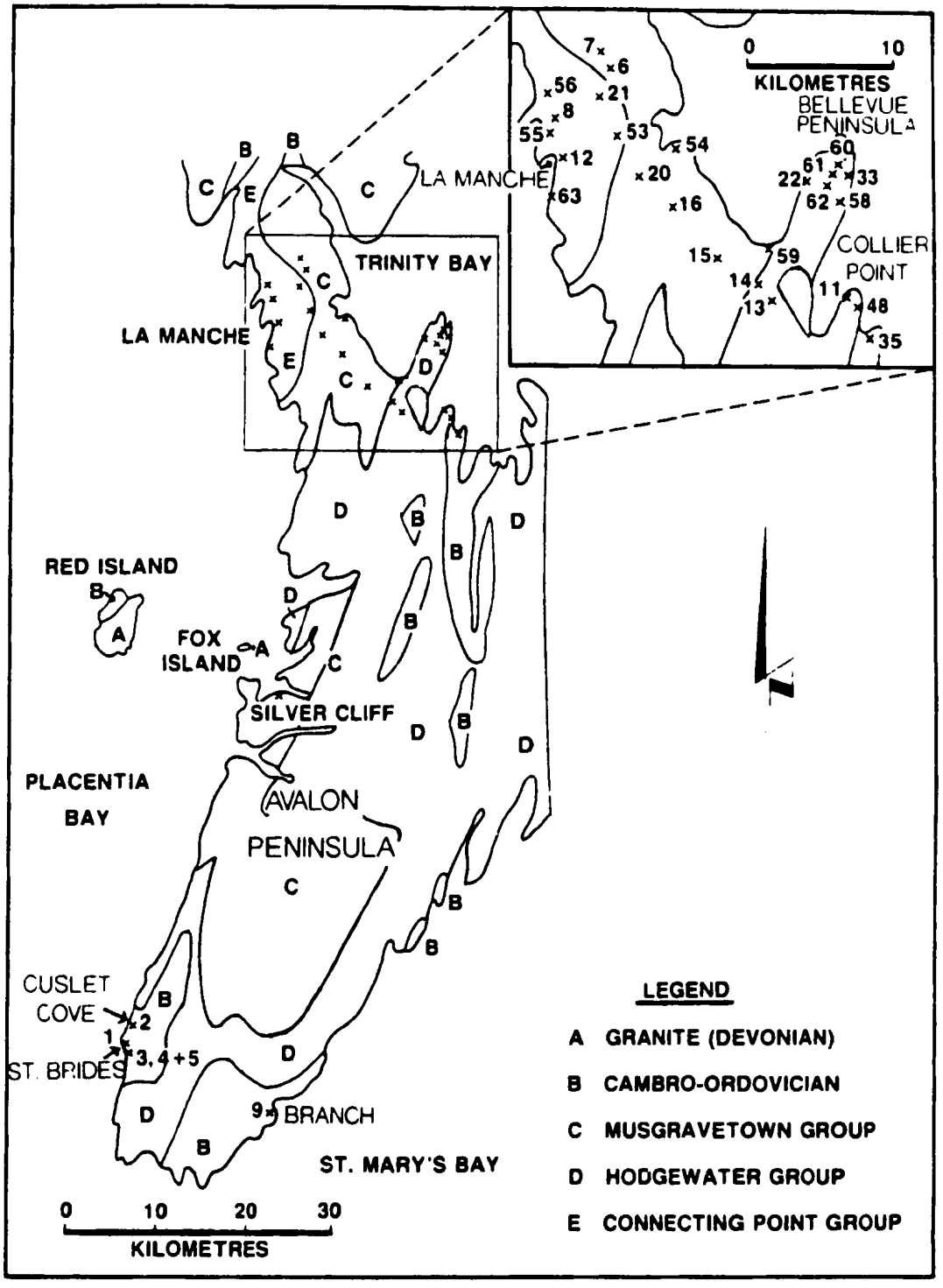

FIGURE 4: FIELD AREA AND GENERAL SAMPLE LOCATION MAP. GEOLOGY FROM HIBBARD (1983).

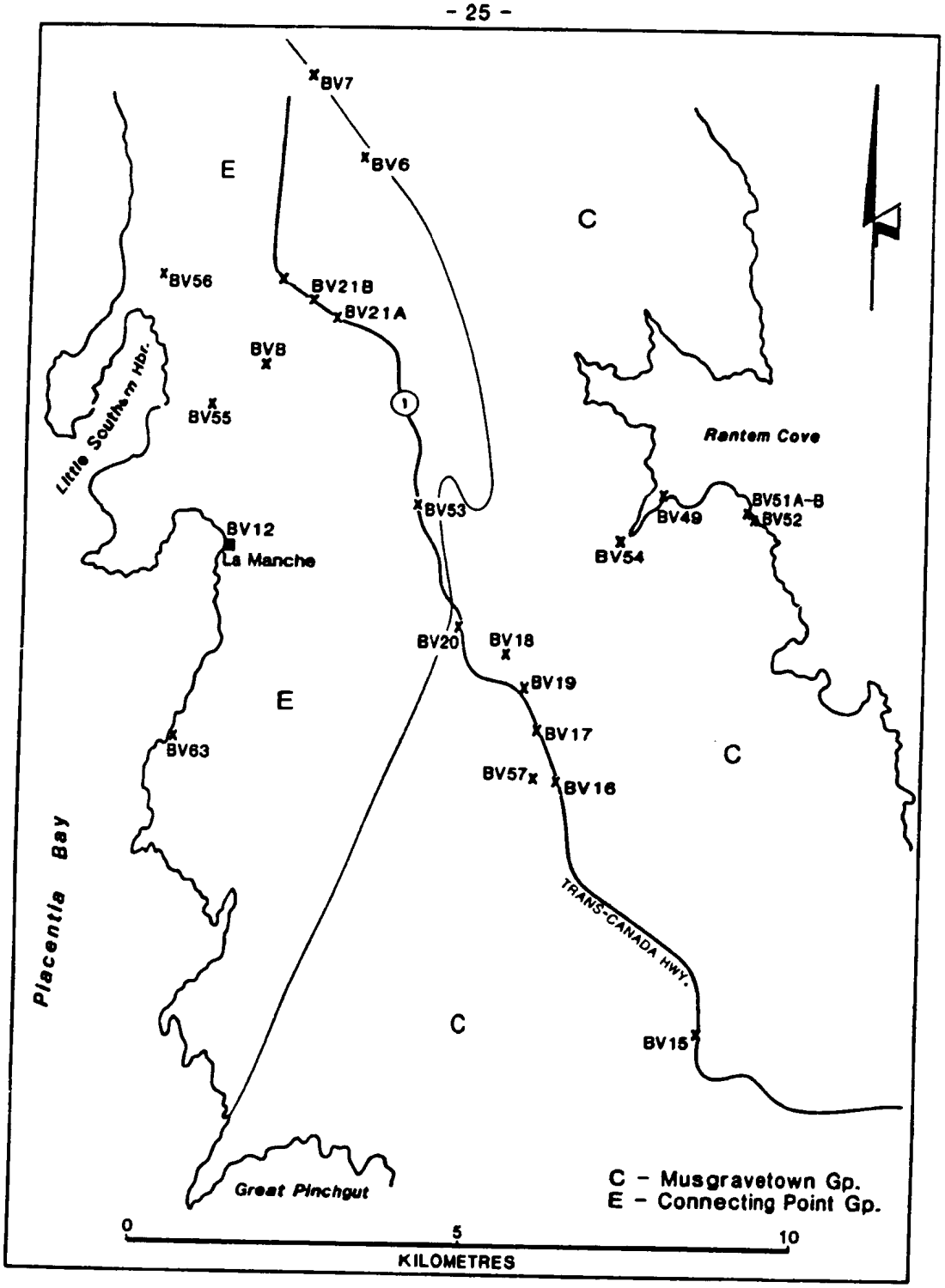

FIGURE 5: SAMPLE LOCATION MAP FOR THE ISTHMUS OF AVALON AREA.

In the southeast segment of the isthmus, clastic rocks of the Connecting Point Group are stratigraphically overlain by volcanic rocks of the Bull Arm Formation. The Bull Arm Formation forms the base of the Musgravetown Group. BCS veins have been observed in these late Haydrinian rocks along both the eastern and western shoreline of the isthmus and along the Trans-Canada Highway (Fig. 5). Malpas (1971) described the occurrence of barite along numerous joint planes in Bull Arm Formation rocks. The MacKay vein and Fowler vein (Figs 6 and 28) of the Silver Cliff mine, occur along the shore of Placentia Bay, just south of the isthmus in rocks of the Bull Arm Formation, on the Argentia naval base. These veins have been previously mined for lead, zinc and silver.

On Bellevue Peninsula and on Collier Point (Figs 4 and 7), along the southern shore of Trinity Bay, several barite and calcite veins occur in late Haydrinian sedimentary rocks of the Hodgewater Group, which are stratigraphically equivalent to rocks in the Musgravetown Group. West of Collier Point, along the southern shore of Long Cove, barite veins (BV39, 40 and 42) occur in Lower Cambrian rocks of the Bonavista Formation (Fig. 7). In the Cape St. Mary's area of the Avalon Peninsula, several barite veins (BV1, 3 and 4) occur in Bonavista Formation rocks, along the coast, south of Cuslet Cove and north of the town of St. Brides (Fig. 8). The barite vein BV-2 occurs in Musgravetown Group rocks

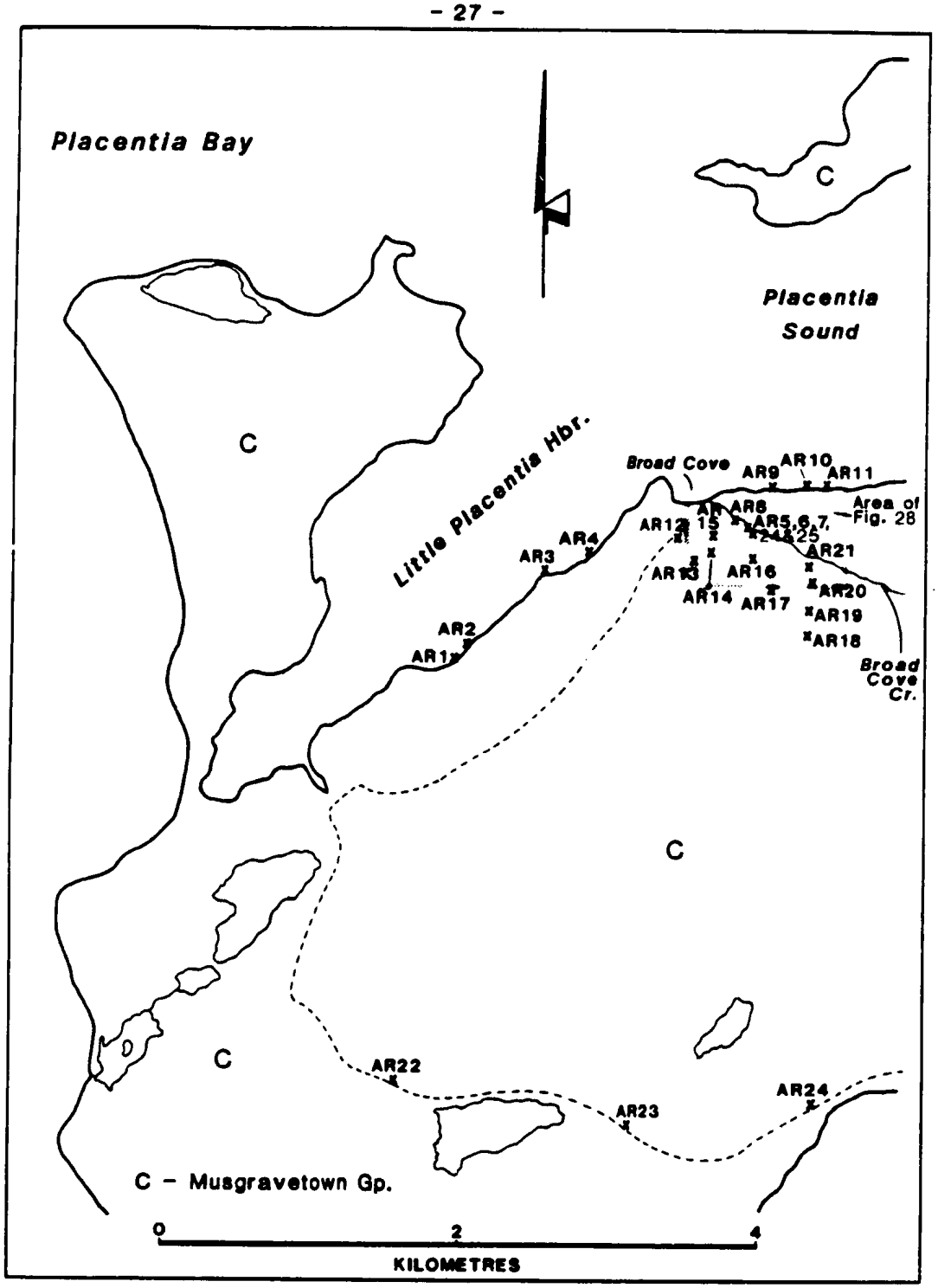

FIGURE 6: SAMPLE LOCATION MAP FOR THE ARGENTIA AREA. REMAINING OPENING OF THE SILVER CLIFF MINE (MACKAY VEIN) IS MARKED BY THE "AR5,6,7,24 & 25" SAMPLES.

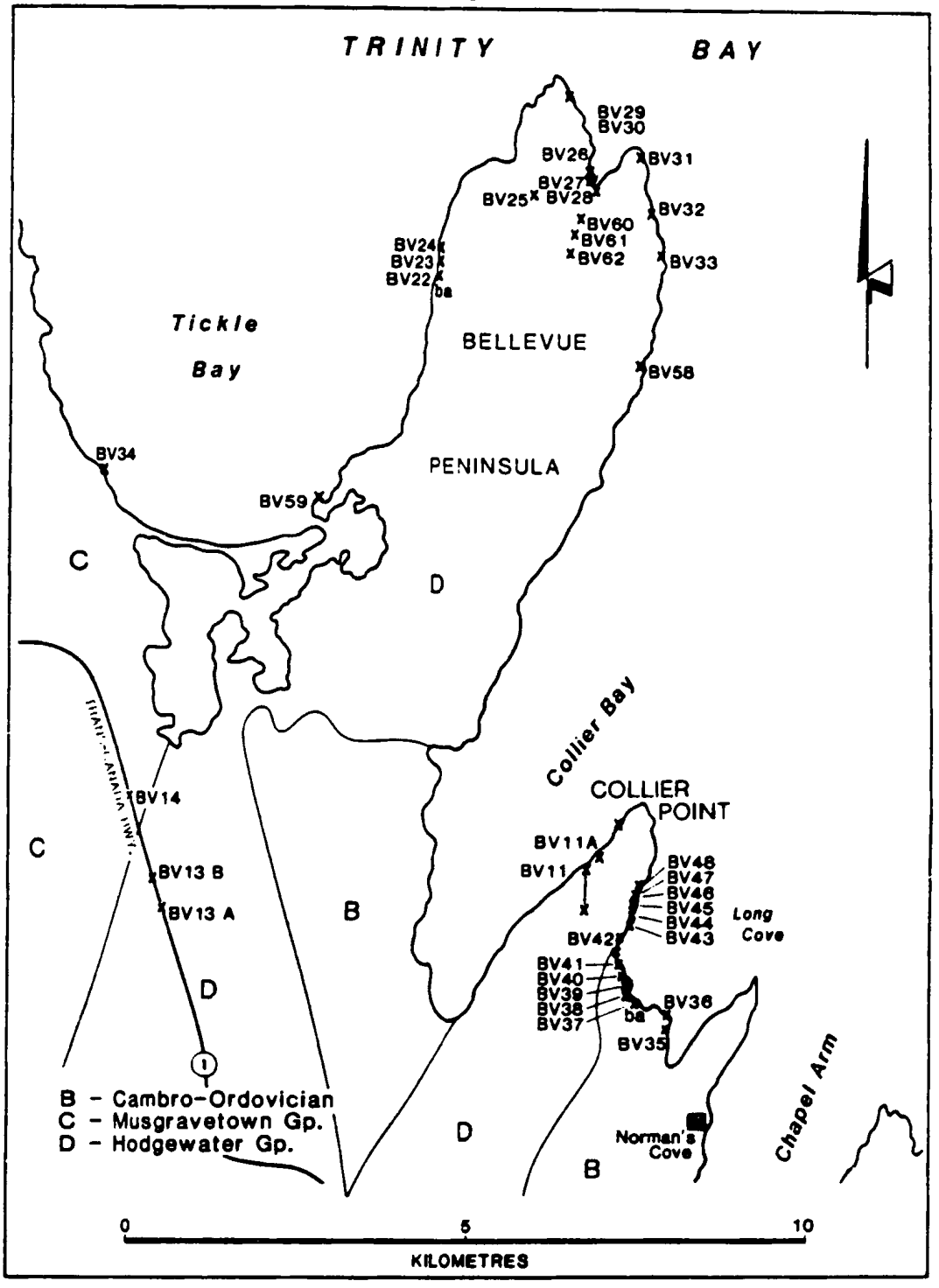

FIGURE 7: SAMPLE LOCATION MAP AND GENERAL GEOLOGY FOR THE BELLEVUE PENINSULA AND COLLIER POINT AREA.

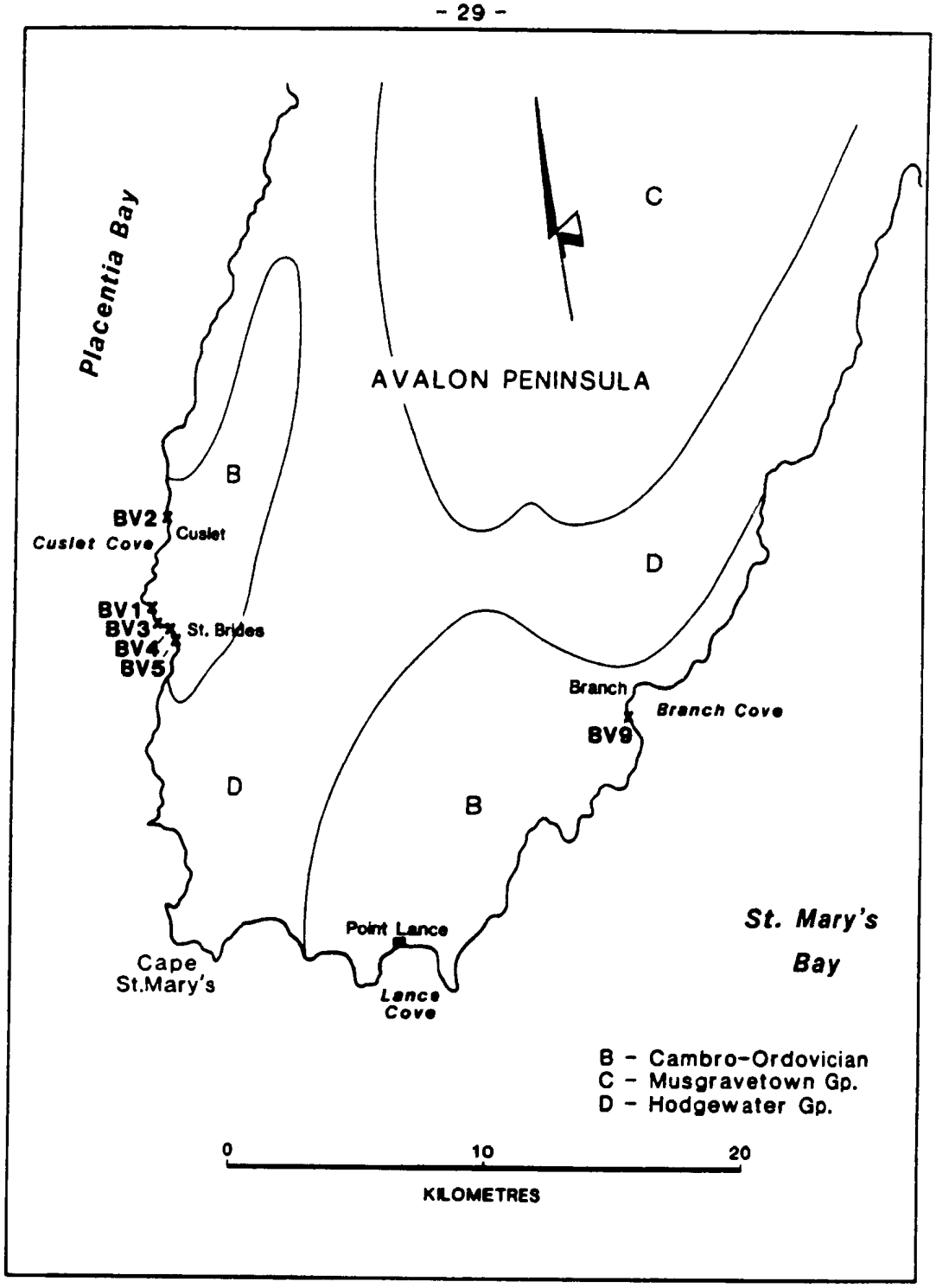

FIGURE 8: SAMPLE LOCATION MAP AND GENERAL GEOLOGY FOR THE CAPE ST. MARY'S AREA OF THE AVALON PENINSULA.

along the coast just north of Cuslet Cove (Fig. 8). One barite vein (BV9) was located on the east coast of this peninsula, just south of the town of Branch, in the Middle Cambrian Chamberlains Brook Formation (Fig. 8). Barite vein formation was therefore at least post-Middle Cambrian.

Most of the veins which were sampled for this study occur along coastal exposures or along the Trans-Canada Highway. While the field work for this study was taking place, the Newfoundland Department of Mines and Energy conducted a stream sediment geochemical survey of the Bellevue Map area (IN/12) and the St. Brides area of the southern portion of the Avalon Peninsula. While traversing these streams a significant number of barite veins were found inland. The results of the geochemical sampling revealed a number of locations with barium anomalies, along with several other elements, indicating the possible presence of many more barite veins in interior locations (Howse et al. 1984).

2.2. Vein Morphology and Paragenesis

All veins observed in this study are of a dilational nature. Euhedral crystal growth into vugs, brecciation of wallrock, comb, ribbon and cockade structures (described below) are textures which indicate open space filling as the process of vein formation. These textures can be found in most veins which have not undergone later deformation.

Based on mineralogy and crosscutting relationships there are two distinct sets of veins recognized in the field area. There exists an early set of quartz ± chlorite ± calcite ± barite veins and a later set of barite ± calcite ± quartz veins. The sulphide-bearing veins at Silver Cliff and La Manche, as well as several smaller veins at other locations, are related to the later set, but are discussed separately.

The early set of quartz ± chlorite ± calcite ± barite veins range in thickness from less than 1 and up to 15 cms, and typically are 2 to 8 cms thick. Although these veins pinch and swell in places, they are more typically constant in thickness. A commmon observation was the pinching out of a vein in close proximity to where another vein either widened or a new vein had formed. The quartz veins generally have a linear to slightly curved trace in outcrop. Intersecting quartz vein sets have resulted in an apparent brecciation of the wall rock at a few locations (e.g., Fig. 9, BV29 on Bellevue Peninsula). An en echelon zone of quartz veins, precipitated into fractures which opened during dextral shear motion, was found near the Silver Cliff mine (Fig. 10). Most quartz veins have undergone some deformation after precipitation, such as the dextral shear which has deformed BV29 (Fig. 11) on Bellevue Peninsula. Wall rock fragments are locally included in quartz veins. Fractures filled by vein material generally have opened with little brecciation of wall rock. Within the rare undeformed

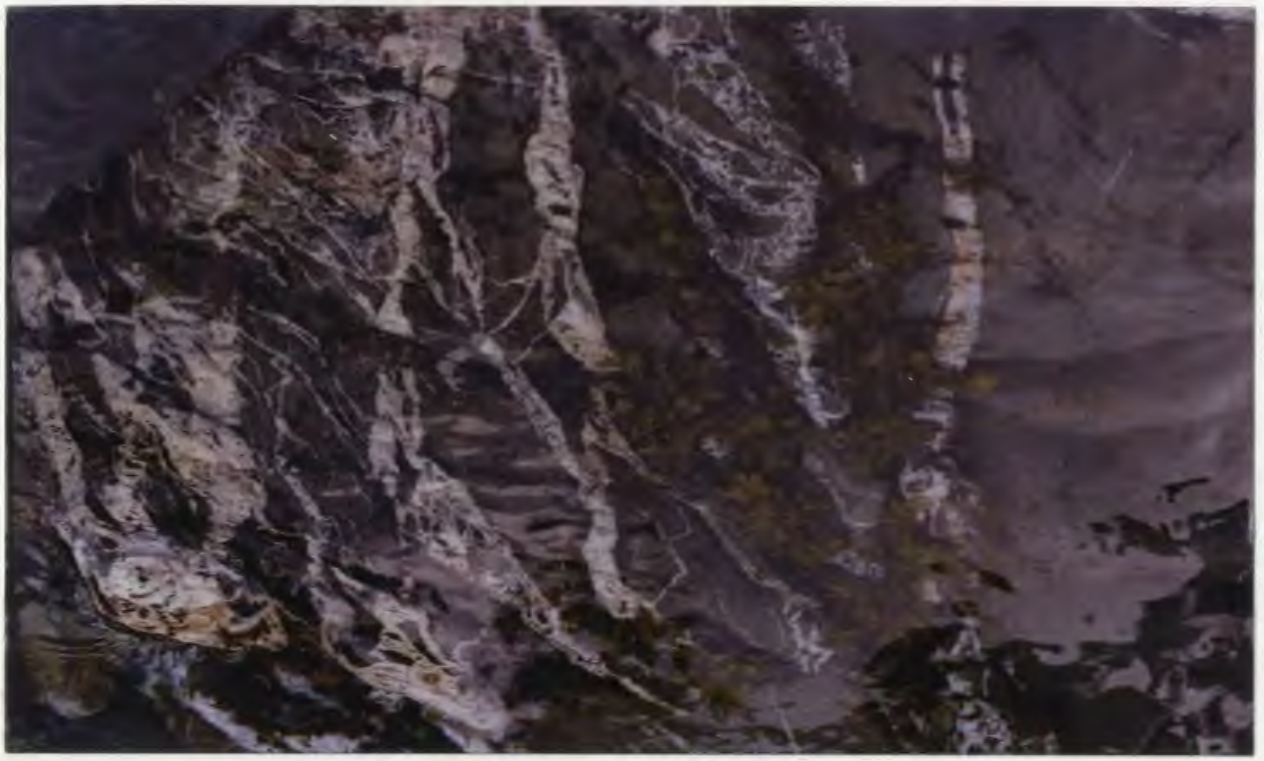

Figure 9. Quartz precipitated into two predominant fracture sets, resulting in a brecciated vein pattern. View is about 2 X 1.2 m, looking down into water. BV29 on Bellevue Peninsula.

Figure 10. En echelon pattern of quartz veins indicating dextral shear. The handle of the hammer is pointing upwards. AR-4 near the Silver Cliff mine.

Figure 11. Deformation caused by dextral shear within a quartz-chlorite vein. BV29 on Bellevue Peninsula.

veins, quartz crystals are coarse, prismatic and typically oriented at a high angle to vein walls, with some comb structures developed. There is no apparent wall rock alteration next to the quartz veins.

Chlorite is a significant constituent of many quartz-dominated veins, generally comprising 10 to 20%, and up to 60%, of a vein. Chlorite exists as fine crystals in undeformed veins, commonly elongate parallel to their crystallographic c-axis, forming pseudo-hexagonal cross sections. These crystals are generally twisted and curved along their length (Fig. 12). Most chlorite exists in solid masses where individual crystals are indistinguishable in the "thick" thin sections prepared for fluid inclusion work. Near the edge of these masses individual curved chlorite crystals (i.e., original form, not subsequently "bent") are surrounded by quartz, indicating co-precipitation with quartz in these veins. Chlorite was frequently observed to exist at the boundary between two quartz crystals as a thin elongate mass, or in fractures which cut through quartz crystals. Chlorite is also typically concentrated within layers in quartz veins, resulting in ribbon structures.

In the early set of quartz-dominated veins, calcite, and less commonly barite, occurs in a subordinate number of veins, usually as late vug-filling crystals surrounding earlier-formed quartz and chlorite crystals (Fig. 13). Calcite was observed to have co-precipitated with quartz and

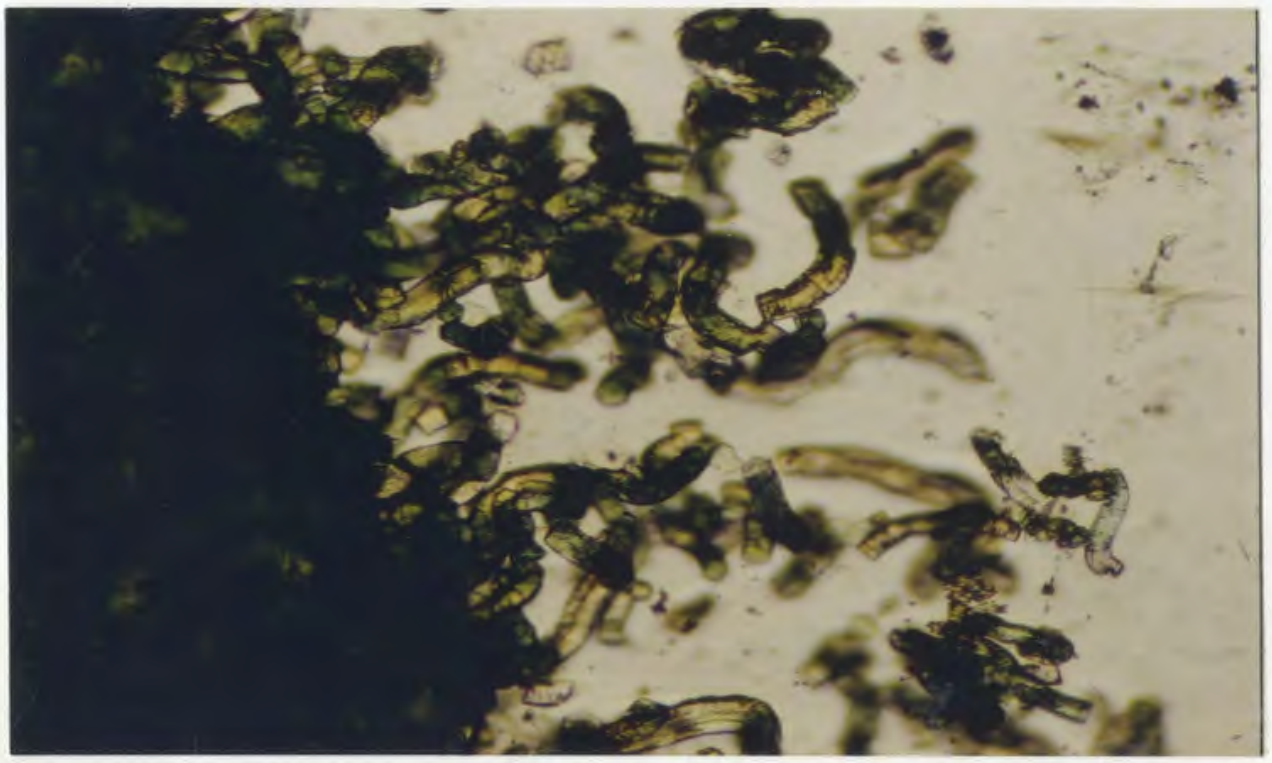

Figure 12. Curved and twisted chlorite crystals surrounded by quartz, next to a solid mass of chlorite. AR1-B2 near the Silver Cliff mine (field of view ~ 10 X 7.5 mm).

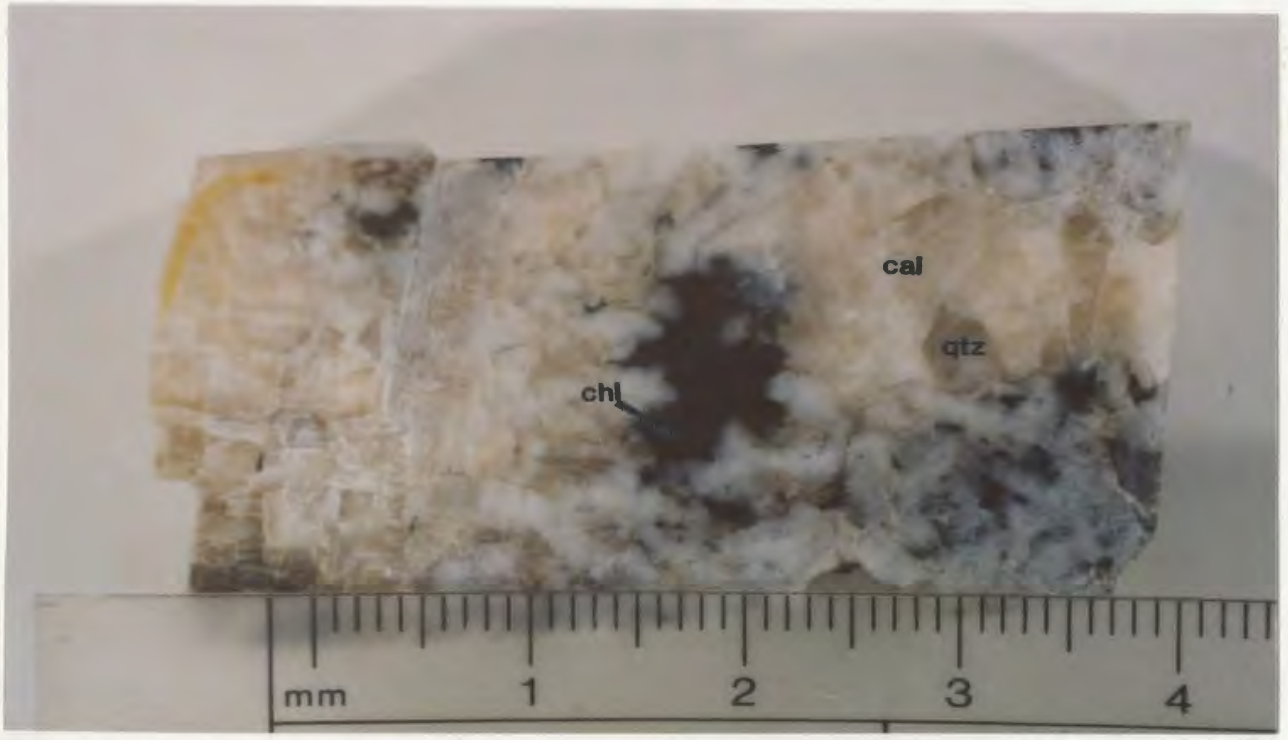

Figure 13. Calcite grown around earlier euhedral quartz crystals. BV35-C near Collier Point. Quartz - qtz, calcite - cal, chlorite - chl.

chlorite in three locations, BV33 (described below) and BV23-B from Bellevue Peninsula (Fig. 7) and BV3-C from St. Brides (Fig. 8).

Figures 14 and 15 are photographs of veins found on the east coast of Bellevue Peninsula (BV33). Figure 14 shows several quartz-chlorite veins of variable strike. To the right of the hammer, a quartz-chlorite vein ends where a pink calcite-dolomite vein, of a different orientation, begins. Figure 15 is a close up of the region where the veins meet. The calcite-dolomite vein can be traced off the photograph for about 10 metres where the outcrop ends. When this vein first opened, quartz and chlorite precipitated on the fissure wall (Fig. 15). Carbonate then precipitated to fill the rest of the vein and has precipitated around earlier euhedral quartz crystals in the center of the carbonate vein, next to the quartz-chlorite vein. This quartz may be connected with the quartz-chlorite vein deeper in the outcrop, or may have been connected above the present outcrop before erosion. There is no indication of any continuation or displacement of either of these two veins past the intersection point. It appears that two fractures of different orientation opened at the same time, and where they intersected they each ended. Quartz and chlorite initiated precipitation in both fissures, but precipitation in the vein on the right was replaced by carbonate phases. Close examination of the carbonate vein reveals that chlorite filled fractures cut through a few early formed

Figure 14. Several orientations of quartz-chlorite veins with one such vein intersecting a carbonate vein, BV33 on Bellevue Peninsula.

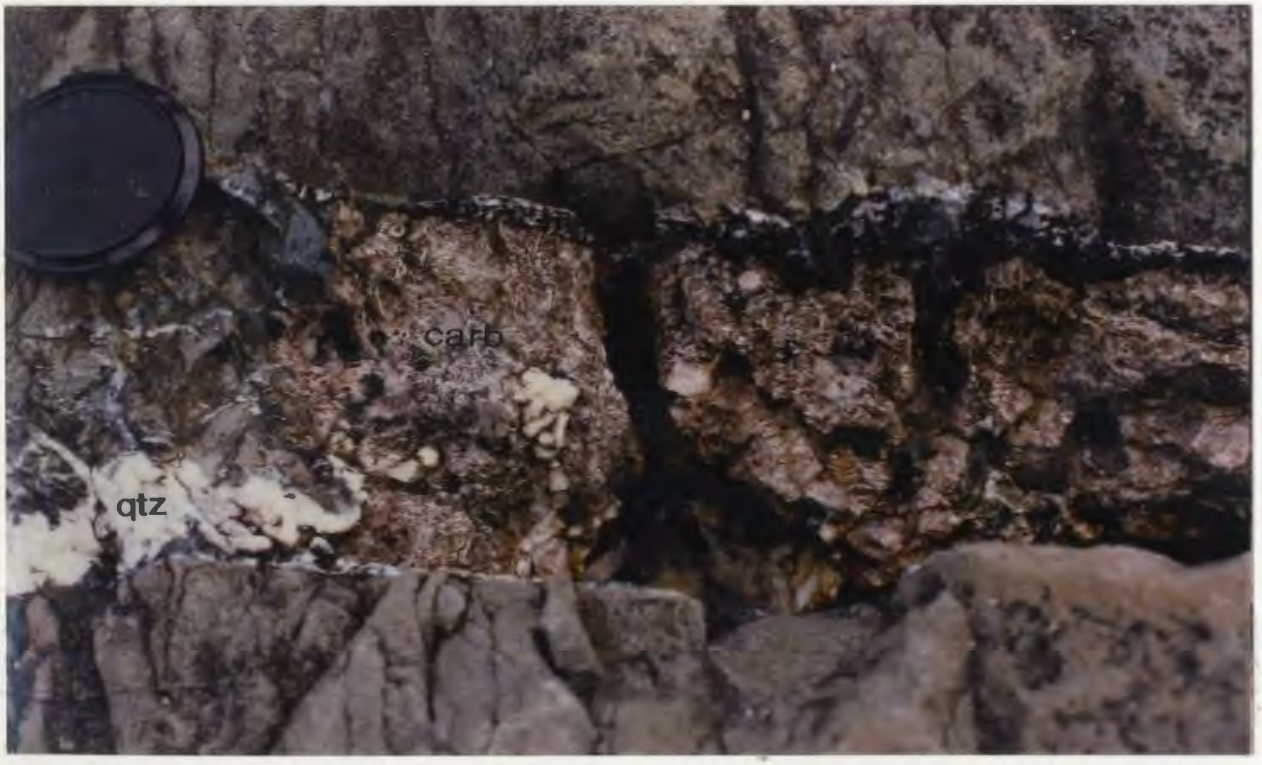

Figure 15. A close up shot of the intersection of a carbonate vein with a quartz-chlorite vein seen in Figure 14. BV33 on Bellevue Peninsula.

quartz-chlorite filled fractures cut through a few early formed carbonate crystals. Carbonate then resumed as the only precipitating phase. It appears that these two veins started off precipitating from a similar fluid. The vein on the right was then filled with fluid from a different source with a different chemistry. Apparently there was a "competition" for space, in the vein on the right, between two different fluids while fissuring progressed. The fluid precipitating carbonate phases eventually replaced the fluid precipitating quartz-chlorite.

The later set of barite ± calcite ± quartz veins cut earlier quartz-chlorite veins (Figs 16 and 17) in all known locations except BV33 described above. These veins range in thickness from coatings on joint surfaces, to veins several metres thick (eg., BV11 Collier Point). BV11 averaged over a metre in thickness and has been mined for barite (Fig. 7).

Minor displacements have affected some barite veins. Figure 18 is a photograph of BV1 (Cross Point vein) located north of St. Brides (Fig. 8) in the Cape St. Mary's area of the Avalon Peninsula. The zig-zag geometry of this vein has resulted from precipitation in an original extensional zig-zag fracture pattern. Some later movements along slip planes have displaced the ribbon structure of the vein. Slickensides have also been found along several barite veins indicating some degree of motion, the magnitude of which is uncertain, but believed to be of only local significance.

Figure 16. Barite vein cutting through an earlier quartz-chlorite-calcite vein on Collier Point. The quartz vein on the left side of the barite vein has been displaced into the top left corner of the photograph.

Figure 17. An early formed zone of quartz-chlorite vein precipitation is cut by a latter barite-calcite vein, again on Collier Point. In the barite vein calcite is the first phase to precipitate and is seen here lining the vein wall.

Figure 18. Cross Point Vein north of St. Brides. Note the zig-zag geometry created by the original extensional fracture pattern. The ribbon structure of the orignal vein has been displaced along later minor slip planes.

Brecciation of wall rock during the fissuring process has occurred at several locations on Collier Point. Figure 19 is a photograph of a unique phenomenon observed in a barite vein (BV48) which occurs along the east coast of Collier Point. During extension and the opening of this vein, numerous fragments of the wall rock broke off and were incorporated into the vein along only one side. Either the fragments were removed only from the one wall to which they are now closest, or they came off of both walls and remained next to the bottom wall with continued fissuring in the vein. The vein dips 72° north and the fragments are along the southern margin. A 72° dip is much greater than the angle of repose and it seems unlikely that the clasts fell off and were resting on the vein footwall at the time of formation, unless there has been a considerable steepening of the vein since formation. As will be discussed later on there has been some rotation of the veins on Collier Point but this particular vein (BV48) probably has undergone a rotation which has lessened its dip by about 10°. It therefore seems likely that this phenomenon is simply related to a shift in the position of fissuring to the top side of the vein after the clasts broke off.

Figure 20 is a photograph of a hand speciman from vein BV11 on Collier Point (Fig. 7), the largest known barite vein in the field area. This speciman displays "cockade structure", which results from precipitation into the open

Figure 19. Vein BV48 located along the east coast of Collier Point. See text for description.

Figure 20. From vein BV11 on Collier Point. This sample displays cockade structure, with included wall rock fragments coated with white calcite crystals. Pink barite crystals fill the remaining space. Scale is in mm.

spaces of a breccia, such that the clasts are coated with a layer of radiating crystals. In the photograph, calcite crystals coat the wall rock clasts, with barite filling the remaining spaces. Calcite also coats the margins of BV11. These are very common features of the BV11 vein and other calcite-barite veins in the field area.

Barite veins range in content from 100% barite, ignoring the very fine hematite which variably stains barite crystals pink, to veins dominated by calcite, quartz or sulphide minerals, containing only a minor amount of barite. An overwhelming proportion of these veins are essentially monomineralic barite veins with traces of late vug-filling calcite or quartz. Barite typically occurs as coarse bladed crystals which are variably white or pink. Barite roses were observed in a few locations (Fig. 21). When calcite and quartz are present as separate fissure-filling phases they may be more or less abundant than barite in the vein.

Figure 22 is a photograph of BV22 in which quartz is more abundant than barite. This vein occurs the west coast of Bellevue Peninsula (Fig. 7). Medium to coarse subhedral quartz crystals form a 10 cm thick lining along each vein wall with a central 5 to 8 cm thick barite core. The quartz in BV22 is different from quartz in the early set of quartz -chlorite veins. In this vein the crystals are equant and lack prismatic forms. The quartz band in BV22 is very porous and weakly consolidated, suggesting that a binding

Figure 21. Barite roses as late precipitating crystal structures in spaces left between earlier calcite crystals in vein BV11 (Collier Point).

Figure 22. Vein BV22 from Bellevue Peninsula. Early quartz precipitation has enclosed a core of later precipitated barite (lens cap shadowed in upper left for scale).

phase, such as calcite, has been leached out of the vein. Furthermore, there has been no precipitation of chlorite accompanying the precipitation of quartz in BV22.

Figure 23 is a photograph of BV30, from the tip of Bellevue Peninsula. Coarse scalenohedral calcite comprises at least 80% of BV30 and is the initial precipitated phase. Coarse, bladed, white and pink barite comprises the rest of the vein. Barite is intergrown with calcite and also occurs as a distinct fissure-filling phase next to the vugs. Figures 24 and 25 are photographs of two offshoot veins from the major BV11 vein on Collier Point. In both veins coarse scalenohedral calcite formed early, lining all vein walls and coating a wall rock fragment seen in Figure 25. Precipitation of coarse, bladed, white and pink barite then followed, filling the remaining space created by extension.

In all of the barite veins found on Collier Point, calcite, where present, has precipitated either as the initial vein-filling phase or very early in the paragenetic sequence of the vein. This is also true of all of the veins in the field area in which quartz and/or calcite form a separate fissure-filling phase. Quartz and calcite can both be found in minor quantities as inter- crystalline material or as vug-filling material throughout the paragenesis of many of these veins. Fine euhedral calcite crystals can also be found as solid inclusions in coarse bladed barite crystals in some veins. However, it is apparent that all

Figure 23. Vein BV30 from Bellevue Peninsula. This vein is composed predominantly of calcite with lesser amounts of interstitial barite. A late fissuring event, lined with coarse scalenohedral calcite and partially filled in with barite, has developed on the right margin of the vein.

Figure 24. A small veinlet on Collier Point which has coarse white euhedral calcite lining the walls, and a pink barite core.

Figure 25. A vein on Collier Point with euhedral calcite lining both the walls of the vein, and a wall rock fragment. Coarse bladed barite has filled the rest of the vein.

Figure 26. Vein BV5 in the town of St. Brides. Calcite has filled one fracture in a pre-existing fracture set. The sediments next to the vein have been altered from red to green, indicating the reducing nature of the source fluid.

significant fissure-filling precipitation of quartz and calcite occurs early in the formatin of these veins.

In general there is no apparent alteration of wall rock next to the barite veins. However, sediments within a distance of about 10 cms on either side of the thin calcite vein (BV5, Figs 8 and 26), in the town of St. Brides, have been altered from red to green, indicating a reducing nature for the source fluid at this location. Such wall rock alteration in not generally apparent in other locations because these wall rocks were green (i.e., reduced) to begin with. This photograph also illustrates that this vein has formed in a pre-existing joint set, a feature discussed in more detail further on in this chapter.

2.3. Sulphide Mineral-Bearing Veins

2.3a. La Manche Vein

The following discussion of the La Manche vein is based primarily on the work of Chute (1939). The La Manche vein (BV12, Figs 4 and 5) formed in siltstones of the Connecting Point Group. For much of its exposed extent it lies within or at the contact of an amygdaloidal basic dyke. Mine workings have exposed the vein for approximately 530 metres. The vein varies from a few cms to 3 metres in width, averaging less than 1 metre along its length. Chute (1939) describes the vein as having an erratically variable

strike which is attributed to pre-vein fractures into which the vein has precipitated. Minor displacements along these fractures have occurred before, during and after vein formation, resulting in a total displacement of a few metres of the wall rock on either side of the vein. Wall rock inclusions are common but generally do not significantly dilute the ore grade of the vein (Chute 1939). Evidence of wall rock alteration is lacking along the vein.

The mineralogy of the La Manche vein is dominated by calcite with abundant galena and minor sphalerite, chalcopyrite, barite and quartz. Murray and Howley (1881) reported finding minor amounts of fluorite but Chute (1939) was not able to repeat this observation. The vein is characterized by comb structures, banding and an abundance of vugs. The banding is a result of changes in colour, texture or mineralogy of crystals which generally occur in parallel aggregates of prismatic crystals grown perpendicular to the wall rocks. Earlier-formed bands are often split and disrupted by later bands.

Figure 27 shows the three-stage paragenetic sequence for minerals in the La Manche vein as determined by Chute (1939). Stage 1 calcite is fine-grained, milky white, and precipitated in ribbon structures due to closely spaced shear fractures. Stage 1 calcite has been brecciated by later vein formation. Stage 2 calcite is medium-grained and pale purple, sometimes grading within crystals to white

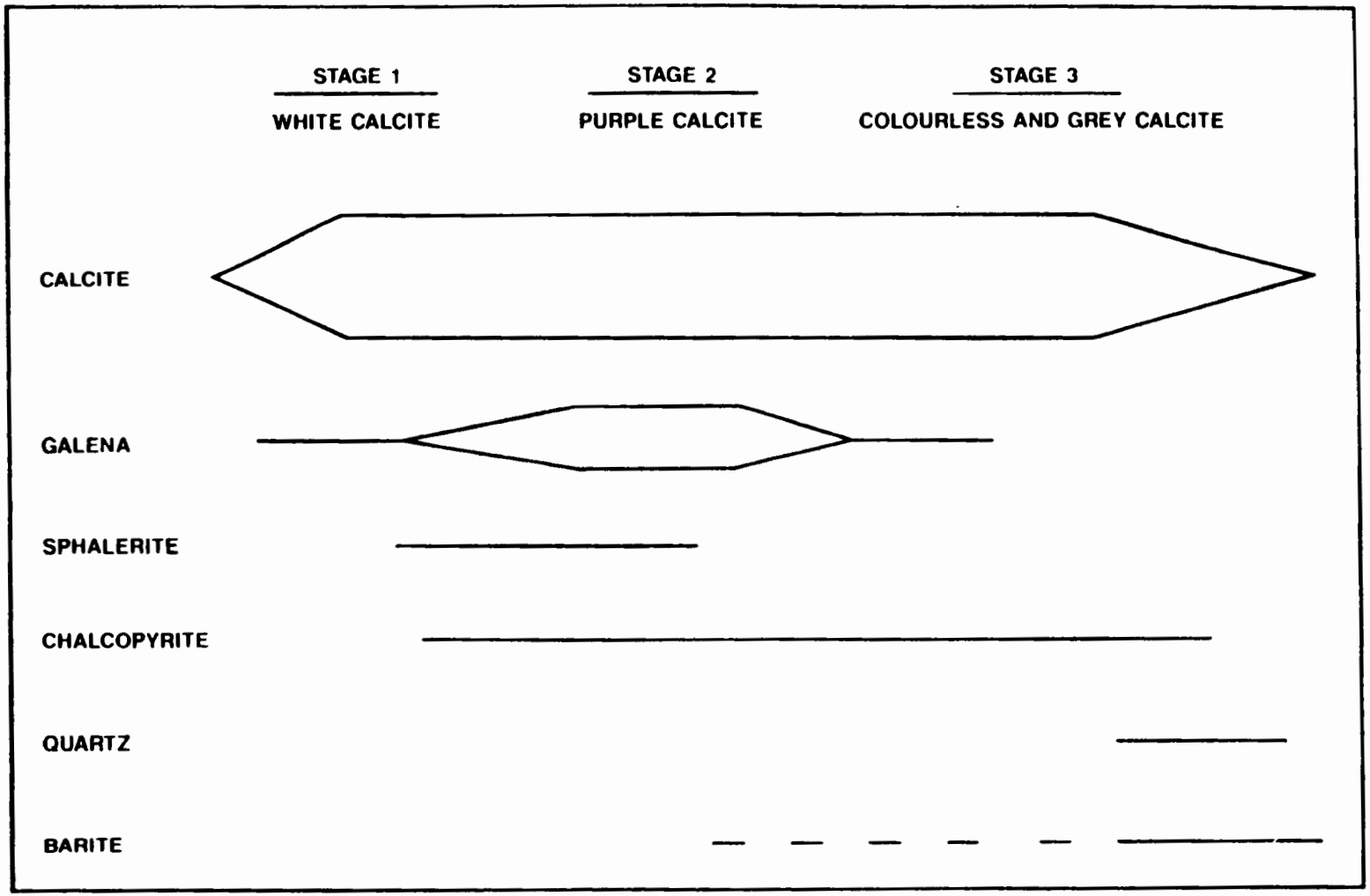

FIGURE 27: PARAGENETIC SEQUENCE OF MINERAL PHASES PRECIPITATED IN THE LA MANCHE VEIN. AFTER CHUTE (1939).

calcite. Comb structures are very common in stage 2 calcite. Stage 3 calcite is smokey grey to colourless and forms comb structures. This calcite lines vugs that are elongate in the plane of the vein and is also found in stringer veins in the wall rock.

Galena occurs primarily in stage 2 calcite, and in lesser amounts in stage 1 calcite, but not with stage 3 calcite. Most galena occurs in irregular "mushroom shaped masses" composed of "semi radiating prismatic crystals" which have co-precipitated with the enclosing calcite. Microscopy indicates that galena is relatively free of other mineral phases, although small amounts of calcite and lesser amounts of chalcopyrite can be found as inclusions.

Sphalerite is found as dark brown radiating crystals occurring in discontinuous bands a few centimetres in width. From his examination of the mine workings, Chute (1939) observed that most sphalerite was separate from galena in the vein, however there was no previous documentation of this observation. Microscopy reveals that "chalcopyrite disease" (Eldrige et al. 1983) is very common in sphalerite from the La Manche samples. Chalcopyrite disease is a texture in which microscopic blebs of chalcopyrite have developed within much larger crystals of sphalerite (an example from the Silver Cliff mine is shown in Fig. 31). Sphalerite crystals containing blebs of chalcopyrite in amounts exceeding that which can be reasonably accounted for

by an equilibrium process of solubility and subsequent exsolution, are common in many sulphide ores (Hutchison and Scott 1981). Eldrige et al. (1983) discuss several possible origins for chalcopyrite disease, and suggest replacement as the most likely origin for this chalcopyrite. This is supported by the recent work of Eldridge et al. (1988), who synthesized this texture in the laboratory by interacting sphalerite with a hot copper-bearing fluid. "Chalcopyrite disease textures were formed only when starving solutions were close to equilibrium with chalcopyrite." They conclude that "chalcopyrite disease represents the earliest stages of replacement of sphalerite by chalcopyrite."

Chalcopyrite is also found as larger crystals, along with galena, within sphalerite crystals. Textures suggest that this chalcopyrite and galena have formed by replacement of the sphalerite. As well as occurring as a replacement phase in sphalerite, chalcopyrite is also found: 1) in bands less than a centimetre wide, 2) as isolated crystals in calcite. Banded chalcopyrite was observed by Chute (1939) only in samples from the mine dump and was not seen in the upper mine workings that he examined. Chute suggested that banded chalcopyrite existed only in the lower mine levels, possibly indicating some depth-controlled mineral zonation. Cross cutting relationships show that there was repeated alternation in the deposition of banded galena, sphalerite and chalcopyrite.

Pyrite is rare in the La Manche vein. It can be found in small quantities in the chalcopyrite bands and in calcite in a few locations. Barite is found in small quantities as tabular white to pink plates irregularly scattered through the vein, but is most abundant in vugs with stage 3 calcite. Barite has also been found in a two centimetre wide monomineralic veinlet 180 metres north of the mine. Quartz occurs only as a late minor phase which lines the walls of some of the many late stage vugs.

In vein BV8A (Fig. 5), which occurs 1.5 km east of Little Southern Harbour along Placentia Bay and only 2.7 km north of the La Manche vein, calcite was the initial precipitating mineral phase, followed by barite and galena which have co-precipitated in this vein. About 2.8 km east-northeast of La Manche, along the Trans Canada Highway, a barite vein known as the "Sutton" vein (BV53, Fig. 5), contains a significant proportion of chalcopyrite. Barite veins occurring in this area generally contain a greater proportion of sulphide mineralization.

2.3b. Silver Cliff Mine

The Silver Cliff mine (Figs 4, 6 and 28) consists of the MacKay and Fowler veins, comprised predominantly of galena, sphalerite and pyrite. All ore mined was from the MacKay vein. Ore grades ranged up to 159 and averaged 30

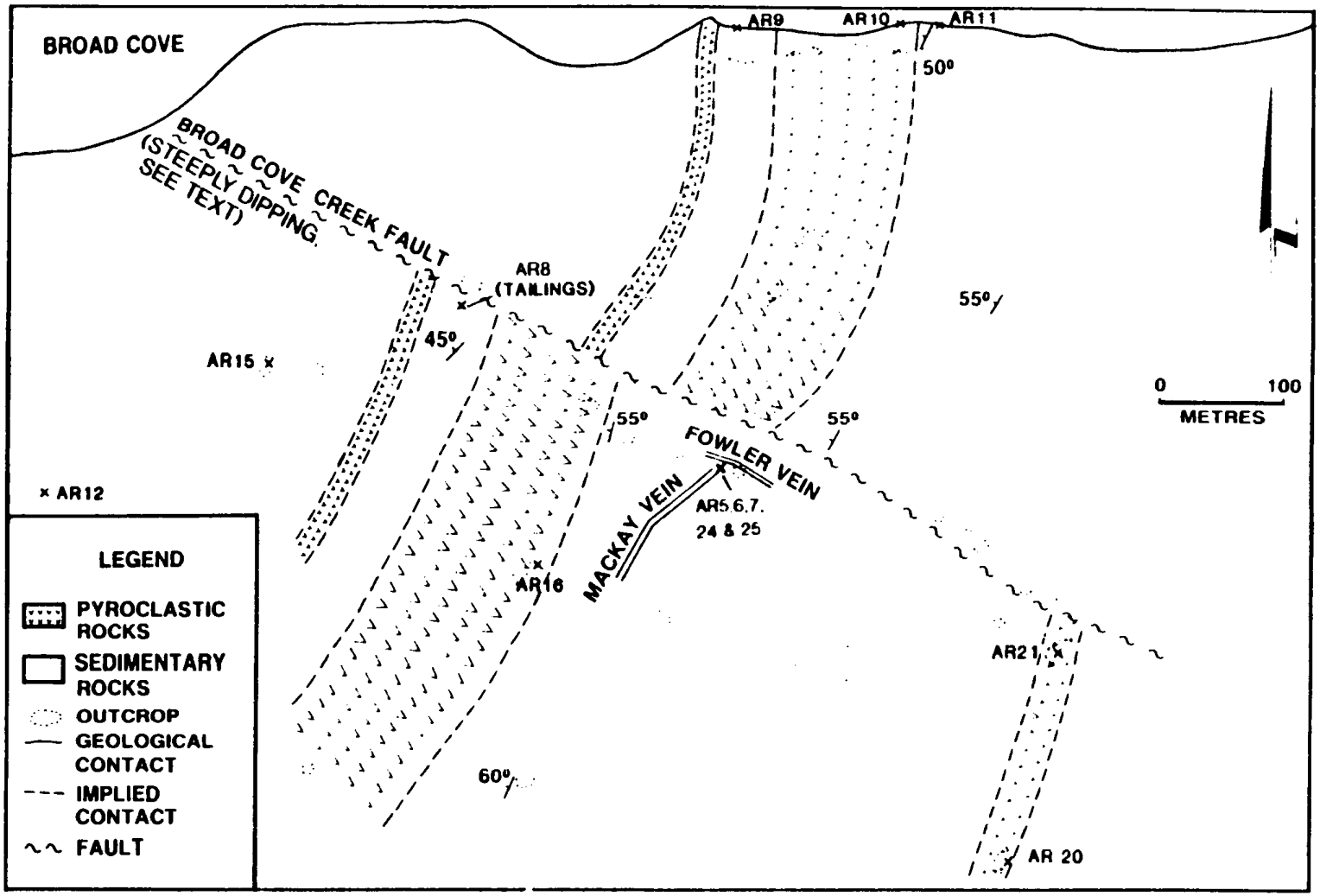

FIGURE 28: GEOLOGY OF THE SILVER CLIFF MINE AREA. FROM CHUTE (1939).

oz/long ton of ore. The mine site is located near the south coast of Placentia Sound along the southwest side of the Broad Cove Creek ravine, which follows the surface intersection of the Broad Cove Creek fault (Fig. 28). The mine occurs in a thick sequence of feldspathic quartzites, pebble conglomerates and lesser amounts of pyroclastic rocks of the Bull Arm Formation in the Musgravetown Group.

The distribution of ore, as described by Chute (1939), is controlled by three sets of faults. All ore discovered was in the MacKay vein which Chute describes as a "fault zone" about a metre wide, with a strike ranging from 030 to 060° Az and a dip ranging from 50° to 80° southeast. However, examination of a map of the mine workings (Chute 1939), indicates that the vein may not display the range of strike suggested by Chute. The strike may be either 030° Az or 060° Az as suggested by the stope orientations indicating that vein material may have precipitated into fractures from two separate sets. Unfortunately the variation in dip described by Chute is not indicated on the map of the mine workings and it is not known if there is an accompanying change in dip with strike. Displacements along the MacKay vein "fault zone" range from centimetres up to a metre.

A set of bedding plane faults hosts no ore. Chute believes that these faults localized ore in the MacKay vein where these structures intersected. A third set of faults, which displaces the other two sets, ranges in strike from

110° to 125° Az and in dip from steeply northeast to steeply southwest. The Broad Cove Creek fault is parallel to these structures. A geophysical survey (Cant 1974) indicates that the ore zone may be displaced by dextral motion along the Broad Cove Creek fault and may continue north of the fault.

The Fowler vein in the Silver Cliff mine is parallel to the third set of faults. Although only a minimal amount of ore was located along this structure, its presence indicates that all three sets of faults developed prior to the final deposition of ore. This conclusion, combined with the observed displacements of the MacKay vein described above, suggests that development of these fracture sets and the event of ore deposition were contemporaneous.

The mined portion of the MacKay vein pinched and swelled rapidly and was discontinuous. It ranged from centimetres to over a metre in width. At the time of Chute's survey only pillars remained of the ore zone, yet it appeared that much of the ore was almost 100% sulphide minerals with very little gangue material. In places, the ore formed a network of closely spaced stringers of sulphide mineralization in brecciated country rock. The ore is most abundant where faults have most shattered the country rock and is less abundant in veins where there is no faulting.

The MacKay vein consists of galena, sphalerite and pyrite with small amounts of chalcopyrite, quartz, carbonate and barite. Pyrite occurs both in the vein and as fine

euhedral disseminated crystals in the wall rock next to the vein. The development of disseminated pyrite was accompanied by silicfication of the wall rock. Chute described pyrite as occurring earlier than other sulphide minerals in the vein and as having been partially replaced by them. He also described a second generation of pyrite crystals deposited in late forming quartz-sulphide stringers which cut through the Mackay vein and enclosing wall rock. In samples of these late quartz-sulphide stringers observed in this study, pyrite is subhedral and sometimes euhedral, having formed both earlier than and contemporaneously with sphalerite and galena.

Sphalerite varies from dark brown to colourless and occurs in aggregates of fine to coarse crystals which surround earlier quartz crystals (Fig. 29). Chute states that it is probable that light coloured sphalerite is younger than darker sphalerite. This is also a feature which is observed in the samples collected for this study (Fig. 30). Chute's description indicates that chalcopyrite disease is a common feature of sphalerite at Silver Cliff. Examination of sphalerite from the samples collected for this study reveals the presence of chalcopyrite disease (Figs. 29 and 31) most commonly in the outer opaque zones within the sphalerite crystals. Chalcopyrite occurs as described above, and also in larger masses in both sphalerite and galena, possibly formed by replacement of

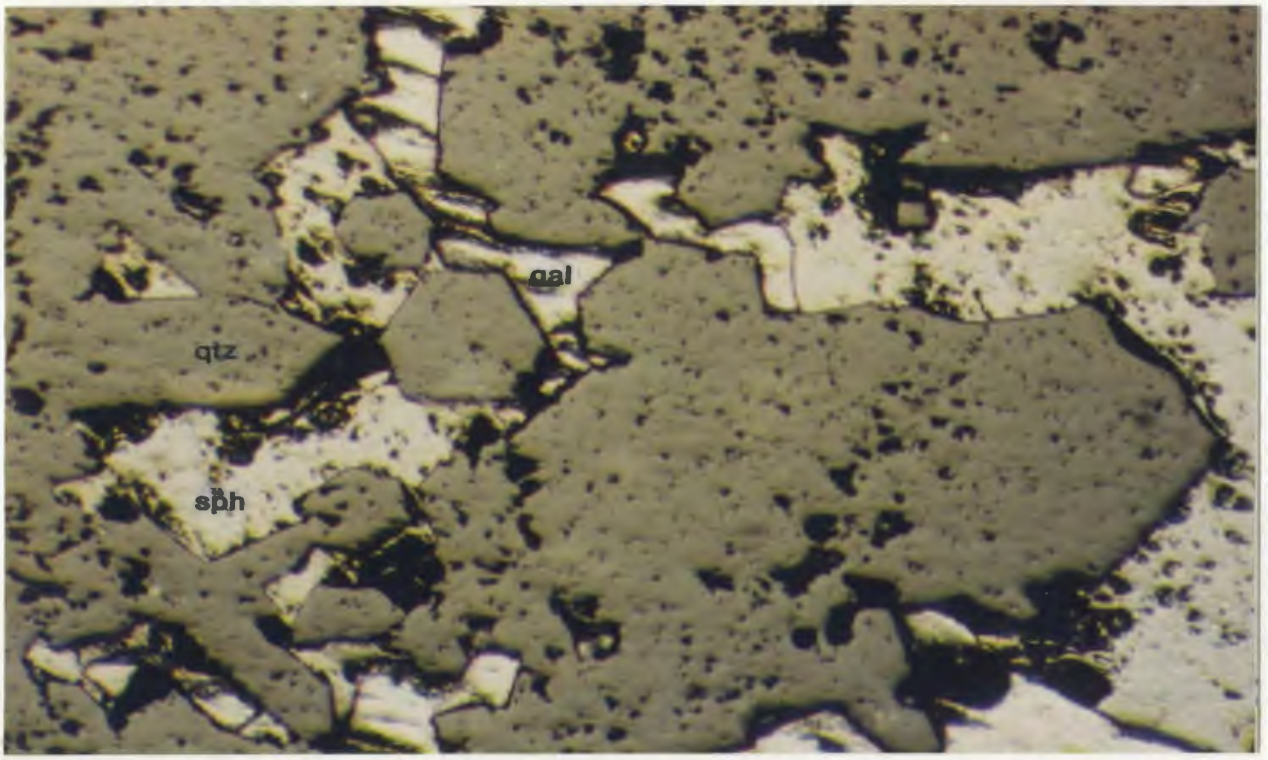

Figure 29. Sphalerite (sph) with chalcopyrite disease has grown around earlier euhedral quartz (qtz) crystals. Galena (gal) has partially replaced sphalerite in the MacKay vein. (AR25-B, field of view is 1.3 X 1.0 cms, very poor polish)

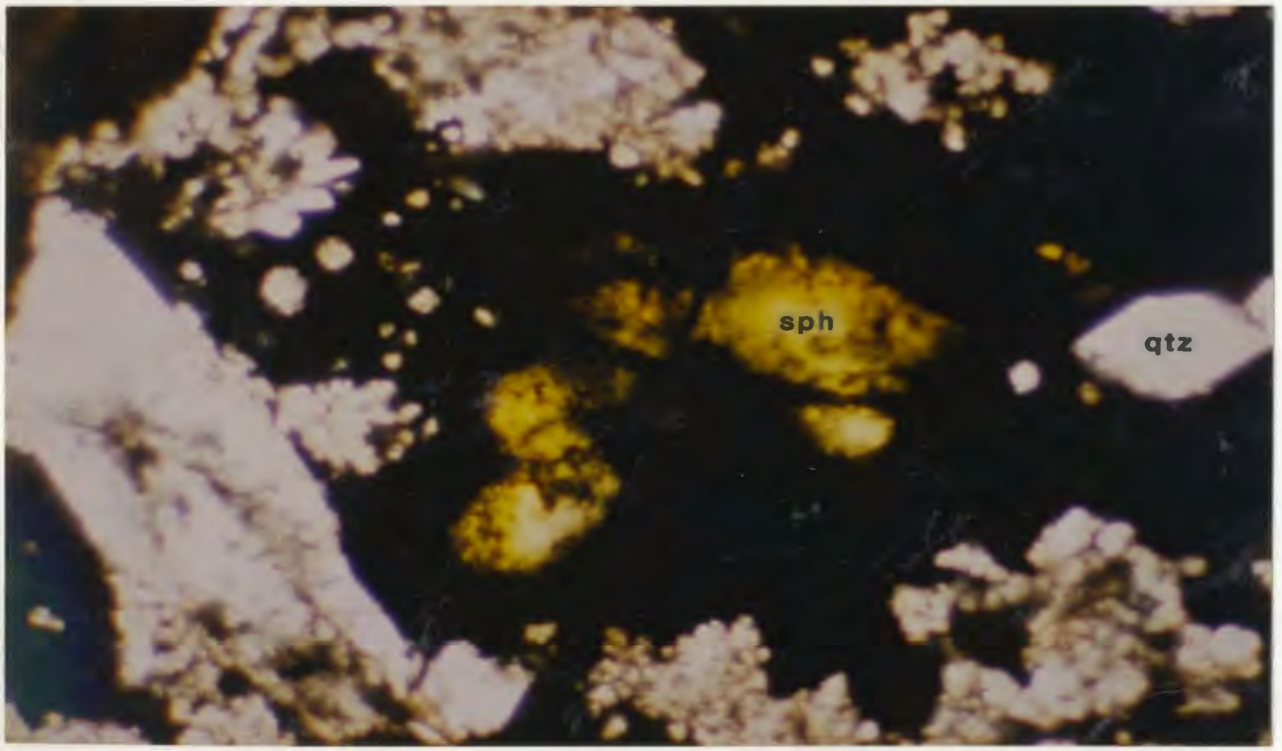

Figure 30. Shows opaque sphalerite (sph) grown around early euhedral quartz (qtz) crystals, grading to light yellow sphalerite in latest stage of open space fill (AR25-C from the MacKay vein, field of view is 4.1 X 2.8 cms).

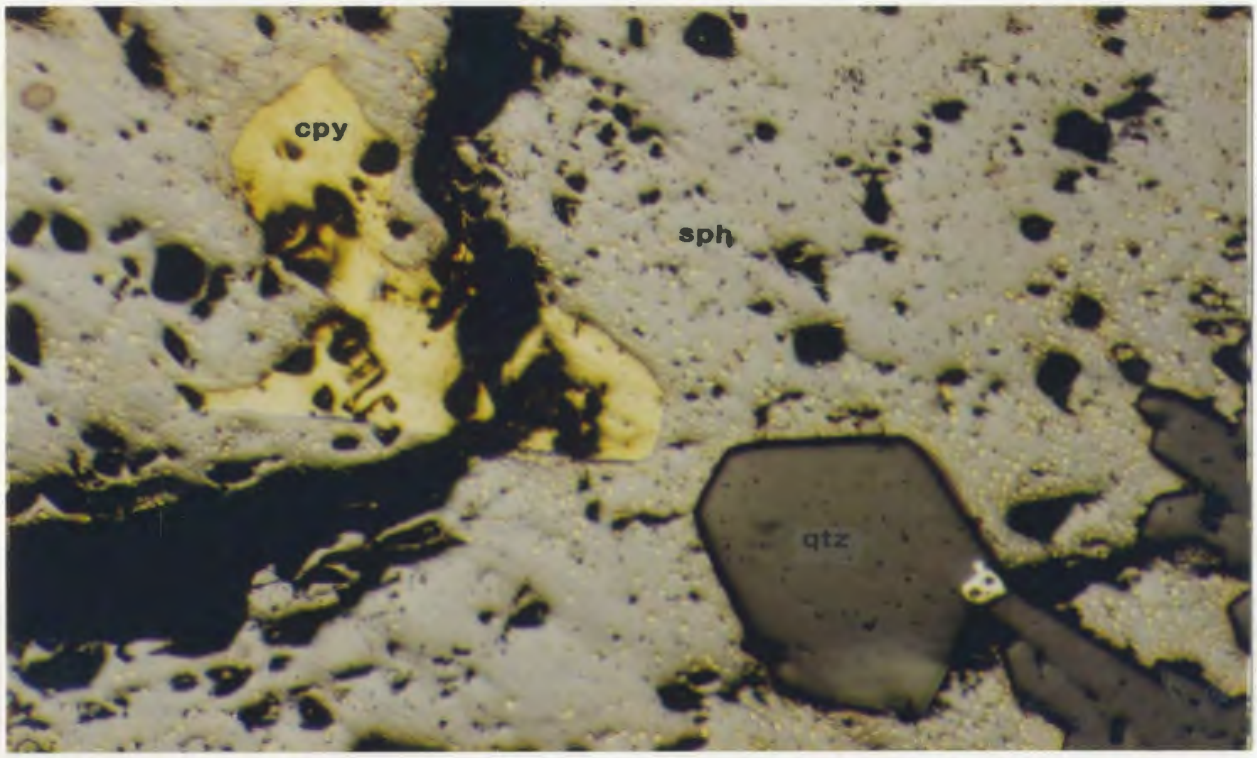

Figure 31. Larger bleb of chalcopyrite (cpy) replacing sphalerite (sph). Small blebs of chalcopyrite as chalcopyrite disease are also visible. Sphalerite has grown around early euhedral quartz (qtz) crystals. AR6-A from the MacKay vein, Silver Cliff (field of view is 1.3 X 1.0 cms).

these minerals (Fig. 31). Chalcopyrite also occurs as small crystals in vugs lined with quartz.

Galena is generally later than sphalerite and pyrite in the MacKay vein and replaces first-generation pyrite and sphalerite (Fig. 29), and chalcopyrite which had previously replaced sphalerite. Galena hosted most of the silver in the vein. No silver mineral has ever been identified. Following deposition of sulphide minerals the vein and enclosing wall rock were cut by quartz veins with minor sulphide mineralization (late quartz-sulphide stringers).

Chute (1939) did not determine the relationship of barite or carbonate to the other minerals in the mine. He suggested that they occurred late in the vein paragenesis but he offered no evidence for this. Examination of the mine dump revealed no barite and only one monomineralic veinlet of carbonate.

A number of other veins, which contain mineralization similar to that of the MacKay vein, have been discovered in the Placentia area (Chute 1939). These veins are generally a few cms wide and contain variable proportions of galena, sphalerite, chalcopyrite, pyrite, quartz, carbonate and barite. Galena is typically the dominant mineral in these veins. Silicification and pyritization within the wall rock has been observed in these veins at several locations.

McCartney (1967), on his map of the Whitbourne area, indicated the presence of flourite on Harbour Island in

Placentia Bay, about 20 kms north of Silver Cliff. This is the closest known occurence of fluorite to the study area, although Murray and Howley (1881) reported minor amounts of fluorite in the La Manche vein. Chute (1939) did not find any fluorite in his examination of the LaManche vein. Large amounts of fluorite, do exist further west on the Burin Peninsula in the St Lawrence Fluorspar deposit. However this deposit is Carboniferous in age and has formed in a "megashear" tectonic setting (Strong 1979). As described below the veins in the present study area are probably older and likely formed in a different tectonic setting.

2.4. Relation of Vein Orientation to Regional Deformation

Acadian deformation (see Chap. 1) resulted in the development of open symmetrical folds in the field area, with essentially vertical axial planes (McCartney 1967). Fold axes are commonly gently curved and axial planes have a general north-northeast strike (Fig. 32). Folds commonly are doubly-plunging (McCartney 1967), and generally plunge less than 15^{o}, resulting in a dome and basin appearance to the overall structure. A gentle re-folding of original Acadian fold axes may explain their curvature and the formation of doubly-plunging structures.

McCartney (1967) indicated on a map of structural elements found on Collier Point in Trinity Bay, the presence of a fold axis to an anticline, situated centrally along the

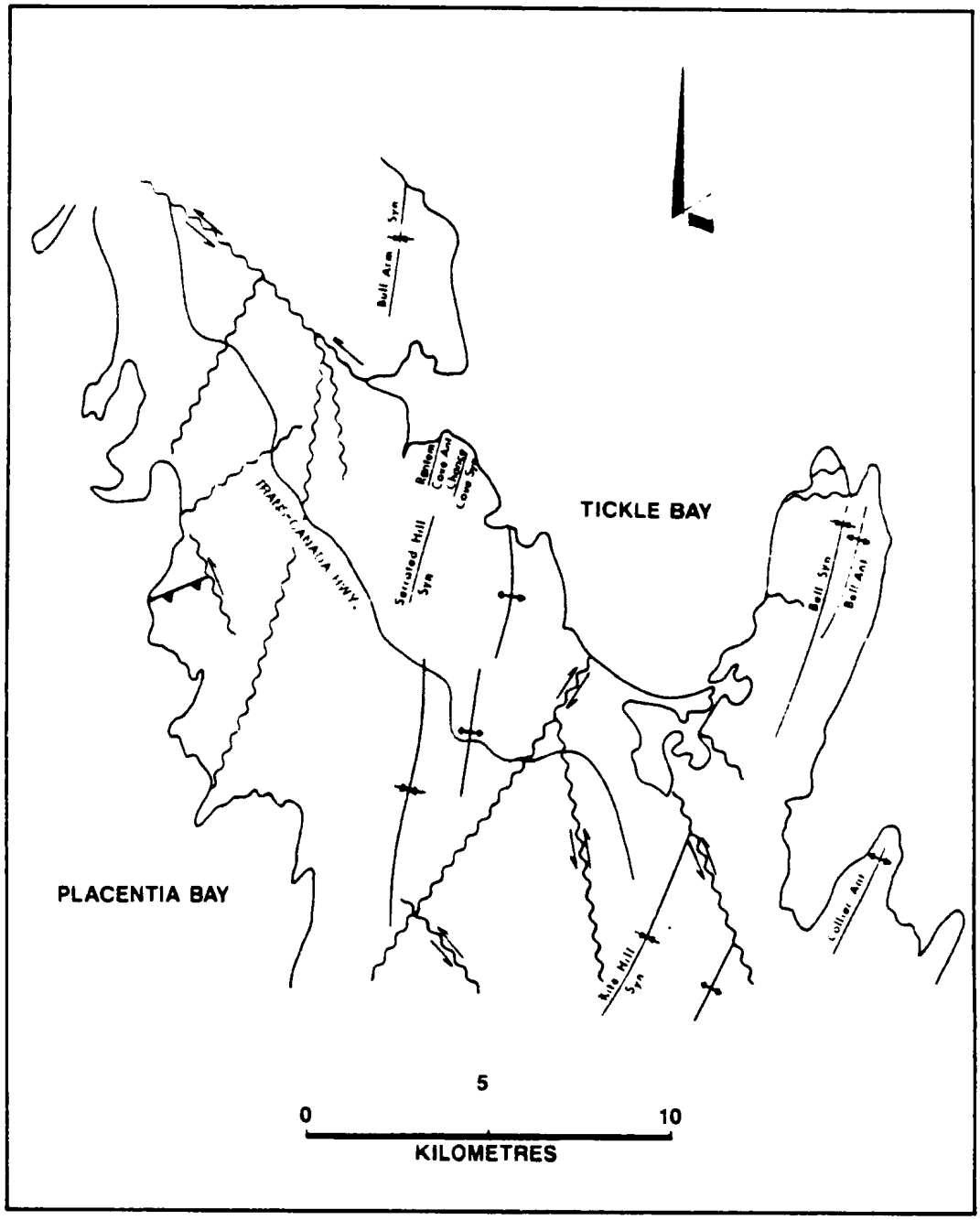

FIGURE 32: STRUCTURAL FEATURES OF THE ISTHMUS OF AVALON FROM McCARTNEY(1967). BELL: BELLEVUE PENINSULA, Syn:SYNCLINE, Ant: ANTICLINE.

length of the point (Fig. 32). A cross section drawn by McCartney (1967) through Collier Point indicates a steep dip for the axial plane of this fold with a possible slight inclination from vertical resulting in a steep westward dip.

Figure 33 is a stereographic (Wulff Net) projection of the poles to quartz and barite veins found on Collier Point and the shore of Long Cove. Poles to barite veins plot in a loose cluster displaying a generally north-northwest strike and steep but variable dip. Poles to quartz veins also define a cluster displaying steeply dipping veins which strike east-northeast. The overall quartz vein cluster can be subdivided in two adjacent sub-clusters. The sub-cluster labelled "west" contains poles to quartz veins occurring on the western limb of the fold, while the "east" sub-cluster contains poles to quartz veins occurring on the east limb of the fold.

Consider a set of joints formed during the initial phase of Acadian compression, striking approximately 065^{o} Az and dipping 82^{o} north (a pre-Acadian joint set is unlikely becuase, as is discussed below, the orientation of joints and faults is consistent with their development during Acadian stress). Subsequent folding of these joints, about a horizontal axis trending 030 Az, would rotatate the joints in an opposite fashion on either side of the fold axis, creating two distinct joint sets. The orientation of these joint sets would be similar to the "east" and "west" quartz

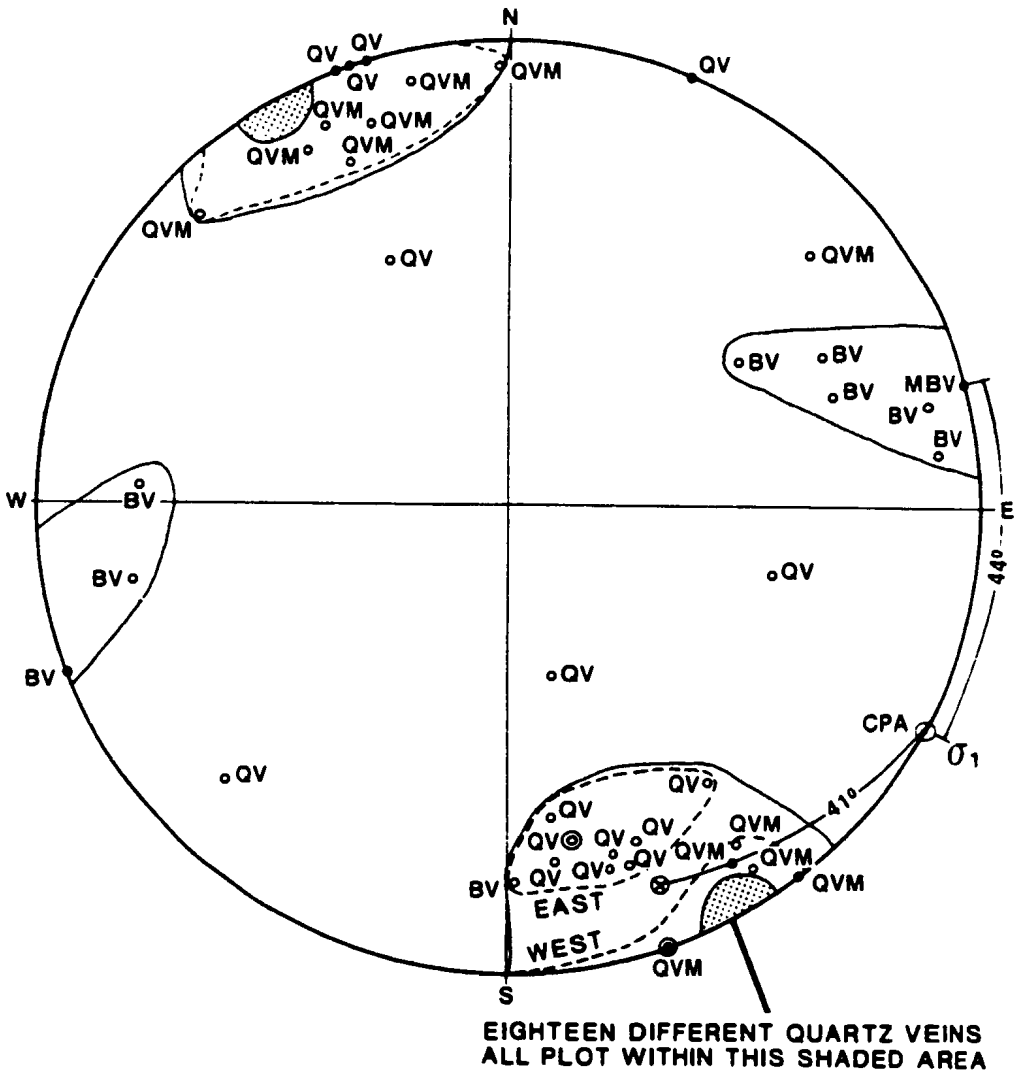

FIGURE 33: STEREONET SHOWING POLES TO VEINS FOUNDS ON COLLIER POINT. QV ARE QUARTZ VEINS, QVM ARE THOSE QUARTZ VEINS FOUND ALONG THE LENGTH OF THE MAIN BARITE VEIN (MBV), BV ARE BARITE VEINS, ⊗ ESTIMATED MIDPOINT, CPA IS THE POLE TO THE AXIAL PLANE OF THE ANTICLINAL FOLD WHICH EXISTS ON COLLIER POINT, FROM McCARTNEY (1967).

vein sets found on Collier Point. Filling of joints by quartz would occur anytime after formation of the joints. Thus vein filling was either syn- or post-tectonic. Most vein material is deformed to varying degrees, suggesting a significant component of syn-tectonic precipitation.

It is not clear if barite veins have also been rotated. Not enough veins have been sampled to distinguish separate sub-clusters of poles on a stereogram. However, with the exception of one vein on Collier Point, barite veins found west of the fold axis are either vertical or dip steeply eastward. Barite veins found east of the fold axis are either vertical or dip steeply westward. If this observation is valid then the nature and timing of rotation of barite veins may be similar to that suggested for quartz veins.

The pole to the axial plane of the Collier Point fold, assumed to be vertical as indicated by McCartney (1967), is plotted on the stereogram in Figure 33 ("CPA"). Ideally, this pole represents the direction of principal stress. The barite vein set and quartz vein set are roughly symmetrical about the direction of Acadian principal stress on Collier Point, with separation angles of approximately 46° and 49° respectively. Ideally, conjugate joints form at less than 45° to the principal stress direction in isotropic rocks, and typically the angle is close to 30° (Badgley 1965). However, on Collier Point it is the obtuse angle of a

conjugate set that is symmetrical about the direction of principal stress. This can occur if the angle was acute upon joint formation and was subsequently widened by rotation of joint planes during continued compression (Badgley 1965).

Rotation of joint planes such that the angle between joint planes and the direction of principal stress widened from 40° at formation to 50° after rotation, requires shortening of the strata along the direction of principal stress by 16%, relative to extension of strata in the direction of the fold hinge in a horizontal plane (Fig. 34). Fluid inclusion work presented in Chapter 3 suggests that quartz vein formation in the Collier Point area occurred at less than a kilometre of depth. Certainly at such a shallow level most strain would be brittle in nature, resulting in the numerous joints, veins and faults that have been described. The country rock was not analysed for indications of ductile deformation. However, Figure 11 clearly shows that there must have been some significant component of ductile deformation in these rocks.

Anisotropy in the rock, such as bedding or a pre-existing fabric, can result in formation of shear fractures at greater than 45° to the direction of principal stress (Badgley 1965). Anisotropy on Collier Point is provided by known stratification. As bedding was not perpendicular to the principal stress direction, it should have contributed

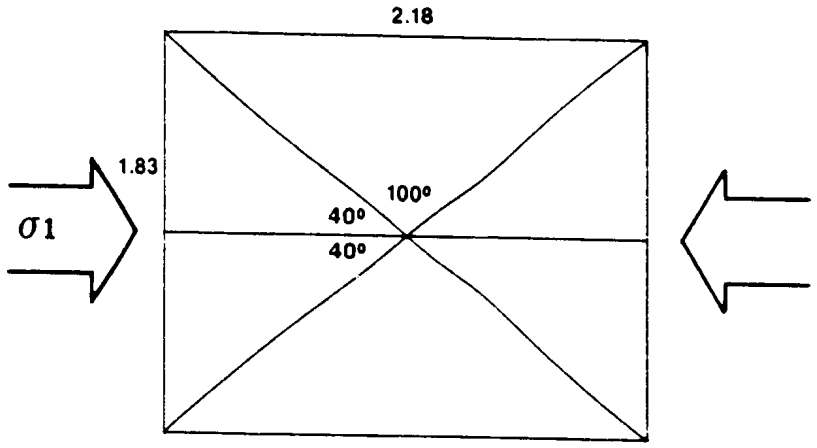

a) INITIALLY JOINTS FORM AT 40° TO $\sigma 1$.

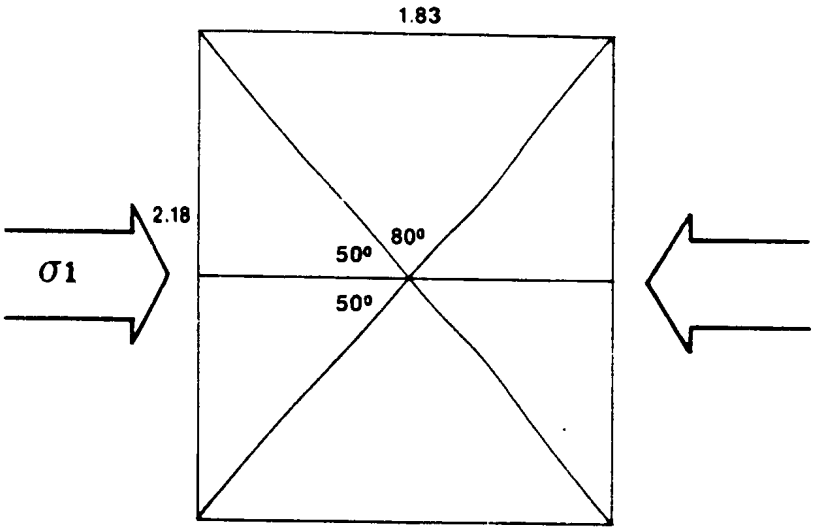

b) WITH CONTINUED COMPRESSION, CRUSTAL SHORTENING TAKES PLACE RESULTING IN A ROTATION OF THE JOINT PLANES.

(2.18 - 1.83) x 100/2.18 = 16% SHORTENING

FIGURE 34: SHORTENING OF 16% IN THE HORIZONTAL PLANE WOULD ROTATE VERTICAL JOINTS FROM 40° TO 50° TO $\sigma 1$.

to variation from the ideal angle of joint formation. The magnitude of this contribution is unknown by the author.

McCartney (1967) indicated the presence of a synclinal and an anticlinal fold axis situated horizontally along the length of Bellevue Peninsula, west of Collier Point (Fig. 32). A steep dip is again used for the axial planes of the folds, as indicated by McCartney (1967). Figure 35 is a Wulff Net stereographic projection of poles to quartz veins, barite veins, one calcite vein and fault planes found on Bellevue Peninsula. The range of strike for axial planes of the synclinal and anticlinal folds are indicated by brackets (range from McCartney 1967). Faults in the Whitbourne map area are described as steeply dipping (McCartney 1967) and are plotted as vertical in Figure 35.

Poles to eight barite veins and two calcite veins form a cluster in Figure 35 which indicates a general north-northeast strike and steep dips for these structures. These veins are roughly parallel to the two fold axes which pass through Bellevue Peninsula and may be classified as radial joints (defined in Hobbs et al. 1976) developed during folding. The limited spread of dips for these structures in Figure 35 is likely due to the open nature of the folding (McCartney 1967) and the limited sampling across fold limbs.

Poles to four quartz veins, two barite veins, one calcite vein, one galena vein and two fault planes, form a second cluster of structures striking east-northeast with

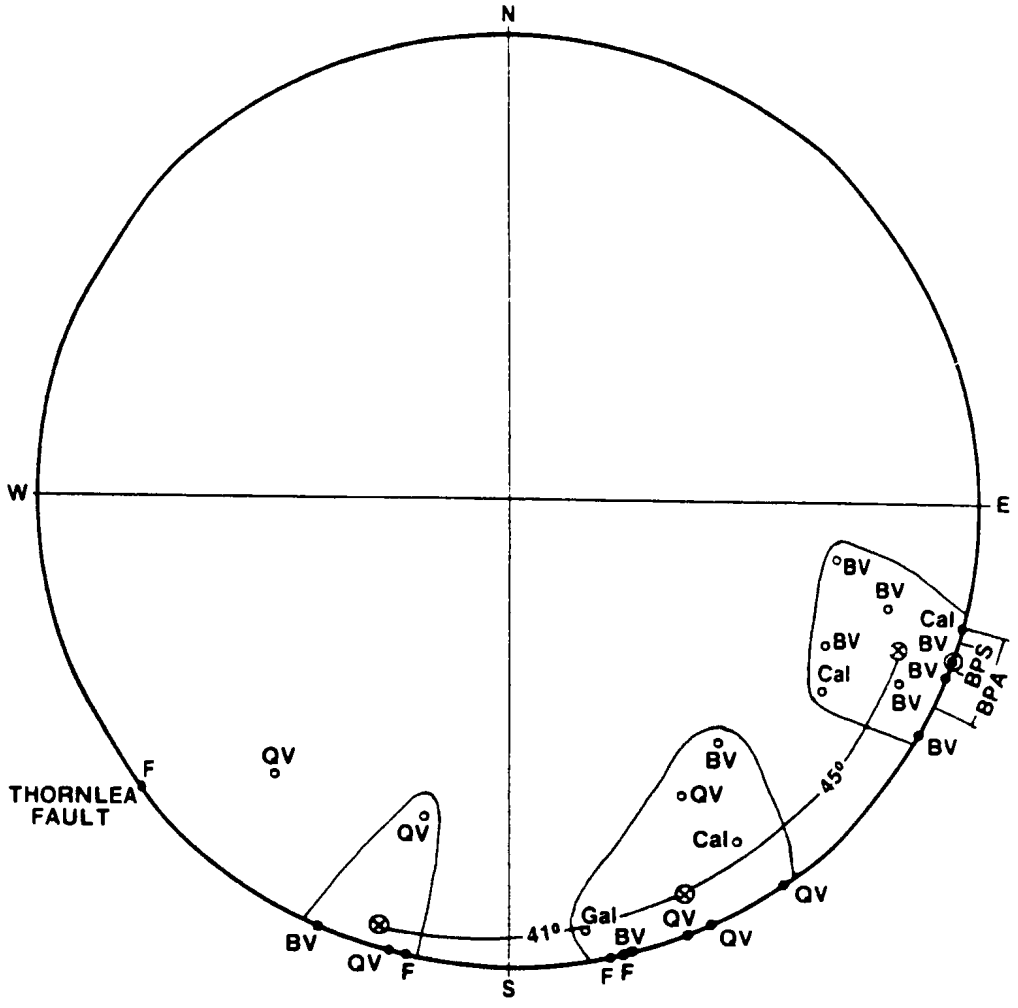

FIGURE 35: STEREONET SHOWING POLES TO VEINS, FAULTS AND AXIAL PLANES FOUND ON BELLEVUE PENINSULA. THE RANGE IN ORIENTATION OF THE AXIS FOR THE BELLEVUE PENINSULA SYNCLINE (BPS) AND THE BELLEVUE PENINSULA ANTICLINE (BPA) ARE INDICATED BY BRACKETS. VISUALLY ESTIMATED MIDPOINTS OF CLUSTERS ARE INDICATED AS⊗. BV-BARITE VEIN, QV-QUARTZ VEIN, Cal-CALCITE VEIN, Gal-GALENA VEIN, F-FAULT.

steep dips. The orientation of these structures is similar to the quartz veins on Collier Point (Fig. 33). If these structures represent one member of a conjugate set with the same orientation as the quartz vein set on Collier Point, the other member is either missing or is represented in Figure 35 only by the Thornlea Fault and possibly one quartz vein (BV29). Badgley (1965) has shown that one member of a conjugate set may be poorly developed or missing in an area.

Poles to two quartz veins, a barite vein and a fault plane form a third cluster in Figure 35 which represents structures striking east-southeast with steep dips. These structures are perpendicular to the axial planes of the two folds on Bellevue Peninsula, and may be a-c joints (defined in Hobbs et al. 1976) formed during Acadian deformation.

Figure 36 is a stereographic projection of poles to veins, faults and axial planes found on the Isthmus of Avalon, including structures found on Collier Point and Bellevue Peninsula. Plotting of all structures in this expanded area on a single stereogram results in expansion of the field of each cluster previously defined on either Collier Point or Bellevue Peninsula, with the exception of the cluster created by the a-c joints (found only on Bellevue Peninsula). A portion of the expansion of these clusters can be explained by the distortion and reorientation of original structures during a later structural event. This postulated event, discussed above,

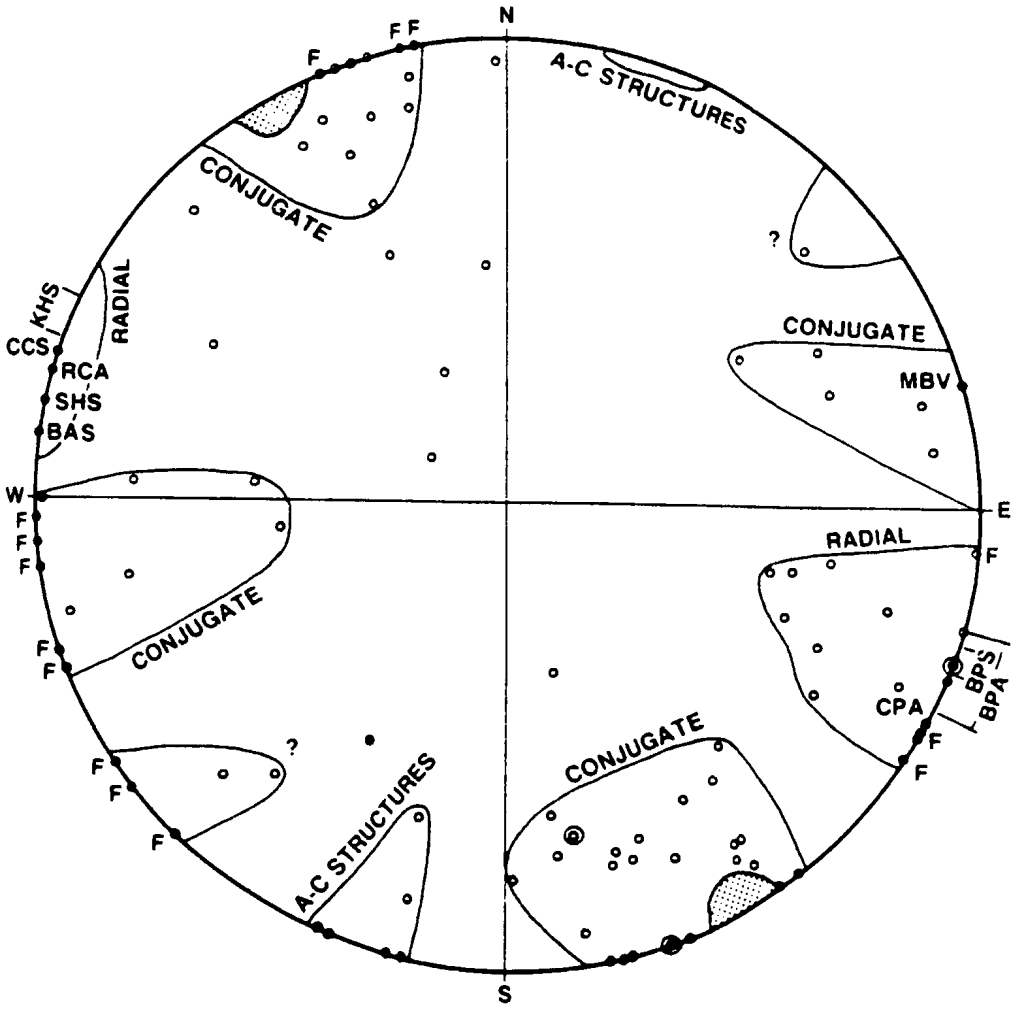

FIGURE 36: STEREOGRAPHIC PROJECTION OF THE POLES TO VEINS, FAULTS AND AXIAL PLANES FOR THE ISTHMUS OF AVALON AREA INCLUDING DATA PRESENTED SEPARATELY FOR BELLEVUE PENINSULA AND COLLIER POINT. F-FAULT, CPA-COLLIER POINT ANTICLINE, BPA-BELLEVUE PENINSULA ANTICLINE, BPS-BELLEVUE PENINSULA SYNCLINE, KHS-KITE HILL SYNCLINE, CCS-CHANCE COVE SYNCLINE, RCA-RANTEM COVE ANTICLINE, SHS-SERRATED HILLS SYNCLINE, BAS-BULL ARM SYNCLINE. MBV - MAIN BARITE VEIN.

might have caused the development of doubly-plunging structures throughout the field area.

Figure 36 illustrates that the Isthmus of Avalon area seems to host a set of conjugate structures, a set of radial structures and a set of a-c structures, the development of which are related to Acadian compression and folding. Figure 36 also shows the presence of a set of steeply dipping structures which strike southeast, including both faults and veins, the origin of which is uncertain. The direction of motion on the vertical faults (see Fig. 32), as described by McCartney (1967), is compatible with some of the faults having developed as conjugate shears during Acadian compression directed east-southeast (Fig. 33).

Figure 37 shows the location of veins sampled in the Cape St. Mary's area of the Avalon Peninsula, as well as significant structures near these veins. Figure 38 is a Wulff Net upon which the poles to veins and fault planes have been plotted (fault planes are again assumed to be vertical). On the west coast of the peninsula, near the town of St. Brides, veins with two general orientations exist. Two barite veins and one calcite vein strike roughly east-northeast and dip vertically. Two barite veins strike north-northeast and dip vertically. These two "sets" of veins are roughly symmetrical about the implied direction of principal stress (derived from the nearest fold axis) with separation angles of 60^{o} and 54^{o} (Fig. 38). Once again it

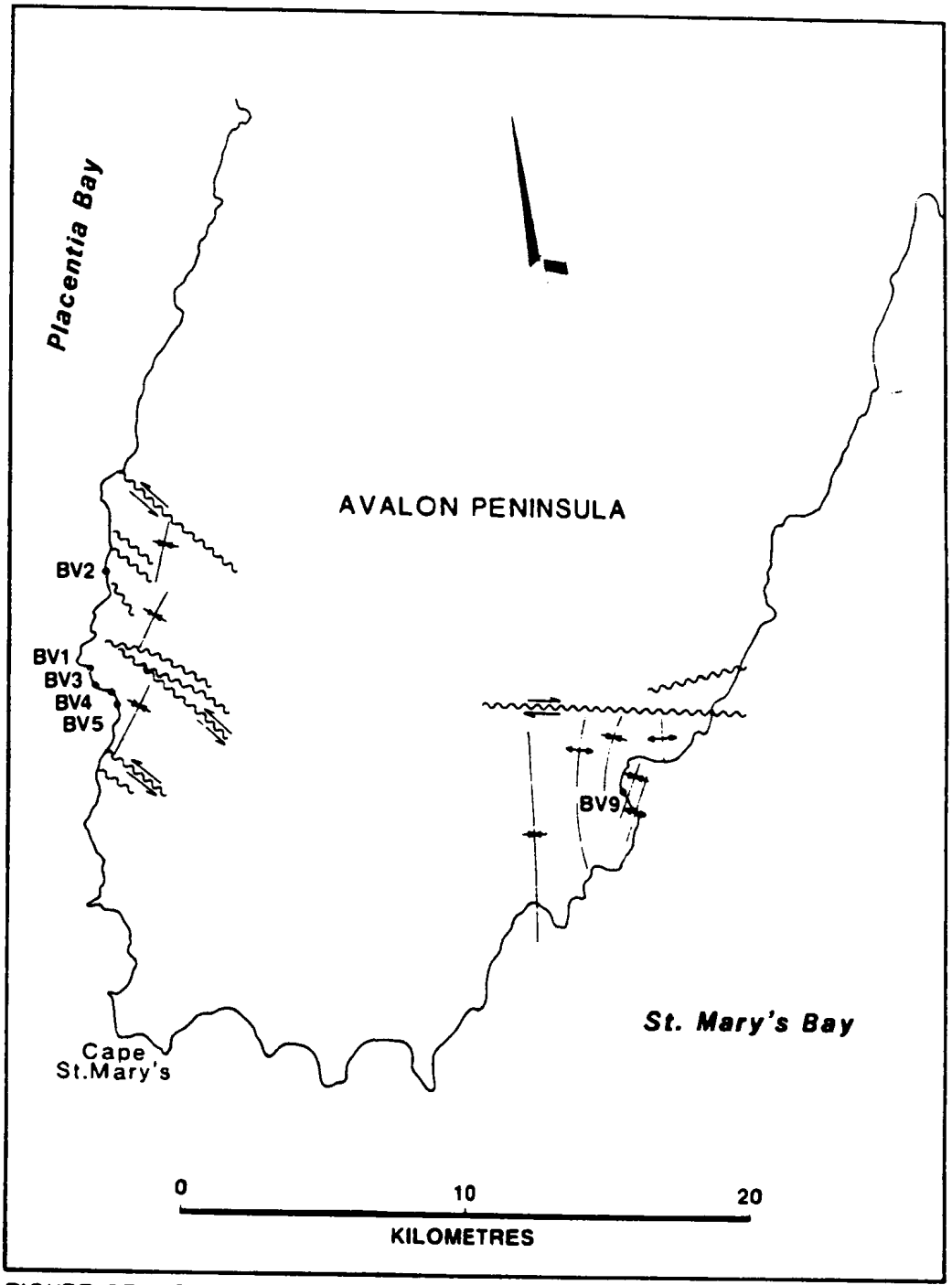

FIGURE 37: STRUCTURAL FEATURES AND VEIN LOCATION IN THE CAPE ST. MARY'S AREA OF THE AVALON PENINSULA. STRUCTURE TAKEN FROM FLETCHER (1971).

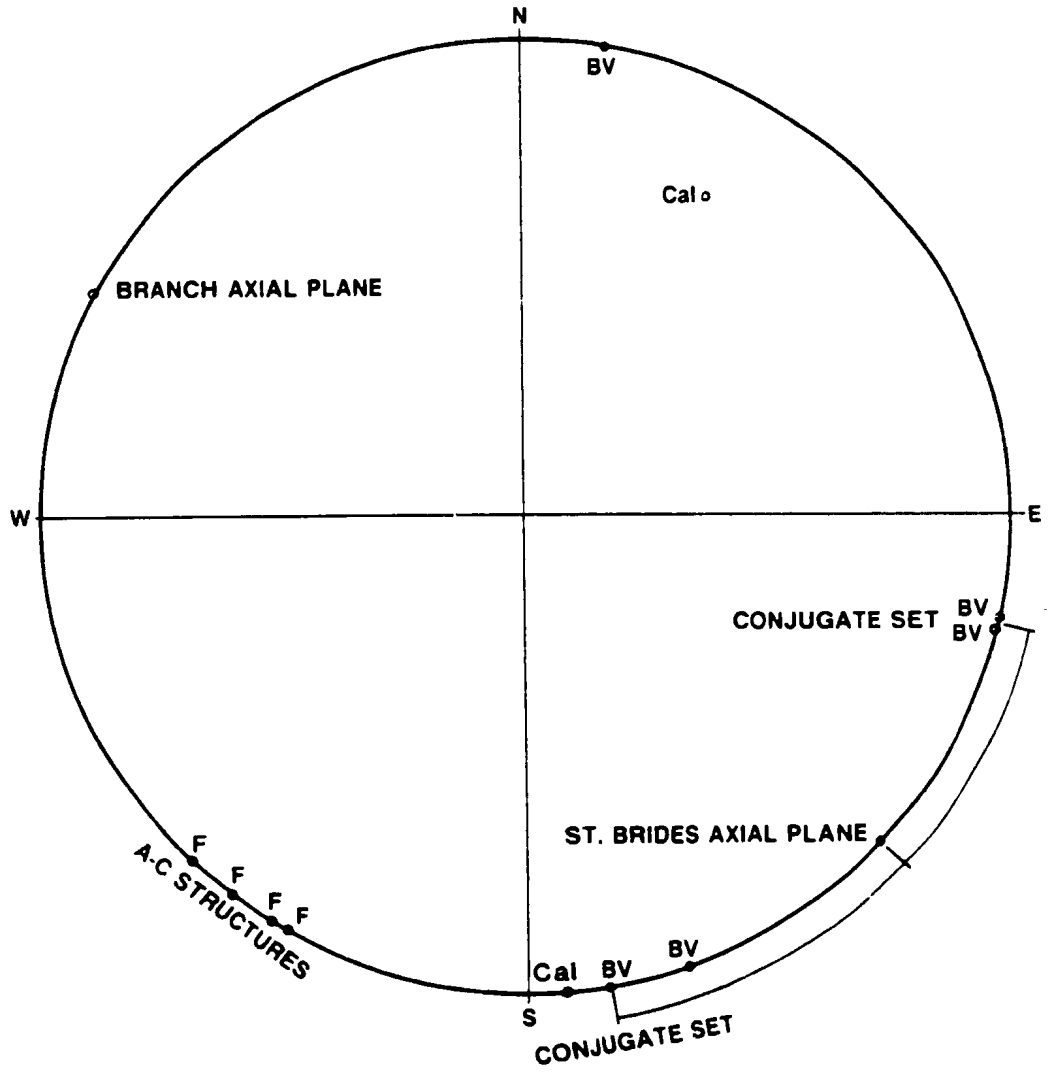

FIGURE 38: STEREOGRAPHIC PROJECTION OF THE POLES TO VEINS, FAULTS AND AXIAL PLANES IN THE CAPE ST. MARY'S AREA OF THE AVALON PENINSULA. BV-BARITE VEIN, Cal-CALCITE VEIN, F-FAULT.

is the obtuse angle of this possible conjugate set which is symmetrical about the direction of principal stress, similar to the relationship found in the Isthmus of Avalon area.

The photograph of BV5, shown in Figure 26, is the calcite vein of the east-northeast set plotted in Figure 38. This photograph shows other fractures which are parallel to the vein and another more prevalent set of fractures which strike approximately northeast and thus are roughly parallel to the local fold axis. This second set is probably a closely spaced set of fractures, radial to the fold axis. Four faults which occur in the St. Brides area are also plotted on the stereogram in Figure 38. These faults are approximately perpendicular to the local fold axis and may have initiated as a-c fractures.

The structure in the area of the town of Branch, where three veins were measured, is more complex. Local fold axes vary in strike over a range of 30° as indicated by Fletcher's map (1971). An interpretation of the three veins relative to the local structure will not be attempted here.

At the Silver Cliff mine, the orientations of only a few structures are known and again an interpretation is difficult. The Silver Cliff mine is on the flank of an anticline, the axis of which is 1800 metres to the southeast of the mine. The fold axis of this anticline trends at 025° Az, similar to the fold axis situated on the Isthmus of Avalon. The axial plane is again assumed to be vertical as

indicated by the open symmetrical style of the folding. The Broad Cove Creek fault and the Fowler vein are approximately perpendicular to the fold axis and may have originated as a-c structures. The MacKay vein follows two trends. At the opening to the MacKay adit the vein strikes at 060° Az and dips 80° southeast. This orientation of the vein is at an angle of approximately 35° to the presumed axial plane of the anticline. The pole to the plane of the vein in this orientation falls within the cluster of poles which were interpreted as representing an east-northeast member of a conjugate set of fractures in the isthmus area. Possibly this portion of the Mackay vein originated as a fracture of this set.

The second orientation of the MacKay vein strikes at 030° Az but the dip of this portion of the vein is uncertain as access is no longer available. Chute (1939) described the dip as variable between 80° to 50° southeast. Where the MacKay vein is accessible at the opening to the adit, the orientation of the vein is 060° Az 80° southeast, and possibly where the strike changes to 030° Az the dip changes to 50° southeast. Unfortunately this cannot be confirmed by present exposures of the vein or by Chute's report. The strike of this portion of the vein at 030° Az is similar to that of the anticlinal fold axis and possibly this structure originated as a radial joint. At a distance of 1800 metres from the fold axis where the beds are dipping 50° northwest

due to folding, a dip of 50° southeast for a radial joint is feasible.

2.5. Summary

Quartz-dominated veins are the most abundant vein type in the field area, with much fewer numbers of barite- and/or calcite-dominated veins and only a few known sulphide mineral-dominated veins. Veins are exposed throughout a section of rocks which range in age from late Haydrinian through to Middle Cambrian. The lithologies of these rocks are quite variable, and include a suite of bimodal volcanic rocks as well as sedimentary rocks derived from the erosion of volcanic rocks.

These veins are all dilational and display textures which indicate open-space filling. Post-precipitation deformation is very common, but sections of veins which have escaped deformation can be found. Cross-cutting relationships indicate that the barite- and calcite-dominated veins are generally later than the quartz-dominated veins. Both calcite and barite can be found as a late vug-filling phase in a few of the quartz-dominated veins. A small number of the quartz-dominated veins have been found cross-cutting the generally later barite- and/or calcite-dominated veins, thus indicating the close timing of development of the different vein types.

In general calcite is earlier than barite and is commonly the earliest precipitated phase in barite-dominated veins. Where sulphide minerals occur in these veins they are either earlier or have co-precipitated with calcite and/or barite, with different paragenetic relationships found in different veins.

Both the orientation and the timing of formation of the veins in the study area are clearly related to the formation of joints and faults during the Acadian deformation event which affected the entire study area. Veins have developed along a conjugate joint set, a radial joint set and an a-c joint set in relation to the principal stress direction of Acadian deformation.

CHAPTER 3. FLUID INCLUSION STUDY OF THE VEIN MINERALS

3.1. Introduction

One hundred and fifty-five doubly-polished wafers of vein material, approximately one mm thick, were prepared from samples of barite, quartz, calcite and sphalerite. Forty-eight of these wafers contained fluid inclusions suitable for further study. Microthermometric measurements were made using a Fluid Inc. adapted, U.S.G.S. gas-flow heating and freezing stage mounted on a Zeiss petrographic microscope. The stage was calibrated using Chaixmeca and BDH organic and inorganic standards. The results of this calibration, shown in Figure 39, indicate that a maximum temperature correction of 1.6°C at 260°C was required. All data are tabulated in Appendix B.

3.2. Results of the Study of Fluid Inclusions in Barite

Fluid inclusions observed in barite crystals are of two types, both of which are believed to be secondary. Type 1 inclusions (Fig. 40) are overwhelmingly the most abundant and are characterized by several common features. Type 1 inclusions are tabular and form groups in a common plane, the result of incomplete healing of fracture planes within individual barite crystals. These fracture planes can commonly be traced right to the edge of the barite crystals. Type 1 inclusions contain either a single liquid phase, or

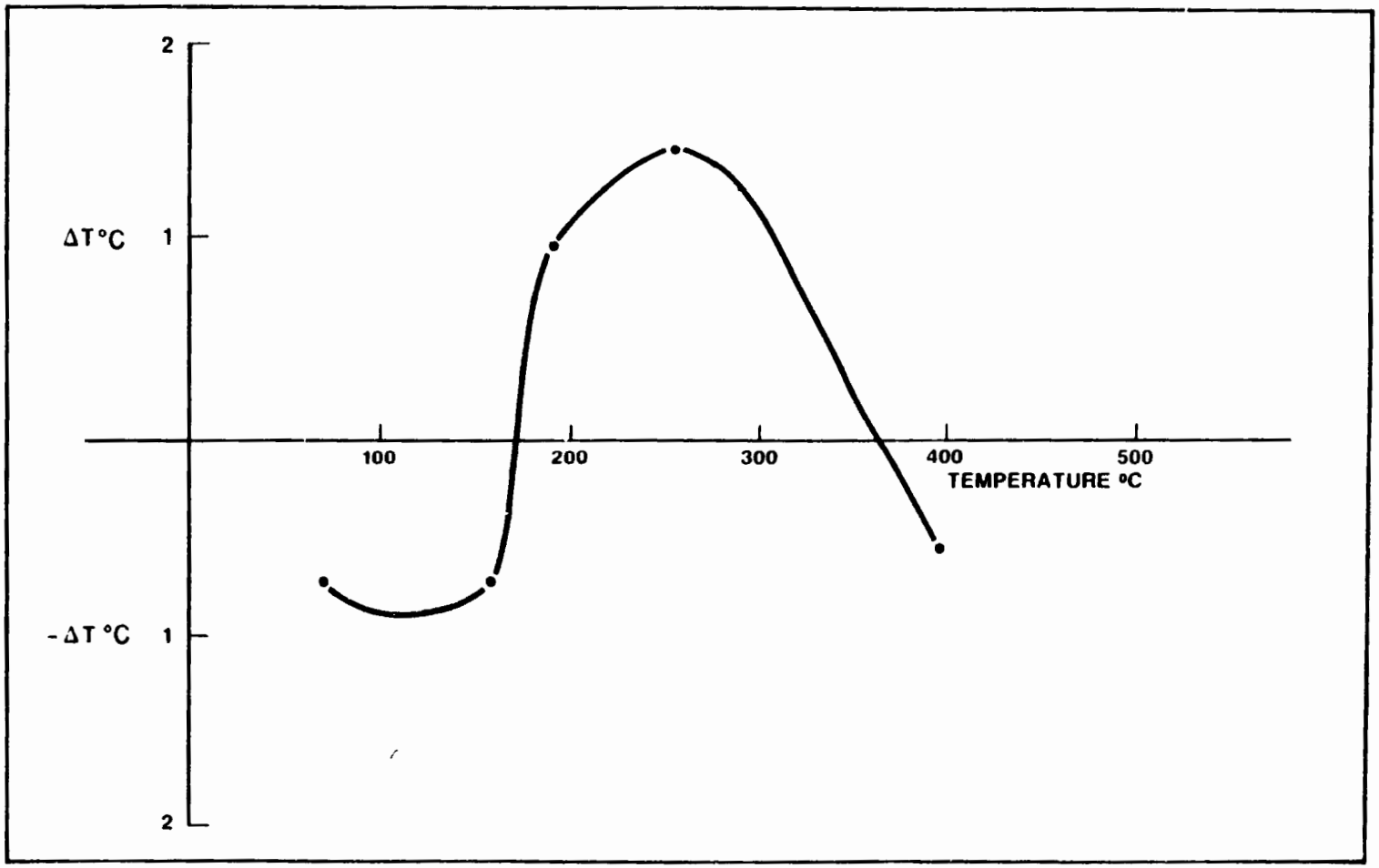

FIGURE 39: CALIBRATION CURVE FOR FLUID INC. ADAPTED U.S.G.S. GAS-FLOW HEATING AND FREEZING STAGE. CALIBRATED USING CHAIXMECA AND BDH ORGANIC AND INORGANIC STANDARDS. ΔT IS THE VARIATION BETWEEN OBSERVED AND KNOWN MELTING TEMPERATURES FOR THE VARIUS STANDARDS USED

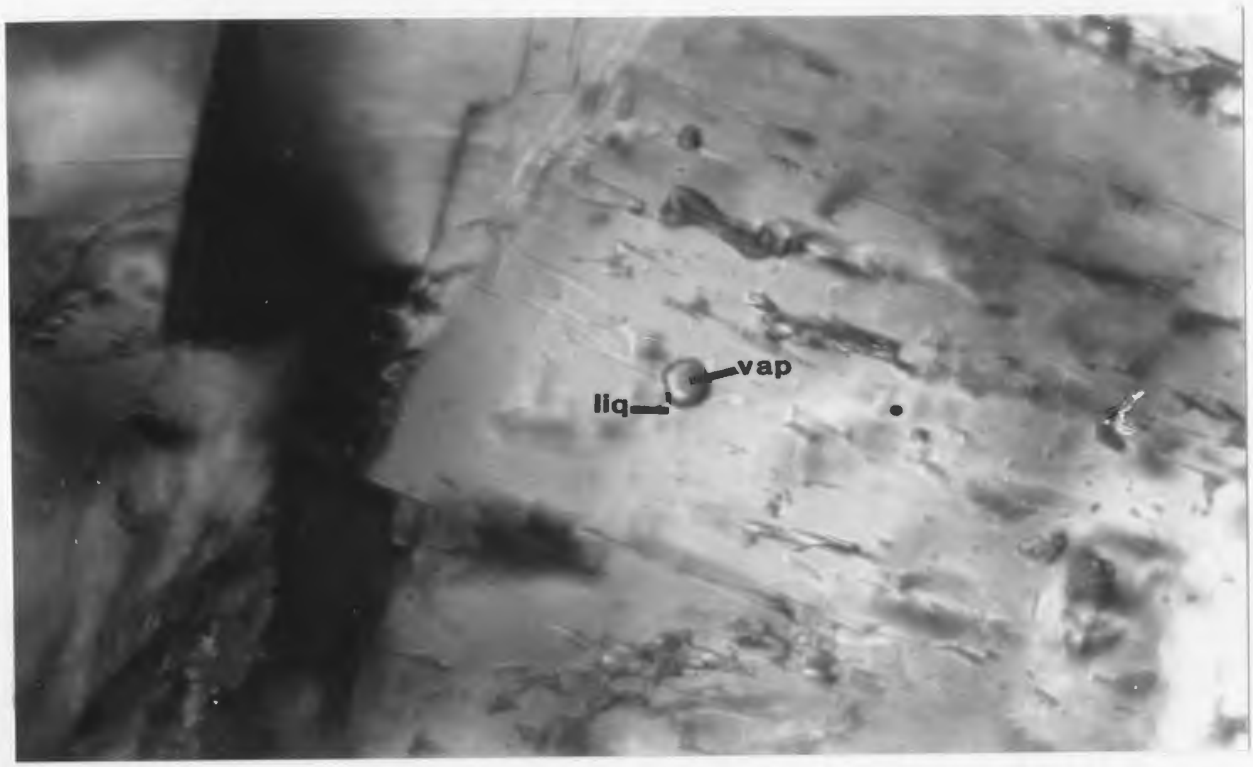

Figure 40. Type 1 fluid inclusion. The vapour bubble (vap) is prominent while the fluid inclusion edge and enclosed liquid (liq) are very faint. A number of other fluid inclusions are in the same plane. BV11-N on Collier Point (500X mag.).

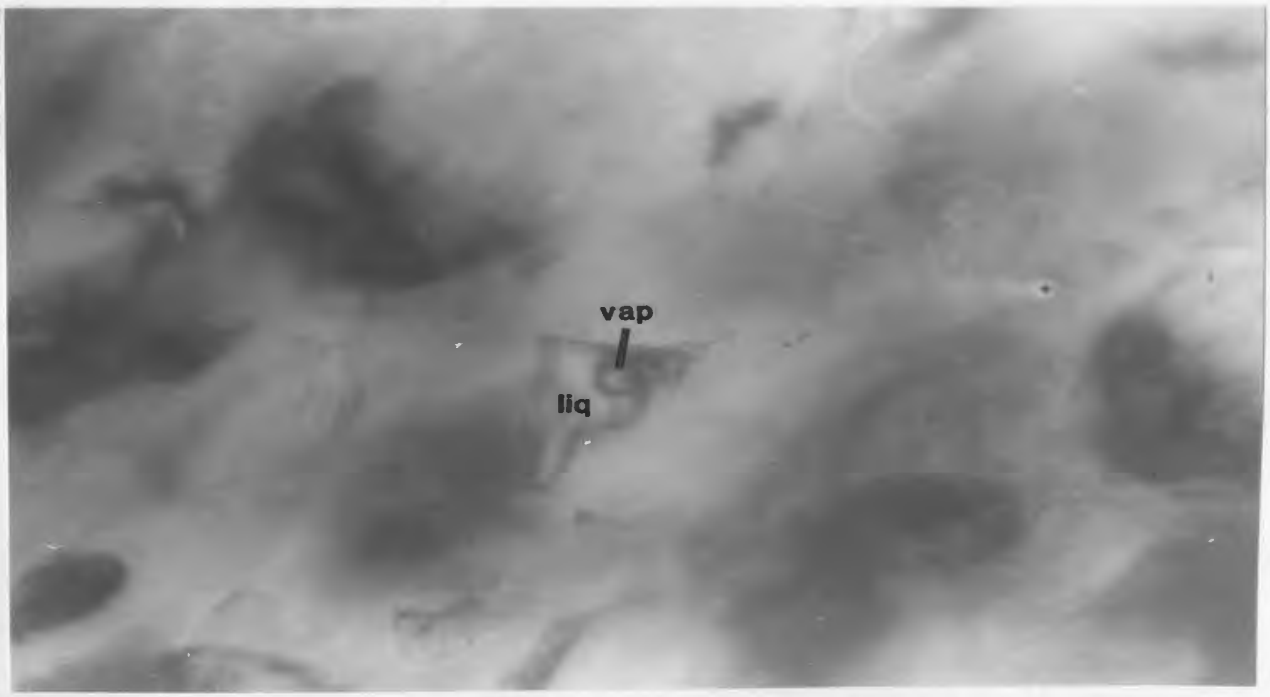

Figure 41. Type 2 fluid inclusion in barite (BV6-A) from Southern Harbour Station South (500X mag.).

liquid and vapour, with vapour forming up to 10% of the inclusion volume. When a vapour is present, type 1 inclusions generally homogenize below 100°C. Eutectic temperatures (Te) observed during controlled melting of the type 1 inclusions (i.e., Te ~ -23°C), indicate the presence of the cations Na^+ and K^+ in solution. Salinity values are consistently near 23 weight percent NaCl equivalent (wt. % NaCl(eq)).

The second fluid inclusion type found in barite samples is much less abundant. These inclusions have more equant dimensions than type 1 inclusions. They are generally sub-rectangular to irregular in shape and range in size from a few microns to 100 microns (Fig. 41). Type 2 inclusions contain variable proportions of liquid and vapour, with a few completely vapour filled. In the type 2 inclusions, evidence for necking down or leakage is almost ubiquitous (Fig. 42), leading to a lack of consistency in observed homogenization temperatures (Th), ranging from room temperature (vapour filled inclusions) to just over 400°C, for the samples measured. Within one sample (BV1-H), a spread of 213°C was found for the values of Th from two separate type 2 inclusions. Salinity is also quite variable in type 2 inclusions, ranging from 0 to 23 wt. % NaCl(eq) with the mode at 0%.

Type 2 inclusions, with more equant dimensions and random distribution, probably originated as primary fluid

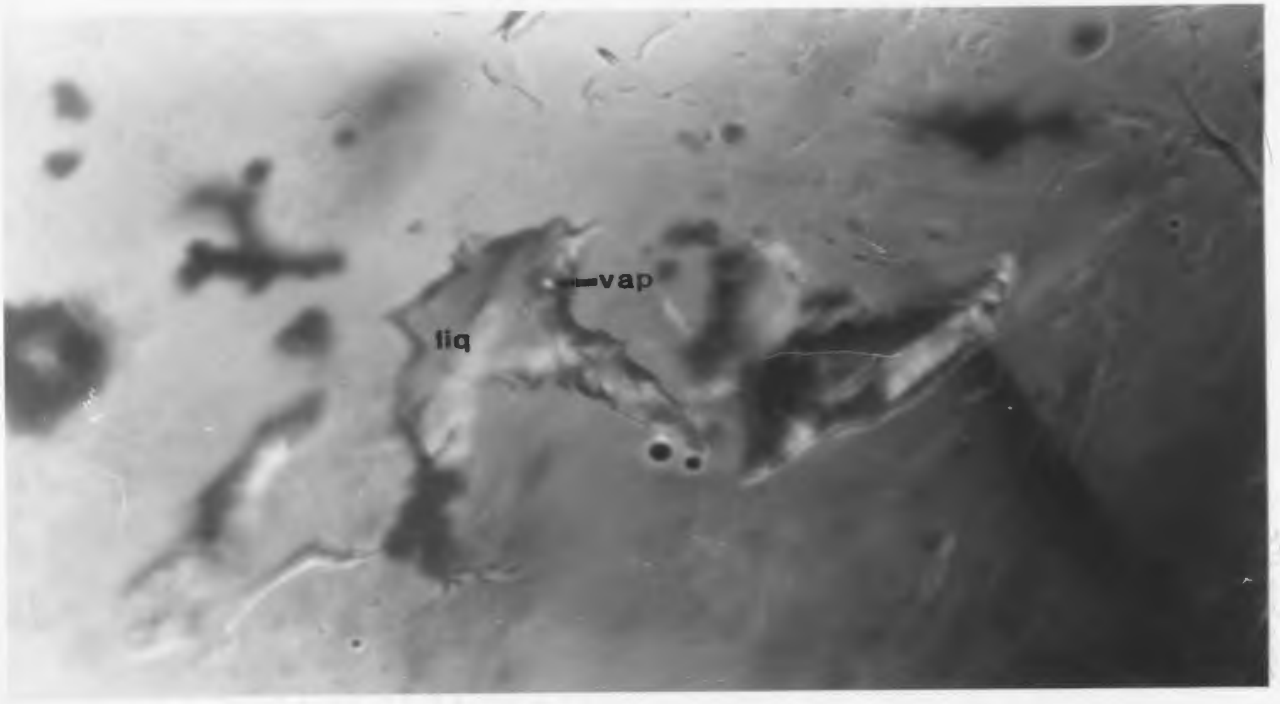

a)

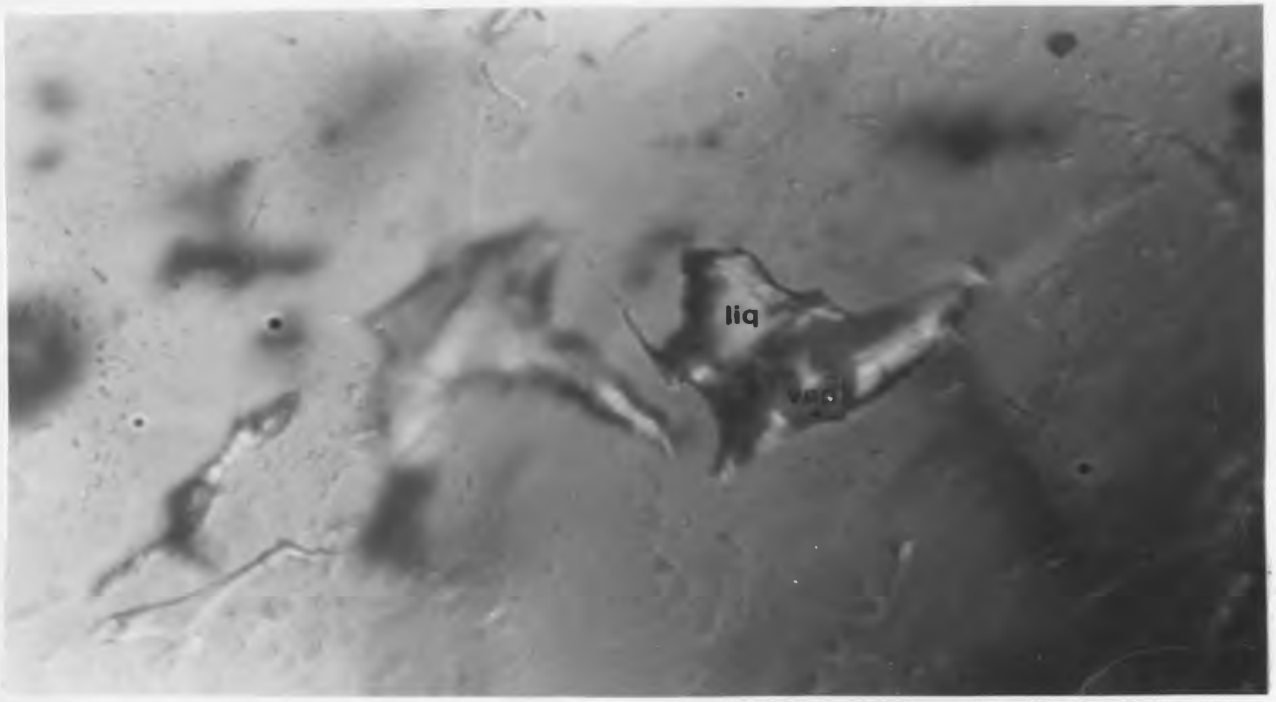

b)

Figure 42. Type 2 fluid inclusions in barite; a) vapour-poor inclusion next to b) a vapour-rich inclusion. These fluid inclusions have obviously necked down from each other (BV6-A, Southern Harbour Station South, 500X mag.).

inclusions and have subsequently been modified by secondary processes. Similar results were obtained by Slack (1980), from a study of fluid inclusions in fissure-filling barite. Slack concluded that there was abundant evidence for post-depositional necking down, resulting in unreliable data.

Another factor which has affected the results of this study is the apparent structural weakness displayed by barite crystals during both the heating and freezing processes. When water freezes it undergoes an expansion in volume of approximately 9% which may exceed the volume of the existing vapour bubble, resulting in a high internal stress and a subsequent stretching of the inclusion (Roedder and Bodnar 1980; Lawler and Crawford 1983). This increase in the volume of the inclusion without any loss or addition of material, results in a reduced density of inclusion fluid and an artificially high Th. In this study, stretching was recognized by an increase in size of vapour bubbles after freezing runs were completed, when viewed at the same temperature before and after a run.

Stretching of fluid inclusions in sphalerite and fluorite during heating runs has been described by Bodnar and Bethke (1984). In these mineral phases it was found that a certain degree of "overheating" above Th was required to produce stretching of inclusions. They also noted that the inclusions became more susceptible to stretching as their size increased. During the present study, while

heating inclusions in barite crystals, an increase in the volume of the vapour bubble was often observed after a heating run was completed. Occasionally while the temperature of the inclusion was increasing, the vapour bubble, which had been slowly decreasing in size, abruptly increased in size, and then returned to its gradual size decrease until homogenization or decrepitation took place. Overheating is therefore not always required to cause stretching of fluid inclusions in barite crystals.

Bodnar and Bethke (1984) also carried out heating runs on four inclusions in barite. Two of these inclusions decrepitated before Th was reached, one stretched when overheated by 30°C and one did not stretch when overheated by 30°C. From these results, they concluded that barite is a very unreliable host mineral for fluid inclusion studies.

The results of the present barite study support the above conclusion from Bodnar and Bethke's limited barite study, but for a different reason. Problems of stretching during heating and freezing can be overcome by careful observation of the size of the vapour bubble. The more significant problem encountered in this study was that of locating unaltered primary fluid inclusions.

3.3. Results of the Study of Fluid Inclusions in Calcite

All fluid inclusions observed in calcite from the veins sampled in this study are believed to be secondary,

with the exception of a group of psuedosecondary inclusions which will be discussed later. Typically these secondary inclusions are very similar to the type 1 fluid inclusions found in barite crystals described above (Fig. 40). They are irregular in shape and most often with one dimension much smaller than the other two. These fluid inclusions are generally aligned in a plane or are near or along a visible fracture in calcite crystals. Vapour generally occupies 1 to 10% of these inclusions by volume.

Microthermometry measurements were carried out on a total of ninety fluid inclusions from eight samples of calcite. These inclusions all homogenized to a liquid between 60° and 100°C (similar to the type 1 barite fluid inclusions). Eutectic temperatures observed during melting indicate the presence of $CaCl_2$ (Te = -49.8°C) in many of these inclusions, and $CaCl_2$ combined with NaCl (Te = -52.0°C), or with NaCl and $MgCl_2$ (Te = -57.0°C) in a few of these inclusions. The salinity of these inclusions ranged from 23 wt. % $CaCl_2$ for inclusions which contained only $CaCl_2$, to 39 wt. % $NaCl_2$(eq) for inclusions which contained $CaCl_2$ + NaCl + $MgCl_2$. Inclusions with $CaCl_2$ + NaCl had Te values which indicated intermediate salinities. Daughter minerals were not observed in any of these inclusions. Similar appearing inclusions were observed in calcite crystals from another twenty samples on which microthermometry was not performed.

The shape, vapour content and range of Th values for these secondary fluid inclusions are similar to that of the type 1 secondary fluid inclusions found in barite. These low temperature inclusions may have formed at the same time in both calcite and barite during the syn-tectonic deformation which has affected these veins (Chap. 2). This event may also have destroyed any existing primary inclusions in the calcite, and may have been responsible for the alteration of primary inclusions in barite.

Sample AR1-B2 is from a quartz-chlorite-calcite vein located about 1500 metres west of the Silver Cliff mine. It contains calcite with equant, rhomboid shaped fluid inclusions, all of which contain approximately 5% vapour (Figs 43 and 44). These inclusions are all situated along fractures which extend to the edge of the calcite crystals and stop without entering neighbouring quartz crystals. Th values for 10 inclusions ranged from 197^{o} to 258^{o}C and the salinity ranged from 0 to 5 wt. % NaCl(eq). The nature of the fluid inclusions in these calcite crystals is clearly exceptional for the veins sampled in the study area.

In the vein AR1-B2, most quartz has co-precipitated with chlorite, generally earlier than calcite precipitation, although some late-formed quartz has apparently precipitated after calcite precipitation was complete. Th values for primary fluid inclusions in quartz range from 235^{o} to 330^{o}C, with most between 250^{o} and 280^{o}C, significantly higher than

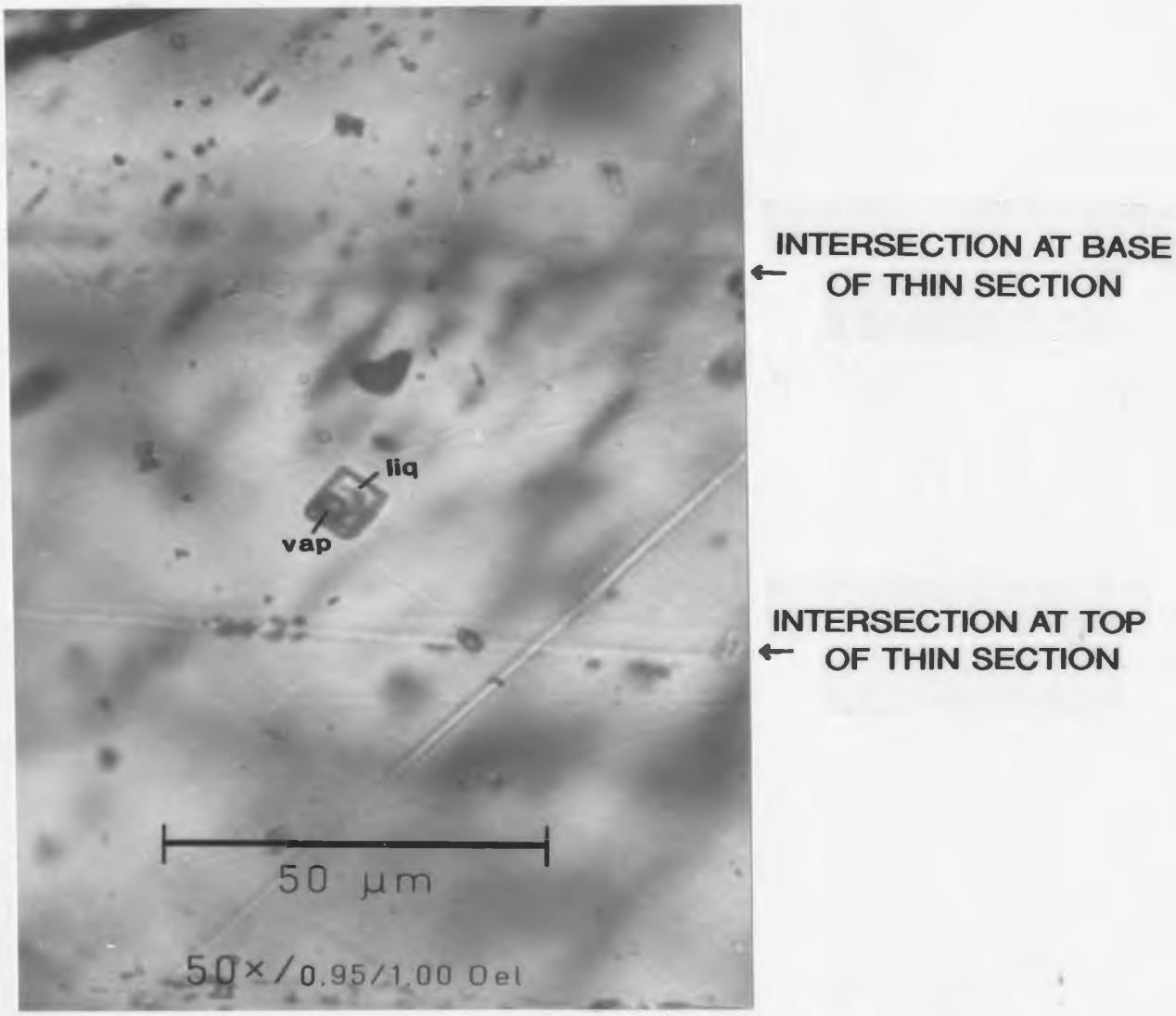

Figure 43. Pseudosecondary rhomboid shaped fluid inclusion in calcite from vein AR1-B2, Argentia. The fracture along which this inclusion has formed can be seen trending from left to right across the photograph. The fracture intersects the front of the thin section just below the inclusion and is visible as white line tilted sligtly downward to the right. The fracture intersects the back of the thin section above the inclusion and is much more blurred as it is further out of focus.

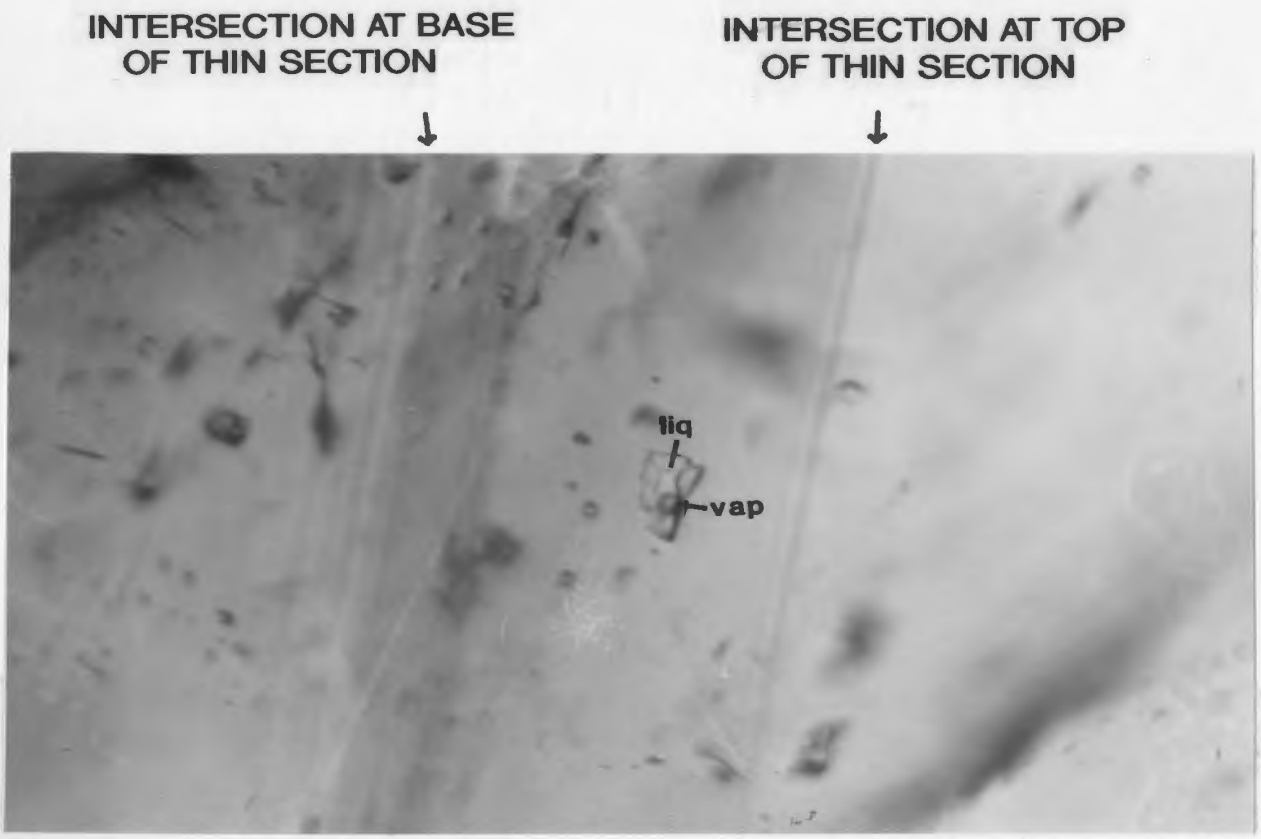

Figure 44. Pseudosecondary fluid inclusion in calcite from vein AR1-B2, Argentia. The fracture along which this inclusion has formed is clearly visible, trending from the top to the bottom of the photograph (500X mag.).

was found in the calcite fluid inclusions described above. The salinity in the quartz fluid inclusions ranges from 0 to 5 wt. % NaCl(eq), similar to the calcite inclusions. Fluid inclusions in calcite crystals of this vein are interpreted as pseudosecondary inclusions which formed during the last stage of calcite precipitation at which time the calcite crystals grew in contact with earlier formed quartz. The fracturing of the weaker calcite structure may have been caused by shearing stress in the vein, which occurred contemporaneously with vein formation (see Chap. 2). Lower Th values observed in the pseudosecondary fluid inclusions in calcite, relative to the primary fluid inclusions analysed in quartz, indicate the lower temperature which existed in the fluids at the time calcite crystals were affected by a deforming stress. The full explanation of how the fluid inclusions found in vein AR1-B formed is very complex and is discussed in detail in the following section.

3.4. Fluid Inclusions in Veins of the Silver Cliff Mine and Surrounding Area

In the Silver Cliff mine the MacKay vein, as described by Chute (1939), was up to a metre thick and was composed almost entirely of sulphide minerals with very little quartz gangue material. Quartz-sulphide mineral veinlets, which cut across the earlier-formed main segment of the MacKay vein, developed during the last vein-forming event in the

mine (see Chap. 2). Samples collected from the Silver Cliff mine for this study are from a surface exposure of the MacKay vein, and from the mine dump. It is believed that all samples which were found to be suitable for primary fluid inclusion work are from the late-formed set of quartz-sulphide mineral veinlets. Thus the fluid inclusion data presented here provide information relevant only to this late stage veinlet formation. Samples were also collected from barren quartz ± chlorite ± epidote veins which occur in an area up to 500 metres from the mine.

Primary fluid inclusions were found only in undeformed portions of quartz and sphalerite crystals (Fig. 45). Undeformed crystalline material was located in vugs where portions of crystals were situated in open space, avoiding transmission of deformational stresses. Fractures with trails of secondary fluid inclusions have developed in most "undeformed" crystals (Fig. 46). These fractures have likely formed either during the application of lithologic stress to other parts of the crystal or during hydraulic stress applied after crystal formation. In regions between such fractures, fluid inclusions can be found which have regular equant to sub-equant shapes, random distributions and which show no signs of leakage or necking down. These are interpreted here as being primary fluid inclusions.

In quartz-chlorite veins sampled from the mine area, undeformed quartz crystals were also found in non-vuggy

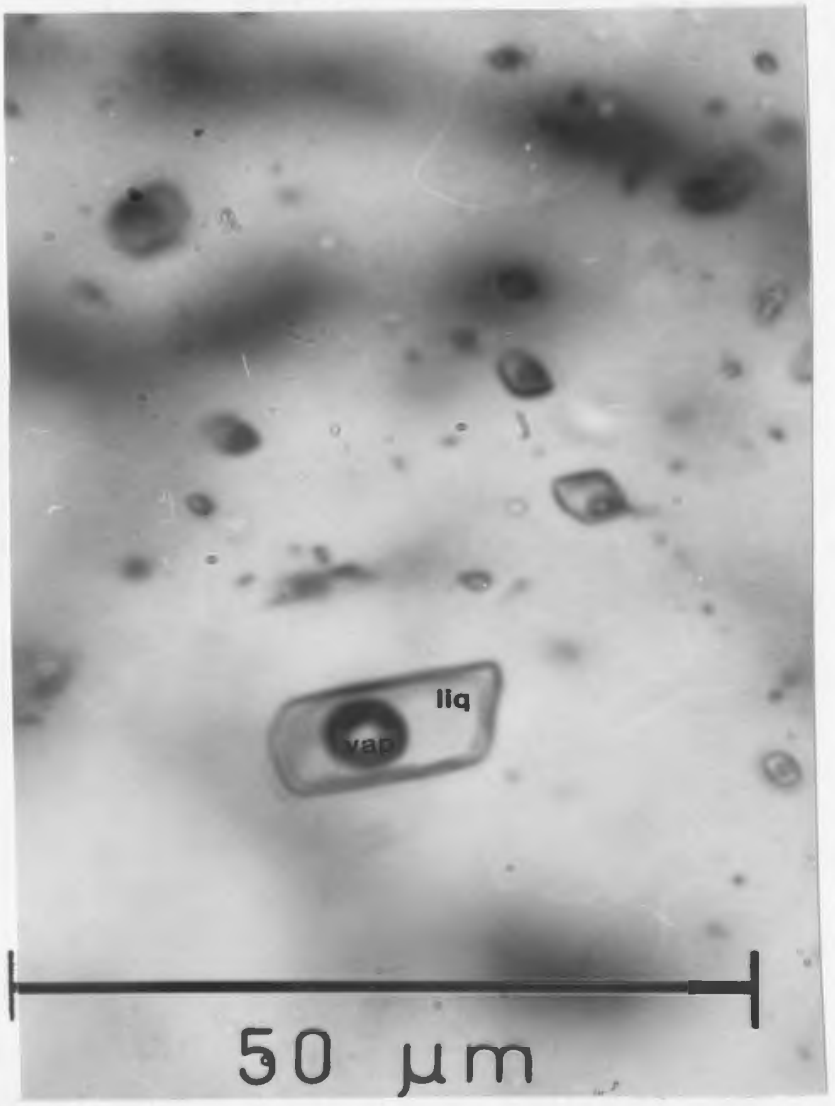

Figure 45. Primary fluid inclusions in quartz. Note the random distribution of these inclusions as suggested by their two dimensional scatter and the variable degree of focus indicating a variable depth within the thin section. Sample AR1-B2, Argentia.

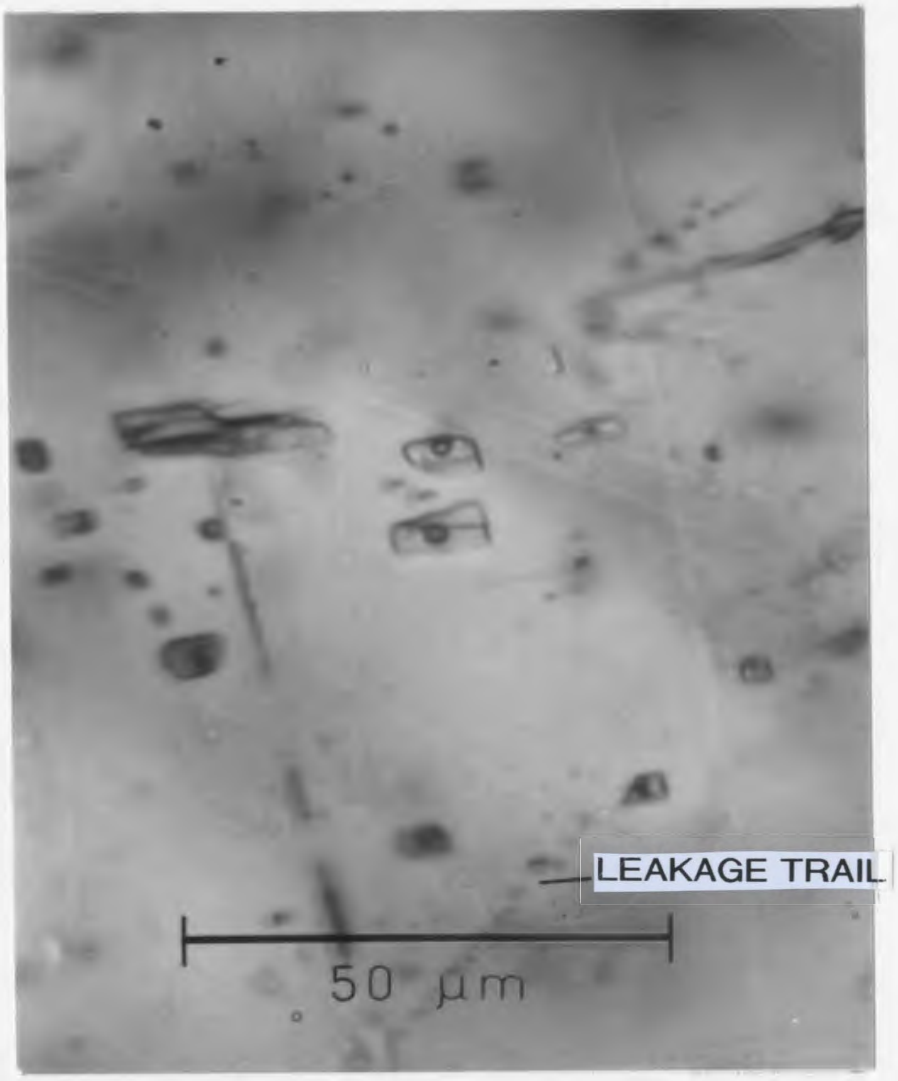

Figure 46. Fluid inclusions in a fractured quartz crystal. Many of the fluid inclusions in this photograph are secondary as indicated by their situation along fractures or by the presence of leakage trails. The two fluid inclusions in focus in the center of the photograph are interpreted as primary. Careful observation during focussing indicates that these inclusions are situated between fractures and that there are no visible leakage trails. This sample BV3-D from St. Brides is used as it best diplays, photographically, primary fluid inclusions found between fractures. This is a feature found throughout the field area.

areas of veins surrounded by chlorite in otherwise deformed veins. The surrounding incompetent chlorite has apparently protected the quartz crystals from stress. Primary fluid inclusions have been located in such quartz crystals.

Salinity data for these fluid inclusions were difficult to obtain with approximately one successful measurement for every nine inclusions studied. The most common cause of failure in attaining a salinity value was metastability, whereby an inclusion fluid would not freeze even though it had been cooled far below its freezing temperature. This metastability arises from the small size of many of the inclusions (i.e., often 2 microns or less), which commonly results in difficulty in the nucleation of ice crystals (Roedder 1984).

Because of the volume expansion which can take place in fluid inclusions during freezing, Th values were determined before melting temperatures to avoid erroneous Th values. However this sequence of operations resulted in a further difficulty. Frequently during heating runs, the Th for several inclusions would be determined from one location. In heating a group of inclusions to the temperature at which the last inclusion of this group homogenized, the earlier homogenized inclusions would sometimes decrepitate, preventing the collection of salinity data. The collection of homogenization data was deemed of more value to this study.

The measured salinity of fluid inclusions in the ore veins ranges from 2.0 to 7.4 wt. % NaCl(eq) and averages 4.5 wt. % NaCl(eq). Although it is very difficult to determine the melting Te of low-salinity inclusions due to the small amount of melt formed at the eutectic point, a first melt was observed in two inclusions at -19.0° and -17.0°C. These temperatures are slightly higher than the Te = -20.8°C for the H_2O-NaCl system. This deviation from the Te for the H_2O-NaCl system probably reflects the difficulty in observing the first melt. It is therefore probable that NaCl is the dominant salt present in these inclusion fluids. It is also possible that a mixture of NaCl and KCl exists in these fluids as such a mixture has a Te of -22.9°C, just slightly lower than that of pure NaCl in H_2O.

Measured salinity values in the barren veins ranges from 0 to 5.5 wt. % and averages 1.8 wt. % NaCl(eq). Chlorite is present in these veins, thus $MgCl_2$ must have been present in the precipitating fluids. Significant quantities of $MgCl_2$ mixed with NaCl will result in Te values of -35.0°C. As this was not observed, it is unlikely that the $MgCl_2$ concentration is very high. Possibly most of the Mg was stripped from the solution by chlorite precipitation. Figures 47 and 48 show the limited salinity data for both the ore veins and the barren veins plotted against both "Th" and "EVC" (Estimated Vapour Content - by volume) at room

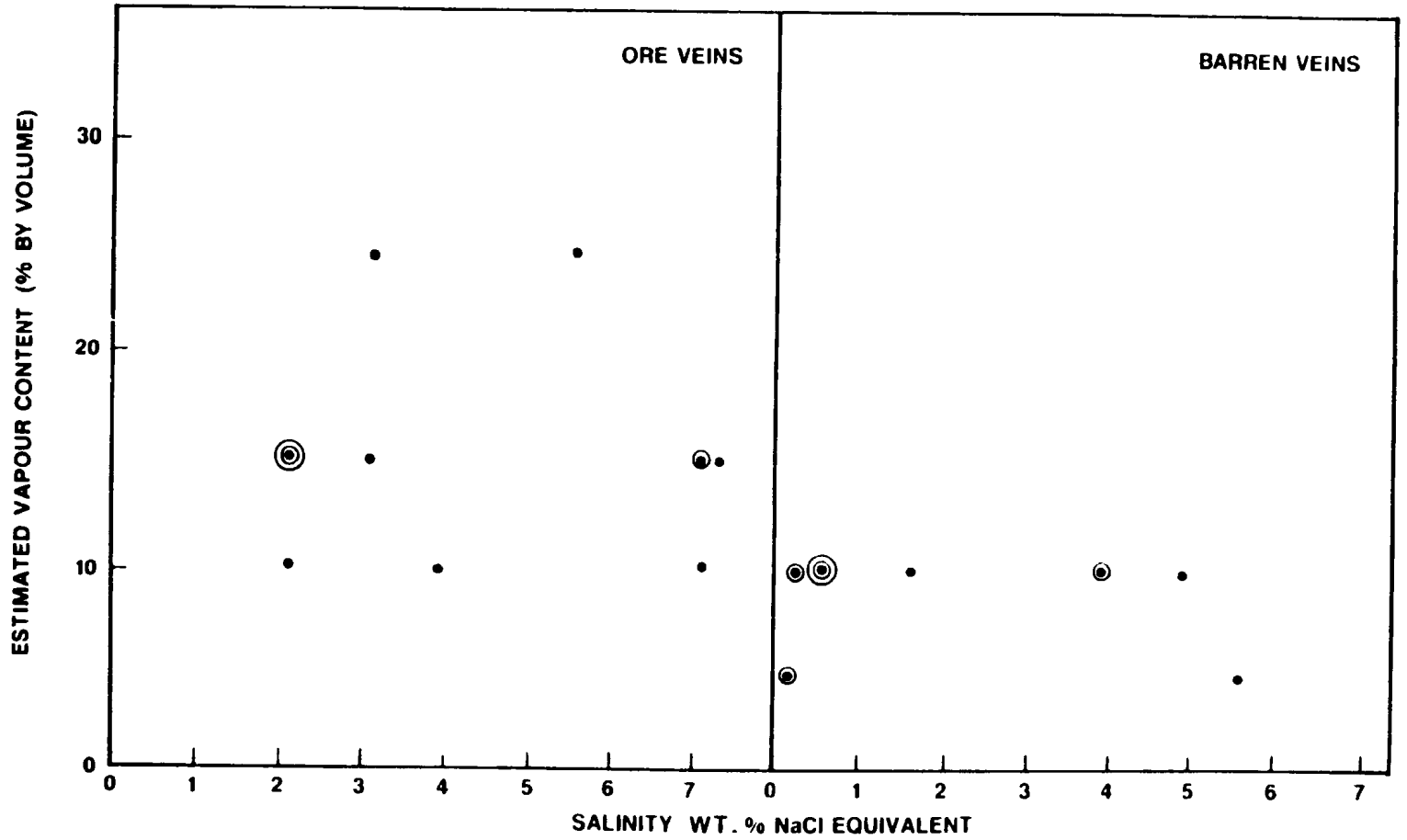

FIGURE 47: SHOWS THE LACK OF CORRELATION BETWEEN THE AVAILABLE SALINITY DATA AND THE ESTIMATED VAPOUR CONTENT AT ROOM TEMPERATURE FOR VEINS AT SILVER CLIFF. COINCIDENT VALUES ARE CIRCLED.

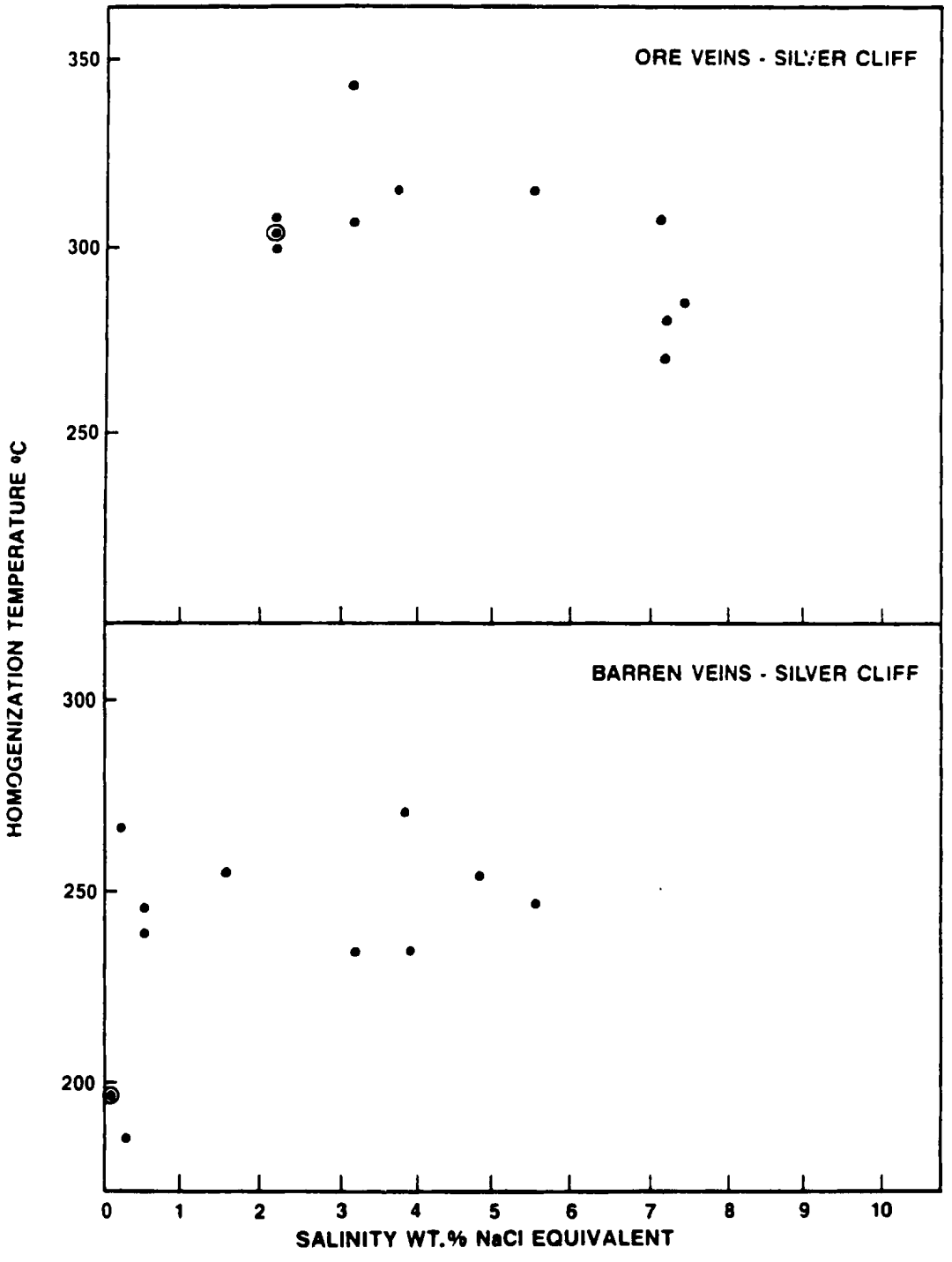

FIGURE 48: SHOWS THE LACK OF CORRELATION BETWEEN HOMOGENIZATION TEMPERATURE AND SALINITY FOR SILVER CLIFF VEINS. COINCIDENT VALUES ARE CIRCLED.

temperature. There is no apparent correlation between salinity and either of these parameters.

Th values for primary fluid inclusions found in quartz crystals and one sphalerite crystal of the late veinlets from the Silver Cliff mine are presented in Figure 49. Temperatures range from 230° to 504°C and form two distinct groupings. The lower temperature group (LTG) contains most of the data and ranges from 230° to 370°C. There is a gap in the data from 370° to 430°C. The high temperature group (HTG) of data ranges from 430° to 504°C. Also significant is the fact that LTG fluid inclusions, with a few exceptions, all homogenized to a liquid, while the HTG inclusions, without exception, homogenized to a vapour.

A further distinction can be made between the LTG and the HTG fluid inclusions. Figure 50 shows that for the LTG inclusions, the EVC of the fluid inclusions, at room temperature, increases with Th. Figure 51 shows that the HTG inclusions display a negative correlation between EVC and Th, opposite to the trend displayed by the LTG data. As will be discussed, an ideal plot would define a non-linear curve. Variation from the expected curve is introduced by the error in accurately estimating the vapour content of inclusions. These estimates are made by visual comparison (two dimensional perspective) of the apparent occupied area of vapour and liquid in these inclusions, to a chart developed by Roedder (1972) which relates surface area in

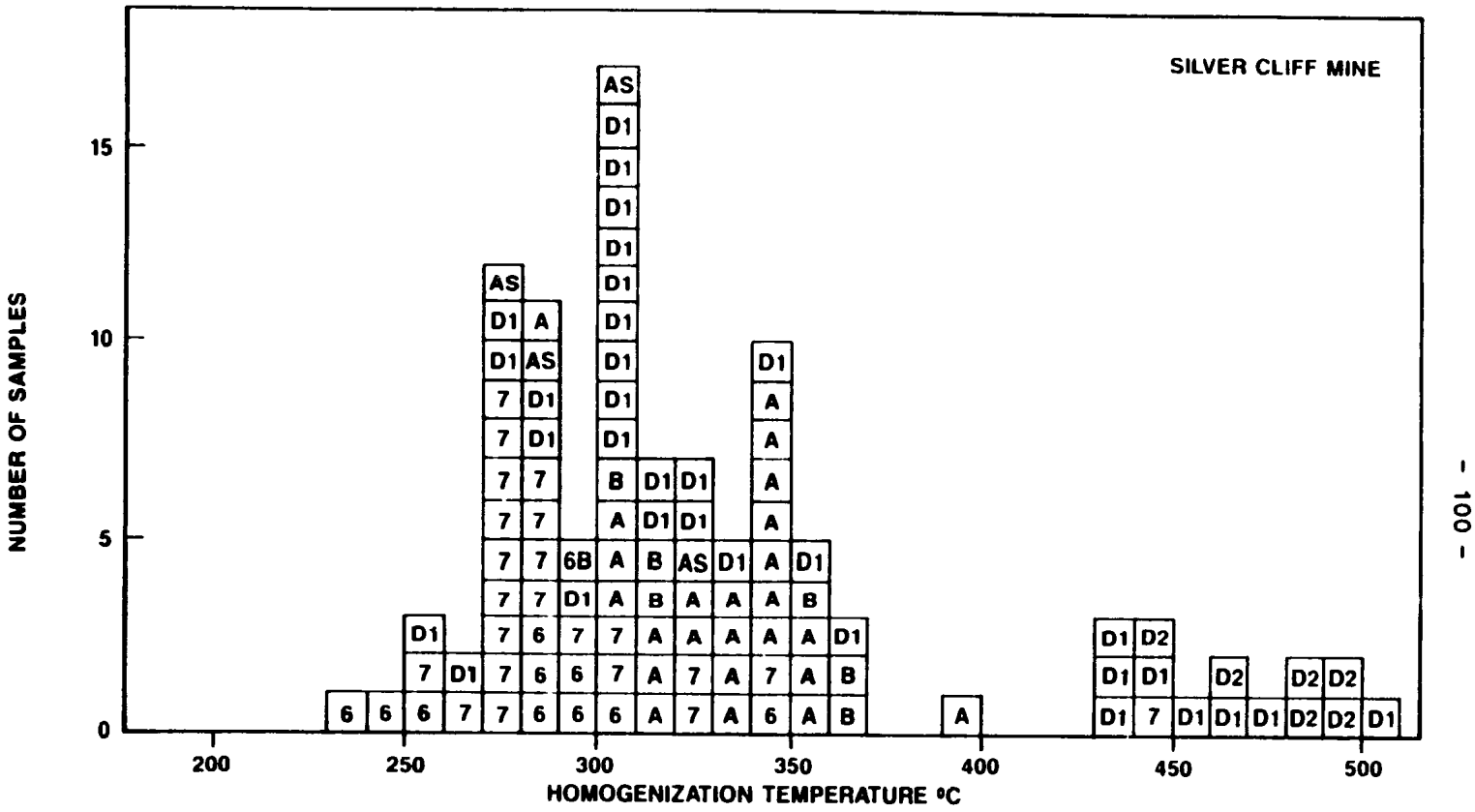

FIGURE 49: HISTOGRAM OF HOMOGENIZATION DATA FROM FLUID INCLUSIONS IN QUARTZ CRYSTALS FORMED IN THE LATE STAGE QUARTZ-SULPHIDE VEINLETS IN THE SILVER CLIFF MINE AND FROM ONE SPHALERITE CRYSTAL. 6 AR6-C, 7 AR7-A, D1 AR25-D1, AS AR25-AS (SPHALERITE), A AR25-A, 6B AR6-B, B AR25-B, D2 AR25-D2.

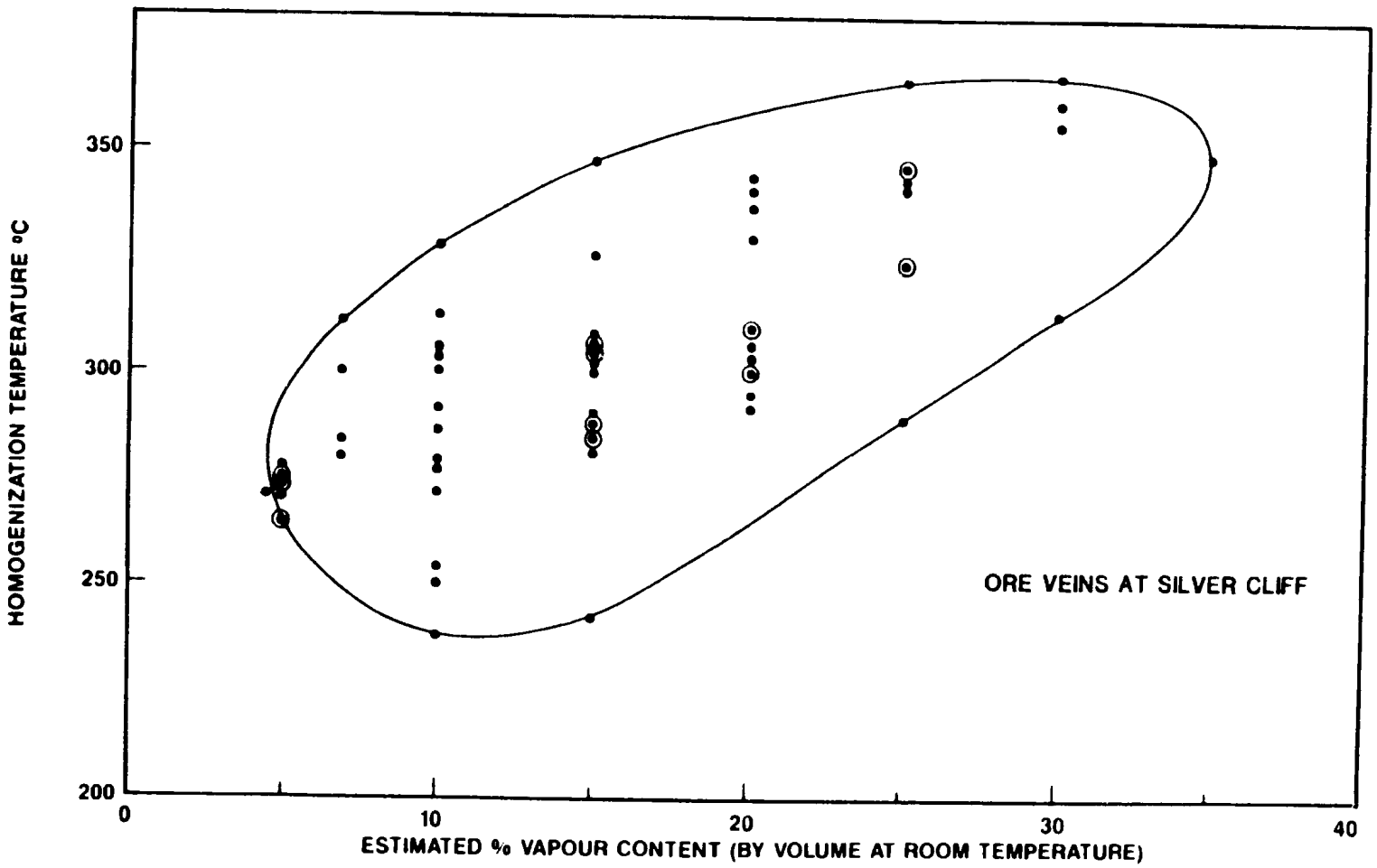

FIGURE 50: INDICATES A CORRELATION BETWEEN HOMOGENIZATION TEMPERATURE AND THE ROOM TEMPERATURE VAPOUR VOLUME OF FLUID INCLUSIONS FROM THE LOW TEMPERATURE DATA GROUP FROM THE VEINS OF THE SILVER CLIFF MINE. COINCIDENT VALUES ARE CIRCLED.

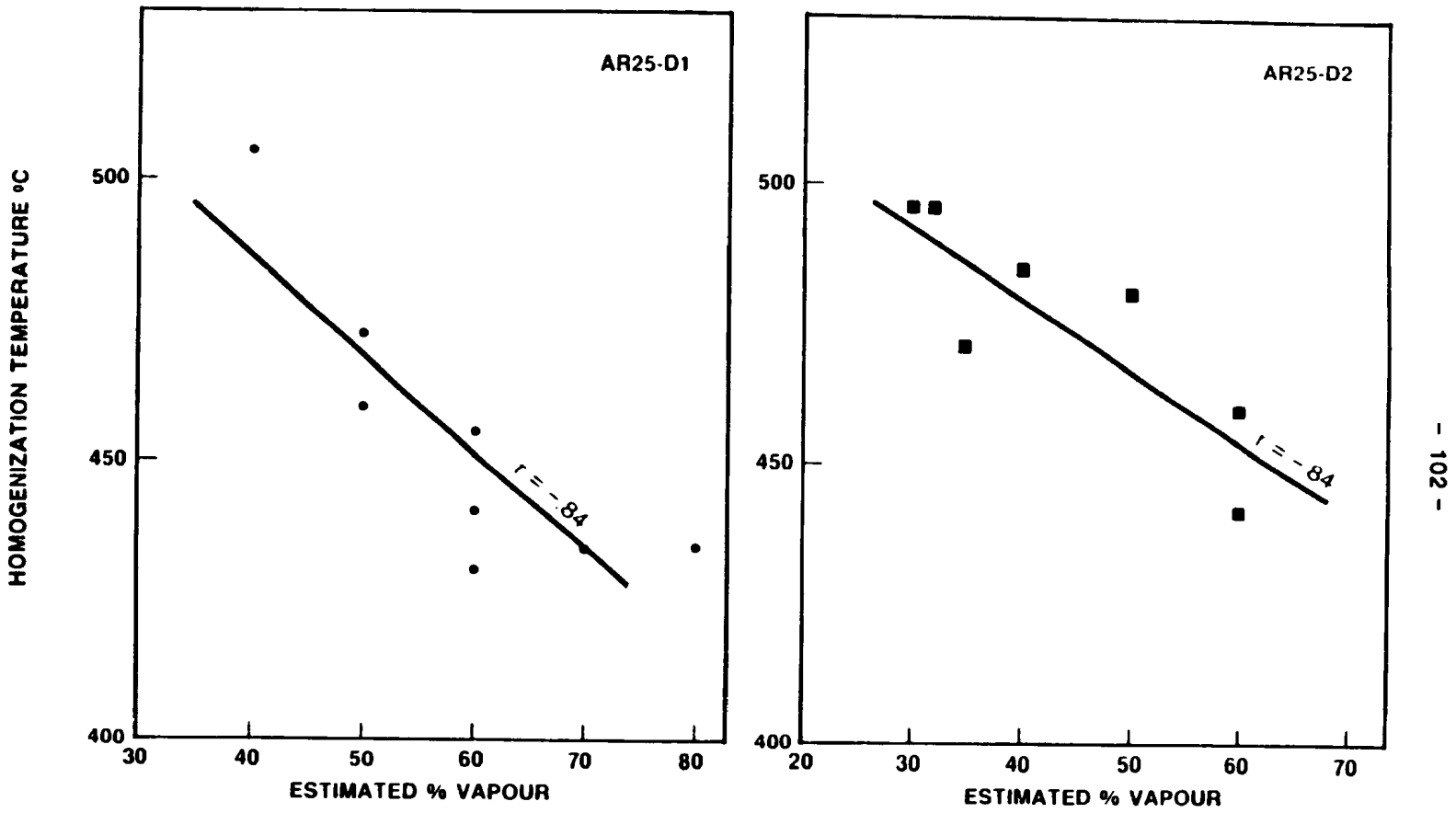

FIGURE 51: SHOWS THE NEGATIVE CORRELATION WHICH EXISTS BETWEEN HOMOGENIZATION TEMPERATURE AND ESTIMATED VAPOUR CONTENT FOR THE HIGHER TEMPERATURE GROUP OF INCLUSIONS. BEST FIT LINES BY LINEAR REGRESSION

spherical inclusions to volume %. A degree of error is introduced because the inclusions have somewhat irregular non-spherical shapes. Also, it is more difficult to estimate the relative proportions of surface areas for the more irregularly shaped inclusions.

Three differences in the nature of the LTG and the HTG have been discussed above: 1) different Th ranges; 2) different homogenization behaviour; 3) opposite correlations between Th Vs EVC. These differences provide the key to understanding how the LTG and HTG fluid inclusions have formed. It is believed that the fluid inclusions formed in the Silver Cliff ore veins trapped fluids over a range of temperatures with boiling taking place at the high temperature end of this range. The LTG is composed of inclusions which have trapped fluid which was not boiling. The HTG inclusions contain fluid which was boiling when trapping occurred. To explain these conclusions it is necessary to review how the fluids involved in trapping behave under conditions of variable pressure, temperature and salinity.

Figure 52 is a temperature-density (T-D) plot for pure H_2O showing the immiscibility field which exists for this system. The maximum temperature of immiscibility occurs at the critical point for pure H_2O at 374^{o}C and 220 bars. The critical point is the point on the immiscibility surface

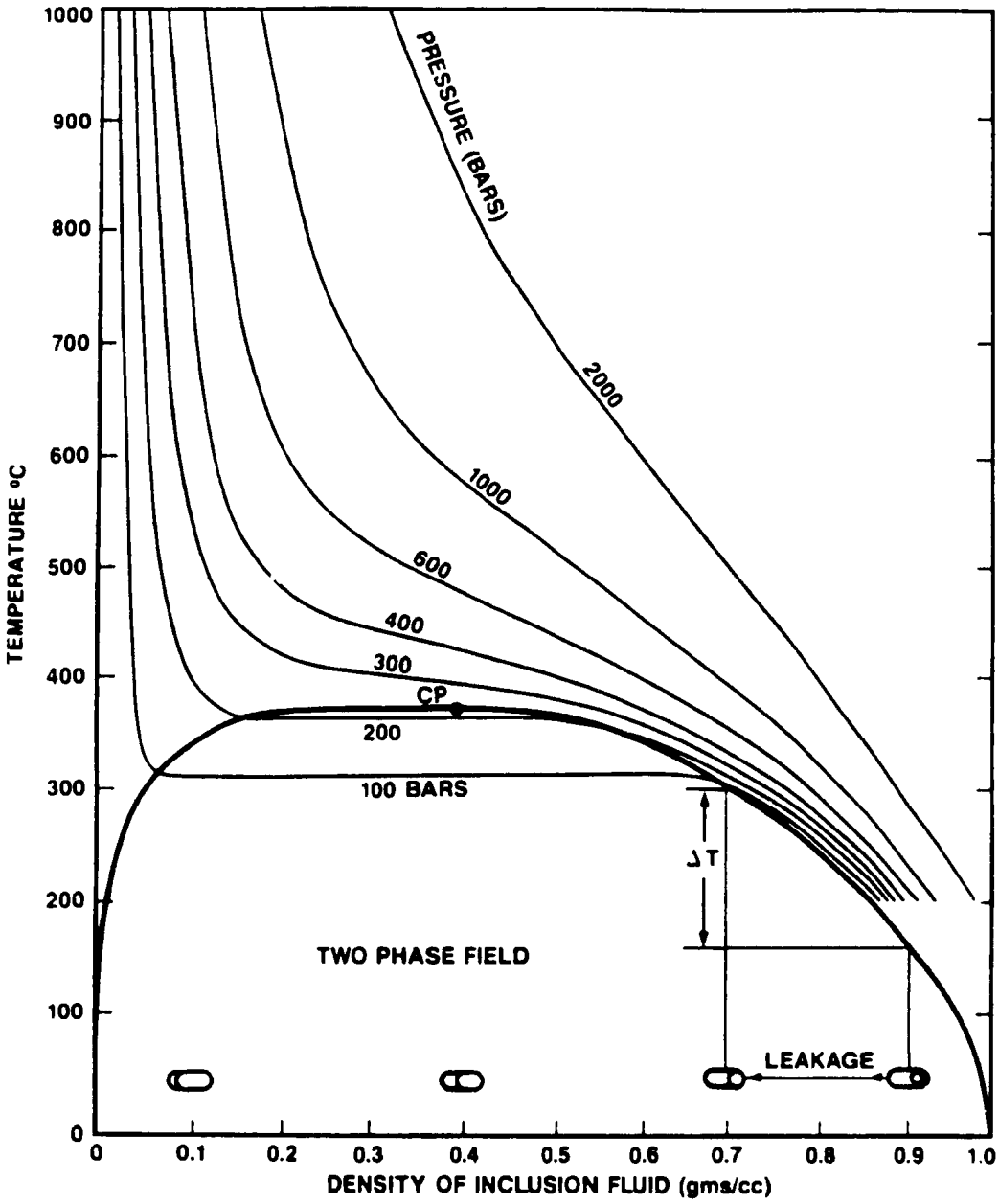

FIGURE 52: TEMPERATURE DENSITY PLOT ILLUSTRATING THE IMMISCIBILITY FIELD OF PURE H_2O. TAKEN FROM ROEDDER (1967). CP - CRITICAL POINT.

which separates fluids which behave more like liquid from those which behave more like vapour. Fluid inclusions with fluid densities greater than the critical density (~ 0.4 gms/cc), will homogenize to a liquid on the immiscibility surface to the right of the critical point in Figure 52. Inclusions with fluid densities less than the critical density, will homogenize to a vapour on the immiscibility surface to the left of the critical point.

It is interesting to note that trapping of fluids above the immiscibility surface, at varying temperatures, holding pressure constant (e.g., along an isobar in Fig. 52), should result in a Th Vs EVC curve which mimics the shape of the isobars in Figure 52. For example the inclusions plotted in Figure 50 are all from veins in the Silver Cliff mine. The mine workings were on two levels which were within 10 metres of each other. Assuming no overpressure development, all fluid inclusion in veins from the mine trapped fluids at essentially a constant pressure. Thus ideally the data points in Figure 50 should define a curve that has a similar shape to the isobars in Figure 52. This should become most noticeable at lower temperatures where the isobars in Figure 52 steepen. In Figure 50 there is no clear steepening of the data in the low temperature region. This may be due to the fact that there are very few inclusions with a Th below 260^{o}C, where the steepening becomes more pronounced in Figure 52. As will be seen

later, other such plots (e.g., Fig. 60) which include lower temperature fluid inclusions do show a pronounced steepening at the low temperature end.

The temperature range for the two plots in Figure 51 is too limited to show anything but a straight line. Also at the pressure conditions (~200 bars as discussed below) and over the temperature range indicated for the fluid inclusion data plotted in Figure 51, the isobar curve in Figure 52 is very close to a straight line.

A potential use of Th Vs EVC plots is the evaluation of overpressure development during fluid inclusion formation. A significant overpressure development in a group of inclusions will show in points plotted on a Th Vs EVC graph as a deviation from the expected trend if the degree of overpressure is sufficient to show up against other variations from the expected curve (discussed above). If the overpressure is constant throughout the formation of the inclusions which are analysed, it will not be detectable on a Th Vs EVC plot. In Figure 50 there is no clear deviation from the expected trend, although there is considerable variation from any one curve. It is not known how much overpressure is necessary to cause a significant deviation from an expected curve. An example of overpressure effects which show clearly on a Th Vs EVC plot is discussed further on in this chapter.

Figure 53 is a pressure-temperature (P-T) plot of the $NaCl-H_2O$ system. The immiscibility field of pure H_2O displayed in Figure 52 as a two dimensional field, is represented in Figure 53 by the solid line which begins at 0^oC and ends at the point C_0, the critical point for pure H_2O. The critical point for pure NaCl is indicated by C_{100}. Also shown in Figure 53 are the immiscibility fields of solutions containing 1, 5 and 20% NaCl, with critical points C_1, C_5 and C_{20} respectively, and the critical curve which joins them. The critical curve is defined by the locus of critical points for all compositions intermediate between, and including, pure H_2O and pure NaCl. Figure 53 shows that the addition of 5% NaCl to pure H_2O, creates a solution with a two-phase immiscibility field which is considerably expanded relative to pure H_2O, such that immiscibility reaches temperatures well over 700^oC. Figure 50 shows that a 0.1% NaCl solution has an immiscibility field which extends up to 650^oC. Thus the addition of NaCl to pure H_2O, even in very minor amounts, results in a pronounced enlargement of the immiscibility field.

The immiscibility curves for all solutions with compositions between 0.0 and 100% NaCl are composed of two segments, a "boiling curve" and a "dew (or condensation) curve", which are separated by the critical point for that composition. In Figure 53, the portion of an immiscibility curve which intersects the critical point from the left is

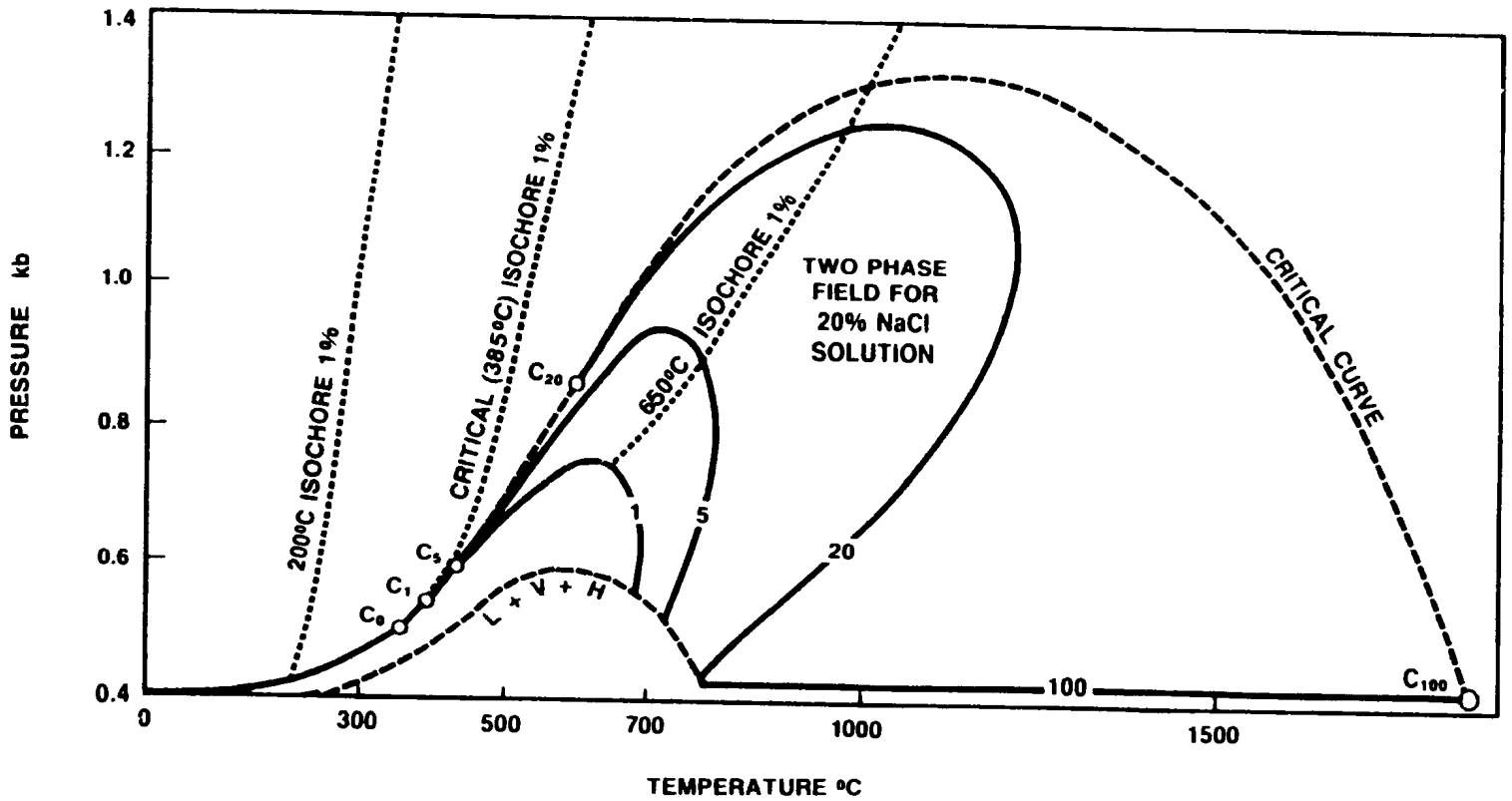

FIGURE 53: PROJECTION OF THE H_2O-NaCl SYSTEM ON THE P-T PLANE. SHOWN ARE THE CRITICAL POINTS FOR PURE H_2O (C_0) AND PURE NaCl (C_{100}), AND THE IMMISCIBILITY FIELDS FOR SOLUTIONS WITH 1, 5 AND 20 WT % NaCl WITH THEIR CORRESPONDING CRITICAL POINTS. THESE CRITICAL POINTS FALL ON THE CRITICAL CURVE WHICH JOINS THE TWO CRITICAL END POINTS. THE LOWER DASHED CURVE DELINEATES THE FIELD IN WHICH HALITE (H) IS PRESENT WITH LIQUID (L) AND VAPOUR (V). FROM PICHAVANT et al.(1982).

the boiling curve, while the dew curve intersects the critical point from the right.

Ideally, fluid trapped within an inclusion maintains an overall constant density through changing temperature and pressure conditions. This is due to the rigidity of the crystal structure which generally maintains a constant inclusion volume (exceptions were discussed above, e.g., inclusions in barite). After trapping, the fluid moves through P-T space along its isochore (constant density path) to progressively lower temperatures and therefore pressures. Eventually the P-T conditions are such that the trapped fluid intersects its immiscibility surface. If the density of the trapped fluid is greater than the critical density, its fluid characteristics are closer to that of a liquid than a vapour. The isochore of such a fluid intersects its boiling curve (e.g., 200°C for an isochore of 1%, Fig. 53), and a vapour is exsolved. A fluid with a density below the critical density behaves more like a vapour than a liquid. Its isochore will intersect its dew curve (e.g., 650°C for an isochore of 1%) and will condense droplets of liquid. The critical density isochore is the line in P-T space, above the immiscibility field for a given composition, which separates fluids with a liquid nature from fluids with a vapour nature (e.g., 385°C for an isochore of 1%, Fig. 53).

The following discussion relates the observations made from the data (discussed above) to the known behaviour of

the H_2O-NaCl system in order to explain the formation of the ore vein fluid inclusions found at Silver Cliff. A constant salinity will be assumed in order to simplify the present discussion. A salinity of 5 wt. % NaCl is chosen as it is close to the average of 4.5 wt. % NaCl(eq) found for the ore veins, and because experimental data are available for 5.0 wt. % NaCl solutions.

It is assumed that the hydrothermal fluid is produced at its source at some undetermined elevated temperature and pressure (refer to Figs 54 and 55 for the following disscussion), and moves upwards in the crust from its source under the influence of an upward decreasing hydraulic pressure gradient. As the fluid ascends, both pressure and temperature decrease. Temperature can change depending on variations in the source temperature and the rate of cooling while the fluid travels from the source to the level of mineral precipitation. Assuming fluid over-pressures were insignificant along the fluid path, fluid pressure will depend on the height of the overlying water column if pressure is hydrostatic, or the height of the overlying rock column if the pressure is lithostatic. The P-T character of the fluid will follow one of an infinite number of possible pathways on its upward migration. The following discussion focusses on two potential pathways shown in Figure 55.

Precipitation of mineral phases may take place at any point along the fluid path. This discussion concerns only

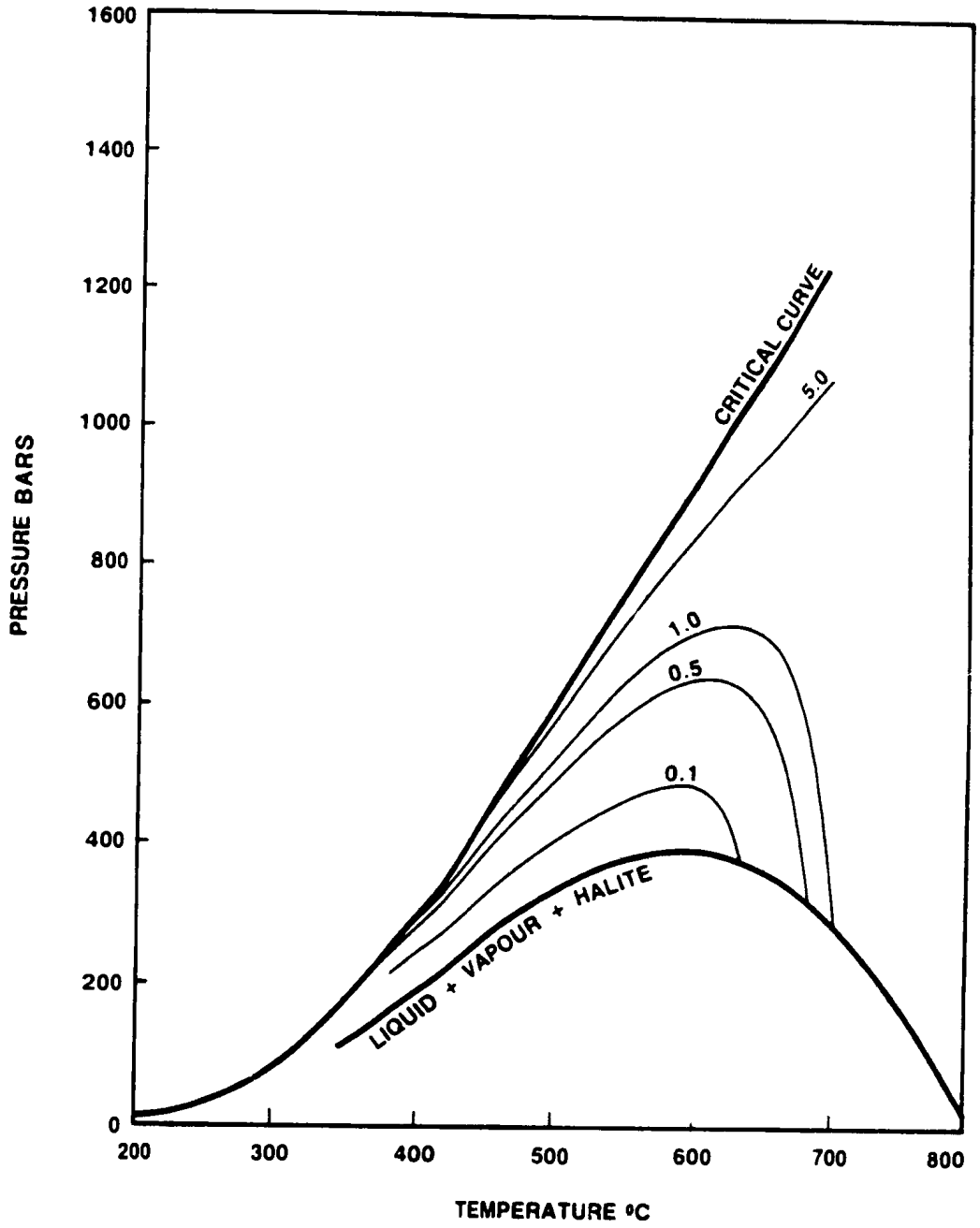

FIGURE 54: IMMISCIBILITY FIELDS FOR 5.0, 1.0, 0.5 AND 0.1 WT.% NaCl—H_2O SOLUTIONS. CURVES ARE FROM SOURIRAJAN AND KENNEDY (1961) AND HAAS (1971).

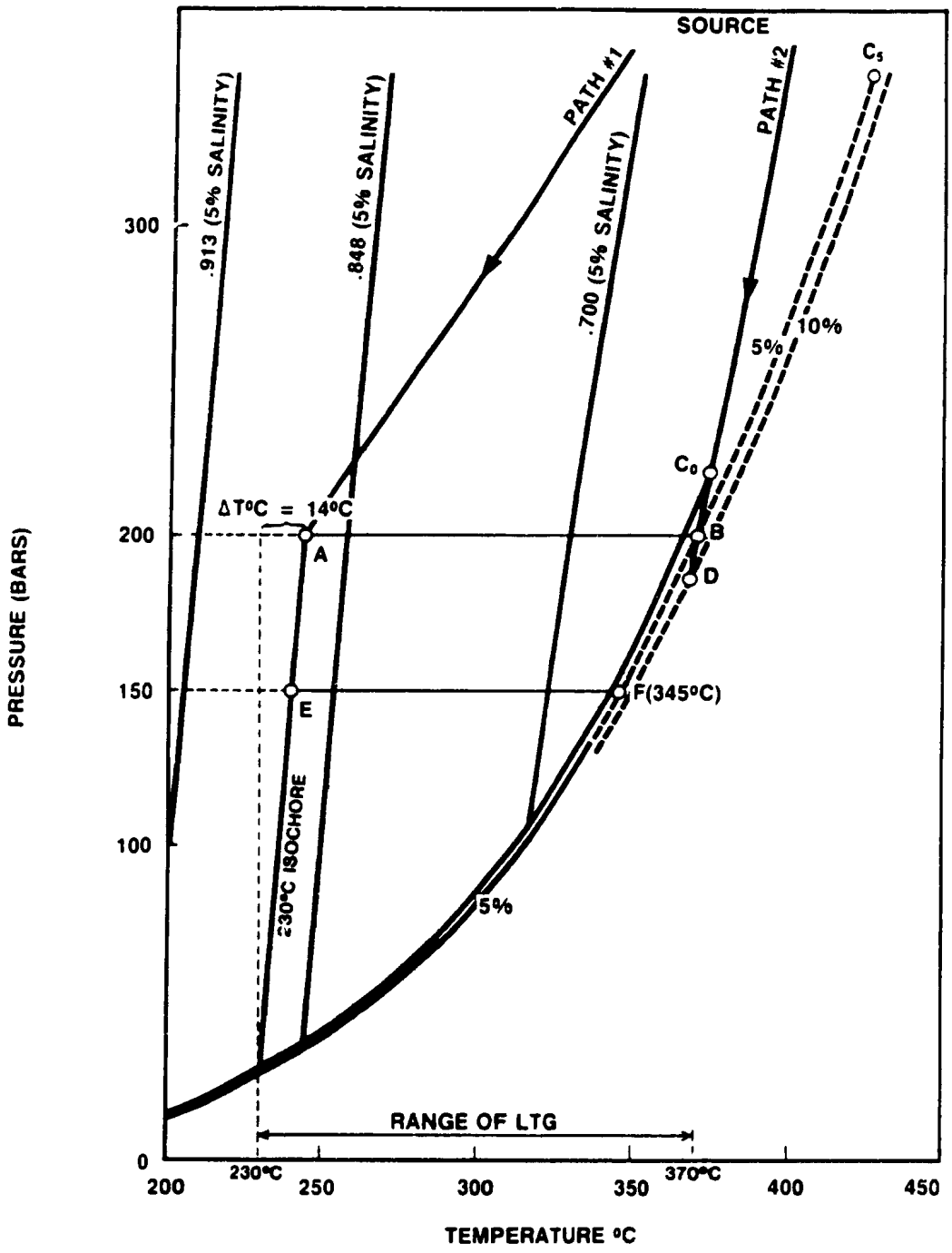

FIGURE 55: ILLUSTRATION OF HOW BOILING CURVES CAN BE USED TO ATTAIN PRESSURE CORRECTIONS. CURVES ARE FROM HAAS (1971). ISOCHORES ARE DRAWN FROM DATA OF POTTER AND BROWN (1977).

that mineral precipitation which takes place at the crustal level of the Silver Cliff mine (i.e., constant pressure, possible overpressure is evaluated below). Fluid inclusion formation at constant pressures and at variable temperatures (and thus variable densities) may occur along the horizontal line A-B in Figure 55. Line A-B is situated such that fluid inclusions which display the range of Th values of the LTG (230°C to 370°C) would have formed above the immiscibility field of a 5% NaCl solution, at a constant pressure. The line A-B does not cover this range of temperatures, but the isochores of fluid inclusions which are trapped along this line will intersect the 5% immiscibility field over this range of temperatures as indicated along the temperature axis in Figure 55. A hydrothermal fluid which rises through the crust along path #1 in Figure 55 might be trapped at the mine paleo-elevation at a temperature above the Th of 230°C, then subsequently (e.g., during uplift and erosion) move along its isochore until it intersects the immiscibility surface at 230°C. When the isochore intersects the immiscibility surface for a 5% NaCl solution, a vapour bubble forms in the inclusion. This is also the point on its immiscibiliby surface that the fluid in this inclusion will homogenize during microthermometry. The higher temperature data within the LTG might result from the trapping of hydrothermal fluids at the mine elevation, which have risen along fluid paths between paths #1 and #2 (i.e.,

progressively more rapid ascent resulting in higher temperatures and/or variable source temperatures).

The trapping of fluids along the line A-B in Figure 55 to form the LTG, would explain the positive correlation between Th and EVC seen in Figure 50. Three isochores have been drawn in Figure 55 using the experimental data of Potter and Brown (1977). These isochores show that trapping of fluids at increasing temperatures along the line A-B in Figure 55 results in lower inclusion fluid densities, which results in increased vapour contents in these inclusions at room temperature.

The explanation of how the HTG fluid inclusions may have formed is more complex. A fluid which moves along path #2 will enter its immiscibility field at point B in Figure 55, resulting in boiling of fluids at that crustal level. The composition of vapour which is exsolved from the liquid at point B can be determined from Figure 56. At 370^{o}C and 200 bars, a liquid of 5% NaCl is in equilibrium with a vapour of such a low salinity that it falls off the left of the diagram (<0.001 wt. % NaCl).

If conditions remain close to equilibrium during ascent the fluid never moves far into the immiscibility field, but remains close to the immiscibility surface, even though temperature and pressure may continue to decrease. This is accomplished by the boiling process which exsolves a vapour with a much lower salinity, thereby increasing the

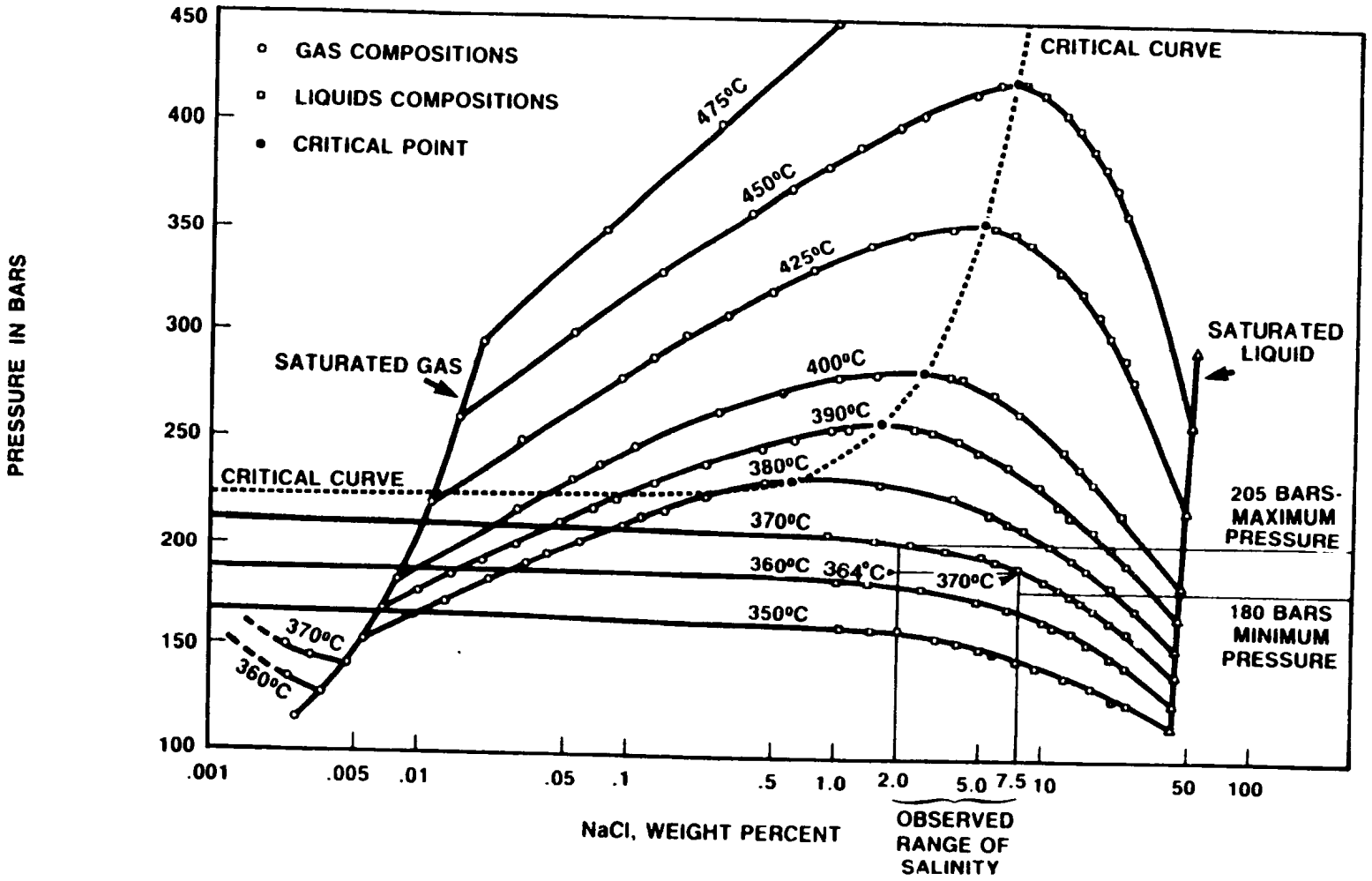

FIGURE 56: CURVES SHOW THE COMPOSITION OF CO-EXISTING GASES AND LIQUIDS AT VARIOUS TEMPERATURES IN PRESSURE-SALINITY SPACE FROM SOURIRAJAN AND KENNEDY (1962). ALSO SHOWN ARE THE MAXIMUM AND MINIMUM TEMPERATURES AND PRESSURE FOR BOILING FLUIDS OBSERVED IN FLUID INCLUSIONS AT THE SILVER CLIFF MINE.

salinity of the remaining liquid. This results in a continuous shift of the boiling curve to higher temperatures (i.e., to the right in Fig. 55), while the fluid continues to decrease in temperature and pressure. Boiling may occur at progressively shallower depths along the path from point B to D. At point D the salinity of the liquid will have increased to 10% NaCl. With the low salinities found in the ore vein fluid inclusions, it is probable that fluids which precipitated minerals in these veins had not experienced significant previous boiling. Shallower veins formed from this same ascending fluid should have higher salinities. Such veins have not been found and may have been eroded.

Fluid inclusions which form at point B in Figure 55, from a 5% NaCl solution, have the potential to trap a liquid of 5% salinity, a vapour of very low salinity (< 0.001%), or variable proportions of these two immiscible fluids. Fluid inclusion studies have shown that small amounts of liquid are more commonly trapped with exsolved steam, than are small amounts of vapour trapped with liquid (Roedder, 1984). If a volume of vapour of very low salinity mixed with a relatively minor volume of liquid with a salinity of 5% NaCl, the resulting fluid could have significantly increased salinity from the original vapour while remaining below the critical density, and thus still homogenize to a vapour (all HTG inclusions homogenized to a vapour). As Figure 54 shows, the immiscibility field of the vapour is readily

expanded to higher temperatures due to the increased vapour salinity. The greater the proportion of liquid, the greater the expansion of the immiscibility field.

The addition of liquid to exsolved vapour results in a new isochore with a different position in P-T space. Figure 57 schematically shows the relative homogenization behavior of fluid inclusions of differing densities. At a constant composition, increasing the density of an inclusion fluid results in a lowering of Th. Thus the addition of liquid to an exsolved vapour of the same composition, causes a lowering of Th. The opposite effect on Th is observed if salinity increases while density remains constant. Increasing salinity results in an expansion of the immiscibility field, resulting in a higher Th. The addition of a small amount of liquid to a vapour results in both an increased salinity and density, each tending to shift the Th of the resulting fluid inclusions in opposite directions. The domination of one of these factors over the other is dependent on the proportion of liquid added to vapour.

The first additions of more saline liquid to extremely low salinity vapour results in the most rapid expansion of the immiscibility field, resulting in increased Th values (Fig. 54) even though fluid density is increasing. With greater proportions of added liquid the effect on Th which results from the salinity increase becomes less significant,

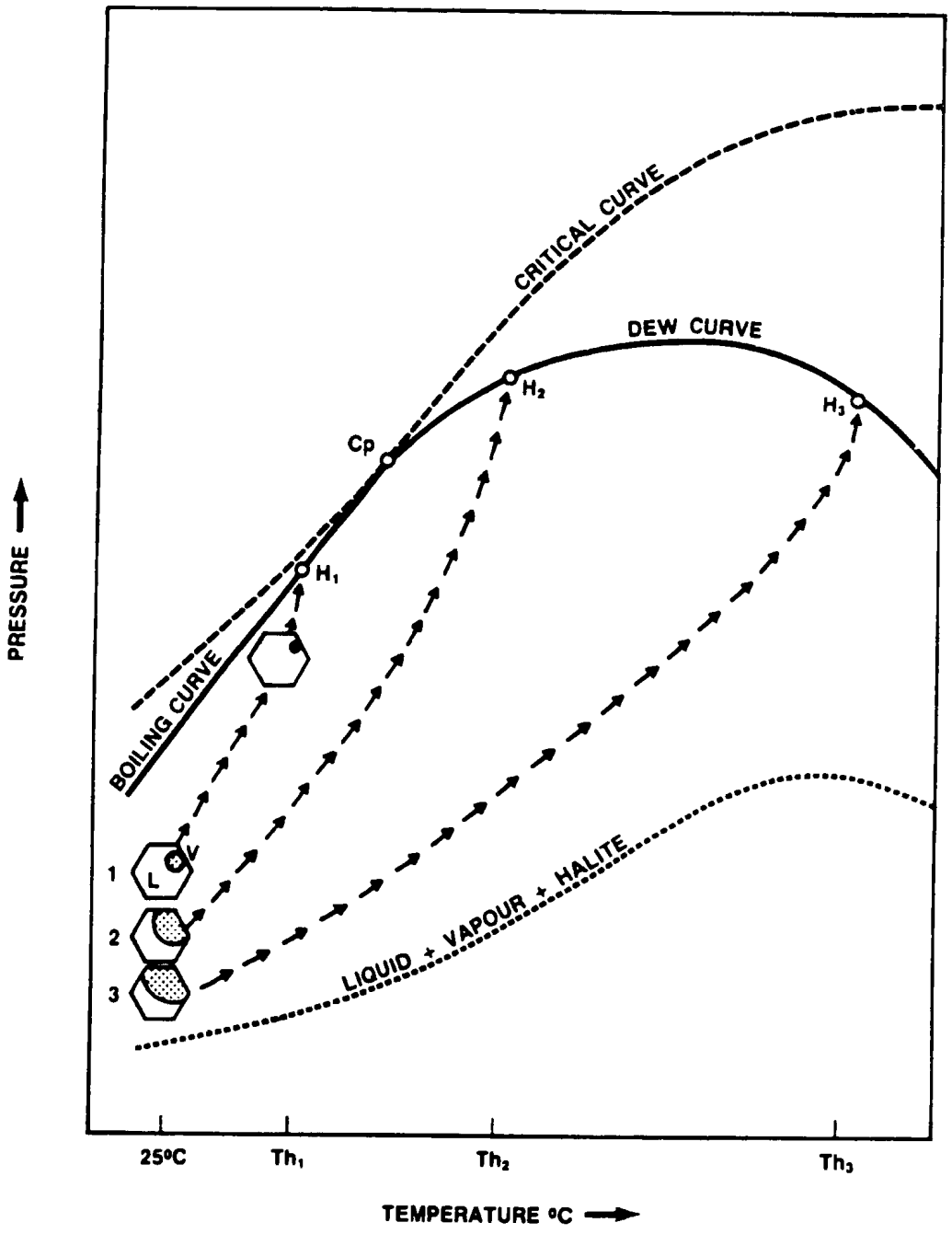

FIGURE 57: SHOWS THE RELATIVE HOMOGENIZATION BEHAVIOUR OF THREE INCLUSIONS OF THE SAME COMPOSITION WITH DENSITITES WHICH DECREASE FROM 1 TO 3.

while the effect of the density increase becomes more significant. Eventually this results in a reversal of the trend to increasing Th values. Further additions of liquid to the vapour-like fluid results in decreasing Th.

The above discussion shows that in inclusions which trap variable yet small proportions of liquid relative to exsolved vapour, such that the effects of increasing salinity dominate over the effects of increasing density, the observed trend in Figure 51 can develop. This is possible if trapping occurs in a boiling system. Thus in Figure 51, inclusions of the HTG which have the highest vapour contents and the lowest Th values, have formed by trapping of the highest proportion of vapour and the lowest proportion of liquid. Those which have the lowest vapour contents and the highest Th values are considered to have trapped the lowest proportion of vapour and the highest proportion of liquid.

The HTG of fluid inclusions have probably formed by trapping of exsolved vapour with variable proportions of higher salinity liquid in a boiling system. The LTG has probably formed by trapping liquid over a range of temperatures. There exists a distinct gap between the two groups of data. This gap has probably developed as a result of a minimum amount of liquid which ends up trapped in the vapour rich inclusions. This has the effect of raising the Th of the HTG by a minimum amount above the actual trapping

temperature. This also implies that there must also be a maximum amount of liquid which gets trapped with the vapour, or again there would be a continuum observed the Th data from the LTG to the HTG. The above explanation for the gap which exists between the LTG and the HTG suggests that boiling was occurring at 370°C, where the gap begins. Inclusions of the LTG which homogenized at or near this temperature, may have trapped liquid which was boiling. Possibly these higher temperature inclusions of the LTG have trapped small amounts of vapour and thus homogenize at a temperature slightly higher than that of trapping.

The range of temperatures over which boiling could have taken place is restricted by the limited range of salinities found in these fluid inclusions. With 370°C as the maximum temperature of boiling, a fluid with the highest observed salinity of 7.4 wt. % NaCl(eq) boils at about 200 bars (Fig. 56). At the same pressure, boiling of a fluid with the lowest observed salinity of 2.0 wt. % NaCl(eq) would take place at 364°C. Thus assuming that the observed salinities are representative and that pressure was constant (Fig. 50 suggests pressure was constant), boiling would have occurred over a limited range of temperatures between 364° and 370°C.

If pressure was not constant, trapping of fluid inclusions could have taken place at lower temperatures. For example, if the pressure in the fluid due to lithostatic

or hydrostatic load is 150 bars, fluid trapping at a constant pressure would take place along the line E-F in Figure 55, and boiling of a 5% NaCl solution would occur at about 345°C. However, this solution could also boil at 370°C, without developing salinities above the observed salinities, if over-pressures in the range of 50 bars were to develop such that boiling at 370°C occurred near point B. Thus the observed salinities allow the possibility of about 50 bars of over-pressure development. If there was over-pressure development the lack of deviation in Figure 50 suggests that it remained relatively constant during LTG fluid inclusion formation.

An estimate of the maximum pressure of trapping in these inclusions (lithostatic + hydrostatic) is attained by plotting the maximum possible temperature of boiling (370°C) and the lowest possible salinity (pure water) on Figure 56. This yields a pressure of 210 bars which is the upper limit for the pressure of formation of fluid inclusions in the Silver Cliff mine. An estimate of the minimum pressure of trapping is attained using the measured maximum salinity of 7.5 wt. % NaCl(eq) and a minimum boiling temperature of 364°C, resulting in a pressure of 180 bars (Fig. 56). It is unlikely that the lowest observed salinities boiled at the highest observed temperatures (and visa versa), thus the actual range between the maximum and minimum pressure is likely much less (i.e., 190 to 200 bars). The likely

maximum pressure of 200 bars corresponds to a depth of about 800 metres if the pressure is purely lithostatic, or about 2000 metres if the pressure is purely hydrostatic. The minimum pressure of approximately 190 bars corresponds to a depth of 760 metres and 1900 metres for lithostatic and hydrostatic pressure respectively.

For fluid inclusions which trapped boiling fluids such as those at the high temperature end of the LTG, the Th is the trapping temperature. However for those inclusion fluids which were trapped above their immiscibility fields, their Th would be lower than their trapping temperatures (Fig. 55). Using boiling curves for saline solutions, constructed by Haas (1971), it is possible to estimate the trapping temperature of fluid inclusions, if the fluid salinity, trapping pressure and the Th are known. To estimate the trapping temperature of the lowest temperature inclusion in Figure 49 (230°C), an isochore is drawn in Figure 55 such that it intersects the 5% NaCl immiscibility surface at 230°C, and has a slope which is estimated from the neighbouring determined isochores (Potter and Brown 1977). Isochores for three different densities of a 5% NaCl solution are shown. The trapping temperature is attained from the point where the constructed 230°C isochore intersects the estimated trapping pressure (i.e., ~ 200 bars). The inclusions which homogenized at 230°C would have been trapped at a temperature of 230° + T°C (≈14°C) =

244°C. The major assumption in this procedure is that the pressure of trapping of this fluid is the same pressure at which the higher temperature fluids boiled.

Temperature corrections to determine trapping temperature from Th are commonly made using the curves developed for the H_2O-NaCl system by Potter (1977). To use these curves, the fluid salinity and the pressure of the fluid during inclusion formation must be known. These curves only work for inclusions which homogenize to a liquid and contain only H_2O and NaCl.

Figure 58 shows the curves developed by Potter (1977), for a 5% NaCl solution. For a pressure of 200 bars (20 MPa) and a Th of 230°C, the temperature correction is 15°C, which is 1°C higher than was determined using Figure 55. The inclusion in Figure 49 which homogenized at 230°C, was probably trapped near 245°C. At 300°C the temperature correction is 10°C, while at 350° it is 8°C. The inclusions which homogenized at 370°C do not require a temperature correction, because they were boiling.

It is apparent from Figure 55 that the temperature correction curves of Potter do not work for all of the data in Figure 49. For inclusions which fall on the line A-B in Figure 55, close to the point of boiling (B), their isochores will obviously intersect the immiscibility field at a temperature closer to the trapping temperature. As the point of boiling is approached the Th must approach the

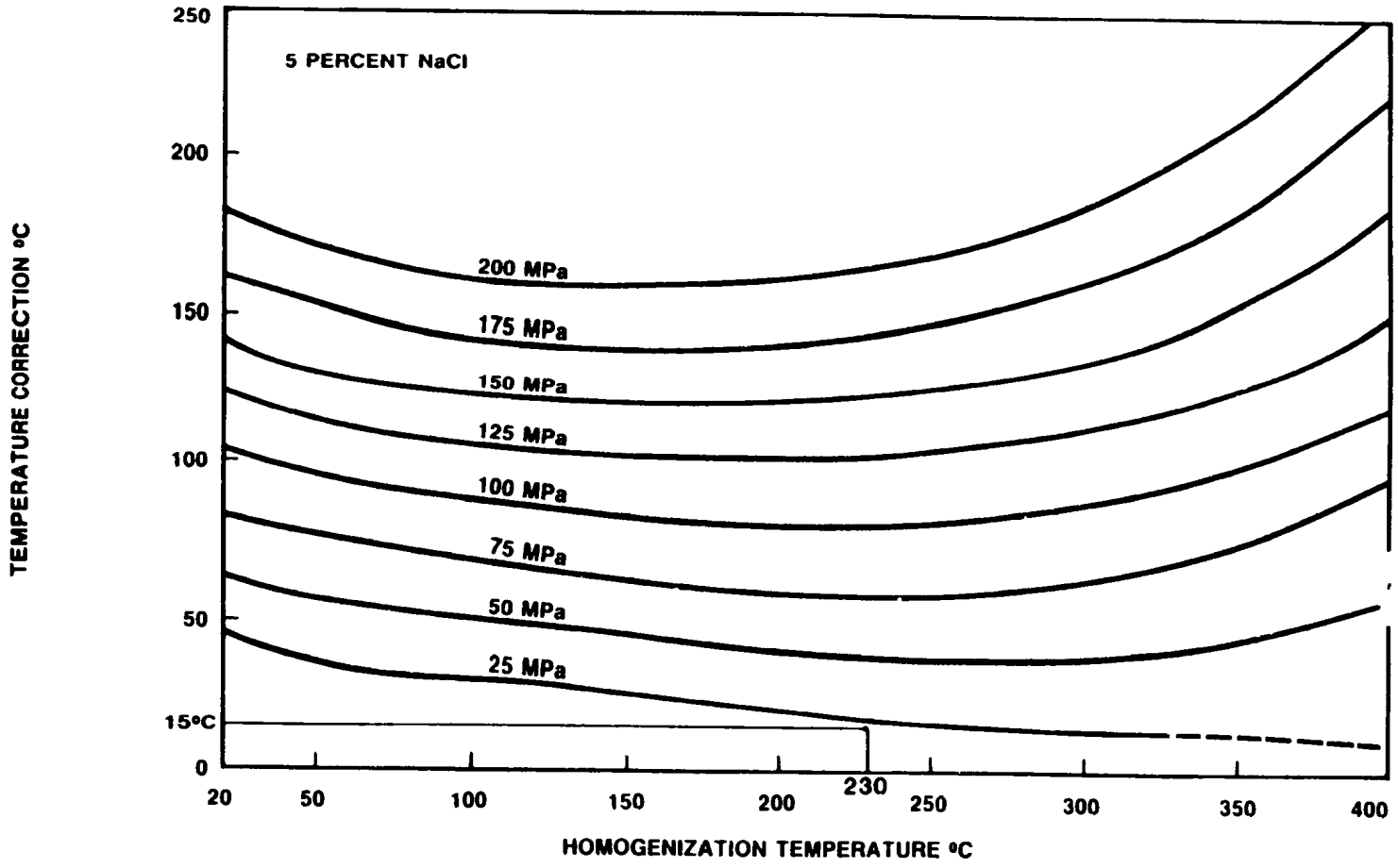

FIGURE 58: TEMPERATURE CORRECTION FOR 5-PERCENT NaCl SOLUTION AS A FUNCTION OF HOMOGENIZATION TEMPERATURE AND PRESSURE. FROM POTTER (1977).

trapping temperature. Thus the curves of Potter (1977) are not useful for inclusions which formed near their immiscibility surface.

The temperature-corrected data indicate that quartz precipitation in late stage veinlets, which cut across the Mackay vein, has taken place over a temperature range from about 245° to 370°C. The temperature data from the primary fluid inclusions found in one sphalerite sample indicate that sphalerite precipitation took place over a temperature-corrected range of at least 285° to 310°C. More sampling is necessary to obtain a more accurate temperature range.

Figure 59 shows the Th data from two barren quartz veins (AR2-A and AR20-A) and one barren quartz-calcite vein (AR1-B) found in the Silver Cliff mine area. Veins AR1-B and AR2-A are located approximately 1500 metres from the mine, while the vein AR20-A is situated about 100 metres from the mine on surface. Measured salinity values range from 0.0 to 4.8 wt. % NaCl(eq) with the average at 1.8%. The Th values range from 180° to 330°C, with a peak at about 255°C. These Th values overlap with those of the LTG ore veins. All of these inclusions homogenized to a liquid.

Figure 60 shows Th Vs EVC at room temperature for these three veins. The B1, B2 and BC inclusions (Fig. 59) are from the same vein. The B2 inclusions are from early-formed quartz which has co-precipitated with chlorite (Fig. 12) before calcite precipitation took place. Th values

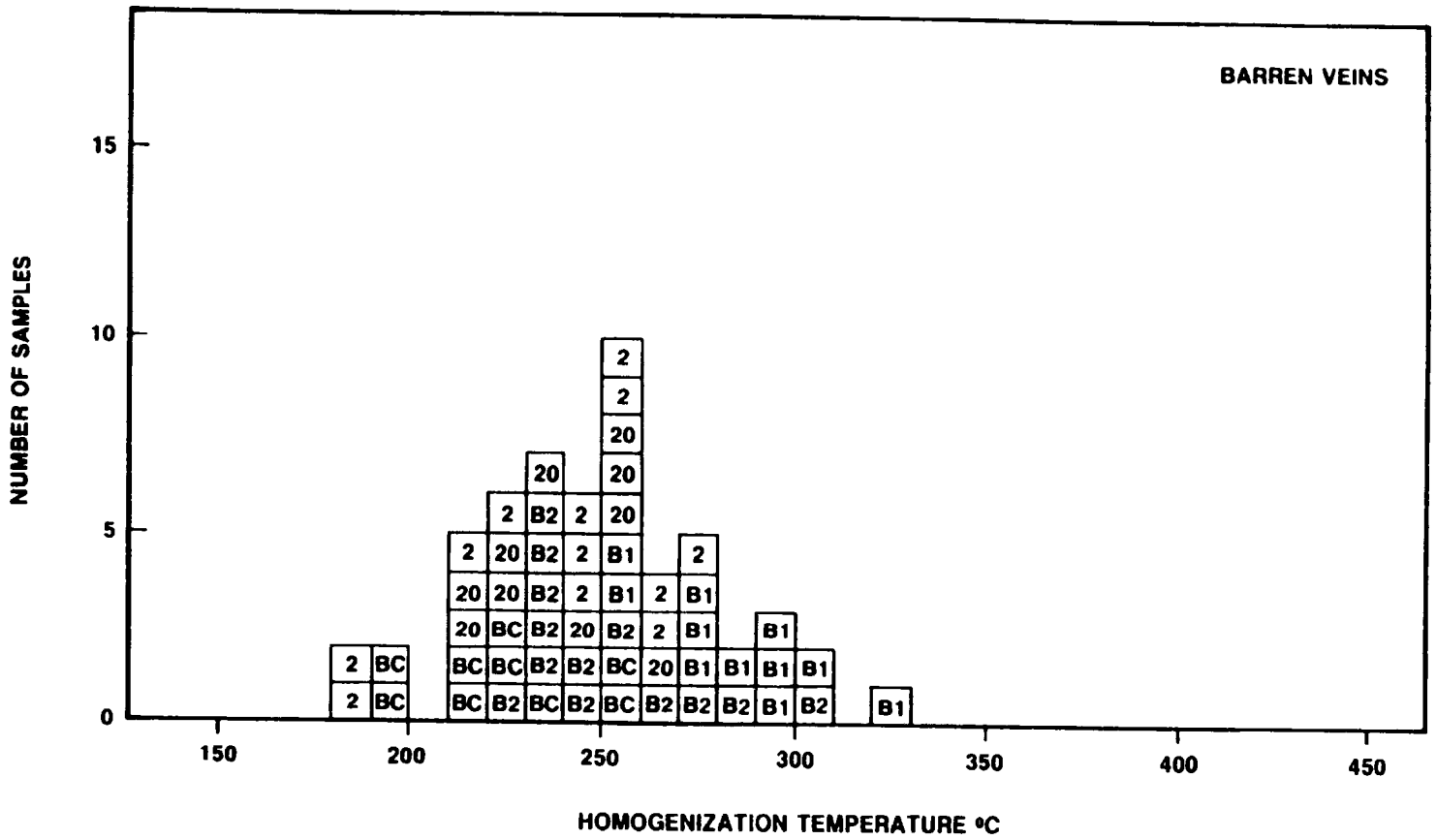

FIGURE 59: HISTOGRAM OF HOMOGENIZATION TEMPERATURE DATA FOR BARREN VEINS IN THE AREA OF THE SILVER CLIFF MINE. BC AR1-B2 (CALCITE), 2 AR2-A, B1 AR1-B1, B2 AR1-B2, 20 AR20-A.

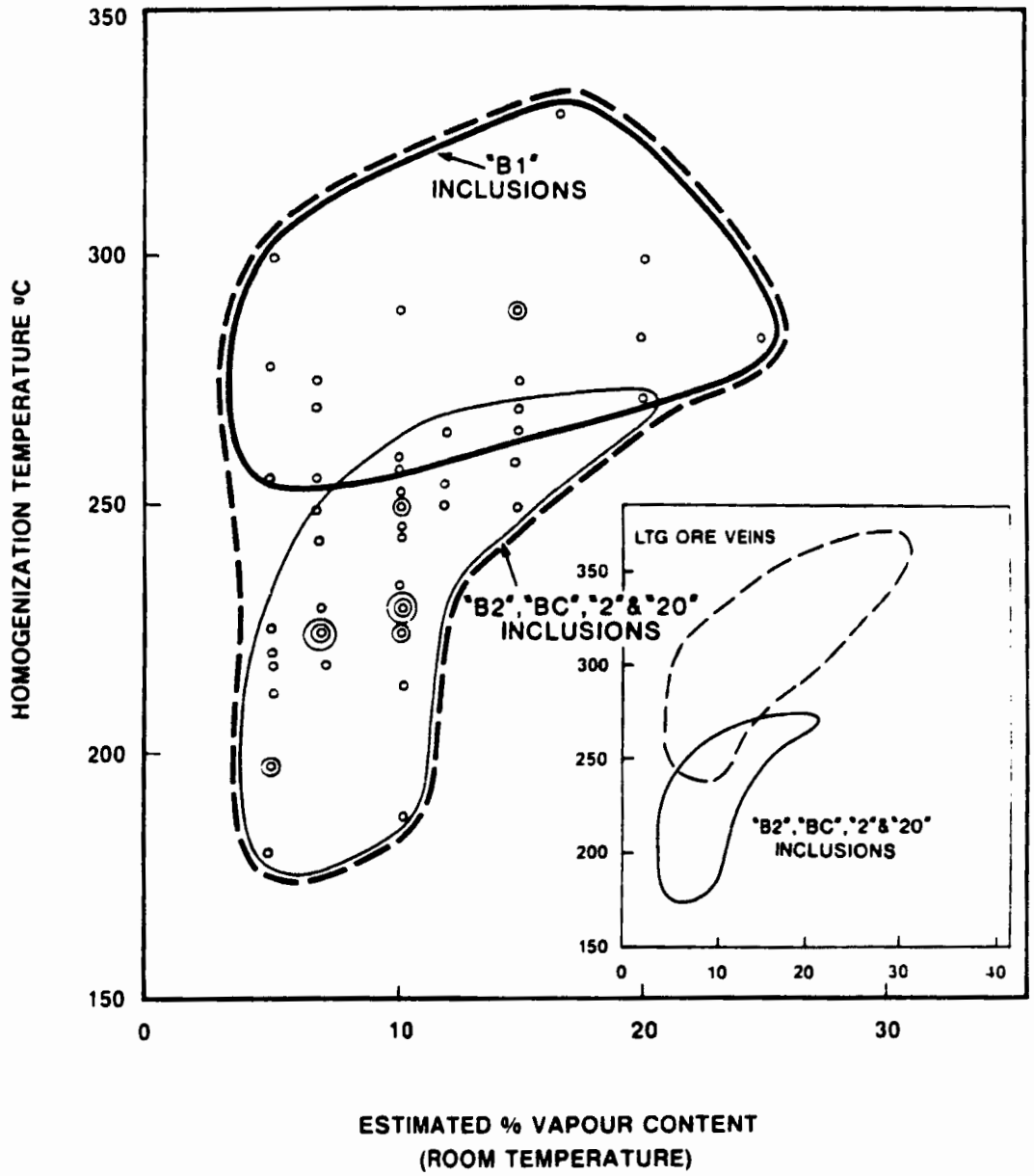

FIGURE 60: COMPARISON OF HOMOGENIZATION TEMPERATURES VERSUS ESTIMATED VAPOUR CONTENT FOR ORE AND NON ORE VEINS AT SILVER CLIFF. REPEATED VALUES ARE CIRCLED.

range from 235 to 300°C for these early-formed inclusions. The B1 inclusions are situated in the latest-formed quartz found in this vein, which has co-precipitated with and formed later than calcite. These later-formed inclusions are hotter with Th values ranging from 255 to 330°C. The BC inclusions are psuedosecondary inclusions found along fractures in calcite (described above) and their origin will be discussed below. The B2 inclusions overlap in Figure 60 with the BC, 2 and 20 inclusions. The 2 and 20 inclusions are from monomineralic quartz veins which are cogenetic with quartz-chlorite precipitation (see chap. 2).

Excluding the B1 inclusions, the remaining data in Figure 60 form a curve which is steep at low temperatures and flattens at higher temperatures. This trend which was predicted earlier from Figure 52 did not show up on the Th Vs EVC plot for the LTG ore vein data (Fig. 50) due to the lack of low temperature data. Down temperature steepening of the data trend is well exemplified in Figure 60 due to the greater abundance of low temperatu e data. The insert in Figure 60 shows the outlines of Th Vs EVC data for both the LTG ore veins and non-ore veins at Silver Cliff (B1 inclusions excluded, ore vein data outside the 95 percentile contour of Fig. 50 alsc excluded).

The flattening trend displayed by the non-ore vein data clearly occurs at a much lower temperature than for the LTG ore vein data. This suggests that the LTG ore veins

formed at a higher pressure and therefore possibly at a greater depth. This results in the trapping of higher density fluids in inclusions which move along a higher pressure isobar in Figure 52. Vein AR1-B (B1, B2 and BC inclusions), and vein AR2-A both occur about 1300 metres higher in the stratigraphy than the ore veins in the mine. However, vein AR20-A occurs lower in the stratigraphy than the ore vein, thus ruling out the use of stratigraphy as an indication of depth of vein formation. The similarity of the data for the B2, BC, 2 and 20 inclusions suggest that they formed at about the same pressure. This suggests that the present relative positions of the veins may be similar to that which existed at the time of vein formation. If this is correct there must have been an overpressure development at the time of formation of the B1 inclusions. The overlap of the B1 data with the LTG data suggests that this overpressure persisted and stabilized during precipitation of the LTG ore veins. The B1 inclusions may have recorded the pressure increase from lower-pressure non-ore veins up to the higher pressure ore veins.

Over-pressure development arising from the boiling process is unlikely. The exsolution of a lower density vapour requires a volume increase for the mass of fluid which becomes vapour. Continued boiling can build up fluid pressure only if vapour release by the boiling process exceeded vapour dissipation by the upward bouyant motion of

vapour bubbles out of the area of boiling. However in doing so the pressure build up moves the fluid to the edge of the immiscibility field (i.e., upwards in Fig. 55) such that boiling would slow down considerably. Boiling would then take place only at the rate allowed by the dissipation of pressure due to the buoyant rise of vapour bubbles out of the zone of boiling. It is unlikely that any significant build up of overpressure can develop from the exsolution of vapour during boiling as it is a self-defeating process.

Another possible mechanism for increasing the pressure during the B1 inclusion formation might be a shift to a greater degree of lithostatic pressure during this phase of quartz precipitation. As earlier described, the formation of the B1 inclusions was contemporaneous with or occurred after calcite deposition in the vein. Factors controlling calcite precipitation are discussed in Chapter 4. Rapid calcite deposition during boiling off of CO_2 gas may have filled fractures faster than they were opening, resulting in plugging of the hydrothermal system. Pressure in the hydrothermal fluid may then have increased having gained a lithostatic component, putting an end to boiling. During such an event the volume of fluid moving through the rock would be a greatly reduced. Fluid inclusions formed in quartz which precipitated during this phase of increasing pressure could produce the pattern observed for Th vs. EVC for the B1 inclusions seen in Figure 60.

Over the range of temperatures indicated from Figure 60 for the formation of the B1 inclusions (255°C to 330°C plus a pressure correction), quartz is more soluble in H_2O as pressure increases (Fig. 61). The increase in pressure caused by plugging of the hydrothermal system would act to reduce quartz precipitation. However falling temperature is the dominant factor controlling quartz precipitation at these pressure-temperature conditions. Precipitation of quartz should proceed even in a plugged system as long as significant cooling of the fluid was occurring.

The remaining question is the absence of CO_2 in these inclusions found in quartz, as would be expected had these inclusions formed in a boiling system. Kerrich et al. (1986) found a similar lack of CO_2 in fluid inclusions in quartz crystals which have co-precipitated with calcite. They explained that the absence of visible CO_2 in quartz inclusions must reflect its essentially complete removal from the hydrothermal fluid before trapping. This they explain by CO_2 effervescence from the hydrothermal fluid during pressure release caused by faulting and fracturing. CO_2 effervescence results in an increased fluid pH, which in turn promotes carbonate precipitation (discussed in chap. 4). Effervescence of CO_2 could thus explain the proposed rapid precipitation of calcite and plugging of the hydrothermal system. All CO_2 is removed from the fluid by effervescence and by calcite precipitation. Subsequent

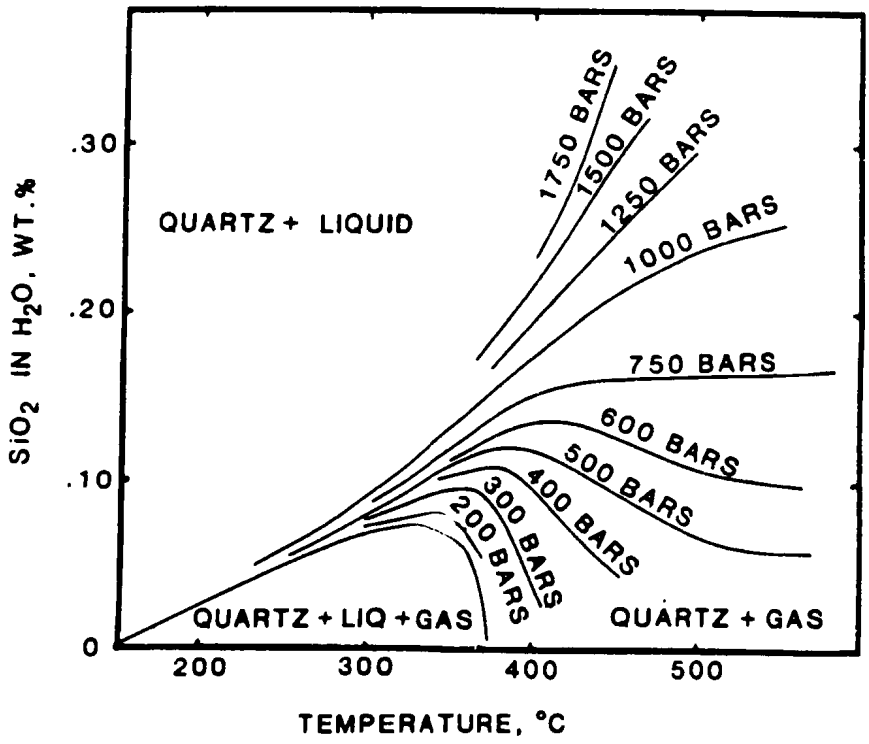

FIGURE 61: SOLUBILITY OF QUARTZ IN WATER (FROM KENNEDY, 1950).

precipitation of quartz in the remaining pore volume would then occur at a higher pressure as indicated by "B1" inclusions in Figure 60, and would be devoid of CO_2. This would also coincide with the formation of the ore veins, also at a higher pressure. Faulting and fracturing was certainly taking place in the field area during vein formation (chap. 2) and may have contributed to, or have been the dominant control in CO_2 effervescence (by sudden pressure release). However it is felt that these processes are not absolutely necessary to cause CO_2 effervescence in these veins. Simple pressure decrease due to fluid ascent in the crust can result in the boiling off of CO_2, similar to the processes described for boiling and formation of the HTG inclusions in Figure 49.

The B1 inclusions, which formed later in the vein paragenesis than the other inclusions in Figure 59, indicate that a fluid which was both higher in temperature and capable of calcite precipitation, passed through the vein. Carbonate is a gangue mineral in the Silver Cliff mine. It is probable that the passage of fluids, from which calcite precipitated in the barren veins, is contemporaneous with carbonate precipitation in the MacKay vein.

The BC inclusions found along fractures in calcites have formed at temperatures and pressures similar to the early-formed quartz (B2, 2 and 20 inclusions) as indicated by the overlap of data points in Figures 59 and 60.

However, calcite is paragenetically later than this quartz. It is therefore believed that these psuedosecondary inclusions formed after all mineral precipitation in this vein was complete and the over-pressure which had developed during formation of the B1 inclusions had dissipated. This pressure dissipation may have been aided by the same fracturing event which resulted in the development of the psuedosecondary fluid inclusions in calcite.

3.5. Fluid Inclusions in Quartz-Chlorite Veins

Figure 62 shows Th data for primary fluid inclusions found in undeformed quartz crystals of the quartz-chlorite veins which occur throughout the field area. Most of the data ranges between 110° and 230°C, with a pronounced peak at 165°C. Above 230°C the data occur discontinuously up to 320°C. From 320° to 370°C there is no data. Above 370°C is a group of sporadic data which reaches up to 470°C.

The salinity of these fluid inclusions ranges from 0.0 to 3.0 wt. %, and averages 0.6 wt. % NaCl(eq). Obtained Te values ranged from 0.0° to -9.0°C. These inclusions may contain variable amounts of KCl forming a solution with a Te of -10.6°C. As with the veins in the Silver Cliff area, NaCl may be present but because of low salinities, the first melt possibly was not detected until temperatures were significantly higher than the Te. NaCl was determined to be the salt most likely present in fluids from which the barren

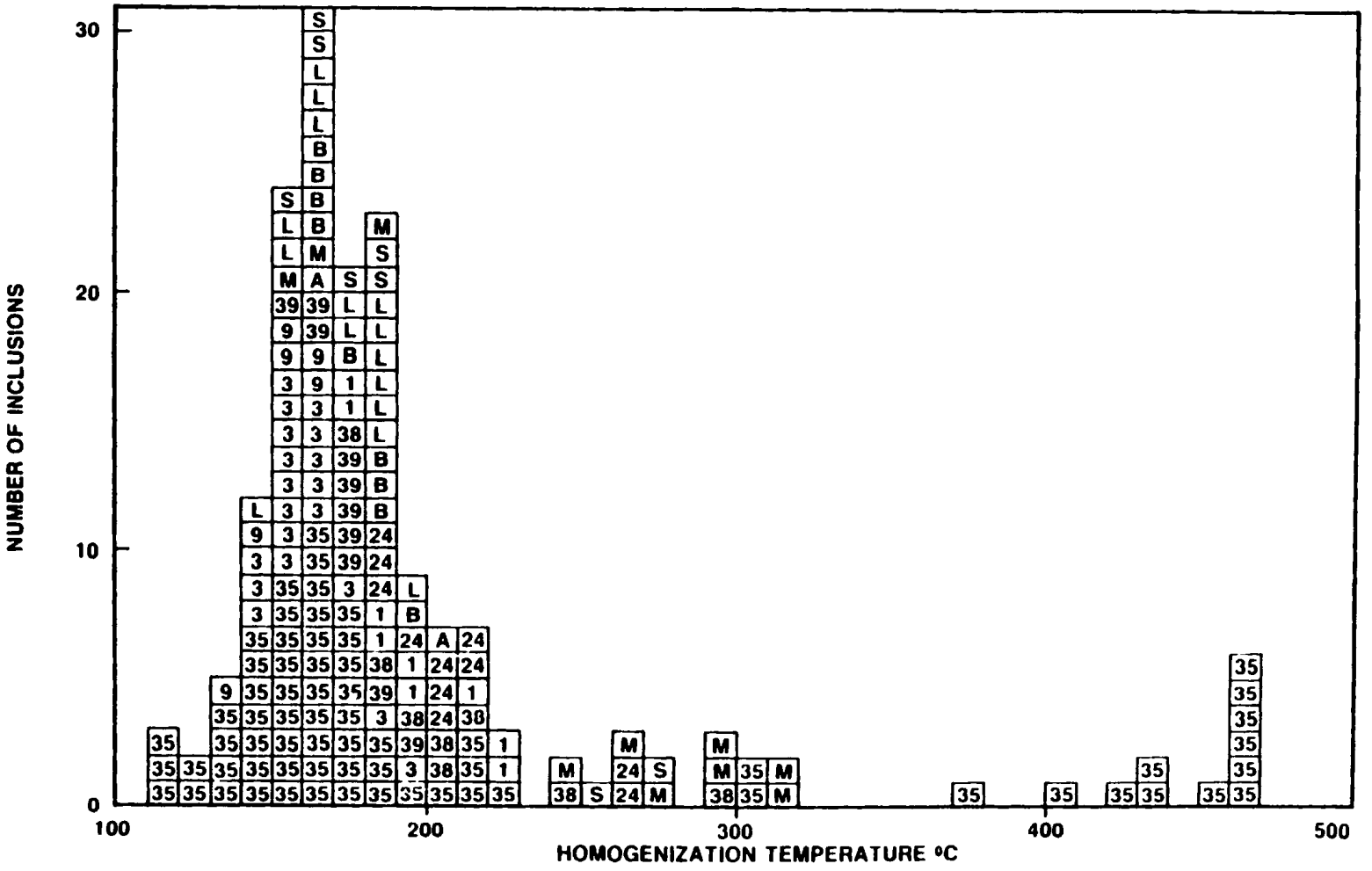

FIGURE 62: HISTOGRAM OF HOMOGENIZATION DATA FROM THE QUARTZ-CHLORITE SET OF VEINS. 1 BV1-K, 3 BV3-C and BV3-D, 9 BV9-D, 24 BV24-B, 35 BV35-C, 38 BV38-A, 39 BV39-A, A QV11-A, B QV11-B, L QV11-L, M QV11-M, S QV11-S.

veins at Silver Cliff were deposited. It is thus most likely the salt present in fluids from which quartz-chlorite veins were deposited throughout the field area.

The large data peak occuring between 110° and 230°C (uncorrected for pressure) indicates the temperatures of precipitation of most quartz in the quartz-chlorite veins. Similar to the AR1-B quartz-chlorite vein at Silver Cliff (discussed above), a late pulse of fluid has passed through some of these veins, depositing late calcite and barite and forming fluid inclusions in quartz with higher Th values. BV24-B is a quartz-chlorite-calcite vein found on Bellevue Peninsula, along with other barite and calcite veins. In BV24-B euhedral quartz crystals are surrounded by later calcite. Th data from BV24-B fall within the main data peak and also in a small data cluster between 240° and 320°C. QV11-M, QV11-S, BV35-C and BV38-A are quartz-chlorite veins found on Collier Point, where several barite and calcite veins occur (e.g., large BV11 barite vein). QV11-M and S both contain minor amounts of late-formed barite. BV35-C and BV38-A each contain late-formed calcite. Th values from each of these four veins fall in both the main data peak and in the small cluster of data between 240° and 320°C.

In BV35-C, higher temperature inclusions occur in the outer growth zones of two quartz crystals. This included inclusions with Th values between 370° and 470°C, with those above 420°C homogenizing to a vapour. Figure 63 shows shows

a poor negative correlation (r = -.41) between Th vs EVC at room temperature for BV35-C vapour rich inclusions. By excluding the one data point at 80% vapour and 450°C the value of r = -.71. There is no visually apparent reason for excluding the data from this inclusion. It is impossible to completely rule out leakage by visual observation. Possibly leakage has affected this one inclusion without leaving a leakage trail. If there is a significant negative correlation between Th and EVC for primary fluid inclusions in BV35-C, it is the same trend observed for vapour-rich inclusions found in the ore veins in the Silver Cliff mine.

Vapour-rich inclusions in BV35-C are interpreted, similar to vapour-rich inclusions in the Silver Cliff mine, to have trapped variable proportions of coexisting vapour and liquid in a boiling system. The two higher temperature inclusions which homogenized to liquid at 373° and 401°C may have trapped enough liquid to have a density greater than the critical density for their composition. The temperature of boiling in BV35-C is not as well defined as it is in the late vienlets of the MacKay vein due to the sparsity of data. However, there is a similarity in the data between Figures 62 and 49. At Silver Cliff it was determined that boiling occurred at the maximum temperature of the LTG, just below the temperature gap which separates vapour-rich from vapour-poor inclusions. Using a similar argument, boiling may have occurred in BV35-C just above 300°C. The two

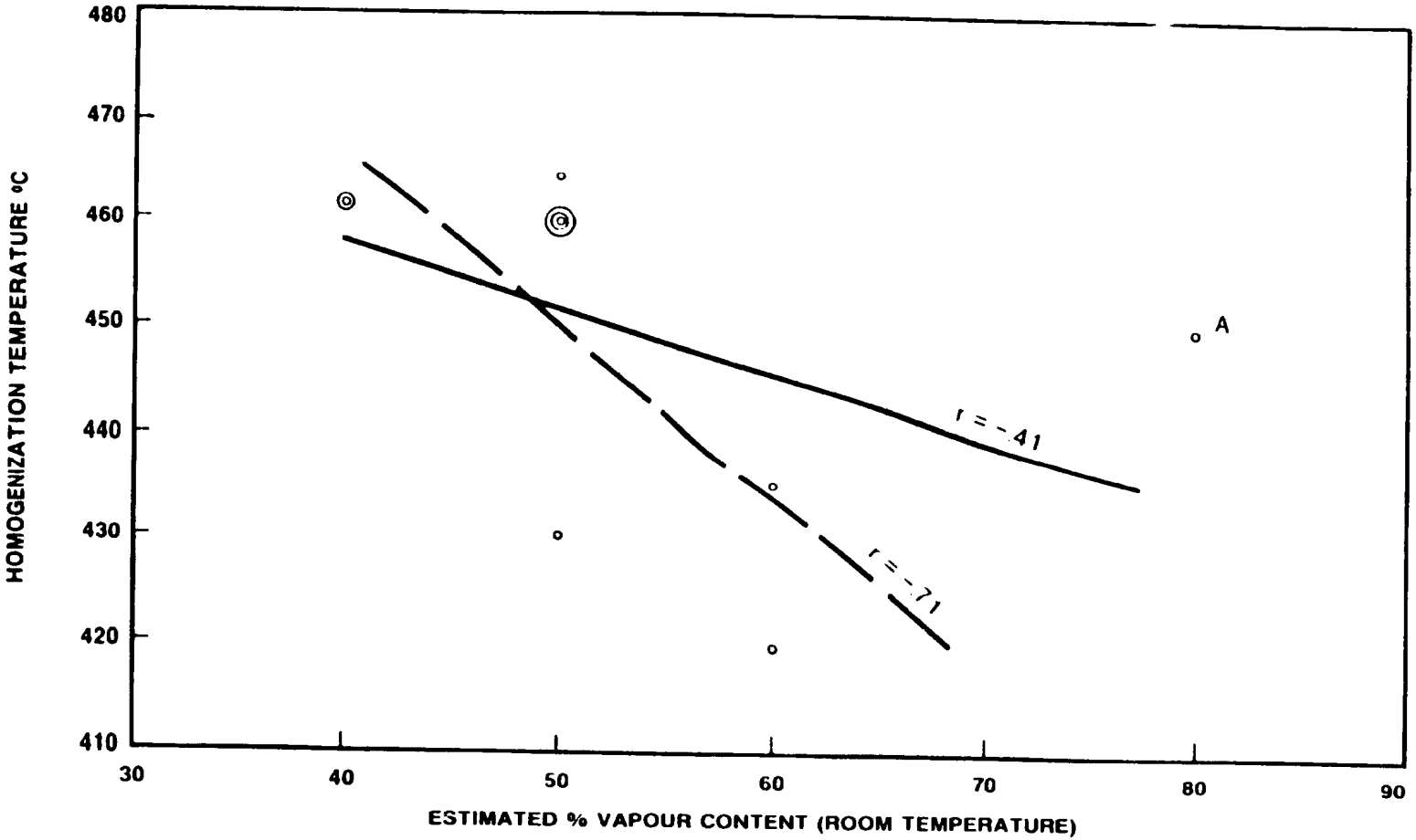

FIGURE 63: SHOWS THE NEGATIVE CORRELATION BETWEEN HOMOGENIZATION TEMPERATURE AND ESTIMATED VAPOUR CONTENT, FOR VAPOUR RICH INCLUSIONS OF BV35-C. COINCIDENT VALUES ARE CIRCLED. BEST FIT LINES BY LINEAR REGRESSION. DASHED LINE IS BEST FIT EXCLUDING DATA POINT "A"

inclusions that homogenized to a liquid just above 300°C represent trapped liquid of the boiling system.

The salinity of one inclusion from BV35-C, which homogenized near 300°C, was determined to be 1.0 wt. % NaCl(eq). The boiling curve for pure water is very similar to that of a 1.0% saline solution at 300°C and thus can be used to estimate trapping pressure. Figure 55 shows that boiling of pure H_2O at 300°C occurs at 80 bars, coinciding with depths of 320 and 800 metres for lithostatic and hydrostatic pressure respectively. Using a Th of 165°C (temperature mode in Figure 62) the temperature correction for these non-boiling fluid inclusions, containing a 1% NaCl solution at 80 bars, is 10°C, indicating trapping at 175°C.

3.6. Summary

Using paragenetic data from Chapter 2, and the fluid inclusion evidence presented above, several conclusions can be made about the formation of veins in the field area.

Quartz-chlorite veins were deposited earliest with quartz precipitation occurring over a temperature range of 110° to 220°C, from a fluid of essentially zero salinity. Deposition of quartz, calcite and/or barite occurred late in the paragenesis of the quartz-chlorite veins, from a fluid with higher temperatures roughly between 240° and 320°C. This fluid boiled above 300°C at a pressure of 80 bars on Collier Point, indicating depths of 320 and 800 metres for

lithostatic and hydrostatic pressure respectively. This event likely coincided with the formation of calcite and barite veins in the field area.

Calcite and barite likely occur late paragenetically in the MacKay vein (Chute, 1939). Ore formation in the MacKay vein is thus likely earlier than barite and calcite vein formation in the field area. Precipitation of quartz and sulphide minerals occurred between 245° and 370°C, with boiling of ore fluids occurring at 360° to 370°C, indicating a pressure of about 200 bars. This corresponds to depths of 800 and 2000 metres for lithostatic and hydrostatic pressure respectively. Anomalous Th Vs EVC behaviour for fluid inclusions found in barren vein quartz from the Silver Cliff area suggest that plugging of the hydrothermal system may have occurred locally during a phase of rapid calcite deposition. This resulted in a shift to more lithostatic conditions in the field area. Ore fluid salinity ranged from 2.0 to 7.5 wt. % NaCl(eq), and averaged 4.5%.

The highest temperatures found in fluid inclusions from the field area are from ore veins at Silver Cliff. It is interesting to note the close proximity of this "hot spot" to suspected syntectonic granites found on Fox Island and Red Island, to the north and north-west (Fig. 4). These granites, or related unexposed granites, represent possible sources of fluid for the hotter veins in the field area. This will be discussed in more detail in the next chapter.

CHAPTER 4. GEOCHEMISTRY

4.1. Stable Isotopes

Natural variations in ratios of stable non-radiogenic isotopes of an element are related to mass-dependent differences in their nuclear properties which cause a separation (fractionation) of the various isotopes of an element during geochemical processes. Heavier isotopes form stronger chemical bonds which are less easily broken, and lighter isotopes have faster reaction rates due to their lower mass. Both effects lead to isotopic fractionation. Such mass differences are less significant in heavier elements where the mass of one neutron does not significantly increase the mass of the nucleus. Mass fractionation effects are usually considered to be insignificant above mass 40 (Cox et al. 1979).

Understanding of stable isotope variations in nature is dependent upon experimental studies and studies of natural systems. The stable isotopes of hydrogen, oxygen and sulphur in hydrothermal systems have received the most study and are the best understood. Carbon isotope variations in hydrothermal systems have also received much study, but comprehensive experimental data are not yet available.

Isotopic ratios are expressed as a value which is normalized to an internationally agreed standard. For example oxygen isotopic ratios are expressed as follows:

$$\delta^{18}O_{sam} = \frac{(^{18}O/^{16}O)_{sam} - (^{18}O/^{16}O)_{std}}{(^{18}O/^{16}O)_{std}} \times 1000 \text{ ‰}$$

where the standard used is SMOW (standard mean ocean water), and " ‰ " represents the term parts per thousand". For carbon, the term $\delta^{13}C$ expresses the ratio $^{13}C/^{12}C$ in a sample relative to the standard PDB (Pedee Formation belemnite). For sulphur, the term $\delta^{34}S$ expresses the ratio of $^{34}S/^{32}S$ in a sample relative to the standard CD (Troilite, from Canyon Diablo meteorite).

4.2. Oxygen and Carbon Isotope Study of Vein Calcites

Calcite crystals were hand picked from samples of quartz-chlorite ± calcite veins and barite ± calcite ± quartz veins. These crystals were screened microscopically to remove visible impurities. Six fine-grained samples were checked for purity by X-ray diffraction analysis resulting in the exclusion of one sample.

Carbon and oxygen isotope ratios in calcites were determined at the University of Waterloo. Carbon and oxygen as CO_2 were extracted from calcite samples by treatment of the calcite with 100% phosphoric acid at 50°C using a method modified from McCrea (1950). $\delta^{13}C$ and $\delta^{18}O$

were then determined directly using a semiautomated V. G. Micromass 903 triple-collecting mass spectrometer. Analytical uncertainty is less than $\pm$ 0.2 ‰ for $\delta^{18}O$ and $\pm$ 0.1 ‰ for $\delta^{13}C$.

On the basis of isotope and REE (Rare Earth Element(s)) data presented in Table 4-1 (discussed below), two groups of geochemically distinct calcites have the following characteristics: group A) $\delta^{18}O$ values from 11.5 to 12.1 ‰, variable $\delta^{13}C$ values from -4.9 to -15.1 ‰, low REE abundances, variable CeN/YbN (N - normalized) ratios and positive Eu anomalies discussed below; group B) higher $\delta^{18}O$ values from 14.5 to 17.3 ‰, a restricted range of $\delta^{13}C$ values from -10.8 to -8.2 ‰, REE abundances which range from under 10 to over 1000 times chondrite, positive correlation between CeN abundance and CeN/YbN ratio and moderate to slight negative Eu anomalies.

The veins of these two groups are geographically interspersed. Most of the veins in group B are greater than 15 cm wide, with the exception of the last three veins listed in Table 4-1, each of which is about 10 cm wide. All of the veins of group A are less than 5 cm wide with the one exception of vein BV8 which occurs about 3 km north of the La Manche vein. This 15 cm wide barite-galena-calcite vein contains calcite from both group A and B. BV8-A calcite is from the vein margin, whereas BV8-Z

TABLE 4-1. OXYGEN AND CARBON ISOTOPIC DATA & REE DATA FOR VEIN CALCITES
REE ABUNDANCES ARE IN PPM

	$\delta^{18}O$ ‰	$\delta^{13}C$ ‰	Ce	Nd	Sm	Eu	Tb	Yb	Lu	CeN/YbN
GROUP A										
B35-C	11.5	-15.1	5.1	3.6	1.1	1.01	0.24	0.51	0.08	2.5
BV8-A	11.5	- 7.4	18.1	9.0	2.7	16.4	0.52	0.40	0.06	11.5
BV3-A	12.0	- 4.9	36.7	24.3	6.7	3.08	0.98	1.13	0.14	8.2
BV9-C	12.1	-10.0	22.4	14.0	3.3	1.65	0.24	0.10	0.01	57.0
GROUP B										
BV11-A	14.5	-10.8	533	310	86	23.8	16.0	15.9	1.71	8.5
BV11-N	14.6	-10.5	433	257	74	20.5	14.4	16.1	1.66	10.5
BV30-A	15.0	- 9.7	602	382	111	31.9	17.5	10.8	1.18	14.2
BV46-A	15.5	-10.0	197	107	31	9.13	6.66	7.65	0.88	6.5
BV8-Z	15.8	- 9.8	1550	854	195	41.2	23.3	14.2	1.91	27.8
BV12-I	15.8	- 9.9	878	560	130	21.3	17.2	11.1	1.50	20.1
BV11-D	16.2	-10.2	518	292	86	24.5	14.1	12.6	1.56	10.5
BV12-E	16.3	- 9.6	1018	633	142	25.7	17.5	10.2	1.43	25.4
BV12-F	16.4	- 9.7	445	226	60	17.9	11.0	10.9	1.27	10.4
BV12-G	16.5	-10.1	494	342	80	13.7	10.3	6.38	0.85	19.7
BV52-A	16.6	- 8.2	34.7	25.7	7.1	2.13	1.44	1.81	0.20	4.9
BV7-B	17.3	- 8.7	15.7	8.7	2.1	0.54	0.41	0.69	0.11	5.8
BV33-A			22.4	10.9	2.1	0.56	0.34	0.48	0.07	11.9

calcite is later and is intergrown with galena and barite. The presence of both types of calcites in this one vein suggests that analysis of more duplicate calcite samples from these veins might well reveal that calcite from both groups occur in more of the veins. The significance of this will be discussed later.

4.2a. Oxygen

Isotopic exchange between precipitating calcite and the hydrothermal fluid takes place according to the reaction

$$H_2{}^{18}O + CaC^{16}O_3 = H_2{}^{16}O + CaC^{18}O_3$$

with an equilibrium constant of

$$\frac{[CaC^{18}O_3]\ [H_2{}^{16}O]}{[CaC^{16}O_3]\ [H_2{}^{18}O]} = K = \alpha_{cal\text{-}H2O} \text{ (fractionation factor).}$$

This simplifies to

$$\frac{(^{18}O/^{16}O)_{cal}}{(^{18}O/^{16}O)_{H2O}} = \alpha_{cal\text{-}H2O}.$$

Substituting in the expression for $\delta^{18}O$ (previous page) for both calcite and H_2O, the following equation can be derived

$$\delta^{18}O_{H2O} = [([(\delta^{18}O_{cal}/1000) + 1]/\alpha_{cal\text{-}H2O}) - 1]\ 1000.$$

The value of $\delta^{18}O_{cal}$ is known by analysis and the $\alpha_{cal\text{-}H2O}$ value can be calculated from the equations used to

construct Figure 64, if the temperature of calcite formation is known. Using a temperature range of 240° to 320°C, as indicated by the fluid inclusion data discussed above, the possible range of values for $\alpha_{cal-H2O}$ is 1.0077 to 1.0049.

Figure 65 shows the possible range of $\delta^{18}O_{H2O}$ values for the two calcite groups, at both the minimum (240°C) and maximum (320°C) observed temperatures of calcite formation as indicated by the fluid inclusion data. Using any one temperature as the temperature of all calcite formation (for the purpose of discussion), there is a distinct break between the values of $\delta^{18}O_{H2O}$ for the two calcite groups. Over the total range of temperatures the calculated values of $\delta^{18}O_{H2O}$ for both the group A and B calcites overlaps the known isotopic compositional fields for both primary magmatic and metamorphic water. The fluid from which either the group A or group B calcites have precipitated could have formed from a single source or a combination of sources (primary magmatic, metamorphic, meteoric or "exchanged" meteoric water). Figure 65 places several restrictions on possible fluid sources. If group A calcites formed at temperatures closer to 240°C, primary magmatic water is eliminated as a possible single source. If either group A or B calcites formed from a single-sourced fluid, meteoric water is eliminated as a possible

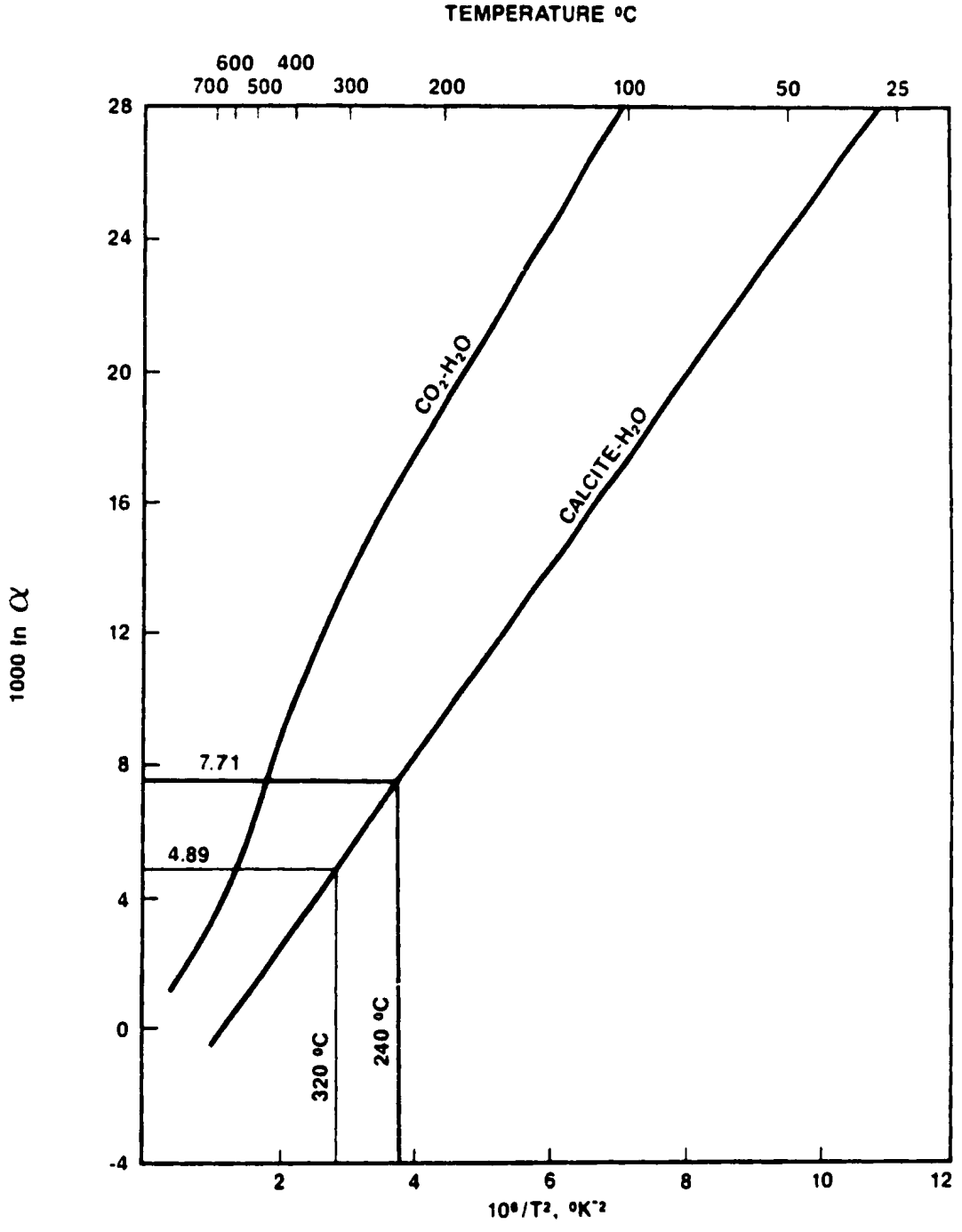

FIGURE 64: EXPERIMENTALLY DETERMINED EQUILIBRIUM OXYGEN ISOTOPE FRACTIONATION CURVES. THE TEMPERATURES OF 240° AND 320° C REPRESENT THE RANGE OVER WHICH CALCITE HAS PRECIPITATED IN THE VEINS AS INDICATED BY THE FLUID INCLUSION STUDY. FIGURE ADAPTED FROM TAYLOR (1979). EQUATIONS USED ARE DISCUSSED IN TAYLOR (1979).

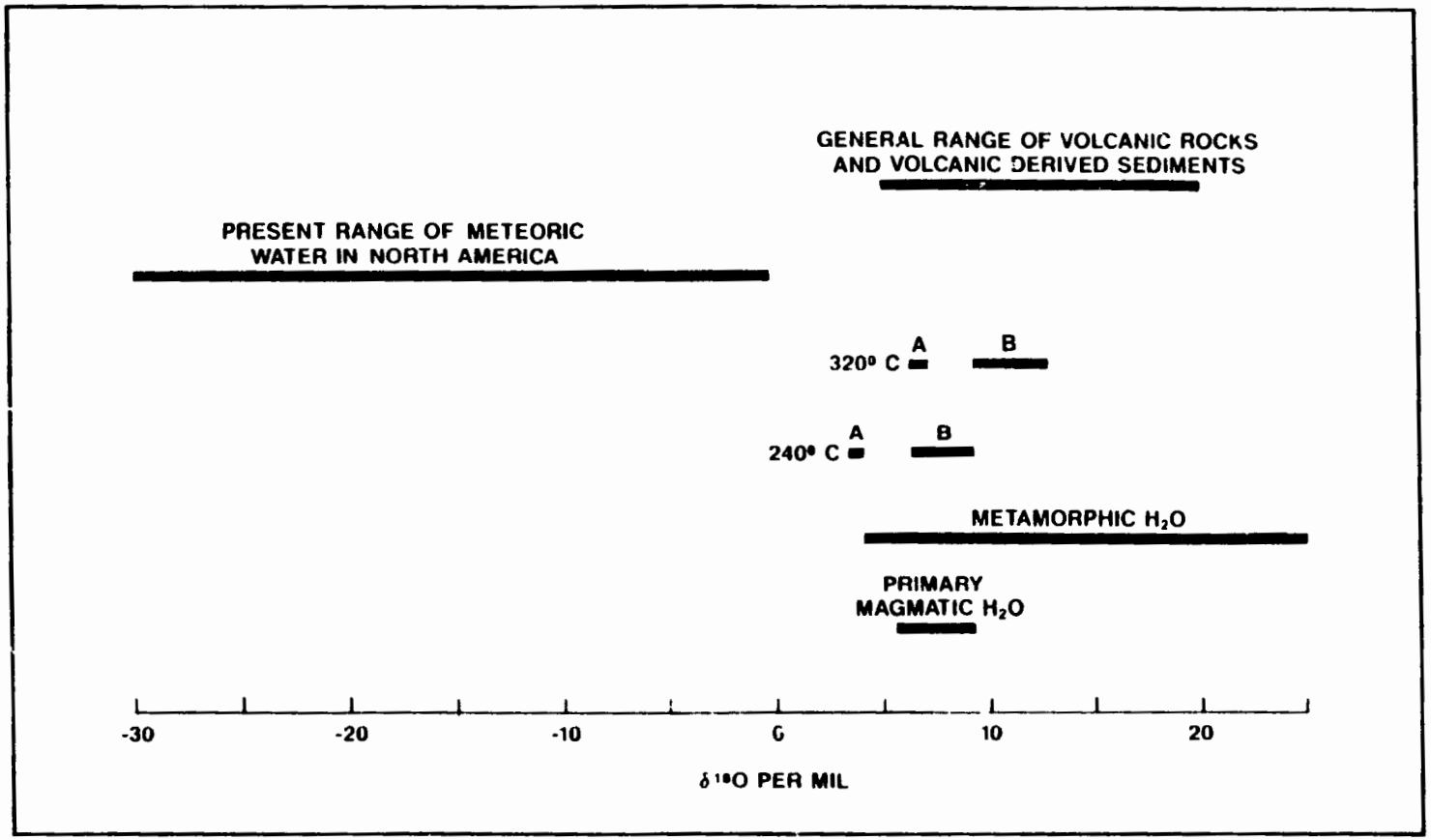

FIGURE 65: RANGE OF $\delta^{18}O$ FOR WATER CO-EXISTING WITH GROUP A AND B CALCITES CALCULATED AT THE MAXIMUM AND MINIMUM TEMPERATURES FOR CALCITE PRECIPITATION INDICATED FROM FLUID INCLUSION DATA. THE RANGE OF $\delta^{18}O$ FOR METAMORPHIC, PRIMARY MAGMATIC AND PRESENT METEORIC WATER, AND OF VOLCANIC AND VOLCANIC DERIVED SEDIMENTS, FROM TAYLOR (1979).

source, unless it had undergone some degree of isotopic exchange with the country rock. Carbon isotope evidence presented below supports the conclusion that meteoric waters, which had undergone a degree of isotopic exchange with the country rock, were involved in the formation of group A calcites. However the carbon isotope and other data presented below do not provide evidence for the involvement of exchanged meteoric water in the precipitation of the group B calcites. This suggests that the group B calcites precipitated from either metamorphic water, primary magmatic water, water which has equilibriated with magmatic rocks or some mixture of these possibile fluids.

Metamorphic and primary magmatic fluids, and fluids which were in equilibrium with magmatic rocks, are all geologically feasible as fluids which may have been sourced in the field area. In Chapter 2, it was established that vein formation took place during Acadian orogenesis, a period of both metamorphism and emplacement of granitoid magmas. Metamorphism of Avalon Zone rocks increases from east to west, reaching mid-greenschist facies (biotite grade) near the Dover fault (Chap. 1). Figure 66 shows that for pelites and greywackes, at low pressures (indicated by the fluid inclusion study, Chap. 3), biotite

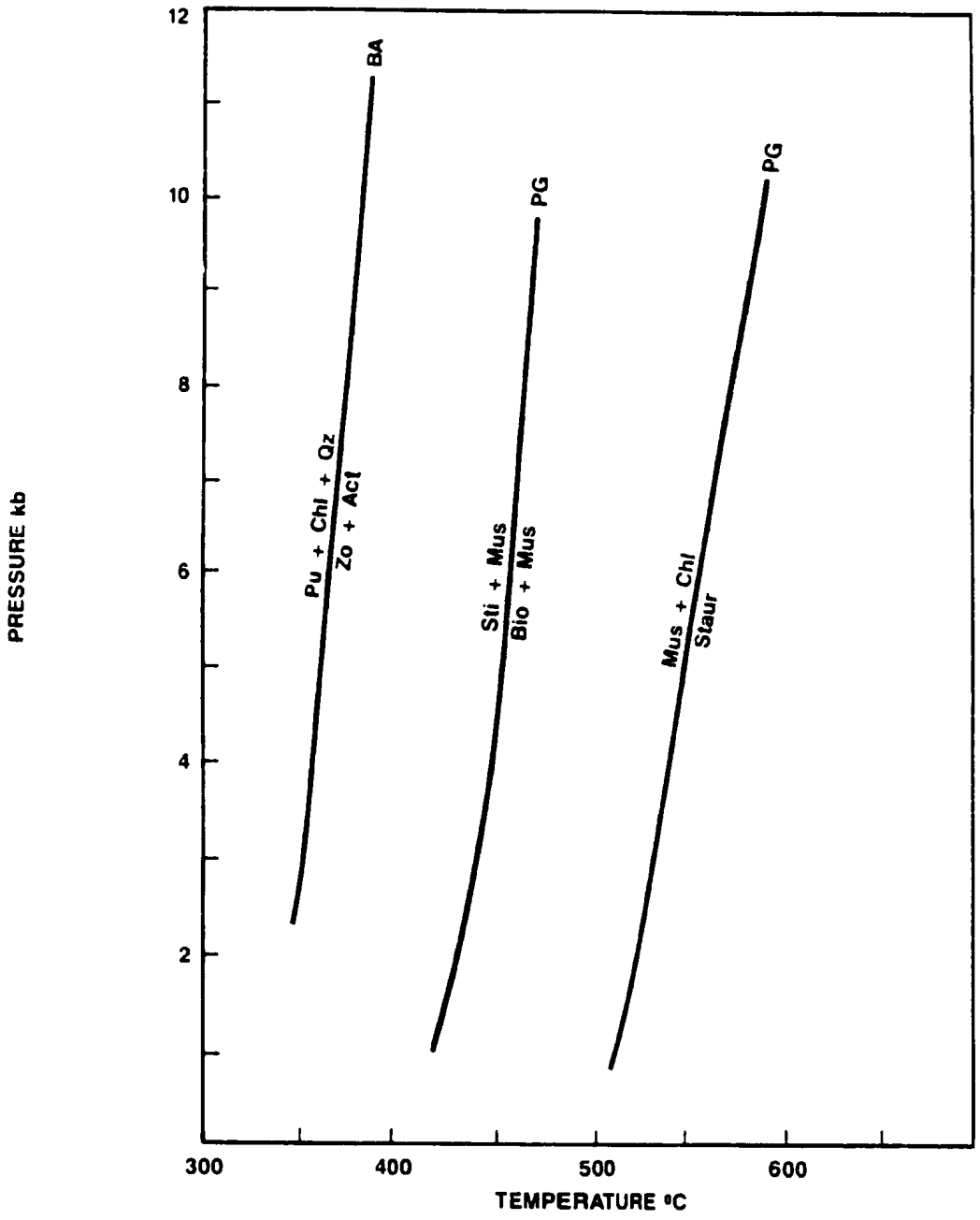

FIGURE 66: SOME LOW GRADE METAMORPHIC REACTIONS WHICH AFFECT PELITES AND GREYWACKES (PG), AND BASALTS (BA). Pu-PUMPELLYITE, Chl-CHLORITE, Qz-QUARTZ, Zo-ZOISITE, Act-ACTINOLITE, Sti-STILPNOMELANE, Mus-MUSCOVITE, Bio-BIOTITE, Staur-STAUROLITE (FROM TURNER, 1968).

grade metamorphism begins just above 400°C. The temperature of metamorphic fluids sourced at the elevation of the present surface in the field area are therefore limited to a maximum temperature of about 400°C. If fluids ascended from deeper rocks, their temperature may have been greater. The maximum temperature of calcite precipitation (320°C, from fluid inclusion data), and even the maximum measured temperature of quartz precipitation in the Silver Cliff mine (370°C), fall within the indicated range of temperatures of metamorphic fluids in the field area.

Metamorphosed sedimentary and igneous rocks tend to retain their original $\delta^{18}O$ values during metamorphism (Taylor 1979). The rock types in the field area are predominantly volcanic rocks, greywackes, arkoses and volcanogenic sediments, which generally have $\delta^{18}O$ values ranging from +5.0 to +13.0 ‰ (Taylor 1979). Water released from these rocks during metamorphism may have $\delta^{18}O$ values close to this range. The values of $\delta^{18}O_{H2O}$ as indicated by the group B $\delta^{18}O_{cal}$ values, also fall within this range. The $\delta^{18}O_{H2O}$ values calculated for the group A calcites falls clearly within this range at the higher temperatures indicated by the fluid inclusion data and fall at the margin of this range at the lower indicated temperatures.

For the range of possible temperatures indicated for calcite precipitation by the fluid inclusion data, it is

not possible for both the group A and group B calcites to have precipitated from fluids of similar $\delta^{18}O_{H2O}$ character. In Figure 65, the lower $\delta^{18}O_{H2O}$ limit of group B calcite at 320°C, is the same as the upper limit at 240°C. It is possible that all group B calcite precipitated from a fluid with a constant $\delta^{18}O_{H2O}$ value of +9.4 ‰ over this range of temperatures. The low $\delta^{18}O_{cal}$ veins of group B would have formed at the highest temperature (320°C), while the highest $\delta^{18}O_{cal}$ veins would have formed at the lowest temperature (240°C). This hypothesis is supported by a similar trend in the $\delta^{13}C_{cal}$ values, as will be described. A fluid with a $\delta^{18}O_{H2O}$ value of +9.4 ‰ is compatible with both a magmatic and a metamorphic source. The limited range of $\delta^{18}O_{cal}$ values in group A calcites indicate a source of limited oxygen isotope variation and a relatively constant temperature. This source must also have had a lower $\delta^{18}O$ character than the source for group B calcites.

To summarize, the oxygen isotope data separate the analyzed calcites into two distinct groups. Group A calcites have precipitated from water of lower $\delta^{18}O$ character than group B. A possible interpretation of the group B data is that the group B calcites may have precipitated from a fluid of constant $\delta^{18}O_{H2O}$ (+9.4 ‰) over a range of temperatures from 320°to 240°C.

4.2b. Carbon

Aqueous carbon species which may be important in hydrothermal fluids are $CO_{2(aq)}$, H_2CO_3, HCO_3^-, CO_3^{2-} and $CH_{4(aq)}$ (Ohmoto 1972). The proportions of these species are controlled by the T (temperature), fO_2 (oxygen fugacity), pH and I (ionic strength) of the hydrothermal fluid. Carbon dioxide is often the most abundant carbon species under conditions of low pH and high fO_2. Carbon dioxide in solution is present predominantly as the CO_2 molecule and partly as the H_2CO_3 molecule. The sum of these two species is commonly expressed as $H_2CO_{3(apparent)}$. Because dissolved carbon dioxide is present predominantly as CO_2 molecule rather than H_2CO_3, the following approximation can be made:

$$\delta^{13}C_{H2CO3(app)} \approx \delta^{13}C_{CO2}$$ (Ohmoto 1972).

Figure 67 shows the fields of dominance for the aqueous carbon species at variable temperatures and pH levels. Over the range of temperatures indicated for precipitation of calcite (240° to 320°C) the CO_3^{2-} field of dominance ends at pH levels below about 11. At lower pH levels which are likely for these veins (discussed below) CO_3^{2-} levels would be insignificant. $CH_{4(aq)}$ is important only under conditions of low fO_2 (i.e., log fO_2 < -38 at 250°C) (Ohmoto 1972). As is demonstrated further on in this chapter the log fO_2 value of the fluid was likely in the range of -32 to -34. CH_4 was thus not likely to have

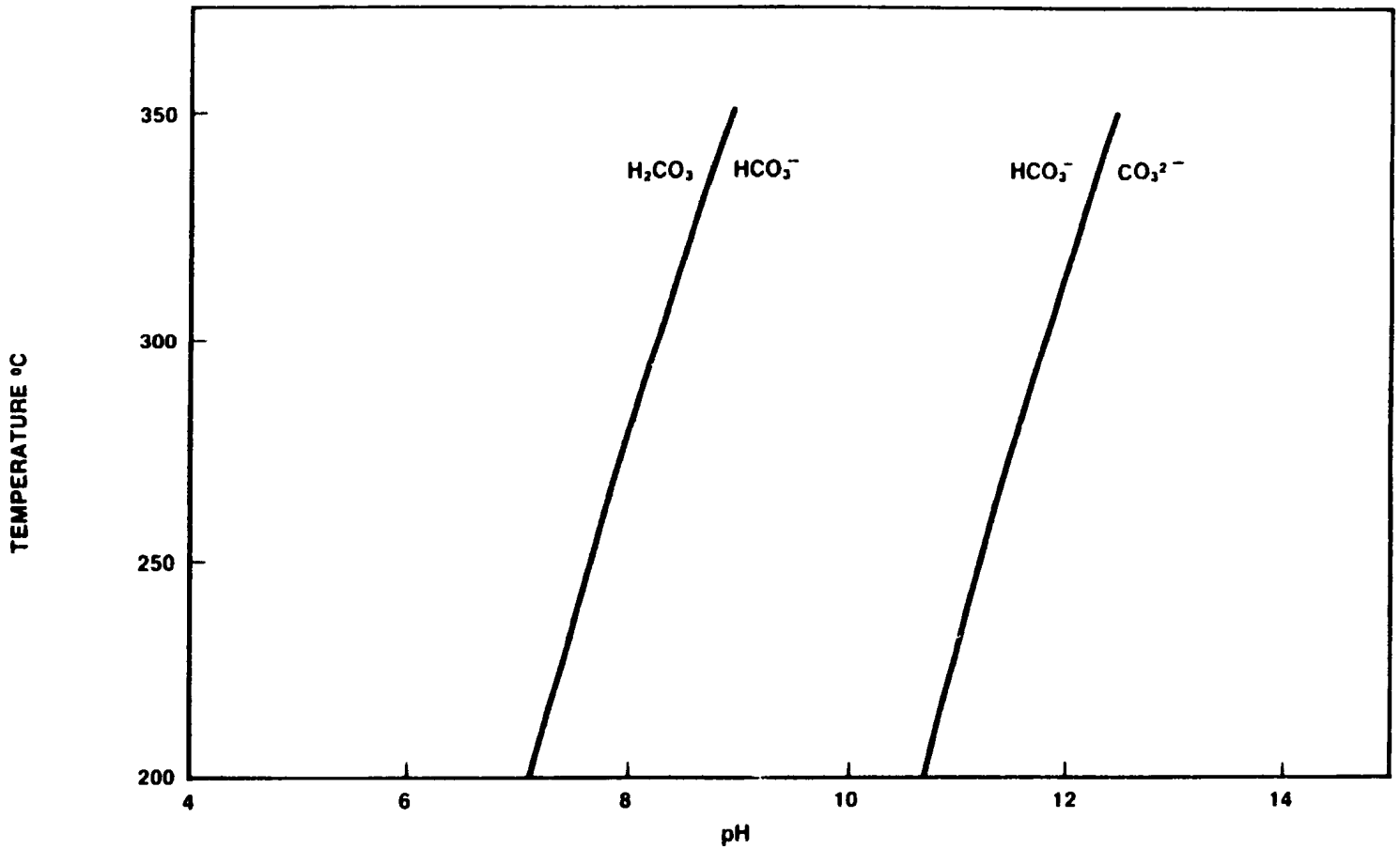

FIGURE 67: CURVES REPRESENT EQUAL ACTIVITIES OF AQUEOUS CARBON SPECIES AND SEPARATE THEIR REGIONS OF PREDOMINANCE (FROM BARNES 1979).

been an important carbon species in the fluid.

The importance of HCO_3^- as a species can be evaluated if the temperature and the pH of the fluid are known. $[HCO_3^-]$ is related to $[H_2CO_{3(app)}]$ by the reaction

$$H_2CO_{3(app)} = H^+ + HCO_3^- \qquad \log K = -7.63 \ (250^\circ C)$$

$$\log K = -8.86 \ (300^\circ C)$$

(Helgeson 1969).

The following equation can be written

$$[HCO_3-] = \frac{[H_2CO_{3(app)}] \ (10^K)}{[H^+]} \ .$$

Table 4-2.

pH	Temp	$[HCO_3^-]$ =
6	250°C	$.02[H_2CO_{3(app)}]$
7	250°C	$.2[H_2CO_{3(app)}]$
6	300°C	$.0014[H_2CO_{3(app)}]$
7	300°C	$.014[H_2CO_{3(app)}]$

As Table 4-2 shows, HCO_3^- becomes an important species in hydrothermal fluids as temperature decreases and as pH increases. Thus at higher temperatures and lower pH values, $[H_2CO_{3(app)}]$ is approximately equal to the sum of all carbon species in the fluid, and therefore

$$\delta^{13}C_{H2CO3(app)} \approx \delta^{13}C_{total\ C}.$$

Isotopic exchange between calcite and $H_2CO_{3(app)}$ in hydrothermal fluid can be described by the equation

$$\frac{(^{13}C/^{12}C)_{cal}}{(^{13}C/^{12}C)_{H2CO3(app)}} = \alpha_{cal\ -\ H2CO3(app)}.$$

The following equation can be derived:

$$\delta^{13}C_{H2CO3(app)} = \left[\frac{[(\delta^{13}C_{cal}/1000) + 1]}{[\alpha_{cal\ -\ H2CO3(app)}]} - 1\right] 1000\ ‰.$$

A similar equation which relates isotopic distribution between the species HCO_3^- and $H_2CO_{3(app)}$ can also be derived. Values of α can be obtained from the equations used to calculate the equilibrium fractionation curves shown in Figure 68. Using these equations and the previously quoted equation relating $\delta^{18}O_{cal}$ with $\delta^{18}O_{H2O}$, the theoretical variation of $\delta^{18}O_{cal}$ with $\delta^{13}C_{cal}$ at changing temperature and pH conditions can be calculated. The two curves in Figure 69 show the theoretical variation in $\delta^{18}O_{cal}$ vs. $\delta^{13}C_{cal}$ which should develop in calcites precipitating at temperatures from 320° to 250°C at a pH of 5.7 and 7.0. $\delta^{18}O_{cal}$ and $\delta^{13}C_{cal}$ data for the group B calcites are also shown in Figure 69. Curve #1 is drawn for all pH values that are low enough at all temperatures

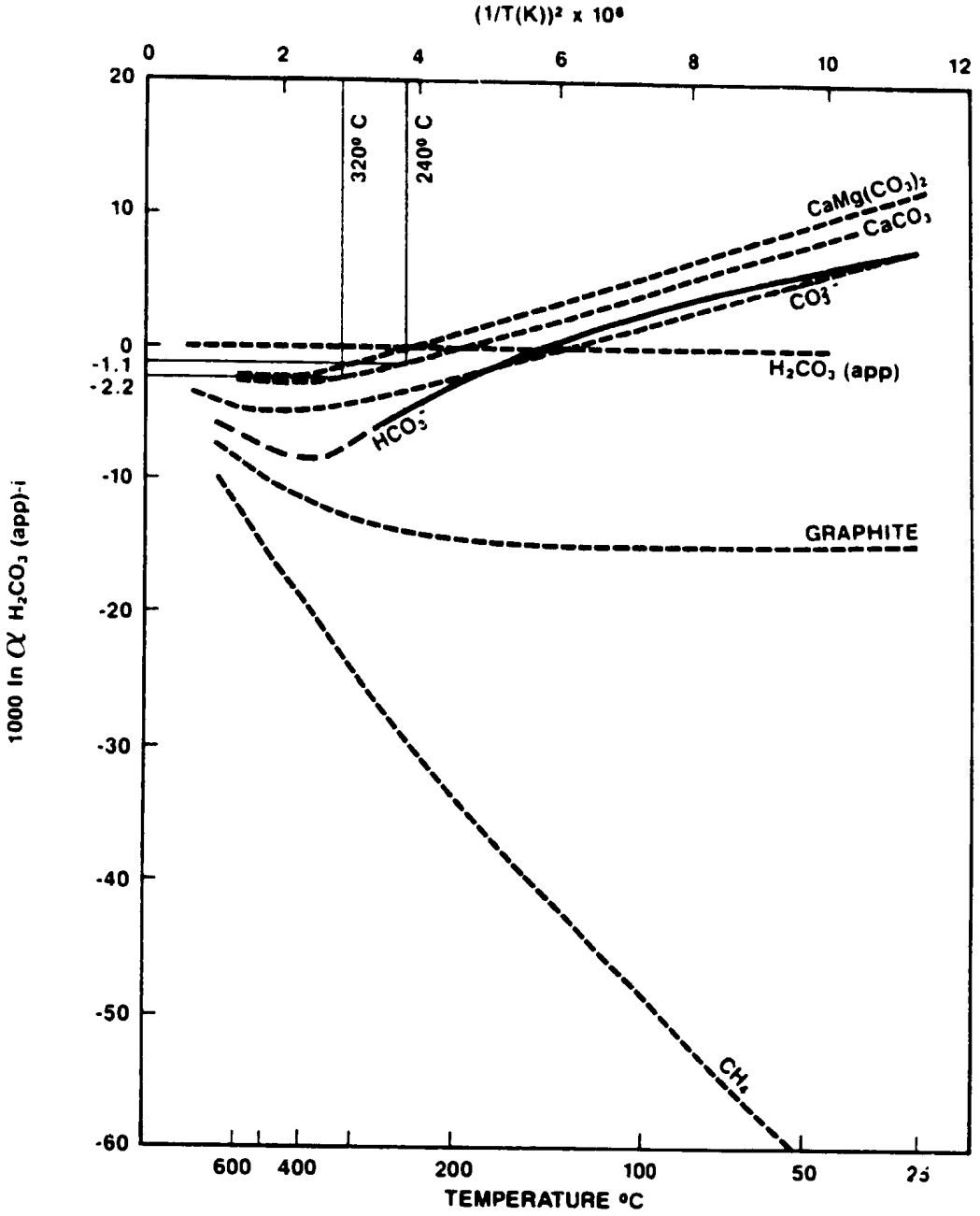

FIGURE 68: EQUILIBRIUM ISOTOPIC FRACTIONATION FACTORS BETWEEN H_2CO_3 (app) AND THE iTH CARBON SPECIES, WHERE H_2CO_3 (app) = H_2CO_3 + CO_2 (aq). ONLY THE HCO_3^- CURVE HAS BEEN PROPERLY EXPERIMENTALLY INVESTIGATED. CURVES FOR OTHER SYSTEMS ARE THEORETICALLY ESTIMATED. FIGURE FROM OHMOTO AND RYE (1979).

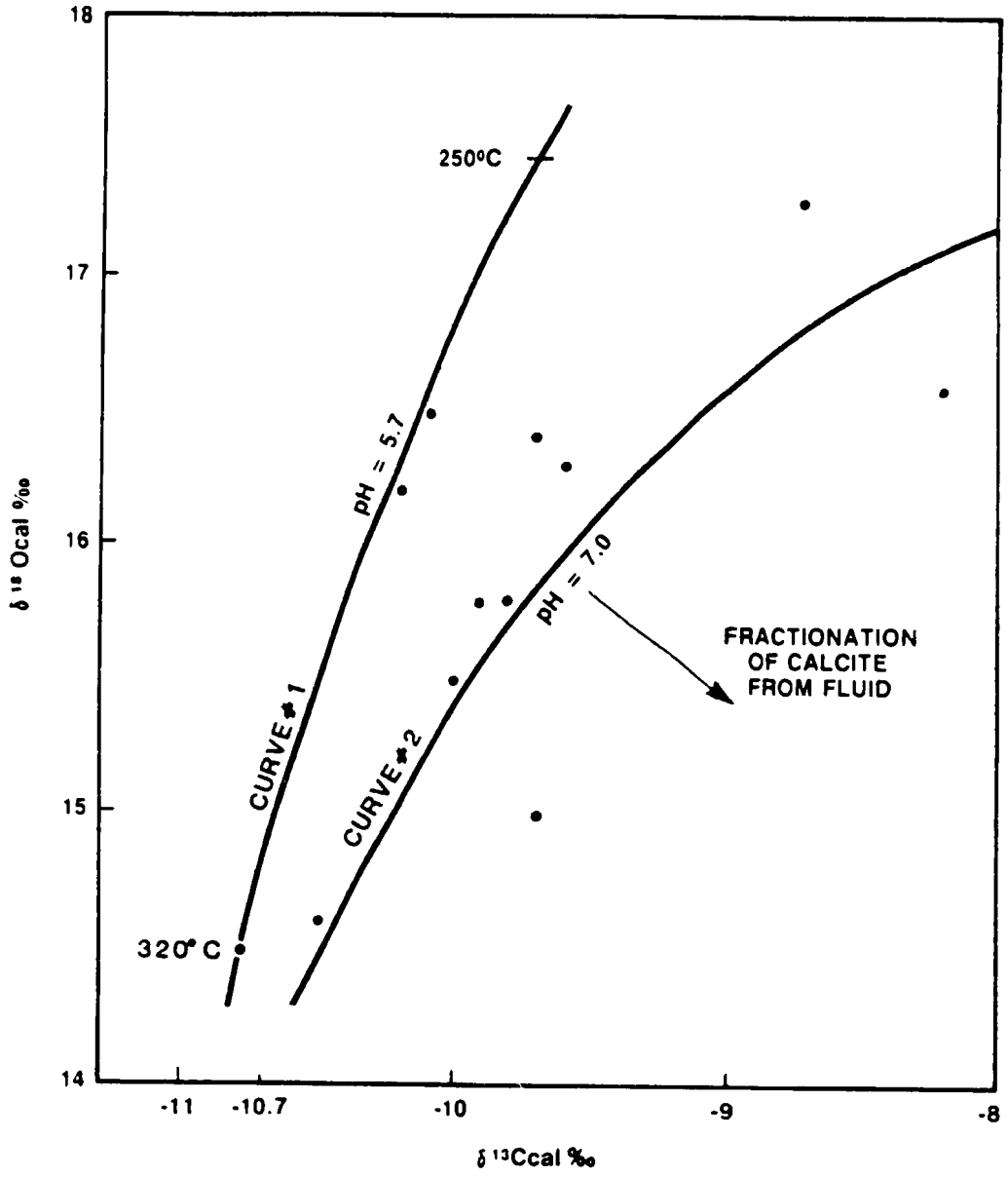

FIGURE 69: **OXYGEN VERSUS CARBON ISOTOPIC RATIOS FOR GROUP B CALCITES. THE TWO CURVES SHOW THE** CALCULATED THEORETICAL VARIATION OF THESE ISOTOPIC RATIOS OVER A TEMPERATURE RANGE OF 250° TO 320°C AT pH = 5.7 AND AT 7.0

considered, such that $[HCO_3^-]$ remains insignificant (at 250°C and pH = 5.7, $[HCO_3^-] = .01[H_2CO_{3(app)}]$). The values of $\delta^{13}C_{total\ C}$ and $\delta^{18}O_{H2O}$ were chosen such that the curve passed through the data point for BV11-E. Curve #2 was calculated using the same values of $\delta^{13}C_{total\ C}$ and $\delta^{18}O_{H2O}$ as for curve #1, but for a pH of 7.0. Either of these two curves can be shifted to better fit the data, without drastically changing the shape of the curve, by varying the starting values of $\delta^{13}C_{total\ C}$ and $\delta^{18}O_{H2O}$. As well, a complete range of intermediate curves exist, representing pH values between 5.7 and 7.0.

Although individual data points will display a considerable amount of deviation from any curve which is calculated to best fit the data, the overall trend of the data more closely matches that of curve #2. Deviation from a single curve may well be due to variation in pH of the hydrothermal fluid. Possibly the higher temperature data for group B fit better with a curve which is closer to curve #1 indicating a lower pH, while the lower temperature calcites may have precipitated from a fluid with a higher pH resulting in a shift to higher $\delta^{13}C_{cal}$ values. Such a shift in pH may be a consequence of falling temperatures, as the dissociation constant of H_2O decreases with decreasing temperature, resulting in a rise in pH.

Precipitation of calcite from the hydrothermal fluid will result in fractionation of both carbon and oxygen

isotopes over the indicated temperature range. However there is no obvious calcite fractionation trend observed in these isotopic data, although some of the variation from the curves of Figure 69 may be due to a subordinate degree of crystal fractionation. One reason for the insignificant amount of isotopic fractionation in these calcites may be that a small amount of calcite precipitation took place relative to the large oxygen and carbon reservoirs in the hydrothermal fluid, composed predominantly of H_2O and CO_2.

The carbon isotope data support the evidence provided by the oxygen isotopes which suggested that the calcites in group B with the lowest $\delta^{18}O_{cal}$ values precipitated at the highest temperature, and those calcites with the highest $\delta^{18}O_{cal}$ values precipitated at the lowest temperatures from a fluid of constant $\delta^{18}O_{H2O}$ and $\delta^{13}C_{total\ C}$ composition.

Using 320°C as a possible temperature of deposition of calcite in sample BV11-E (lowest $\delta^{13}C$ value), and assuming that the value of $[HCO_3^-]$ is insignificant at this temperature, $\delta^{13}C_{total\ C}$ for the hydrothermal fluid is estimated to be -8.6 ‰. Using 240°C as the temperature of deposition for calcite in vein BV52-A (highest $\delta^{13}C$ value) and assuming a pH = 7.0, $\delta^{13}C_{total\ C}$ = -8.1 ‰. These values are within the range of possible $\delta^{13}C_{total\ C}$ values (+2.0 to -10.0 ‰) indicated by Ohmoto and Rye (1979) for magmatic carbon. Other possible sources include fresh

water limestone, organic carbon and reduced carbon in sedimentary and metamorphic rocks.

The Lower Cambrian Smith Point Formation is the only significant limestone unit on the Avalon Peninsula. It is a thin marine limestone found in both the northern (McCartney 1967) and southern (Fletcher 1971) regions of the field area. The carbon isotopic character of the Smith Point formation is unknown, but most marine carbonates, regardless of age, have $\delta^{13}C$ values between -4 and 4 ‰ (Ohmoto and Rye 1979). As Figure 68 shows, isotopic fractionation between calcite and $H_2CO_{3(app)}$ is not sufficient over the temperature range indicated to allow for a marine limestone to be the carbon source for these veins, with the exception of BV3A ($\delta^{13}C_{cal}$ = -4.9 ‰).

Variations in the amount of organic and reduced carbon in sedimentary or metamorphic rocks are expected over the expanse of the field area. This would result in variable $\delta^{13}C_{cal}$ values in veins from different areas, which had an organic or reduced carbon source, as is observed for the $\delta^{13}C_{cal}$ values from the group A calcites. The value of -15.1 ‰ certainly argues for isotopic exchange with a graphitic source for carbon in BV35-C. A likely source for this graphite would be metamorphosed sedimentary rocks in the field area which contain organic carbon, converted to graphite during metamorphism. The limited range in $\delta^{13}C_{cal}$ values for group B calcites (-8.2

to -10.8 ‰) argue against an organic or a reduced carbon source. This suggests that the carbon is most likely of magmatic origin.

In summary, the carbon isotopic data support the oxygen isotope data in separating calcites into two groups. Group A calcites appear to have precipitated from a fluid which has undergone isotopic exchange with sources of differing carbon signature, but which had a relatively constant oxygen isotopic character. Group B calcites have probably precipitated from a fluid of relatively constant oxygen and carbon isotopic composition, over a range of temperature from approximately 240° to 320°C. A magmatic source is indicated for the group B carbon and oxygen.

As described above, the group A veins are thin relative to the group B veins. The rate of fluid flow through these smaller fracture networks would be diminished resulting in longer residence times. Also, the surface area of wall rock exposure per unit volume of fluid is increased. Fluids in these smaller veins thus have more opportunity for contamination by ground water mixing.

4.3. Rare Earth Elements

Rare earth elements (REE) in calcites, and in one dolomite sample (BV33-A), were determined at the University of Waterloo, using Instrumental Neutron Activation Analysis, as described by Hertogen and Gijbels (1971) and Gibson and

Jagam (1980). The REE, La through Lu in group IIIB of the periodic table, typically form trivalent ionic species with ionic radii (1.13 to 0.94 Å) which allows them to substitute for Ca^{2+} (1.08 Å) in calcite. In aqueous solution the REE form complexes with ligands such as OH^-, F^-, SO_4^{2-}, HPO_4^{2-}, HCO_3^-, CO_3^{2-}, etc. The stability of these complexes tends to increase from La to Lu, due to a systematic change in the physical and chemical behavior of the REE. Fractionation of REE may thus result during: hydrothermal fluid formation and solution of REE; interaction of this solution with country rocks during transport; precipitation of minerals containing REE; remobilization and alteration of REE-bearing phases after deposition (Moller and Morteani 1983).

Anomalies in abundances of Ce and Eu found in REE-bearing phases develop when these elements form ionic species other than the trivalent species common to REE. In a fluid with high fO_2, Ce^{3+} will oxidize to Ce^{4+} and will readily be absorbed by any oxyhydrates (e.g., FeO(OH)) encountered during transport, resulting in Ce depletion from the fluid. A Ca^{2+} bearing mineral phase (e.g., calcite) precipitating from a Ce-depleted fluid, regardless of oxidation conditions at the site of deposition, will have a negative Ce anomaly (Moller and Morteani 1983).

Positive Eu anomalies can develop in hydrothermal fluids by alteration of feldspar crystals, which commonly contain a positive Eu anomaly. Ca^{2+}-bearing mineral phases

precipitating from a Eu-rich fluid will develop a positive Eu anomaly only if Eh conditions at the site of deposition are high enough such that Eu^{3+} is the stable ionic species in the fluid. Under reducing conditions, Eu^{2+} is stable and tends not to co-precipitate with other REE, resulting in a negative Eu anomaly (Moller and Morteani 1983).

Figures 70 and 71 illustrate REE patterns from group A and B calcites (data in Table 4-1, REE normalized to chondrite values of Frey et al. 1968). The four group A samples have distinct positive Eu anomalies of variable magnitude which show no correlation to REE abundance or steepness of REE pattern. Group A REE have twice the variation in CeN/YbN ratios relative to group B REE, yet there is no correlation between this ratio and abundances of any of the REE. The only other feature common to group A REE is their relatively low overall abundance, which is similar to calcites with the lowest REE abundances in Group B. Sample BV9-C is exceptional in that it is very depleted in HREE relative to the other three group A samples.

The lack of correlation between group A REE abundances and the steepness of REE patterns suggests that REE distributions in group A calcites were not controlled by a fractionation process, supporting a similar conclusion drawn from carbon isotopic data. From the variable $\delta^{13}C_{cal}$ values it was suggested that group A calcites precipitated from fluids which had reacted with variable host rocks,

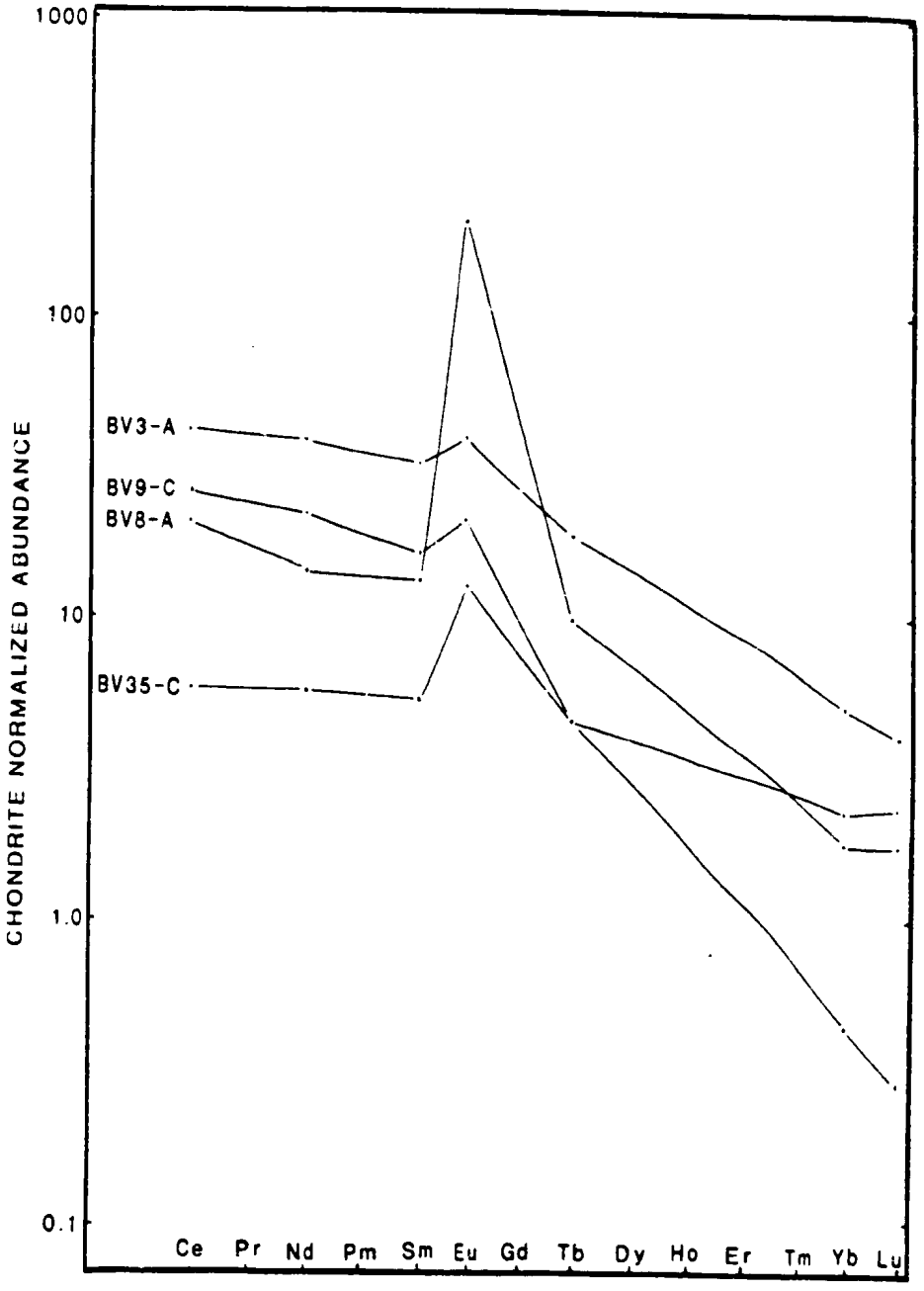

FIGURE 70: REE PATTERNS FOR GROUP A CALCITES.

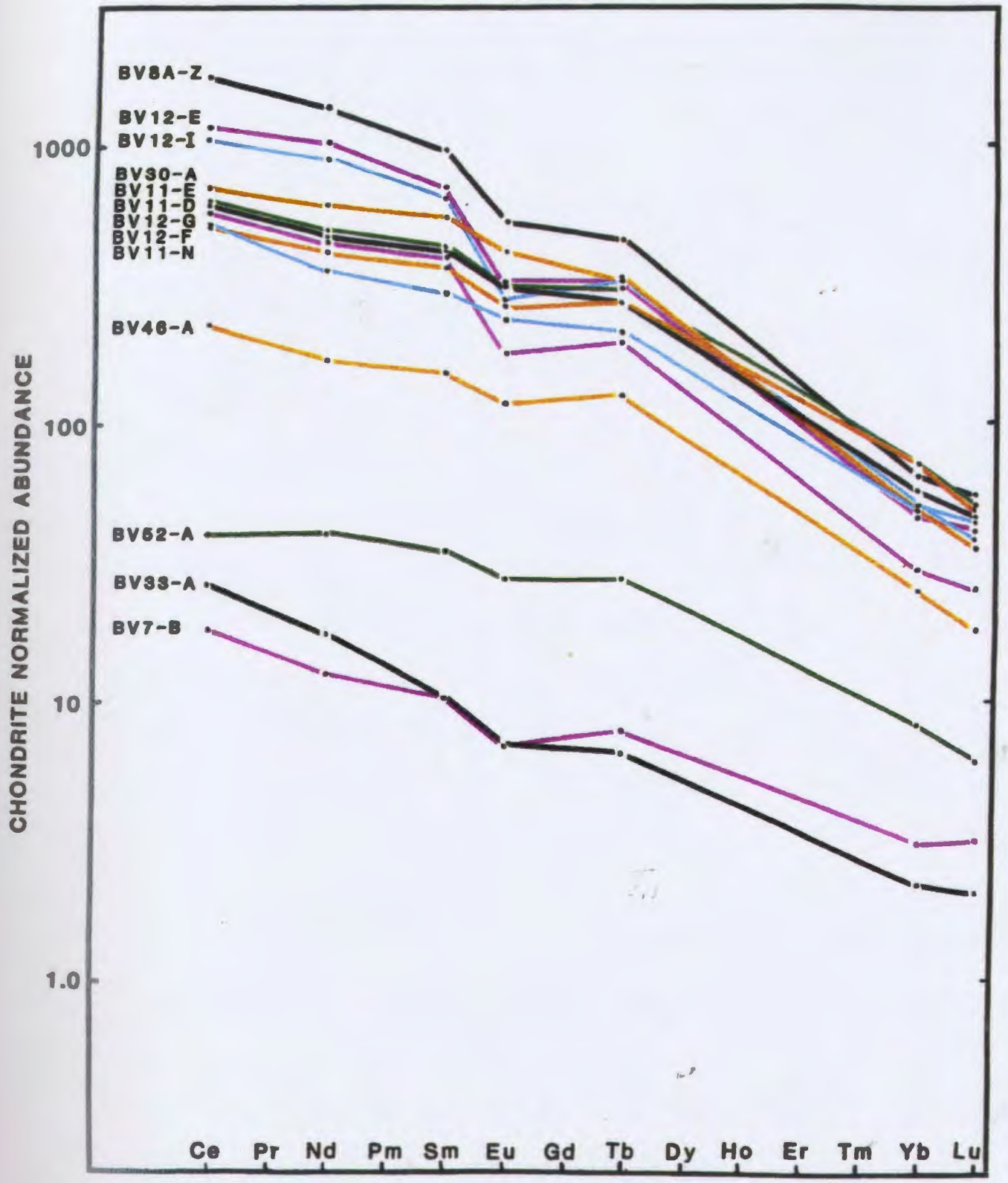

FIGURE 71: REE PATTERNS FOR THE GROUP B CALCITES.

one of which was graphitic. Such reactions may have affected REE abundances in the hydrothermal fluid, which may explain the lack of correlation between CeN/YbN and REE abundance. The vein host rocks are predominantly volcanic rocks and sedimentary rocks formed by erosion of volcanic rocks. REE and isotopic abundances in the fluid would vary with variable degrees of equilibriation of fluids with the different host rocks. These fluids could readily develop positive Eu anomalies by alteration of feldpars in the host rocks. Even in host rocks depleted in Eu, selective alteration of feldspars, which tend to be Eu-rich, could result in a Eu-rich alteration fluid.

Thirteen samples which comprise group B all have small but distinct negative Eu anomalies. The ratio of CeN/YbN increases proportionally with increasing abundance of LREE (light REE) within group B. This is illustrated in Figure 72 which shows a strong positive correlation ($r = 0.91$) between Ce abundance and CeN/YbN. Group B calcites become more LREE enriched with increasing overall REE abundance. The correlation between CeN/YbN and REE abundance diminishes as the REE atomic number increases. This correlation suggests that fractionation is a process which exerted a significant degree of control over the distribution of REE in group B calcites.

To understand the nature of the observed Eu anomalies and the fractionation trend it is first necessary to

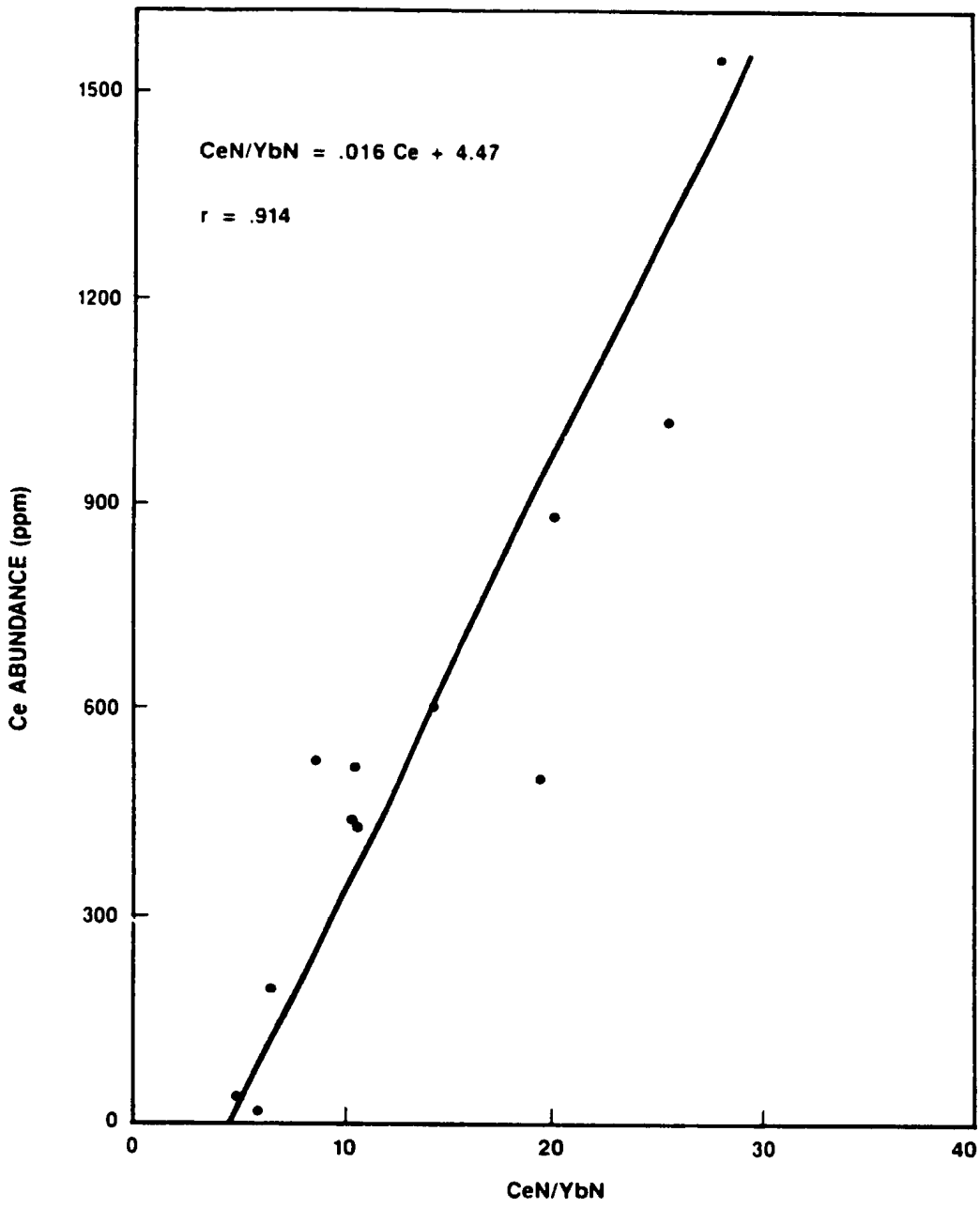

FIGURE 72: PLOT OF Ce ABUNDANCE vs. CeN/YbN FOR GROUP B CALCITES.

understand how the REE are complexed in the hydrothermal solution. Ultimitely this requires a knowledge of the distribution coefficients between each of the REE and the solution, at its source, during transport and at the site of depositon. Such complete understanding is not presently possible due in part to the lack of reliable experimental data dealing with REE complexing. However, the existing experimental data, combined with observations of natural systems, allows for a degree of valid interpretation.

A number of possible complexing agents for REE in natural systems have been described in the literature (Cl^-, F^-, OH^-, SO_4^{2-}, HCO_3^-, CO_3^{2-}). Experimental work carried out by Bilal et al. (1979), Bilal and Becker (1979), and Bilal and Kob (1980) at 25°C, showed that at low fluorine concentrations ([F] = 10^{-3} M), where monofluoro complexes predominate, REE stability constants have a maximum at Tb. Where concentrations of F exceed 10^{-3}M, difluoro complexes predominate and the stability constants of complexes formed with REE increase gradually from La to Lu. The assumption made in using these data to interpret natural hydrothermal systems is that similar complexing relationships exist under natural hydrothermal conditions of elevated temperature and pressure.

Flynn and Burnham (1978) showed that fluorine does complex REE at magmatic conditions in hydrothermal fluids but they did not determine differences between mono and

difluoro complexes. In the St. Lawrence fluorspar deposit on the Burin Peninsula, Strong et al. (1984) suggested that REE in hydrothermal fluids which precipitated fluorite in fluorspar veins, were complexed by difluoro anions, based on the shape of REE patterns in fluorites. Fluorite was absent from all vein material examined in this study. Murray and Howley (1881) report the existance of minor fluorite in La Manche vein. McCartney (1967) did not find any fluorite in the La Manche vein, but he described minor fluorite existing on Harbour Island in Placentia Bay. This general lack of fluorite suggests that if F concentrations in the hydrothermal fluids which precipitated group B calcites would be low, and any REE-F complexes would be of the monofluoro type with maximum stability at Tb. The REE patterns for group B suggest that the the stability of the REE complexing anion increased gradually from La to Lu. This suggests that fluorine was not involved as a significant complexing ion in these fluids.

There are very few experimental data evaluating SO_4^{2-} as a REE complexing agent. Bilal et al. (1979) showed that at 25°C and pH=3.6, SO_4^{2-} did complex REE when sulphate concentrations were significantly higher than other better complexing agents (e.g., F^-). Guichard et al. (1979) demonstrated that natural barites from hydrothermal and marine systems contain significant quantities of REE. They describe barites with up to 1000 times chondritic values of

La. Sulphate may have been a complexing agent for REE in some of these chemical systems. Several barite samples from the present study area were analyzed and were found to have REE levels below the reliable detection limit of the analytical technique (INAA). It does not appear that sulphate acted as a significant complexing agent in the barite veins of this study.

At the higher temperatures of sulphide mineral precipitation (up to 370°C from the fluid inclusion study, 307°C for one galena-sphalerite pair using $\delta^{34}S$ ratios [discussed later in this chapter]) H_2S was the dominant sulphur species in the hydrothermal fluid and sulphate would be insignificant. Therefore, REE found in calcites which co-precipitated with sulphide minerals (e.g., La Manche vein) could not have been complexed by sulphate.

It is still curious that no significant REE abundances were found in barite, although this was not rigorously tested. Possibly all REE were stripped from the hydrothermal fluid by early calcite precipitation. Another possible explanation is that a completely separate fluid, depleted in REE, was responsible for barite precipitation in these veins. However the sulphur isotope data (to be discussed) do not support that interpretation.

As discussed, the CO_3^{2-} abundance is not significant at the pH levels involved, and HCO_3^- is only significant at the lower temperatures involved. Thus these two species

are discounted as possible complexing agents. Burnham and Flynn (1978) attempted and failed to get quantitative data on REE-CO_2 complexing under magmatic conditions.

It is difficult to evaluate the role of OH^- as a complexing ion in these solutions. Bilal et al. (1979) found that at 25°C, REE-fluoro complexes were unaffected by variations in pH below values of 5. At pH levels higher than 5, OH^- affected the formation of REE-fluoro complexes. At higher temperatures the dissociation constant of water increases thus lowering the pH level of fluids, accompanied by an increase in the activity of the OH^- ion. Clearly more experimental work is needed to evaluate the role of OH^- as a REE complexing agent under natural hydrothermal conditions.

The overall syn-depositional nature of calcite and sulphide minerals at La Manche (samples BV12-E, F, G and I) and in other veins (e.g., BV8 at Little Southern Harbour) indicates that calcite deposition marked the onset of sulphide mineral deposition in the vein system. In barren quartz-chlorite veins, calcite often occurs as a late vug filling phase which may coincide with the calcite deposition associated with sulphide mineral precipitation.

Fluid inclusion data suggest that low salinities existed in the hydrothermal fluid during precipitation of quartz in quartz-chlorite veins (average 0.6 wt. % NaCl(eq)). At Silver Cliff higher concentrations of NaCl(eq) are found in fluid inclusions in quartz crystals

associated with sulphide mineral deposition (average of 4.5 wt. % NaCl(eq)). Thus it is reasonable to assume that the introduction of fluids into the vein system which were capable of precipitation of calcite coincided with an increase in the NaCl(eq) content of the fluid.

Flynn and Burnham (1978) conducted experimental work at magmatic temperatures and pressures which showed that Cl^- is a good complexing agent for REE (slightly better than F^-). Their experiments used chlorine concentrations which ranged from 0.6M to 0.9M, which is approximately 3 to 5 wt. % NaCl and is similar to the concentrations found at Silver Cliff. Thus it is possible that the chloride ion was the dominant complexing agent in the hydrothermal fluids from which the group B calcites precipitated.

Negative Eu anomalies found in all group B calcites may have developed as a result of source fluid generation processes, equilibriation with country rock during transport or by precipitation under reducing conditions. Figure 73 shows REE patterns for four sedimentary rocks from various locations on the Isthmus of Avalon. The patterns are very similar except for the presence of one negative Ce anomaly. All four samples have a slightly negative Eu anomaly and are moderately enriched in the LREE. It is possible that fluids which equilibriated with such rocks could then have precipitated calcites which yield REE patterns observed in the group B calcites.

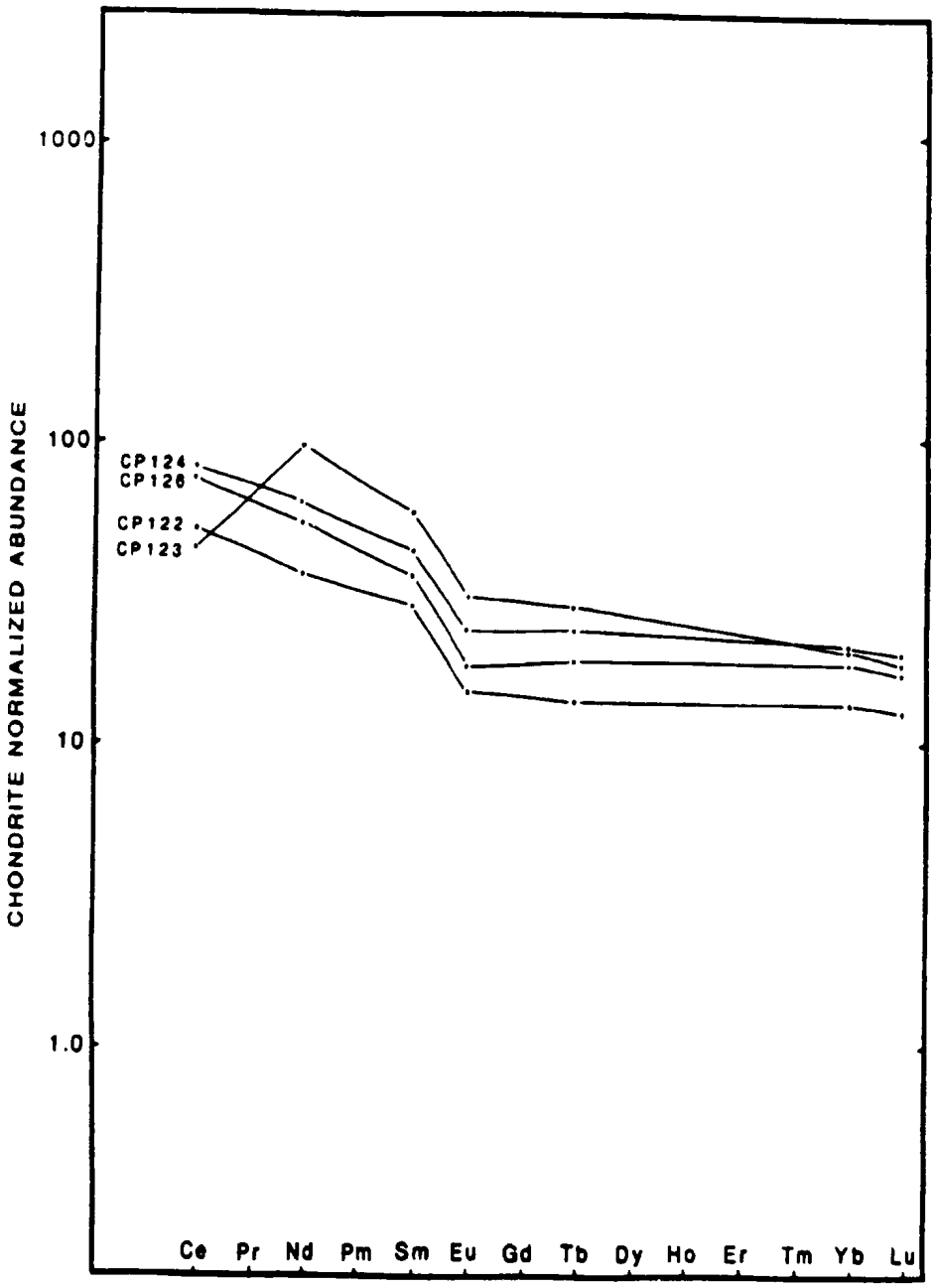

FIGURE 73: REE PATTERNS FOR FOUR SEDIMENTARY ROCKS FROM VARIOUS LOCATIONS ON THE ISTHMUS OF AVALON.

However if a fluid was in contact with such rock long enough to equilibriate its REE abundances, possibly the carbon isotopic ratios in the fluid would also be affected and show a greater variation, as has apparently happened to group A calcites. The lack of variation in carbon isotopic ratios in group B calcites may be evidence that negative Eu anomalies found in group B calcites is not related to transport processes.

Carbon and oxygen isotopic data suggest a magmatic source for hydrothermal fluids from which group B calcites precipitated. A magmatic source can expell Eu-depleted fluids capable of precipitating calcites with negative Eu anomalies. Flynn and Burnham (1978) showed that fluid exsolved from a granitic melt at low pressures (i.e., 1.25 kb at QFM buffer conditions), with no previous Eu depletion and with Cl^- as a complexing agent, would have a well developed negative Eu anomaly and would be LREE-enriched.

Figure 74 shows six REE patterns from granitic rocks taken from Fox Island and Red Island in Placentia Bay (Fig. 4). Tb values for FOX-CG and FOX-FG were discarded due to interferences developed in the neutron activation process. As described in Chapter 1, these granites are post-Cambrian and are believed to be syntectonic, formed roughly at the same time as the veins. The evidence for this is based on their association with other dated granites. They represent possible fluid source rocks for the veins.

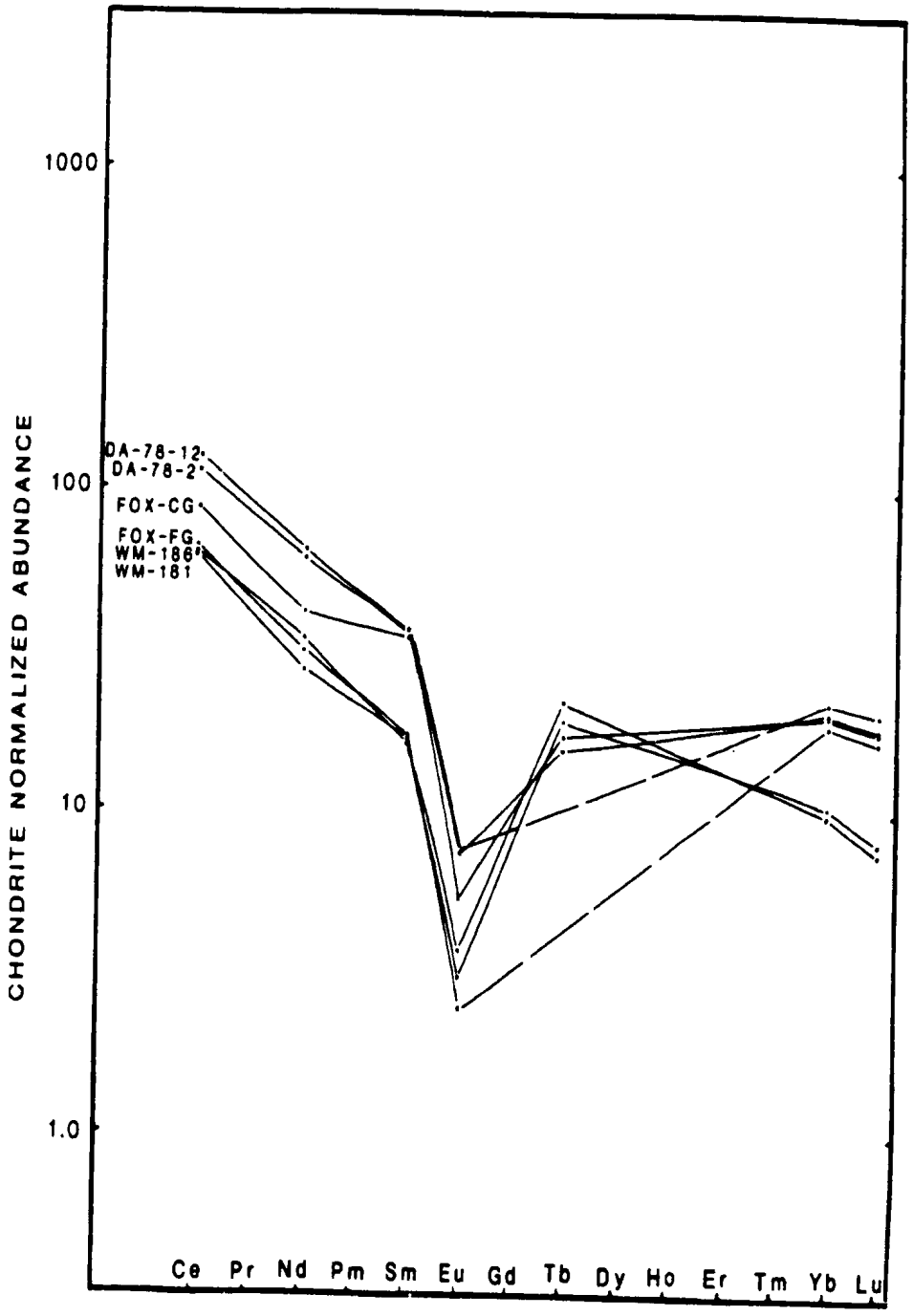

FIGURE 74: REE PATTERNS FOR SIX GRANITIC SAMPLES TAKEN FROM FOX ISLAND AND RED ISLAND IN PLACENTIA BAY.

The large negative Eu anomaly developed in all six samples suggests that it may not be necessary to exsolve hydrothermal fluids from magmas at shallow levels as was discussed. These magmas were probably strongly depleted in Eu before they reached shallow crustal levels, probably due to feldspar fractionation. Eu depletion in the hydrothermal fluid may simply be the result of having equilibriated with a Eu-depleted melt. Strong et al. (1984) concluded that negative Eu anomalies developed in fluorite in the St. Lawrence fluorspar veins (on the Burin Peninsula west of Placentia Bay) were the result of precipitation from a fluid which had exsolved from a Eu-depleted melt. These veins and the St. Lawrence granite are believed to be cogenetic.

To summarize, if the negative Eu anomalies observed in the group B calcites of the present study developed due to source processes, the cause of Eu depletion in the source fluid may be due to exsolution at shallow crustal levels or to exsolution of fluid from a Eu-depleted melt or some combination of the two processes.

Finally, there is evidence that negative Eu anomalies may have developed in some of the calcites as a result of reducing conditions during precipitation. Three of the four calcites from the La Manche vein (BV12-I,E and G) which precipitated with sphalerite and galena have the most pronounced Eu anomalies (Fig. 71) (BV12-F is a

monomineralic calcite sample from the tailings pile and is of uncertain paragenesis). As is discussed later in this chapter, the precipitation of sphalerite and galena in this vein probably took place while H_2S was the dominant sulphur species in the hydrothermal fluid. Under such reducing conditions negative Eu anomalies may have developed in co-precipitating calcite as the reduced Eu^{2+} ion would not precipitate with the other REE ions as discussed earlier. The presence of barite instead of sulphide minerals indicates a more oxidizing fluid with SO_4^{2-} (or HSO_4^-) as the dominant sulphur species. Under such conditions more of the Eu would be in the trivalent state and thus more readily accommodated in the calcite structure resulting in less anomalous behaviour. Thus calcite in veins that have barite as the main sulphur species such as those samples from the Collier Point barite vein (BV11 samples) have smaller negative Eu anomalies.

Before discussing the development of the fractionation trend observed for REE in group B calcites, a brief discussion of the processes controlling calcite deposition is in order. Holland and Malinin (1979) reviewed various factors affecting calcite solubility in hydrothermal fluids. Figure 75 shows that the cooling of the fluid below 300°C results in an increase in the calcite solubility, promoting dissolution of existing calcite and

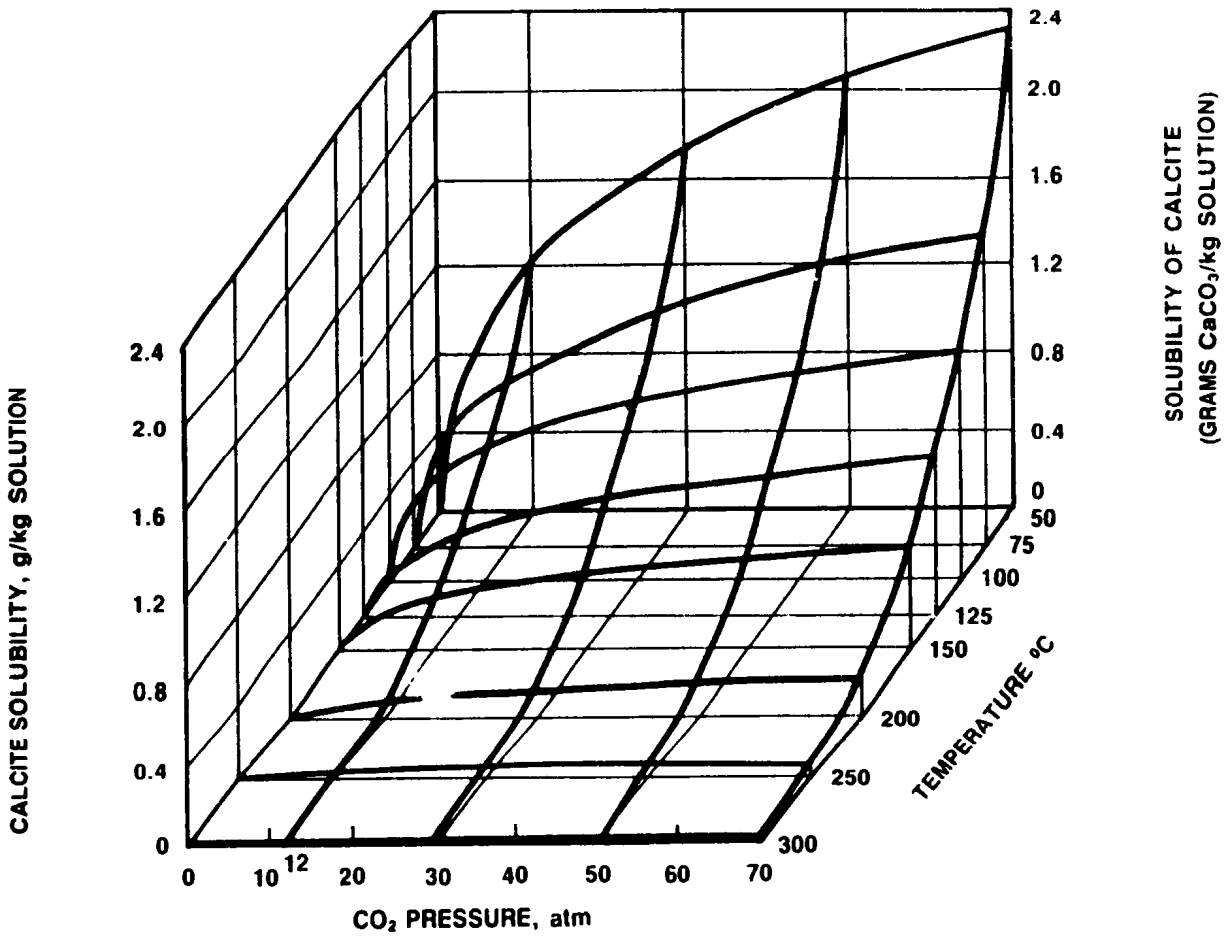

FIGURE 75: THE SOLUBILITY SURFACE OF CALCITE IN THE SYSTEM $CaCO_3$-CO_2- H_2O BETWEEN 50° AND 300°C AND BETWEEN 0 AND 70 atm CO_2. TAKEN FROM HOLLAND AND MALININ (1979).

the possible development of an undersaturated condition. Figure 75 also shows that as PCO_2 decreases calcite solubility decreases, promoting an oversaturated condition and precipitation of calcite. If the temperature and pressure conditions of the rising hydrothermal fluid intersect the immiscibility surface for the CO_2-H_2O system (see Chap. 3 for a discussion of immiscibility surfaces), CO_2 will effervesce resulting in a rapid reduction in the PCO_2 level in the hydrothermal fluid and an accompanying increase in pH. Loss of CO_2 due to effervescence strongly promotes calcite precipitation.

Holland and Malinin (1979) suggest that in hydrothermal fluids which rise without CO_2 effervescence, the decrease in calcite solubility due to decreasing pressure is normally more than compensated for by the increase in calcite solubility due to falling temperatures in the direction of fluid flow. This adds support to the hypothesis that CO_2 effervescence did occur, resulting in calcite precipitation, as was inferred above by the fluid inclusion data.

The REE fractionation trend developed in the group B calcites can be explained by both precipitation and source processes. Using a magmatic source for the hydrothermal fluid, fractionation which results only from precipitation processes requires that fluids, which are continuously exsolved from a crystallizing melt, remain relatively

constant in composition. The earliest-formed calcites from any one pulse of hydrothermal fluid would be the most REE-enriched, and the most LREE-enriched relative to the HREE's (due to the increase in stability of complexes from La to Lu, as discussed earlier). Continued precipitation from the same fluid pulse would result in calcites that contained progressively lower levels of REE and that were progressively less LREE-enriched. Using this model a zonation of REE character is expected, with the most enriched calcites precipitated closest to the source at the highest temperatures, and the most depleted calcites precipitated furthest from the source at the lowest temperatures. Other factors, such as a variable precipitation rate and variable flow rate at which the hydrothermal fluid moves through the vein system, will tend to mask this zonation.

The present sampling density is too sparse to document this zonation in the field area. However, the calcites which have the highest REE abundances are those from the La Manche vein (BV12) where sulphide minerals were deposited, and thusthis vein was likely relatively closer to its fluid source. The calcite sample from the vein BV8-2 (Little Southern Harbour vein) also has very high REE abundances. This vein contains up to 40% galena with the remainder consisting of barite and calcite. Thus the highest REE abundances are found in calcites associated

with sulphide mineralization. It is unfortunate that calcite associated with sulphide mineralization was not discovered in the tailings pile or in the vein exposure at Silver Cliff. Calcites from the large Collier Point barite vein (BV11) contain the next highest abundances. Although there is no sulphide mineralization in BV11, the vein thickness and length suggests that fluid permeabilities would have been quite high, and thus the ratio of flow rate to precipitation rate would be relatively high. This may have resulted in high REE abundances in calcites from the BV11 vein compared to other smaller veins found on Collier Point (i.e., BV46-A, Fig.7). Similarly, on Bellevue Peninsula, calcite from BV30-A, which is a 60 cm thick zoned calcite-barite vein (Fig. 23) found along strike with several other thicker vein exposures, has relatively high REE abundances. The much smaller BV33-A vein (5 cm thick), located 1400m from the BV30 vein has one of the lowest REE abundance levels of any of the group B samples (BV33-A is dolomite). Fluid would have moved more slowly through these smaller and more discontinuous veins and thus have more time to cool and precipitate calcite resulting in lower REE abundances.

The observed fractionation may also result from exsolution of a continuously evolving hydrothermal fluid from a source melt. To date there has been no experimental work done to determine how the REE chemistry of exsolved

hydrothermal fluid changes with progressive crystallization of the melt. Flynn and Burnham (1978) determined that for granitic melts at the QFM oxygen buffer (Q=quartz, F=fayalite, M-magnetite), REE distribution coefficients (K, defined as ppm REE in vapour/ppm REE in melt) decrease from Ce to Yb. This work also showed that with exsolution occurring at decreasing pressures there was an enrichment of REE in the vapour phase. Most importantly Flynn and Burnham (1978) showed that as the chloride content of the solution in equilibrium with the melt increases, the ratio of ppm REE in vapour/ppm REE in melt increases in cubic proportionality. However this ratio was never greater than 0.2 for trivalent REE under all conditions studied.

Once exsolution of vapour from a melt has begun, more vapour continually exsolves from the melt in an effort to maintain equilibrium as crystallization proceeds. It is not clear, from experimental or field data, whether subsequent volumes of exsolved vapour are richer or poorer in REE than preceeding volumes. Strong et al. (1984) suggested the latter for fluids associated with the St. Lawrence Fluorite veins. The partition coefficient for chlorine very strongly favours the aqueous (vapour) phase (Kilinc and Burnham 1972). Since chlorine is a good complexing agent for REE in the vapour phase, there is a strong possibility that the REE follow chlorine into the aqueous phase. Kilinc and Burnham (1972) showed that for a granodioritic melt with 3% H_2O and

a low chlorine concentration of 0.1%, the first vapour phase formed at 0.6 Kb (exsolution occurs when melt has undergone 10% crystallization) contains 4.6 wt. % chlorine. At 2.1 Kb (exsolution occurs when melt has undergone 53% crystallization) the exsolved vapour contains 7.5 wt. % chlorine. Thus the chlorine composition of the exsolved vapour is very pressure dependent and it is therefore also likely true of the REE composition.

The process of exsolution itself can cause variation in the pressure of exsolution as there is limited pore volume in the country rock to hold the exsolved vapour. As exsolution proceeds pressure will build up if there are no conduits to allow the fluid to escape. However Burnham (1979) suggests that the amount of pressure build-up would rarely exceed 400 bars at shallow crustal levels, before causing brittle deformation of the surrounding rock and allowing escape of the exsolved fluid. Pressure build up due to exsolution is therefore not likely to greatly affect chlorine and thus REE concentration in the exsolved fluid.

Kilinc and Burnham (1972) also showed that in an open system, where exsolved fluids are able to move away from the melt (as likely existed during formation of the veins in the present study, before calcite precipitation; discussed in Chap. 3), the chlorine content of the evolving aqueous phase in the 2.1 Kb example above, decreases by a factor of 20 or more as exsolution evolves. In the lower

pressure case of 0.6 Kb the chlorine content actually increased with progressive exsolution. Thus the evolution of the chlorine content, and therefore possibly the REE content, of the exsolved fluids from a melt, may be strongly dependent on the crustal level at which the melt crystallizes. Clearly the source granites would have to be identified and studied to determine the nature of their composition and history of crystallization to evaluate fully how evolution processes may have caused the observed fractionation pattern.

4.4. Summary of Results of REE Study of Calcites

There are two distinct groups of calcites indicated by their REE geochemistry.

Group A: 1) These calcites are inferred to have precipitated from fluids which have exchanged REE with the country rock.

Group B: 1) Prior to incorporation into these calcites, the REE were likely complexed by chloride ions in the hydrothermal solution, although other complexing ions remain a possibility.

2) Slightly stronger negative Eu anomalies observed in the La Manche vein and other calcites probably are the result of precipitation under reducing conditions.

3) Less pronounced negative Eu anomalies may be the result of precipitation under less reducing conditions, or

from a Eu-depleted fluid. Eu depletion in the fluid could result from exsolution of fluid from a magma at very shallow crustal levels or by exsolution from a Eu-depleted melt.

4) The observed REE abundance trend is probably due to fractionation during precipitation. Possibly some of the variation in the REE abundances is due to evolution of the REE chemistry of the hydrothermal fluid during progressive exsolution from the magma.

4.5. Sulphur Isotopes

Table 4-3 lists the $\delta^{34}S$ values determined for eighteen barite, five galena and six sphalerite samples collected in the field area. The isotopic determinations were carried out at McMaster University. Sulphide samples were converted to sulphur dioxide by reaction under vacuum with copper oxide at 1200°C. Carbon dioxide was removed from the sulphur dioxide by fractional distillation at the freezing temperature of liquid pentane. Sulphur dioxide was separated from water by fractional distillation at the temperature of dry ice. Sulphur dioxide samples were stored in pyrex tubes prior to mass spectrometry. Values of $\delta^{34}S$ were determined by analysis in a double inlet-double collector mass spectrometer with a 6 inch radius and 90° magnetic sector analyser. Measurement precision was $\pm$ 0.2 ‰ . No standards or duplicates were analysed.

Table 4-3 - $\delta^{34}S$ Values

Sample	Barite	Galena	Sphalerite
BV1-I	10.0		
BV1-G	10.8		
BV2-A	9.6		
BV3-B	10.4		
BV6-A	11.8		
BV8-DG		-3.8	
BV8-H	10.6		
BV8-ZG		-3.3	
BV9-A	9.9		
BV11-AB	13.9		
BV11-F	15.4		
BV11-V	12.9		
BV12-F	10.9		
BV15-A	11.4		
BV17-B	12.5		
BV22-B	12.2		
BV30-A2	13.0		
BV39-B	14.0		
BV48-A	14.6		
BV55-A	13.2		
BV12-DS			1.5
BV12-IS			0.7
BV12-GS			0.2
BV12-ES			1.7
AR5-AG		-3.1	
AR25-CS			-0.7
AR25-AG		-5.5	
AR6-B		-2.3	-0.5

4.5a. Geothermometry

The value of $\delta^{34}S$ for both sphalerite and galena was determined from one sample (AR6-B) for the purpose of geothermometry. The calibration equation of Czamanske and Rye (1974) for sphalerite-galena pairs was used to determine the temperature of isotopic equilibriation:

$$1000 \ln \alpha_{sph\text{-}gal} = 7.0 \times 10^5 / T^2$$

From the determined values of $\delta^{34}S$ for sphalerite and galena from AR6-B, $\alpha_{sph\text{-}gal}$ $(=(^{34}S/^{32}S)_{sph}/(^{34}S/^{32}S)_{gal})$ is +1.8 yielding a calculated temperature of equilibration of 307°C. This isotopic temperature determination is at the high end of the range in measured Th values found in fluid inclusions in sphalerite crystals in the Silver Cliff vein (273° to 300°C, Fig. 49). With a temperature correction of 13°C for the fluid inclusion with Th = 273°C and 10°C for the fluid inclusion with a Th at 300°C (see Chap. 3), the isotopic temperature determination actually falls within the range indicated by the fluid inclusions (285° to 310°C).

4.5b. Sulphur Source and Paragenesis of Sulphur-Bearing Mineral Phases

The variation of sulphur isotopic compositions of naturally occurring sulphide minerals is illustrated in Figure 76. Clearly there is much overlap between igneous and sedimentary sulphide mineral isotopic compositions. It is therefore necessary to combine sulphur isotopic studies

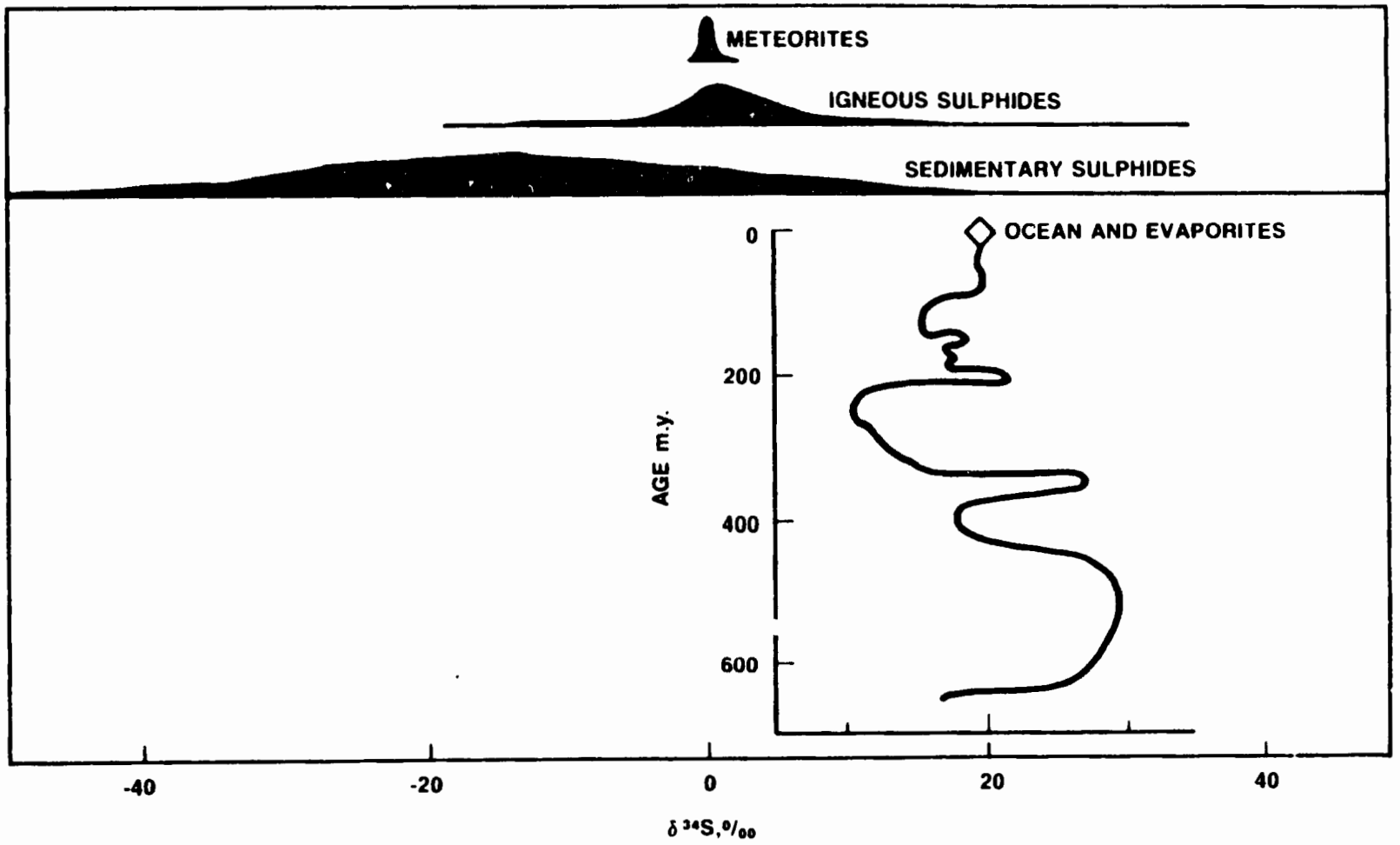

FIGURE 76: SULPHUR ISOTOPIC VARIATION IN NATURE. FROM OHMOTO AND RYE (1979).

with other geological and geochemical data to determine a most likely sulphur source.

The five galena samples analyzed, three from the Silver Cliff veins ("AR" samples in Table 4-3) and two from the Little Southern Harbour vein ("BV8" samples), have $\delta^{34}S$ values ranging from -2.3 to -5.5 ‰. Both the highest and the lowest values are from the Silver Cliff veins. Six sphalerite samples from the La Manche vein (BV12) and the Silver Cliff veins have $\delta^{34}S$ values ranging from -0.7 to 1.7 ‰, with the two lowest values from the Silver Cliff vein. The $\delta^{34}S$ values for barite samples range from +9.6 to +15.4 ‰. Barite from two sulphide-bearing veins (Little Southern Harbour - BV8, La Manche - BV12) had $\delta^{34}S$ values of +10.6 and +10.9 ‰ (respectively) at the low end of the $\delta^{34}S$ range for the barites. Barite veins which contain no other sulphur-bearing mineral phases have $\delta^{34}S$ values ranging from the lowest value of +9.6 ‰ to the highest value of +15.4 ‰.

Before discussing the observed variations in the $\delta^{34}S$ values for galena, sphalerite and barite, a discussion of the conditions and the processes under which precipitation of these phases occurred is in order. Paragenetically, barite occurs after sulphide mineral precipitation, in both the La Manche and Silver Cliff veins. The early paragenesis of the sulphide minerals relative to barite, and the higher indicated temperatures of sulphide

mineralization suggests that H_2S was the initial dominant sulphur species in the hydrothermal fluid. Figures 77 and 78 show the stability fields for the various sulphur species at 350° and 250°C. At 350°C H_2S is stable below a pH of 9 and at log aO_2 levels less than -29. As pH decreases the H_2S stability field boundary is found at progressively higher levels of log aO_2 (i.e., log aO_2 = 25, pH = 5). Figures 77 and 78 also show the stability fields of barite and calcite. In the early paragenesis of the Silver Cliff vein neither calcite or barite are observed and thus it is inferred that the pH and aO_2 conditions were outside of the stability fields of these phases while sulphide mineralization was taking place. At 250°C the stability fields for the various sulphur species shift to lower values of log aO_2 and pH. A fluid which is at 350°C and has a log aO_2 of -33 and pH of 5.7 (neutral pH at 350° C) is within the H_2S-dominant field outside the stability field of both barite and calcite ("X" in Fig. 77). This same fluid at 250°C has a pH of 5.0 and (assuming a constant value of log aO_2) is within the stability field of HSO_4^-, with both barite and calcite stable ("X" in Fig. 78).

If one envisages the progressive shift of the stability fields with decreasing temperature the paragenetic sequence observed in these veins area can be

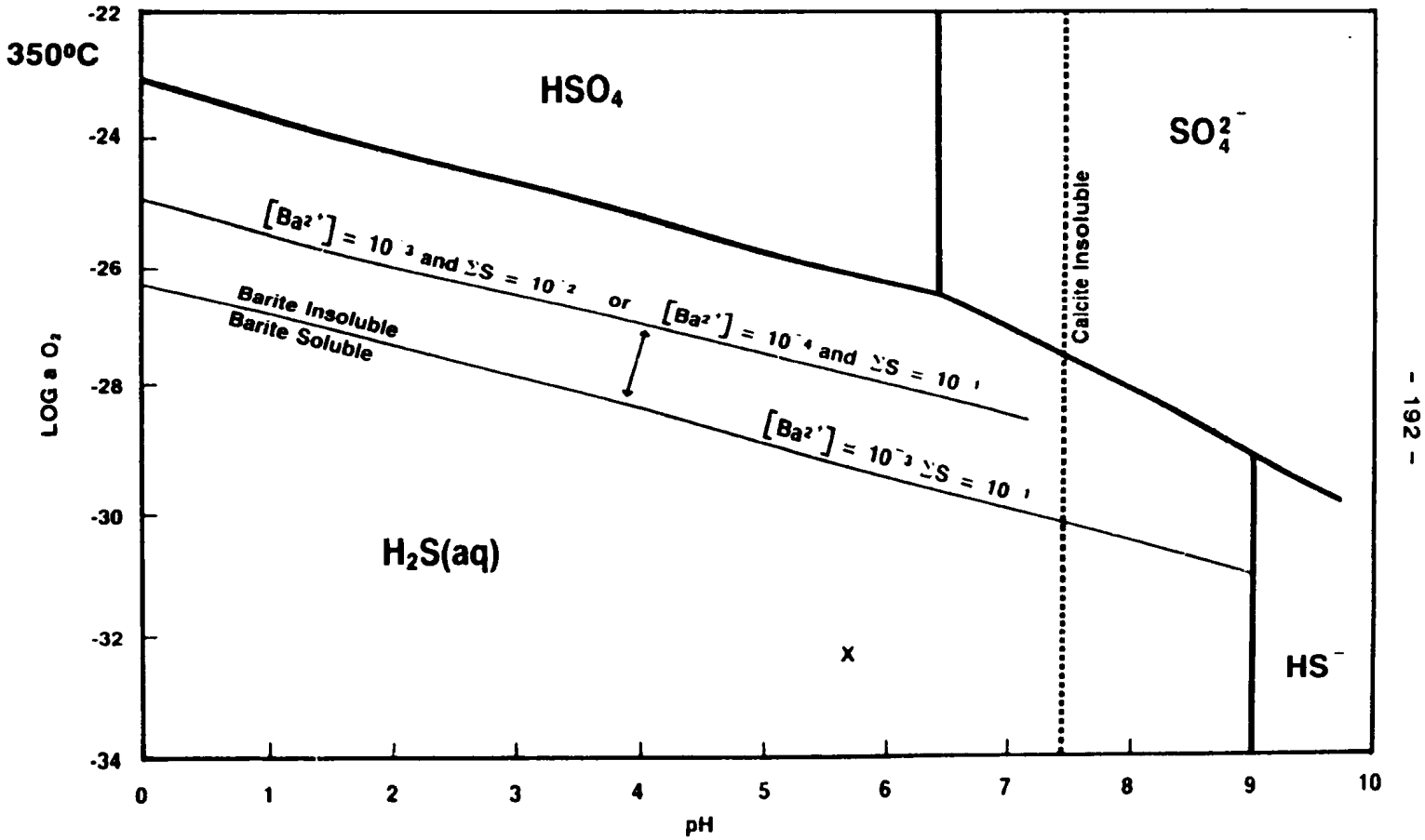

FIGURE 77: SHOWS THE FIELDS OF DOMINANCE FOR THE VARIOUS SULPHUR SPECIES, AND ALSO SHOWS HOW, AT 350° C, THE BARITE SOLUBILITY LINE IS AFFECTED BY VARIABLE CONCENTRATIONS OF Ba^{2+} ION AND ΣS CONTENT. CALCITE SOLUBILITY LINE IS FROM SO, RYE AND SHELTON (1983). FIELDS WERE CONSTRUCTED USING THERMODYNAMIC DATA FROM HELGESON (1969).

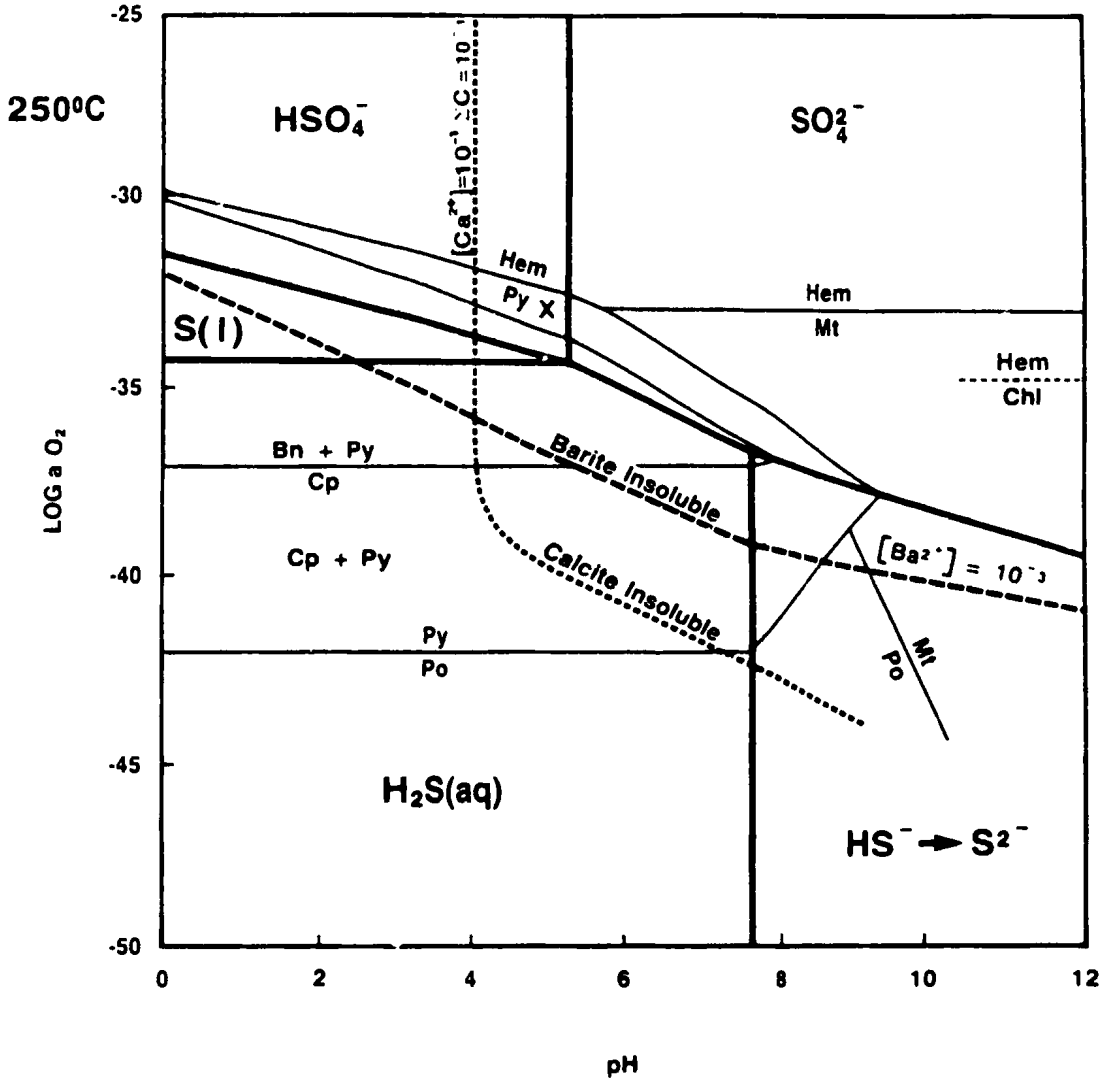

FIGURE 78: SHOWS THE FIELDS OF DOMINANCE FOR THE VARIOUS SULPHUR SPECIES, AND THE STABILITY FIELDS FOR SEVERAL SULPHIDE MINERALS OVER VARIABLE pH AND OXYGEN ACTIVITY CONDITIONS AT 250°C. FROM BARNES (1979).

traced. At the highest temperatures ($\approx 360^{\circ}C$, "A" in Fig. 79) H_2S is the dominant sulphur species and sulphide mineral deposition takes place without calcite or barite at Silver Cliff. In the La Manche vein the fluid was cooler, stabilizing calcite ("B" in Fig. 79) by shifting the stability field to lower pH levels (effervescence of CO_2 discussed below). Sulphide mineralization would still have occurred because the fluid was still in the $H_2S(aq)$ dominant field. The Little Southern Harbour vein (BV8) displays the next step in the sequence with early-formed calcite found in the same vein with galena and barite. Thus with further cooling the stability field of barite had moved to sufficiently low levels of aO_2 and pH that barite became stable ("C" in Fig. 79), but probably was still near the H_2S-dominant field, possibly just inside of it. The Sutton vein (BV53, Fig.5), situated about 4 km east of the Little Southern Harbour vein (BV8), contains barite and chalcopyrite and was probably deposited at pH and aO_2 conditions similar to that of the Little Southern Harbour vein. The rest of the veins to the north and east contain mineral assemblages dominated by barite and/or calcite, with no significant sulphide mineral content. During precipitation of these veins further cooling resulted in pH and aO_2 conditions which were either in the HSO_4^- or SO_4^{2-} dominant fields and which were outside of sulphide mineral stability fields ("D" in Fig. 79).

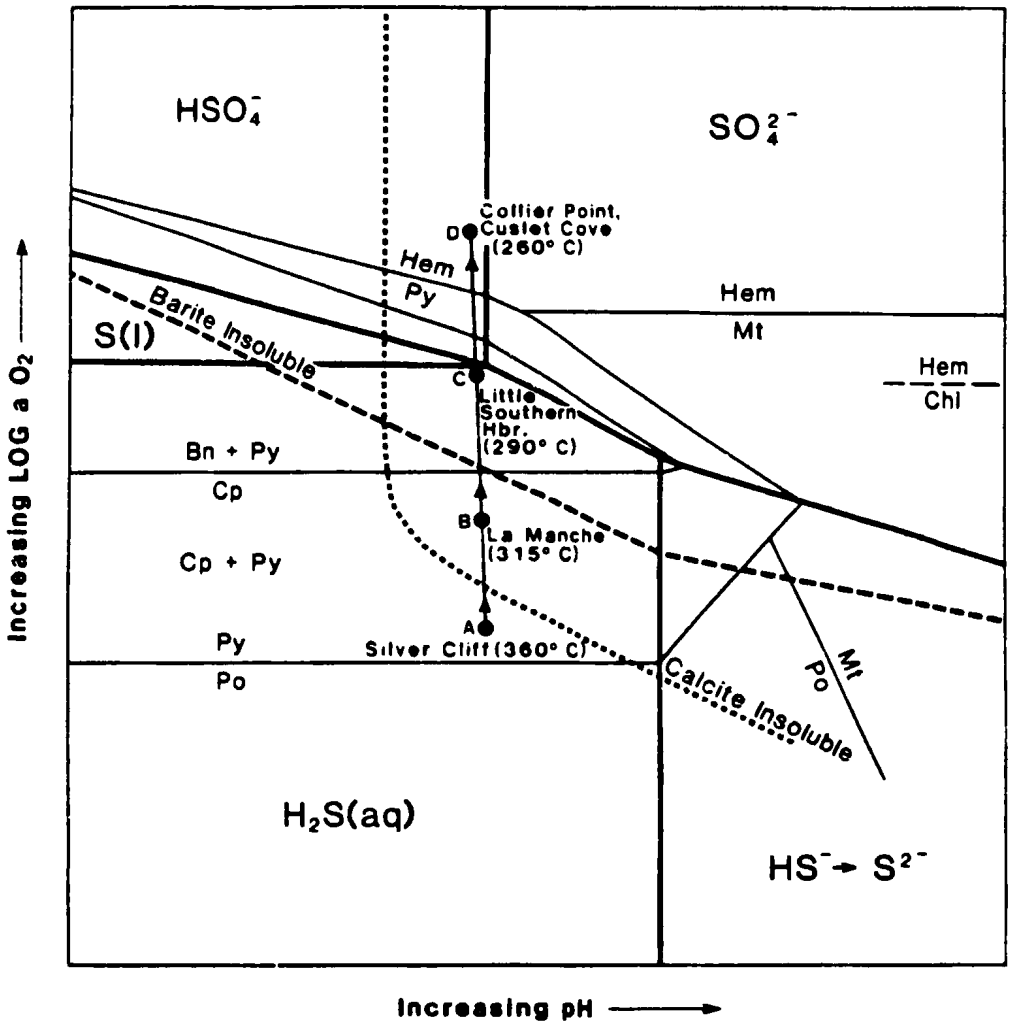

FIGURE 79: SHOWS THE FLUID COOLING PATHWAYS AND THE APPROXIMATE RELATIVE POSITIONS OF THE VARIOUS MINERAL ASSEMBLAGES ON A GENERALIZED PLOT OF AQUEOUS SULPHUR SPECIES STABILITY FIELDS.

In all cases where calcite occurs with barite, calcite has formed early in the paragenesis of the vein, as predicted by the cooling model. The other feature that changes in these sulphide-free veins is that the barite becomes very hematite-rich, which according to the stability field for hematite in Figure 78, suggests further cooling and oxidation of the fluid. This model assumes that the concentrations of ions in the hydrothermal fluid remain constant except for depletion due to precipitation.

In the veins found in the southern reaches of the field area, to the south of the Silver Cliff area, calcite occurs late in the vein paragenesis in numerous quartz-calcite ($\pm$ chlorite) veins. These veins have subsequently been cut by later-formed monomineralic barite veins, which is compatible with the paragenetic sequence observed in veins in the northern areas.

The above "cooling" model was likely enhanced and may have even been dominated by the rise in pH which would take place during CO_2 effervescence. As Figures 77 and 78 show, any increase in pH would favour the precipitation of both calcite and barite. It would also favour SO_4^{2-} as the stable aqueous sulphur species in the hydrothermal fluid, as oxidation progressed.

It has been inferred above that when sulphide mineralization began in the Silver Cliff veins, H_2S was the dominant sulphur species in the hydrothermal fluid.

Figure 80 shows the equilibrium isotopic fractionation factors for sulphur compounds, relative to H_2S at variable temperatures. Sulphate minerals are not on this diagram due to the lack of fractionation between sulphate in solution and precipitating sulphate phases (Sakai, 1968). Using the sulphur isotopic temperature determination of 307° C and the $\delta^{34}S$ values for sphalerite and galena determined for sample AR6-B, the $\delta^{34}S$ ratio in the coexisting H_2S is calculated to be -0.20 and -0.43 ‰ respectively for sphalerite and galena (equations from Ohmoto and Rye 1979). These values are probably indicative of the value of $\delta^{34}S_{\text{total S}}$ in the hydrothermal fluid at or very close to the end of precipitation of sulphur-bearing phases from the fluid at Silver Cliff. $\delta^{34}S_{\text{total S}}$ in the hydrothermal fluid at the source of the sulphur may be slightly different than is indicated by the AR6 crystals, if there was any significant precipitation of sulphur-bearing phases from the fluid before it reached the crustal level of the Silver Cliff vein. Evidence presented below suggests that there was early precipitation of galena and the development of a degree of significant fractionation before precipitation of the AR6-B sample. A $\delta^{34}S_{\text{total S}}$ value of about -0.3 ‰ as indicated by the AR6 spalerite-galena pair, is therefore likely a few ‰ higher than the value of $\delta^{34}S_{\text{total S}}$ for the sulphur source (assuming no isotopic exchange during transport).

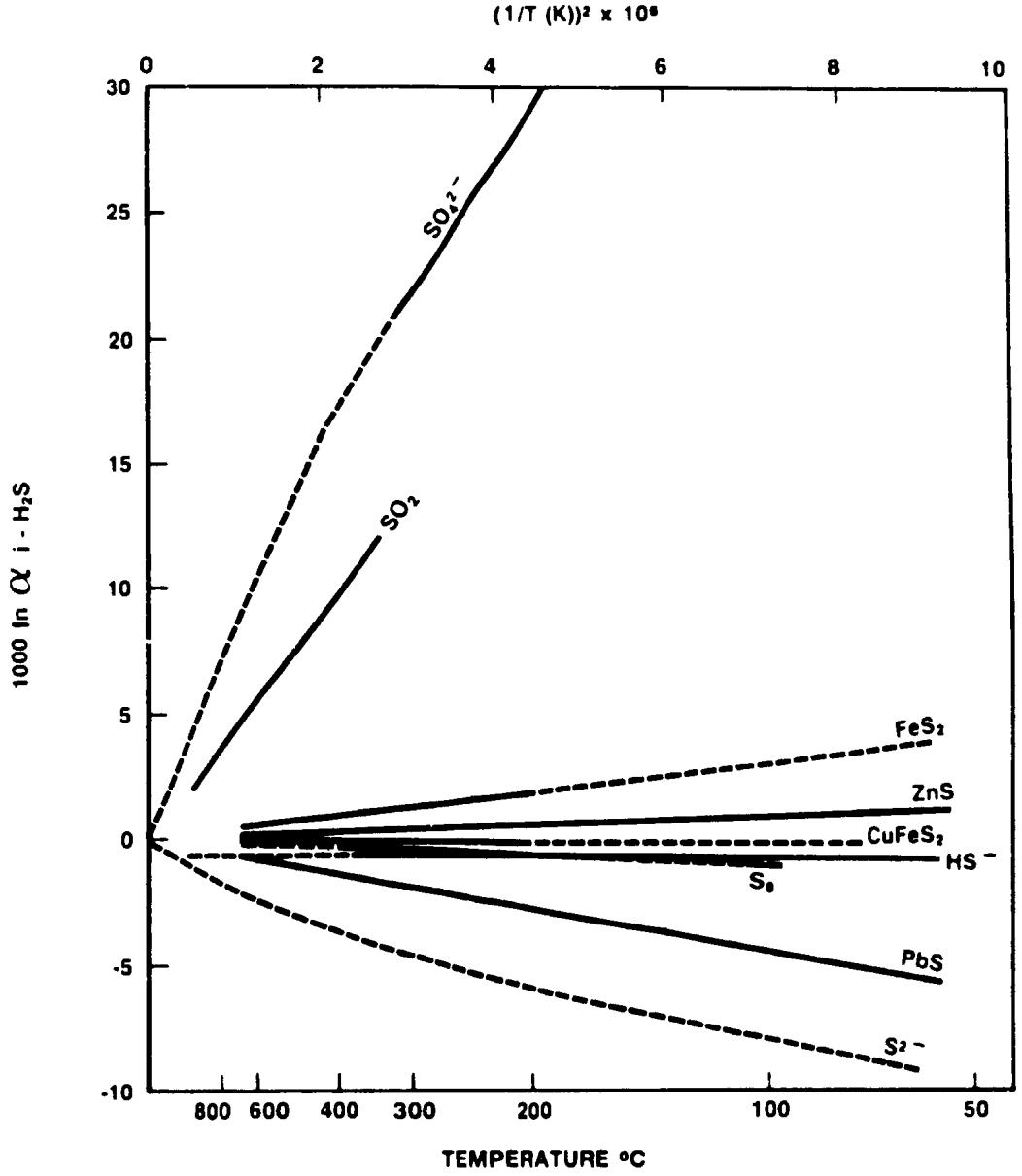

FIGURE 80: EQUILIBRIUM ISOTOPIC FRACTIONATION FACTORS AMONG SULPHUR COMPOUNDS RELATIVE TO H_2S. SOLID LINES EXPERIMENTALLY DETERMINED. DASHED LINES EXTRAPOLATED OR THEORETICALLY CALCULATED. FROM OHMOTO AND RYE (1979).

After the initial formation of the hydrothermal fluid, and assuming that there was no addition or subtraction of sulphur to the system during transport, there are three processes which can significantly affect the $\delta^{34}S$ values of sulphide and sulphate minerals precipitated from the fluid. These three processes are: 1) Temperature variation: This results in increasing sulphur isotope fractionation between sulphur-bearing species as the fluid cools (Fig. 80). Cooling alone does not affect the value of $\delta^{34}S_{total\ S}$ in the fluid; 2) Crystal fractionation: As predicted from Figure 80, precipitation of galena will result in an upward shift in the $\delta^{34}S_{H2S(aq)}$ value, and thus $\delta^{34}S_{total\ S}$, in the remaining hydrothermal fluid. Precipitation of pyrite has the opposite effect to that of galena, while the effect of sphalerite and chalcopyrite precipitation is minimal; 3) Oxidation: At higher temperatures almost all of the sulphur in the hydrothermal fluid is in the form of H_2S with only a very small proportion in an oxidized state. The $\delta^{34}S_{total\ S}$ value is therefore very close to $\delta^{34}S_{H2S(aq)}$, and actually is just slightly higher due to the existence of a small component of oxidized sulphur which has a higher $\delta^{34}S$ value as indicated in Figure 80.

Upon cooling of the fluid, oxidation of H_2S transforms progressively more of the total sulphur to SO_4^{2-} (or HSO_4^-). The value of $\delta^{34}S_{SO4^{2-}(aq)}$ shifts

progressively closer to $\delta^{34}S_{total\ S}$ which remains constant. The value of $\delta^{34}S_{H2S(aq)}$ decreases during oxidation, maintaining isotopic equilibrium with the sulphate species according to Figure 80. Precipitation of sulphur-bearing minerals from a fluid which is undergoing oxidation will result in progressively lower $\delta^{34}S$ values for both sulphide and sulphate minerals. The relative importance of any one of these three processes in controlling the isotopic ratios in the various sulphur species will depend on the relative rates at which cooling, precipitation and oxidation take place.

The limited number of analyzed samples from the Silver Cliff veins and the La Manche vein, combined with the lack of paragenetic control for the samples which were collected (i.e., a number of samples were from tailings piles), make it difficult to say much about how sulphur isotopic conditions varied during precipitation within individual veins. However it is observed that there exists a significant variation between the three galena samples analyzed from the Silver Cliff veins with $\delta^{34}S_{gal}$ ranging from -5.5 ‰ (AR25-A) to -2.3 ‰ (AR6-B) with a difference of 3.2 ‰. Oxidation is not likely to have been a significant process until very late in paragenesis of this vein as suggested by the lack of calcite and barite in these samples. As well, an unrealistic amount of cooling

would be required to account for this variation between samples (see PbS curve in Fig. 80).

Unfortunately Chute (1939) did not indicate the relative proportions of the various sulphide minerals precipitated at Silver Cliff. However from his description of the La Manche vein and a number of other mineralized veins in the area (Jersyside, Strouter adit, Verrains Island, Galleons Point, Black Point and Bay de l'Eau River), it is apparent that galena is the dominant sulphide mineral precipitated in the area and may well have been the dominant sulphide mineral precipitated in the Silver Cliff veins.

The variation in the sulphur isotope ratios observed in these galena samples could be due to fractionation caused by galena precipitation. If fractionation was the controlling process the galena in sample AR25-A would have precipitated earliest, followed by the galena in AR5-A and then AR6-B. This suggests that the initial $\delta^{34}S_{\text{total S}}$ in the hydrothermal fluid was a few per mil lower (-4.0 ‰ for AR25-A, assuming precipitation at the maximum temperature of 370°C as indicated by fluid inclusions) than was calculated using AR6-B. The other possible cause for the variation is a simple variation in the sulphur isotope ratios in the source fluid. However, fractionation, combined with temperature variation and oxidation models, also explains the variation in sulphur isotopes from Silver Cliff to La Manche and to the other veins.

Four sphalerite samples were analyzed from the La Manche vein. These samples all have higher $\delta^{34}S$ values (0.2 to -1.7 ‰) than the sphalerite samples from Silver Cliff. For any of the $\delta^{34}S_{sphal}$ values from the La Manche vein, the previously calculated value of $\delta^{34}S_{H2S}$ (-0.3 ‰ from AR6-B) is too low to be in equilibrium over the likely temperature range of precipitation of this vein (325° to 275°C is a likely range by comparing the known paragenesis of the vein with stability fields in Figs 77 and 78). This suggests that galena fractionation continued to drive up the value of $\delta^{34}S_{H2S}$ at least until after the time of deposition of the La Manche vein. Despite the fact that galena was by far the most abundant sulphide mineral in the La Manche vein and can still be found in abundance in the existing tailings, no galena samples were obtained due to a sampling error.

The one barite sample analyzed from the La Manche vein has $\delta^{34}S$ value of +10.9 ‰ (BV12-F). When this value and the values determined for the sphalerite crystals from this vein are compared using Figure 80, it is clear that sphalerite and barite are far from equilibrium at any reasonable temperature for the precipitation of this vein. By the time barite precipitated late in the paragenesis of the vein, the temperature of the fluid had dropped significantly such that a large proportion of the original H_2S had been oxidized to SO_4^{2-}. As discussed above, this

results in much lower values of $\delta^{34}S$ for both SO_4^{2-} and H_2S remaining in the fluid, which explains the low values for $\delta^{34}S_{bar}$ observed for the La Manche samples. This also suggests that the analysed sphalerite had precipitated before much oxidation had taken place. Otherwise it would have had much lower $\delta^{34}S$ ratios.

The Little Southern Harbour vein (BV8) also contains galena, calcite and barite. However in this vein these mineral phases were deposited closer together paragenetically. Even though galena precipitation continued up to the time of deposition of this vein, the values of $\delta^{34}S_{gal}$ for the two BV8 samples are lower than would be expected had sulphur isotope fractionation due to galena precipitation continued to be the dominant isotope-controlling process. The observed $\delta^{34}S_{gal}$ values of -3.8 and -3.3 ‰ are similar to those found at Silver Cliff. The galena in this vein was deposited while conditions were close to the H_2S - SO_4^{2-} stability field boundary as indicated by co-precipitated barite. Oxidation of H_2S was a significant process here even during galena precipitation which resulted in lowering $\delta^{34}S_{H2S}$ and thus the $\delta^{34}S_{gal}$ values as observed. Unfortunately the barite sample BV8-H is not directly from the Little Southern Harbour vein but from a small barite vein about 10 m away which contains no sulphide mineralization. The $\delta^{34}S_{bar}$ value of +10.6 ‰

indicates that oxidation of much of the $H_2S_{(aq)}$ had taken place by the time this barite had been deposited.

Three barite samples from the Collier Point vein have values of $\delta^{34}S_{bar}$ ranging from +15.4 to +12.9 ‰. The presence of an almost ubiquitous hematite staining of the barite suggests that the oxidation of H_2S to SO_4^{2-} in the hydrothermal fluid was complete by the time most of the fluid reached the site of deposition of the Collier Point vein (Fig. 79). The earliest fluid which resulted in calcite deposition may have been less oxidized. $\delta^{34}S_{bar}$ values are higher in the Collier Point vein than they are at Little Southern Harbour and La Manche. Possibly the fluid from which the Collier Point vein precipitated had a higher $\delta^{34}S$ source. However it could have the same source as the other veins if more galena precipitation, and therefore fractionation, had taken place from the hydrothermal fluid before it flowed through the Collier Point fracture. Possibly the availability of Pb in each area controlled the amount of galena precipitation.

Obviously there was an abundance of H_2S which survived sulphide precipitation to be later oxidized and deposited as barite on Collier Point. The variation in sulphur isotopes between the three samples from Collier Point (15.4 to 12.9 ‰) can be explained by varying degrees of previous galena precipitation before the barite in each sample was precipitated. The different barite samples may

have been deposited from different pulses of hydrothermal fluid, each of which had experienced different amounts of galena precipitation at deeper levels and higher temperatures beneath or lateral to the Collier Point vein. Those pulses of fluid from which more galena precipitation took place would later have precipitated barite with higher values of $\delta^{34}S_{bar}$.

BV39-B and BV48-A (Fig. 7) are samples from two much smaller barite veins found on Collier Point about 2 kms and 1 km respectively, from the large Collier Point barite vein (BV11). These two veins also have high $\delta^{34}S_{bar}$ values of 14.0 and 14.6 ‰ respectively, in line with the values determined for BV11 barite, again indicating a high proportion of previous galena precipitation.

The rest of the barite veins in the field area have values of $\delta^{34}S_{bar}$ ranging from 13.2 (BV55-A) to 9.6 ‰ (BV2-A) with the variation between these samples possibly reflecting the variation in the amount of galena precipitation which took place in each area. It is interesting that the $\delta^{34}S_{bar}$ values for all the veins found in the southern portion of the field area (St. Brides, Branch) are relatively low, suggesting that galena precipitation may have been minimal in this region. From an exploration viewpoint the northern area appears to hold more potential for discovery of sulphide-mineralized veins.

The values of $\delta^{34}S$ determined for sphalerite and galena, and the values of $\delta^{34}S_{H2S}$ determined for the co-existing hydrothermal fluid, fall within the peak range for igneous sulphides illustrated in Figure 76. This evidence, combined with the other geochemical and geologic evidence already presented (C, O, REE data, potential syntectonic intrusion of granitoid magmas), suggests that sulphur, as well as carbon, oxygen and the REE were all emplaced in the hydrothermal fluid during the expulsion of this fluid from a magma.

In summary the sulphur isotope data support the following conclusions:

1) Sphalerite precipitation in the late veinlets of the Silver Cliff mine occurred at about 300°C.

2) The sulphur found in both the sulphide and the sulphate minerals had an igneous source.

3) The ratios of sulphur isotopes found in the various sulphur-bearing minerals were controlled initially by the source and the temperature of precipitation. As vein formation proceeded, galena precipitation exerted a dominating control over isotopic fractionation. Finally the process of oxidation of H_2S to SO_4^{2-} (or HSO_4-), in the hydrothermal fluid, became the dominant control.

Figure 81 attempts to show how the sulphur isotopic ratios varied in the hydrothermal fluid and in the

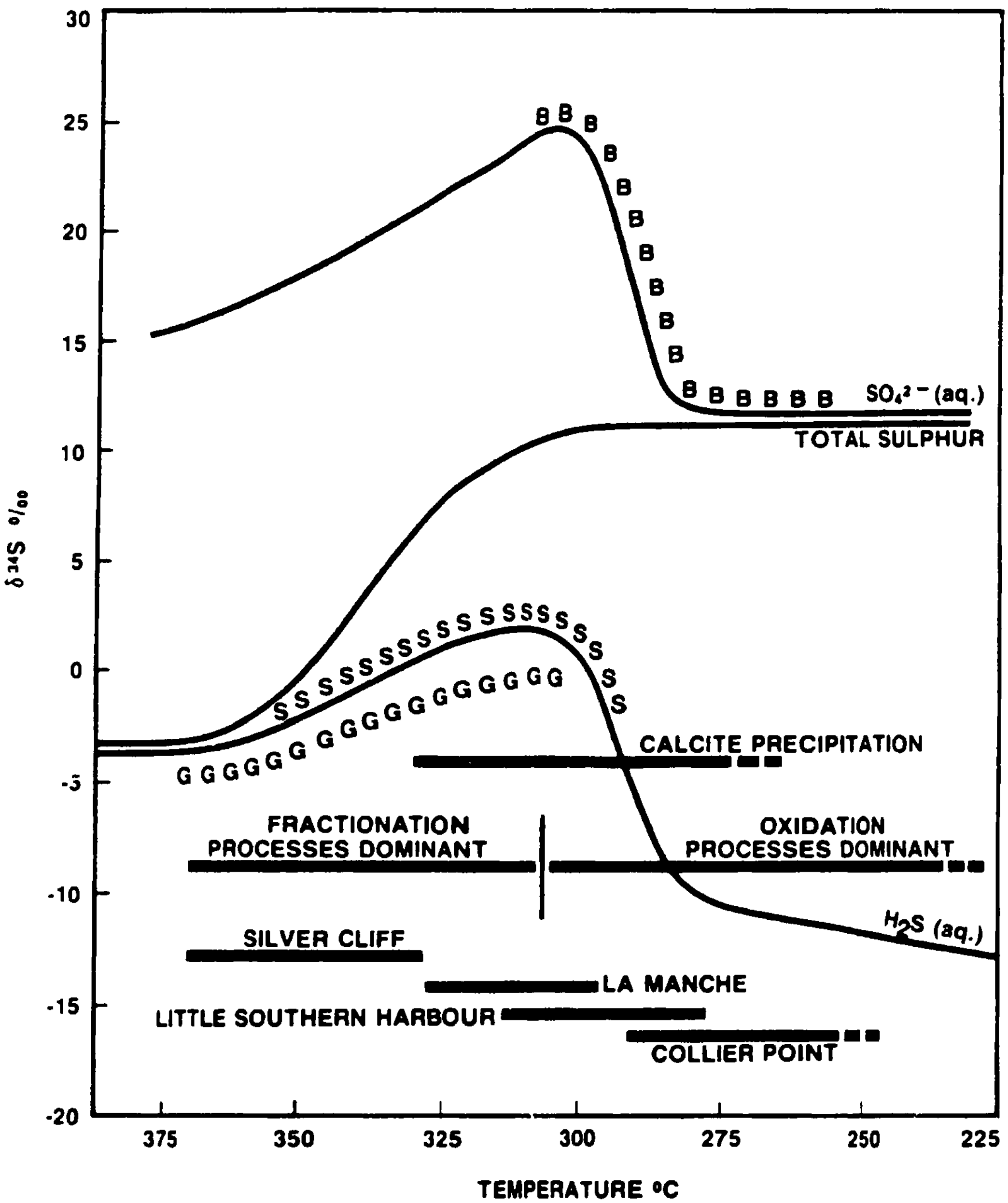

FIGURE 81: VARIATION IN SULPHUR ISOTOPIC RATIOS FOR THE SULPHUR SPECIES IN THE HYDROTHERMAL FLUID AND FOR THE PRECIPITATED SULPHUR BEARING PHASES AS VEIN FORMATION IN THE FIELD AREA PROGRESSED. ADAPTED FROM DING AND REES (1984).
B-BARITE, S-SPHALERITE, G-GALENA.

precipitated sulphur phases as vein formation progressed in the field area.

CHAPTER 5. SUMMARY OF DATA AND CONCLUSIONS, WITH COMPARISONS TO OTHER DEPOSITS

5.1. Summary of Data and Conclusions

In Chapter 2, it was shown that vein formation had taken place by mineral precipitation in a fracture set which developed during Devonian Acadian deformation. Quartz ± chlorite (± minor calcite and barite) veins are the most common and earliest-formed vein type. Veins that are dominated by calcite, barite and/or sulphide minerals are paragenetically later than the quartz-chlorite veins. Amongst these later veins, sulphide minerals are generally earliest, followed by calcite and then barite.

In Chapter 3, a study of fluid inclusions in quartz crystals from the early set of quartz-chlorite veins showed that the bulk of quartz precipitation in these veins took place at temperatures between 110°C and 230°C from a fluid with no significant salt content. Late in the paragenesis of these veins higher temperature fluids moved through the vein openings and precipitated quartz and late calcite and/or barite at higher temperatures and pressures. The higher pressure is believed due to throttling of the fracture network during rapid calcite precipitation. This resulted in a shift in the nature of the pressure to more lithostatic conditions. The fluid

inclusion evidence for samples from Collier Point indicates that this late fluid boiled at just above 300°C.

In the area of the Silver Cliff veins, fluid inclusion data from the barren quartz ± chlorite veins indicates that quartz precipitation took place over a higher range of temperatures (180°C to 330°C) than the quartz ± chlorite veins of the rest of the field area. As with the other quartz ± chlorite veins the highest temperature inclusions are from quartz which precipitated with calcite rather than chlorite. Thus the depositon of calcite and barite as late phases in the quartz-chlorite veins coincides with the introduction of a much hotter pulse of hydrothermal fluid moving through the fracture system in the entire field area. This hotter fluid was apparently hottest in the Silver Cliff mine and resulted in formation of the sulphide-mineral-dominated MacKay and Fowler veins, as well as a number of other sulphide-mineral-dominated veins in the Silver Cliff area. Fluid inclusion evidence indicates that this fluid boiled at about 370°C in the Silver Cliff mine. Away from the Silver Cliff area, where this hotter pulse of fluid was of lower temperatures, calcite- and barite-dominated veins were formed at this time.

In Chapter 4 the sulphur isotope geochemistry of galena, sphalerite and barite was shown to be consistent with a magmatic source for sulphur (other sources are also

possible as discussed). The observed evolution of sulphur isotopes through the paragenesis of galena, sphalerite and barite indicate that fractionation due to galena precipitation controlled the distribution of sulphur isotopes in sulphide minerals during the early phase of sulphide mineral-dominated precipitation. Progressive cooling resulted in oxidation of $H_2S_{(aq)}$ in the hydrothermal fluid to $SO_4^{2-}{}_{(aq)}$ (and/or $HSO_4^-{}_{(aq)}$). This resulted in a shift from sulphide- to sulphate-dominated mineral precipitation. The distribution of sulphur isotopes in sulphur bearing minerals precipitated during the oxidation process is controlled by the degree of oxidation, which in turn is highly temperature dependent.

In Chapter 4 two groups of calcites were distinguished by their REE geochemistry, as well as by their carbon and oxygen isotope geochemistry. The group A calcites precipitated from fluids which had exchanged REE and carbon isotopes with the country rock. The group B calcites have REE, carbon and oxygen isotopic distributions which suggest a magmatic source. The distribution of carbon and oxygen isotopes within the group B calcites suggests precipitation from a fluid which underwent progressive cooling during crystallization.

The transition described above, from reducing to oxidizing conditions in the hydrothermal fluid, also manifests itself in the nature of Eu anomalies developed

in group B calcites. Early calcites precipitated with sulphide minerals under reducing conditions have well developed negative Eu anomalies. Paragenetically later calcites precipitated with barite have much smaller negative Eu anomalies, reflecting the more oxidizing nature of the hydrothermal fluid at that time. Finally, there is a well developed REE crystal fractionation trend observed for the group B calcites created during progressive calcite precipitation.

The data collected in this study (field relationships, paragenetic data, fluid inclusion data, carbon, oxygen and sulphur isotope data, REE data) allow the following conclusions to be made about the veins in the field area.

1) The early quartz $\pm$ chlorite veins were formed during a regional deformational and low grade metamorphic event, by precipitation in fracture sets developed during this deformation.

2) During this deformational event a much hotter pulse of hydrothermal fluid moved through the same fracture set. This later fluid pulse deposited sulphide-mineral-dominated veins where it was hottest and presumably closest to its source (Silver Cliff, La Manche). Further from the source, where the fluid was cooler, calcite- and barite-dominated veins were precipitated (Collier Point, Bellevue Peninsula, Cuslet Cove, etc..).

3) The proximity of the "hottest" sulphide dominated veins to suspected syndeformational granitic intrusions, combined with the geochemical evidence, strongly suggest that the hot fluid pulse was sourced by exsolution of fluid during crystallization of these granitic magmas. Carbon, oxygen, sulphur and REE were all likely sourced from these granitic melts as well. In some of the veins studied, there is evidence that elemental and isotopic exchange took place between this magmatic fluid and either the surrounding country rock or meteoric waters.

5.2. Comparison to Other Deposits

The Taolin Zn-Pb-fluorite deposit, of the Hunan province in China, displays a number of similarities to the Silver Cliff deposit. The Taolin deposits occur along a major fault zone between the Mofushian granite batholith (136 Ma, Li et al. 1964) and Proterozoic aged metamorphic phyllites and quartzites (Ding and Rees 1984). The fault zone is 50-300 m wide and trends east-northeast for over 20 km (Ding et al. 1986). Mineralization developed as fissure filling veins and as cementation of brecciated ore and country rock, in part concentrated at fault intersections (Ding et al. 1986). The MacKay vein at Silver Cliff was formed by fissure filling in a fault zone with brecciation of ore and country rock increasing near the intersection of faults (Chute 1939). Chute believed

that ore was concentrated near these fault intersections. Silver Cliff vein formation has taken place close to where much younger granitic rocks have intruded Proterozoic metamorphic rocks. Thus both the geological setting and the nature of mineral emplacement are similar for both deposits.

Mineralogically there are both similarities and differences. At Taolin there is a pre-ore stage of barren quartz described by Roedder and Howard (1988), comparable to the early barren quartz veins found in the present study area. Ding and Rees (1984) describe an early stage of ore mineralization (stage 1) consisting of galena, dark brown sphalerite, chalcopyrite, quartz and fluorite. At Silver Cliff the ore mineralization stage consists of galena, sphalerite (dark earlier than light), quartz, pyrite and chalcopyrite. The obvious differences are the presence of fluorite at Taolin, absent from Silver Cliff (and La Manche) and the absence of early pyrite at Taolin. The second ore mineralization stage (stage 2) described by Ding and Rees (1984) at Taolin consists of barite, galena, light sphalerite, calcite and chalcopyrite. The introduction of later barite, calcite and lighter coloured sphalerite are all features observed at Silver Cliff. "Later" calcite and barite is a feature also found in a number of other veins in the present study area (i.e., La Manche, Little Southern Harbour, etc.).

Ding and Rees (1984) studied sulphur isotopes in the sulphide minerals at Taolin. Sulphur isotope geothermometry at Taolin indicates that stage 1 veins precipitated over a temperature range from 345°C to 265°C, while stage 2 veins precipitated over a lower temperature range from 265°C to 220°C. These results are similar to those of this study using fluid inclusion evidence and one sulphur isotope pair. At Silver Cliff the highest temperatures found were 370°C ranging down to around 285°C for the ore assemblage. These are modestly higher temperatures than those found by Ding And Rees (1984) at Taolin, but this is easily explained by a modest difference in the depth of formation. Roedder and Howard (1988) conducted a fluid inclusion study of one of the Taolin deposits (Shangtangchong mine) but were not able to find a reliable geobarometer to determine pressure and therefore the depth of formation of the deposit that they studied.

The trend towards lower temperatures during later calcite and barite precipitation is similar for both deposits. Roedder and Howard (1988) found a much lower temperature range of 200°C to 120°C using fluid inclusions from quartz, sphalerite fluorite and barite. However their study was limited to only eight "representative" samples. Also they admit that it is questionable as to whether or not any of the fluid inclusions found in both

barite and sphalerite were primary. Perhaps further study of quartz from contemporaneous quartz-ore mineral assemblages would yield higher temperatures.

Ding and Rees (1984) modelled the variation of sulphur isotope ratios found in various sulphur-bearing species in the hydrothermal fluid and the resulting precipitated sulphide minerals at Taolin. Figure 82 illustrates the result of their modelling and shows, similar to what was shown for the Avalon veins, that the earlier sulphide and later co-precipitated barite and sulphide minerals all had the same sulphur source, which they describe as primary, either from the mantle or from partial melting of a deep crustal source. The sulphur-bearing minerals of stage 2 precipitated from a fluid which was a residue of stage 1 precipitation. Similar to Avalon veins, Ding and Rees (1984) showed that the sulphur isotope variations found in the sulphur-bearing mineral species can be explained by processes of: 1) increasing fractionation between various sulphur-bearing species in the hydrothermal fluid and the precipitating sulphide minerals with decreasing temperature; 2) oxidation of sulphide to sulphate. However Ding and Rees (1984) also state that the precipitation of sulphide minerals involved no isotope fractionation. Yet Figure 80 clearly shows that there will be sulphur isotope fractionation between precipitated galena and $H_2S_{(aq)}$ over the temperature range

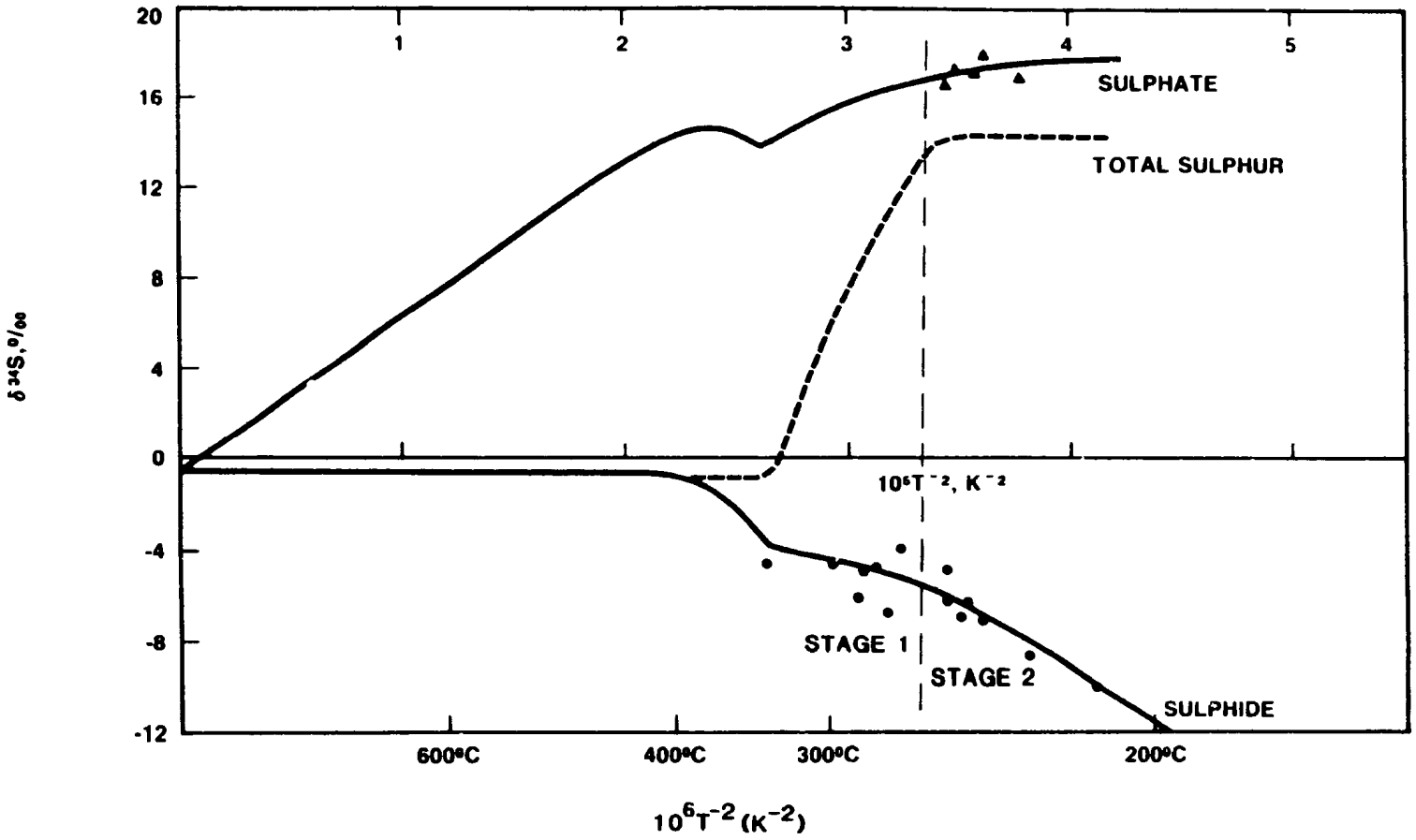

FIGURE 82: CALCULATED VARIATIONS OF $\delta^{34}S$ WITH $1/T^2$ FOR SULPHATE IN SOLUTION, SULPHIDE IN SOLUTION AND TOTAL SULPHUR IN SOLUTION FOR THE OPTIMUM SET OF FITTING CONDITIONS, FOR THE TAOLIN DEPOSIT (DING AND REES 1984).

indicated for all sulphide mineral deposition in the Taolin deposit. However if the amount of galena precipitation is relatively small the effects of galena precipitation may be minimal relative to the other two processes. They have not demonstrated this to be the case in the Taolin deposit.

Ding et al. (1986) studied oxygen and lead isotopes from the Taolin deposit. They suggested that lead was probably derived from the Mofushian granite. Water from the hydrothermal fluid from which the Taolin deposit formed contains oxygen which either exchanged with the granite or was partially magmatic in origin. This is similar to results found for oxygen from the calcites of the Avalon veins. As well the carbon and sulphur from the Avalon veins have an indicated magmatic source.

Another similarity between the Taolin and the Avalon veins is the low salinity indicated for the hydrothermal fluid from which the deposits precipitated. Roedder and Howard (1988) describe salinities ranging from 0 to 14 wt. % NaCl(eq). The range found for the Silver Cliff veins was 0 to 7 wt. % NaCl(eq) which is somewhat lower on average. This may be due to a greater depth of formation of the Silver Cliff deposit which would result in a lesser degree of previous boiling which takes place before the fluids reached the deeper level of the Silver Cliff veins. Fluids rising to the shallower levels of the Taolin veins

have a greater opportunity for boiling and thus for developing higher salinities.

Finally both deposits have alteration zones next to the veins. Ding and Rees (1984) report wall rock alteration consisting predominantly of silicification with lesser chloritization and sericitization. At Silver Cliff the wall rock next to veins has been altered to quartz and pyrite. Roedder and Howard (1988) reported that there was a lack of wall-rock alteration in the Shangtangchong mine, which appears to be at odds with the results of Ding and Rees (1984).

Kamilli and Ohmoto (1977) studied the paragenesis of the Finlandia vein of the Colqui District in Central Peru. This vein is situated in a belt of Tertiary andesitic volcanic rocks with norite and andesite porpyhry stocks intruded into the area. The Colqui district has been subjected to a folding event of moderate intensity with contemporaneous faulting developed along two principal fracture orientations. Radiometric dating of muscovites from the vein yielded two overlapping ages of 10.0 $\pm$ 5 Ma and 10.6 $\pm$ 5 Ma (K-Ar), corresponding to the age of intense volcanism in the Central Andes, which also corresponds to the age of deformation and intrusive activity in this area (Kamilli and Ohmoto 1977). The geological setting of the Finlandia vein is thus very similar to the setting of the Avalon veins in terms of

folding, faulting and fracture development, with contemporaneous intrusion of magmas.

Samples were collected from the Finlandia vein as mining progressed, resulting in very good paragenetic control. This degree of control allowed for the recognition of seven distinct stages of precipitation (Kamilli and Ohmoto 1977). Quartz dominated the first three stages of precipitation. Sphalerite and galena are dominant or very significant through stages IV to VII. Quartz was variably important through these last four stages and present in all seven stages. Siderite is present in the final three stages of vein precipitation and barite was deposited in the final stage of vein formation. This sequence of mineral precipitation from early quartz to later sulphide minerals to later carbonate and finally barite, is similar to that found at Silver Cliff and throughout the Avalon study area.

In the Finlandia vein, muscovite is present in minor amounts throughout much of the paragenesis of the vein. Minor amounts of argentite and tetrahedrite are also present from stage I through to stage VI precipitation. In particular stage II contains high silver and gold values (up to 43 and 1.8 oz/short ton respectively). In the MacKay vein at Silver Cliff, silver was found in galena giving ore grades up to 159 oz/short ton averaging

30 oz/short ton. No silver mineral has yet been recognized at Silver Cliff.

The fluid inclusion study carried out by Kamilli and Ohmoto (1977) using quartz crystals from the Finlandia vein shows similarities to the Avalon fluid inclusion study. Primary fluid inclusions in quartz crystals from the Finlandia vein contain predominantly vapour-poor inclusions and a much smaller number of vapour-rich inclusions which have much higher homogenization temperatures, similar to the distribution of fluid inclusions found in quartz crystals in the Avalon veins. Also similar is the interpretation of these vapour-rich high temperature inclusions as having trapped variable proportions of liquid and vapour during a time when the hydrothermal fluid was boiling (stage II in Finlandia vein).

A pressure study using fluid inclusions which boiled indicated that the Finlandia vein formed at a depth of about 1000 metres, compared with 2000 metres for the Silver Cliff veins, using purely hydrostatic models. The fluid inclusion evidence from the present study suggests that there was a component of lithostatic pressure during the formation of the Silver Cliff vein (and other late-formed veins). Thus there may not have been that much difference in the depth of formation of the Silver Cliff and the Finlandia veins. Possible shallower depths

indicated for the Finlandia vein would correspond with lower temperatures of boiling of the fluid (290°C at Finlandia compared with 370°C at Silver Cliff) and vein formation. Salinity values measured for the fluid inclusions in quartz from the Finlandia vein range from 0 to 13 wt. % NaCl(eq) (Kamilli and Ohmoto 1977). These higher salinities again indicate a larger proportion of previous boiling than is indicated for the Silver Cliff veins, possibly the result of vein formation at shallower levels.

Figure 83 shows how the sulphur isotopic compositions of galena and sphalerite vary through the paragenetic stages of precipitation in the Finlandia vein. For both minerals the $\delta^{34}S$ values increase progressively from stage I through to stage VI. In stage VII, when precipitation of barite begins, with its much higher $\delta^{34}S$ values, the $\delta^{34}S$ values of galena and sphalerite drop sharply. These observed trends match very well with the hypothesised trend shown in Figure 81 for the veins in the Avalon area. As with the Avalon veins the $\delta^{34}S$ trends in the Finlandia vein can be explained by early galena precipitation with fractionation processes dominating. Fractionation, due to galena precipitation, gradually drove up the value of $\delta^{34}S_{(H2S)}$ in the hydrothermal fluid and thus subsequent sulphide minerals. This is followed

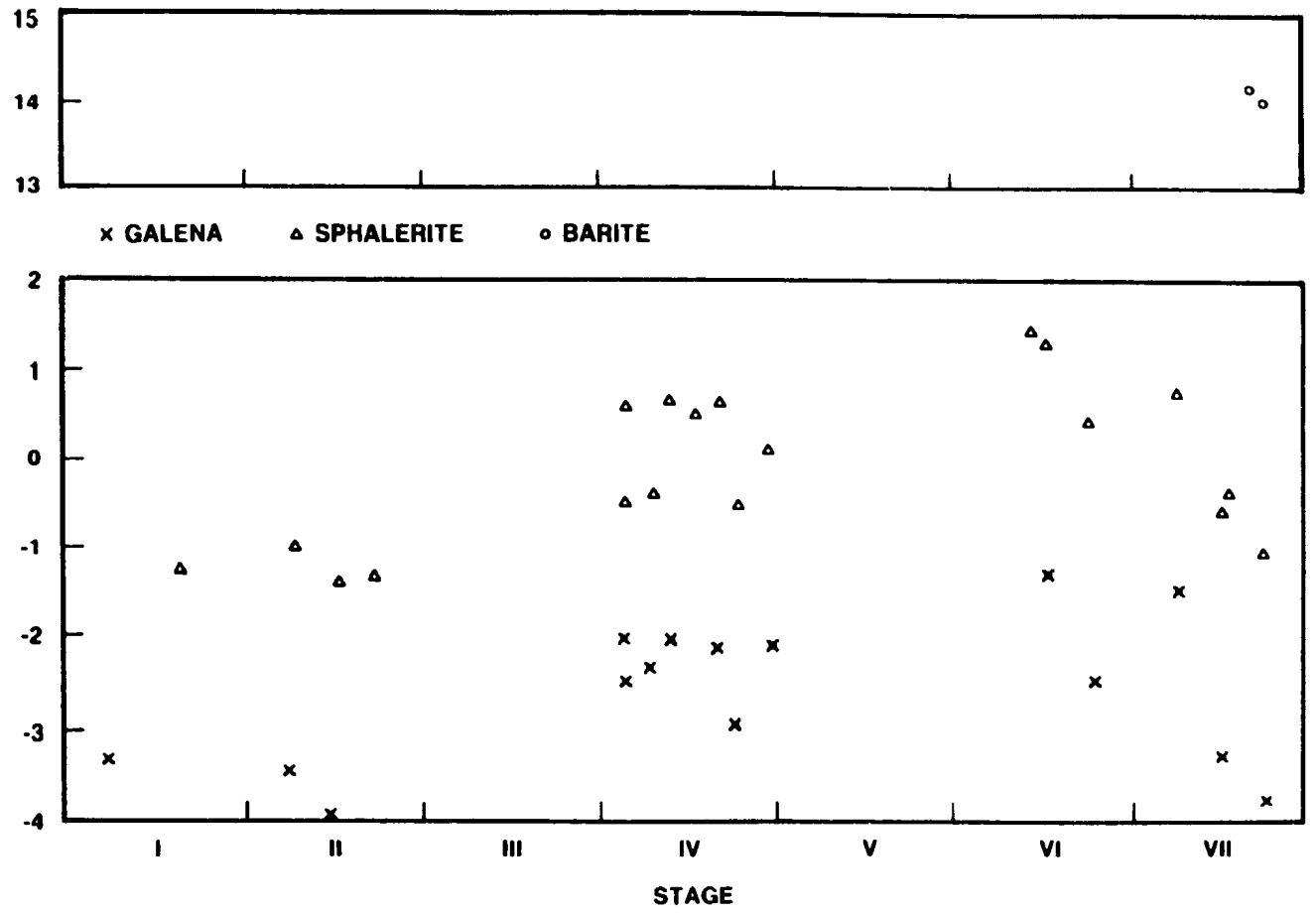

FIGURE 83: VARIATION IN SULPHUR ISOTOPIC COMPOSITIONS OF GALENA AND SPHALERITE THROUGH THE STAGES OF VEIN PRECIPITATION IN THE FINLANDIA VEIN. FROM KAMILLI AND OHMOTO (1977).

by a later oxidation dominant process which converted $H_2S_{(aq)}$ to $SO_4^{2-}{}_{(aq)}$ (or $HSO_4^-{}_{(aq)}$). This oxidation drove down the $\delta^{34}S_{H2S}$ value and results in much higher $\delta^{34}S$ values for sulphate (see Chap. 4). Kamilli and Ohmoto (1977) favour an explanation whereby the fO_2-pH conditions are such that oxidized sulphur species are dominant throughout the vein paragenesis. This explanation favours a sedimentary origin for the sulphur whereas the explanation suggested here favours an igneous origin for the sulphur. The explanation suggested by Kamilli and Ohmoto (1977) fails to account for the observed isotopic trends which are similar to those shown in Figures 81 and 82.

Oxygen isotope data from quartz, and hydrogen isotope data from the Finlandia hydrothermal fluid trapped in fluid inclusion in quartz strongly suggest that meteoric water dominated the fluid from which quartz precipitated. Such an isotopic study was not undertaken for the Avalon veins and it is not known if meteroic water was involved in the precipitation of quartz in these veins. However if this were so, the mixing of meteoric fluid with igneous derived fluid would aid in the cooling and possibly the oxidation of the igneous sulphur-bearing fluid, promoting the mineral paragenesis observed in both veins.

So et al. (1984) described the Sambo Pb-Zn-barite deposit, located 45 km south of Seoul, South Korea. This deposit is composed of fissure-filling ore veins which developed in Proterozoic biotite schists. The area has been intruded by Jurassic granodiorite stocks (177.3 ± 3.6 Ma, K-Ar from biotite in granite; 163.6 ± 3.3 Ma, K-Ar from muscovite in granodiorite) which are believed to have the same age as the ore deposit. The Jurassic age of the ore deposit is implied by its similarity in mineralogy, which is Ba-rich, to a known Korean Jurassic to Early Cretaceous Ba-rich metallogenic epoch.

Three distinct stages of mineralization have been recognized, from earliest to latest: 1) abundant quartz with small amounts of barite and minor sphalerite, galena, pyrite and chalcopyrite; 2) main ore stage composed of quartz and barite as the dominant minerals with abundant sphalerite and galena, and minor pyrite, chalcopyrite, calcite and dolomite; 3) quartz dominant stage with lesser barite, galena and sphalerite and minor pyrite, chalcopyrite, calcite and dolomite. There is no clear separation of the major minerals described above by their stages, with only their abundance in each stage changing. Thus despite the similarity in the minerals found in the Sambo veins with those of the Avalon veins, the paragenetic distribution of these minerals is distinctly different. The presence of barite in the early stage of

vein formation suggests that conditions were more oxidizing in the Sambo hydrothermal fluid earlier in the vein paragenesis. The presence of sulphide minerals late in the vein paragenesis suggests that the hydrothermal fluid maintained a similar level of oxidizing character throughout vein formation.

A fluid inclusion study was carried out on the quartz crystals from each stage of the vein (So et al. 1984). No obvious spatial or temporal trends could be documented by this study. However an analysis of the data presented by So et al. (1984) shows that all fluid inclusions in quartz from a mineral assemblage which contains barite homogenized at or below 270°C. Fluid inclusions in quartz found in mineral assemblages with sulphide minerals, but with no barite, homogenized up to 324°C. There was considerable overlap in the Th values for the various assemblages analysed. Pressure data suggest that trapping of inclusions took place at 500 m or 1250 m for lithostatic and hydrostatic conditions respectively. Salinities ranged from 0.7 to 16.9 wt. ‰ NaCl(eq). Thus slightly shallower depths and higher salinities are indicated for the Sambo deposit relative to the Silver Cliff veins, and again may suggest a greater degree of previous boiling at Sambo.

Sphalerites from the Sambo deposit have $\delta^{34}S$ values ranging from -3.7 to -9.6 ‰, while $\delta^{34}S$ values from

galena range from -6.4 to -11.8 ‰ (So et al. 1984). Barites have $\delta^{34}S$ values ranging from +14.7 to +17.2 ‰. No systematic temporal or spatial variations of the $\delta^{34}S$ values in these minerals were found. It is interesting to compare these $\delta^{34}S$ values with those found for the same minerals in the Avalon veins. The $\delta^{34}S$ values for the sulphide minerals are significantly lower at Sambo, while the values for barite are significantly higher (Avalon values: galena -2.3 to -5.5 ‰; sphalerite +1.7 to -0.7 ‰; barite +9.6 to +15.4 ‰). In the Avalon veins most of the sulphide mineral precipitation was complete before barite precipitation began. Thus the values of $\delta^{34}S$ obtained for the sulphide minerals reflect equilibrium with $\delta^{34}S_{H2S}$ in the hydrothermal fluid during a period in which most of the sulphur in the hydrothermal fluid was in the $H_2S_{(aq)}$ form. Similarly, when barite precipitated, most of the sulphur in the hydrothermal fluid existed as $SO_4^{2-}{}_{(aq)}$ (or $HSO_4^{-}{}_{(aq)}$). At Sambo, however, barite and sulphide minerals precipitated from a hydrothermal fluid which must have constantly contained significant quantities of both $H_2S_{(aq)}$ and $SO_4^{2-}{}_{(aq)}$ (or $HSO_4^{-}{}_{(aq)}$) at the same time. The modelling that Ding and Rees (1984) did for the Taolin deposit shows that there can be a considerable range of temperatures over which both $H_2S_{(aq)}$ and $SO_4^{2-}{}_{(aq)}$ will be significant components of the precipitating fluid. This range is illustrated by the

total sulphur line in Figure 81 where it undergoes the transition from $H_2S_{(aq)}$ to $SO_4^{2-}{}_{(aq)}$ dominated fluids.

As can be seen from Figure 80, assuming a primary magmatic sulphur source similar to the Avalon veins, barite which is precipitated under conditions of incomplete oxidation can develop $\delta^{34}S_{(bar)}$ values up to +25 ‰. Under "oxidation-dominant" to "oxidation-complete" conditions, values for $\delta^{34}S$ in sulphide minerals can easily reach down to -12 ‰. Thus the mineralogical differences between the Sambo and the Avalon veins may be due only to the constancy in the character of the hydrothermal fluid, being partially oxidized at Sambo, relative to that seen for the Avalon veins. This constancy may be due only to the limited geographic nature of the study conducted by So et al. (1984) which was restricted to the mine itself.

5.3. Summary

The Avalon veins which formed during the quartz-galena-sphalerite-calcite-barite mineralization event have fundamental similarities to a number of veins in other deposits described in published literature, three of which were described here (Taolin, Finlandia and Sambo). Other deposits not described here include the veins of "Lake City District", Colorado (Slack 1980); the "Mainland" group veins near Thunder Bay, Ontario (Franklin et al.

1986); the "Fresmillo" silver-lead-zinc mine in Mexico (Macdonald et al. 1986). These deposits are all formed by an event of crystal precipitation in fissure-filling veins associated with contemporaneous granitic intrusion. Where geochemical analysis has been performed the granitic magmas invariably are found to have acted as the heat source for the deposits and also to have supplied many of the components for both gangue and ore minerals. Where the mineralogic evolution has been documented these deposits have similar mineral assemblages and show similar evolution of these assemblages.

It is clear from comparing these various studies to the study presented above that the presentation of data from only a few aspects of vein formation, or from only a limited geographical area, can result in erroneous conclusions, or conclusions which are limited in their scope. This study greatly benefited from covering an area much larger than a single mine site. It has also benefited from the wide range of analysis techniques that have been employed (structural geology, paragenetic study, fluid inclusions, REE, carbon, oxygen and sulphur isotopes).

REFERENCES

Anderson, M. M., 1981. The Random Formation of southeastern Newfoundland: A discussion aimed at establishing its age and relationship to bounding formations. Am. J. Sci., v. 281, pp. 807-830.

Anderson, M. M., Bruckner, W. D., King, A. F., and Maher, J. B., 1975. The late Proterozoic "H. D. Lilly Unconformity" at Red Head, northeastern Avalon Peninsula, Newfoundland. Am. J. Sci., v. 27, pp. 1012-1027.

Badgley, P. C., 1965. Structural and Tectonic Principles. Harper and Row, New York, 521 p.

Barnes, H. L., 1979. Solubilities of ore minerals. In: Geochemistry of Hydrothermal Ore Deposits, ed., Barnes, H. L., John Wiley and Sons, New York, pp. 404-460.

Bell, K., Blenkinsop, J., and Strong, D. F., 1977. The geochronology of some granitic bodies from eastern Newfoundland and its bearing on Appalachian evolution. Can. J. Earth Sci., v. 14, pp. 456-476.

Bell, K., and Blenkinsop, J., 1977. Geochronological evidence of Hercynian activity in Newfoundland. Nature, v. 265, No. 5595, pp. 616-618.

Bell, K., and Blenkinsop, J., 1975. Geochronology of Eastern Newfoundland. Nature, 254, pp. 410-411.

Bengston, S., and Fletcher, T. P., 1983. The oldest sequence of skeletal fossils in the lower Cambrian of southeastern Newfoundland. Can. J. Earth Sci., v. 20, pp. 525-536.

Bilal, B. A., and Becker, P., 1979. Complex formation of trace elements in geochemical systems. II: Stability of rare earth fluoro-complexes in fluorite-bearing model systems of varying ionic strengths. J. Inorg. Nuclear Chem., v. 41, pp. 1607-1608.

Bilal, B. A., Herrmann, F., and Fleischer, W., 1979. Complex formation of trace elements in geochemical systems. I: Potentiometric study of fluoro-complexes of rare earth elements in fluorite-bearing model systems. J. Inorg. Nuclear Chem., v. 41, pp. 347-350.

Bilal, B. A. and Kob, V., 1980. Complex formation of trace elements in geochemical systems. III: Studies on the distribution of fluoro-complexes of rare earth elements in fluorite-bearing model systems. J. Inorg. Nuclear Chem., v. 42, pp. 629-630.

Blackwood, R. F. and O'Driscoll, C. F., 1976. The Gander-Avalon boundary in northeastern Newfoundland. Can. J. Earth Sci., v. 13, pp. 1155-1159.

Blackwood, R. F. and Kennedy, M. J., 1975. The Dover Fault: Western boundary of the Avalon Zone in northeastern Newfoundland. Can. J. Earth Sci., v. 12, pp. 320-325.

Bodnar, R. J. and Bethke, P. M., 1984. Systematics of stretching of fluid inclusions I: fluorite and sphalerite at 1 atmosphere confining pressure. Econ. Geol., v. 79, pp. 141-161.

Bruckner, W. D., 1969. Geology of the eastern part of the Avalon Peninsula, Newfoundland - a summary. AAPG Memior 12, pp. 130-138.

Buddington, A. F., 1919. Pre-Cambrian rocks of southeast Newfoundland. J. Geol., v. 27, pp. 449-479.

Burnham, C. W., 1979. Magmas and hydrothermal fluids. In: Geochemistry of Hydrothermal Ore Deposits, ed., Barnes, H.L., John Wiley and Sons, New York, pp. 71-136.

Cant, J. W., 1974. A VLF-EM and geochemical survey of the Silver Cliff property, Argentia, Newfoundland. Commodore Mining Company, unpublished. Nfld. MDD File - 1N/5, 226 p.

Chappell, B. W. and White, A. J. R., 1974. Two contrasting granite types. Pacific Geol., v. 8, pp. 173-174.

Chute, N. E., 1939. Mineral deposits of the Placentia Bay area. Geol. Surv., Nfld. unpubl. rept., Open File IN (16).

Cox, K. G., Bell, J. D. and Pankhurst, R. J., 1979. The Interpretation of Igneous Rocks. George Allen and Unwin, London, 450 p.

Czamanske, G. K., and Rye, R. O., 1974. Experimentally determined sulfur isotope fractionations between sphalerite and galena in the temperature range 600oC to 275oC. Econ. Geol., v. 69, pp. 17-25.

Dallmeyer, R. D., Hussey, E. M., O'Brien, S. J., and O'Driscoll, C. F., 1983. Chronology of tectonothermal activity in the western Avalon Zone of the Newfoundland Appalachians. Can. J. Earth Sci., v. 20, pp. 355-363.

Dallmeyer, R. D., Blackwood, R. F. and Odom, A. L., 1981b. Age and origin of the Dover Fault: tectonic boundary between the Gander and Avalon Zones of the northeastern Newfoundland Appalachians. Can. J. Earth Sci., v. 18, pp. 1431-1442.

Dallmeyer, R. D., Odom, A. L., O'Driscoll, C. F. and Hussey, E. M., 1981a. Geochronolgy of the Swift Current Granite and host volcanic rocks of the Love Cove Group, southwestern Avalon Zone, Newfoundland: evidence of a late Proterozoic volcanic-subvolcanic association. Can. J. Earth Sci., v. 18, No. 4, pp. 699-707.

Dallmeyer, R. D., 1980. Geochronology report. Current Research. Newfoundland Dept. of Mines and Energy, Min. Dev. Div., Report 80-1.

Dickson, W. L., Elias, P., and Talkington, R. W., 1980. Geology and geochemistry of the Ackley Granite, southeast Newfoundland. Current Research. Nfld. Dept. of Mines and Energy, Min. Dev. Div., Report 80-1.

Ding, T., Younge, C., Schwarcz, H. P. and Peng, Z., 1986. Oxygen, hydrogen and lead isotope studies of the Taolin lead-zinc ore deposit, China. Econ. Geol., v. 81, pp. 421-29.

Ding, T. and Rees, C. E., 1984. The sulpher isotope systematics of the Taolin lead-zinc ore deposits, China. Geochim. Cosmochim. Acta, v. 48, pp. 2381-92.

Dudas, F. O., Campbell, I. H., and Gorton, M. P., 1983. Geochemistry of igneous rocks in the Hokuroku District, northern Japan. In: Ohmoto, H. and Skinner, B. J., editors, The Kuroko and Related Volcanogenic Massive Sulphide Deposits. Econ. Geol. Mon. 5, pp. 115-133.

Elias, P., and Strong, D. F., 1982. Paleozoic granitoid plutonism of southern Newfoundland: contrasts in timing, tectonic setting and levels of emplacement. Transactions of the Royal Society of Edinburgh: Earth Sciences, v. 73, pp. 43-57.

Eldridge, C. S., Barton, Jr., P. B., and Ohmoto, H., 1983. Mineral textures and their bearing on formation of Kuroko orebodies. Econ. Geol. Mon. 5, pp. 241-281.

Eldridge, C. S., Bourcier, W. L., Ohmoto, H. and Barnes, H. L., 1988. Hydrothermal inoculation and incubation of calcopyrite disease in sphalerite. Econ. Geol., v. 83, pp. 978-989.

Fletcher, T. P., 1972. Geology and Lower to Middle Cambrian trilobite faunas of southwest Avalon, Newfoundland, Unpub. Ph.D. Thesis, Univ. of Cambridge, England, 530 p.

Flynn, R. T., and Burnham, W. C., 1978. An experimental determination of rare earth partition coefficients between a chloride containing vapour phase and silicate melts. Geochim. Cosmochim. Acta, v. 42, pp. 685-701.

Franklin, J. M., Kissin, S. A., Smyk, M. C. and Scott, S. D., 1986. Silver deposits associated with the Proterozoic rocks of the Thunder Bay District, Ontario. Can. J. Earth Sci., v. 23, pp. 1576-91.

Frey, F. A., Haskin, M. A., Poetz J. O. and Haskin L. A. 1968. Rare Earth Element Abundances in Some Basic Rocks. J. Geophysical Res., v. 73, pp. 6085-98.

Gibson, I. L. and Jagam, P., 1980. Instrumental nuetron activation analysis of rocks and minerals. In: Mineralogical Association of Canada - Short Course in Neutron Activation Analysis, ed., Muecke, G. K., pp. 109-131.

Green, R. E., 1981. Genesis of the La Manche vein and comparisons with similar Caledonide deposits. B.Sc. Thesis, Memorial Univ. Nfld., St. John's, Nfld.

Greene, B. A. and Williams, H., 1974. Fossil localities and the base of the Cambrian in southeastern Newfoundland. Can. J. Earth Sci., v. 11, pp. 319-323.

Greene, B. A., 1973. Burin-Bonavista Project. Geology of the Marystown and St. Lawrence Map Areas (1M/3, 1L/14). Summary based on literature and 1973 field work. Nfld. Dept. of Mines and Energy, unpublished report.

Guichard, F., Church, T. M., Treuil, M. and Jaffrezic, H., 1979. Rare earth in barites: distribution and effect on aqueous partitioning. Geochim. Cosmochim. Acta, 43, pp. 983-997.

Haas, J. L., Jr., 1976. Physical properties of the co-existing phases and thermochemical properties of the H2O component in boiling NaCl solutions. U.S. Geol. Surv., Bulletin 1421-A, 73 p.

Haas, J. L., Jr., 1971. The effect of salinity on the maximum thermal gradient of a hydrothermal system at hydrostatic pressure. Econ. Geol., v. 66, pp. 940-946.

Hanor, J. S., 1979. The sedimentary genesis of hydrothermal fluids. In: Geochemistry of Hydrothermal Ore Deposits, ed., Barnes, H.L., John Wiley and Sons, New York, pp. 137-172.

Haworth, R. T. and Lefort, J. P., 1979. Geophysical evidence for the extent of the Avalon Zone in Atlantic Canada. Can. J. Earth Sci., v. 16, pp. 552-567.

Hayes, A. O., 1948. Geology of the area between Bonavista and Trinity Bays, Eastern Newfoundland. Geol. Surv. Nfld., Bulletin 32, pt. 1.

Helgeson, H. C., 1969. Thermodynamics of the hydrothermal systems at elevated temperatures and pressures. Am. J. Sci., v. 267, pp. 729-8C4.

Hertogen, I. and Gijbels, R., 1971. Instrumental neutron activation of rocks with a low-energy photon detector. Anal. Chem. Acta, v. 56, pp. 61-82.

Hibbard, J., 1983. Geology of the Island of Newfoundland. Nfld. Dept. of Mines and Energy, Min. Div., Map 83-106.

Hiscott, R. N., 1982. Tidal deposits of the Lower Cambrian Random Formation, eastern Newfoundland: facies and paleoenvironments. Can. J. Earth Sci., v. 19, pp. 2028-2042.

Hobbs, B. E., Means, W. D. and Williams, P. F., 1976. An outline of Structural Geology. John Wiley and Sons, New York, 571 p.

Hoffmann, H. J., Hill, J. and King, A. F., 1979. Late Precambrian microfossils, southeastern Newfoundland. Current Research. Part B, Geol. Surv. Can., Paper 79-1B, pp. 83-98.

Holland, D. H., and Malinin, S. D., 1979. The solubiiity and occurrence of non-ore minerals. In: Geochemistry of Hydrothermal Ore Deposits, ed., Barnes, H.L., John Wiley and Sons, New York, pp 461-508.

Howley, J. P. and Murray, A., 1918. Reports of Progress, 1881-1909. Geol. Surv., Nfld.

Howse, A. F., Butler, A. J. and Collins, C. J., 1984. Stream sediment geochemistry of the St. Brides area, Avalon Peninsula, Bewfoundland. Nfld. Dept. of Mines and Energy, Min. Dev. Div., Open File 1L/16, p. 90.

Howse, A. F., Butler, A. J. and Collins, C. J., 1984. Stream sediment geochemistry of the Bellevue Map Area (1N/12), Avalon Peninsula, Newfoundland. Nfld. Dept of Mines and Energy, Min. Dev. Div., Open File 1N/12, p. 452.

Hughes, C. J., 1973. Late Precambrian volcanic rocks of Avalon, Newfoundland - a spilite/keratophyre province: recognition and implications. Can. J. Earth Sci., v. 10, pp. 272-282.

Hughes, C. J. and Bruckner, W. D., 1971. Late Precambrian rocks of eastern Avalon Peninsula, Newfoundland - a volcanic island complex. Can. J. Earth Sci., v. 8, pp. 899-915.

Hughes, C. J. and Malpas, J. G., 1971. Metasomatism in the late Precambrian Bull Arm Formation in southeastern Newfoundland: recognition and implications. Geol. Assoc. Can. Proc., v. 24, No. 1, pp. 85-93.

Hussey, E. M., 1980. Geology of the Clode Sound area, Newfoundland. Unpublished M.Sc. thesis, Memorial University of Newfoundland, St. John's, Canada.

Hutchinson, M. N. and Scott, S. D., 1981. Sphalerite geobarometry in the Cu-Fe-Zn-S system. Econ. Geol., v. 76, pp. 143-153.

Jenness, S. E., 1963. Terra Nova and Bonavista map areas, Newfoundland. Geol. Surv. Can., Mem. 327, 184 p.

Jenness, S. E., 1957. Gander Lake (east half), Newfoundland. Geol. Surv. Can., Map 3 - 1957.

Kay, M., 1967. Stratigraphy and structure of northeastern Newfoundland bearing on drift in North Atlantic. A.A.P.G. Bulletin, v. 51, No. 4, pp. 579-600.

Kay, M. and Colbert, E. H., 1965. Stratigraphy and Life History. John Wiley and Sons, Inc., New York, 736 p.

Kennedy, G. C., 1950. A portion of the system silica-water. Econ. Geol., v. 45, pp. 629-53.

Keppie, J. D. (compiler), 1979. Geological map of Nova Scotia. Nova Scotia Dept. of Mines, Canada.

Kerrich, R., Strong, D. F., Andrews, A. J., and Owsiacki, L., 1986. The silver deposits at Cobalt and Gowganda, Ontario. III: Hydrothermal regimes and source reservoirs - evidence from H, O, C, and Sr isotopes and fluid inclusions. Can. J. Earth Sci., v. 23, No. 10, pp. 1519-1550.

Kilinc, I. A., and Burnham, C. S., 1972. Partitioning of chloride between a silicate melt and co-existing aqueous phase from 2 to 8 kilobars. Econ, Geol., v. 67, pp. 231-235.

King, A. F., 1980. The birth of the Caledonides: Late Precambrian rocks of the Avalon Peninsula, Newfoundland and their correlatives in the Appalachian Orogen. In: Proceedings, "The Caledonides in the U.S.A.." Int. Geol. Cor. Proj., Caledonide Orogen, I.G.C.P. 1980, Blacksburg, Virginia.

King, A. F., Bruckner, W. D., Anderson, M. M. and Fletcher, T. P., 1974. Late Precambrian and Cambrian sedimentary sequences of eastern Newfoundland. Geol. Assoc. Can. Ann. Mtg., Field Trip Manual B-6.

Kontak, D. J., Tuach, J., Strong, D. F., Archibald, D. A., and Farrar, E., 1988. Plutonic and hydrothermal events in the Ackley Granite, southeast Newfoundland, as indicated by total-fusion 40Ar/39Ar geochronology. Can. J. Earth Sci., v. 25, No. 8, pp. 1151-1160.

Krogh, T. E., Strong, D. F., O'Brien, S. J., and Papezik, V.S., 1988. Precise U-Pb zircon dates from the Avalon Terrane in Newfoundland. Can. J. Earth Sci., v. 25, No. 3, pp. 442-453.

Krogh, T. E., Strong, D. F., and Papezik, V. S., 1983,. Precise U-Pb ages of zircons from volcanic and plutonic units in the Avalon Peninsula: Abstacts with Programs, Northeastern Section--G.S.A., v. 15, no. 3, p. 135.

Krogh, T. E., 1982. Improved accuracy of U-Pb zircon ages by the creation of more concordant systems using an air abrasion technique. Geochim. Cosmochim. Acta., v. 46, pp. 637-649.

Kusakabe, M., and Robinson, B. W., 1977. Oxygen and sulphur isotope equilibria in the BaSo4-HSO4--H2O system from 110 to 350C and applications. Geochim. Cosmochim. Acta, v. 41, pp. 1033-1040.

Lawler, J. P. and Crawford, M. L., 1983. Stretching of fluid inclusions resulting from a low temperature microthermometric technique. Econ. Geol., v. 78, pp. 527-529.

Li, P., Dai, T. M., Qiu, C. Y., and Wang, J. W., 1964. A report of absolute dating of rocks and minerals by K-Ar method. Scientia Geologica Simica, 1964, pp. 24-34.

Lilly, H. D., 1966. Late Precambrian and Appalachian tectonics in light of submarine exploration of the Great Bank of Newfoundland in the Gulf of St. Lawrence: preliminary views. Am. J. Sci., v. 264, pp. 569-574.

Macdonald, A. J., Kreczmer, M. J. and Kesler, S. E., 1986. Vein, manto and chimney mineralization at the Frezno silver-lead-zinc mine, Mexico. Can. J. Earth Sci., v. 23. pp. 1603-14.

Malpas, J. G., 1971. The Petrochemistry of the Bull Arm Formation near Rantem Station, Southeast Newfoundland. M.Sc. Thesis, Memorial Univ. Nfld., St. John's Nfld.

McCartney, W. D., 1969. Geology of the Avalon Peninsula, southeast Newfoundland. AAPG Memior 12, pp. 115-129.

McCartney, W. D., 1967. Whitbourne map area, Newfoundland. Geol. Surv. Can., Mem. 341, 135 p.

McCartney, W. D., Pool, W. H., Wanless, R. K., Williams, H. and Loveridge, W. D., 1966. Rb/Sr age and geological setting of the Holyrood granite, southeast Newfoundland. Can. J. Earth Sci., v. 3, pp. 947-957.

McCrea, J. M., 1950. On the isotopic chemistry of carbonates and paleotemperature scale. J. Chem. Phys., v. 18, pp. 849-857.

Miller, H. G., 1987. A geophysical interpretation of the onshore and offshore geology of the Southern Avalon Terrane, Newfoundland. Can. J. Earth Sci., v. 24, pp. 60-69.

Miller, H. G., 1977. Gravity zoning in Newfoundland. Tectonophysics, v. 38, pp. 317-326.

Miller, H. G., Goodacre, A. K., Cooper, R. V., and Halliday, D., 1985. Offshore extensions of the Avalon Zone of Newfoundland. Can. J. Earth Sci., v. 22, pp. 1163-1170.

Moller, P., and Morteani, G., 1983. On the geochemical fractionation of Rare Earth Elements during the formation of Ca-minerals and its application to problems of the genesis of ore deposits. In: Augusthithis, S.S. (ed.), The Significance of Trace Elements in Solving Petrogenetic Problems, Athen (Theophrastus) pp. 747-791.

Moller, P., Morteani, G., Hoefs, J. and Parekh, P. P., 1979. The origin of the ore bearing solution in the Pb-Zn veins of the Western Harz/Germany as deduced from rare earth element and isotope distributions in calcite. Chem. Geol., v. 26, pp. 197-225.

Murray, A. and Howley, J. P., 1881. Geological Survey of Newfoundland from 1864 to 1880, London.

Nockolds, S. R., and Mitchell, R. L., 1948. The geochemistry of some Caledonian plutonic rocks: A study in the relationship between major and trace elements of igneous rocks and their minerals. Trans. Roy. Soc. Edinburgh, v. 61, pp. 533-75.

O'Brien, S. J., Wardle, R. J. and King, A. F., 1983. The Avalon Zone: A Pan-African terrane in the Appalachian Orogen of Canada. Geological Journal, v. 18, pp. 195-222.

O'Brien, S. J., 1979. Volcanic stratigraphy, petrology and geochemistry of the Marystown Group, Burin Peninsula, Newfoundland. Unpublished M.Sc. thesis, Memorial University of Newfoundland, St. John's, Canada.

O'Driscoll, C. F. and Muggeridge, W. W., 1979. Geology of Merasheen and Harbour Buffett map area, Newfoundland. In: Report of Activities for 1978, ed., Gibbons, R. V., Nfld. Dept. of Mines and Energy, Min. Dev. Div., Report 79-1, pp. 82-89.

O'Driscoll, C. F., 1977. Geology, petrology and geochemistry of the Hermitage Peninsula, southern Newfoundland. Unpublished M.Sc. thesis, Memorial University of Newfoundland, St. John's, Canada.

Ohmoto, H., 1983. Geologic setting of Kuroko deposits, Japan: Part I. Geologic history of the Green Tuff Region. In: The Kuroko and Related Volcanogenic Massive Sulphide Deposits, eds., Ohmoto, H. and Skinner, B. J., Econ. Geol. Mon. 5, pp. 9-23.

Ohmoto, H., 1972. Systematics of sulphur and carbon isotopes in hydrothermal ore deposits. Econ. Geol., v. 67, pp. 551-578.

Ohmoto, H., and Rye, R.O., 1979. Isotopes of Sulphur and Carbon. In: Geochemistry of Hydrothermal Ore Deposits, ed., Barnes, H.L., John Wiley and Sons, New York, pp 509-67.

O'Neil, J. R., Shaw, S. E. and Flood, R. H., 1977. Oxygen and hydrogen isotope compositions as indicators of granite genesis in the New England Batholith, Australia. Cont. Min. Pet., v. 62, pp. 312-328.

O'Neil, F. R. and Taylor, H. P., 1969. Oxygen isotope fractionation between muscovite and water. J. Geophys. Res., v. 74, pp. 6012-6022.

Papezik, V. S., 1970. Petrochemistry of volcanic rocks of the Harbour Main Group, Avalon Peninsula, Newfoundland. Can. J. Earth Sci., v. 7, pp. 1485-1498.

Pelletier, B. R., 1971. A granodioritic drill core from the Flemish Cap, eastern Canadian continental margin. Can. J. Earth Sci., v. 8, pp. 1499-1503.

Pichavant, M., Ramboz, C. and Weisbrod, A., 1982. Fluid immiscibility in natural processes: use and misuse. I Phase equilibria analysis--a theoretical and geometrical approach. Chem. Geol., v. 37, pp. 1-27.

Potter, II, R. W., 1977. Pressure corrections for fluid-inclusion homogenization temperatures based on the volumetric properties of the system NaCl-H2O. U.S. Geol. Survey J. Res., v. 5, pp. 603-607.

Potter, II, R. W. and Brown, D. L., 1977. The volumetric properties of aqueous sodium chloride solutions from 0oC to 500oC and pressure up to 2000 bars based on a regression of available data in the literature. U.S. Geol. Survey Bulletin 1421-C, 36 p.

Rast, N., 1979. The Avalonian plate in the northern Appalachian and Caledonides. In: Proceedings: "The Caledonides in the U.S.A.," ed., Wones, D., Int. Geol. Cor. Proj. 27, Caledonide Orogen, 1979 meeting, Blacksburg, Va., pp. 63-66.

Roedder, E., 1984. Fluid Inclusions. In: Reviews in Mineralogy, ed., Ribbe, P. H., v. 12, Mineralogical Society of America, 644 p.

Roedder, E., 1972. Composition of fluid inclusions. U.S. Geol. Survey Prof. Paper 440JJ, 164 p.

Roedder, E., 1967. Fluid inclusions as samples of ore fluids. In: Geochemistry of Hydrothermal Ore Deposits, ed., Barnes, H. L., 1st edition, Holt, Rinehart and Winston, New York, NY, pp. 515-574.

Roedder, E. and Howard, K. W., 1988. Taolin Zn-Pb-fluorite deposit, Peoples Republic of China: an example of some problems in fluid inclusion research on mineral deposits. J. Geol. Soc. Lon., v. 145, pp. 163-74.

Roedder, E. and Bodnar, R. J., 1980. Geologic pressure determination from fluid inclusion studies. Ann. Rev. Earth Planet Sci., v. 8, pp. 263-301.

Rose, E. R., 1952. Torbay map area, Newfoundland. Mem. Geol. Surv. Can., 265 p.

Sakai, H., 1968. Isotopic properties of sulphur compounds in hydrothermal processes. Geochem. J., v. 2, pp. 29-49.

Shieh, Y. N., 1985. High 18O granitic plutons from the Frontenac Axis, Grenville Province of Ontario, Canada. Geochim. Cosmochim. Acta, v. 49, pp. 117-123.

Slack, J. F., 1980. Multistage vein ores of the Lake City District, western San Juan Mountains, Colorado. Econ. Geol., v. 75, N. 7, pp. 963-991.

So, C., Park, M., Shelton, K. L., and Seidemann, D. E., 1984. Geology and geochemistry of the Sambo Pb-Zn deposit, Republic of Korea. Econ. Geol., v. 79, pp. 656-670.

So, C., Rye, D. M., and Shelton, K. L., 1983. Carbon, hydrogen, oxygen and sulfur isotope and fluid inclusion study of the Weolag Tungsten-Molybdenum deposit, Republic of Korea: Fluid histories of metamorphic and ore-forming events. Econ. Geol., v. 78, No. 8, pp. 1551-1573.

Sourirajan, S. and Kennedy, G. C., 1962. The system H2O - NaCl at elevated temperatures and pressures. Am. J. Science, v. 260, pp. 115-141.

Strong, D. F., 1980. Granitoid rocks and associated mineral deposits of eastern Canada and western Europe. In: The Continental Crust and its Mineral Deposits, ed., Strangway, D. W., Geol. Assoc. Can., Spec. Pap. 20, pp. 741-769.

Strong, D. F., 1979. Proterozoic tectonics of northwestern Gondwanaland: new evidence from eastern Newfoundland. Tectonophysics, v. 54, pp. 81-101.

Strong, D. F., Fryer, F. J., and Kerrich, R., 1984. Genesis of the St. Lawrence fluorspar deposits as indicated by fluid inclusion, rare earth element and isotopic data. Econ. Geol., v. 79, No. 5, pp. 1142-1158.

Strong, D. F., O'Brien, S. J., Taylor, S. W., Strong, P. G. and Wilton, D. H., 1978. Aborted proterozoic rifting in eastern Newfoundland. Can. J. Earth Sci., v. 15, pp. 117-131.

Strong, D. F., O'Brien, S. J., Taylor, S., Strong, P. and Wilton, D. H., 1976. Geology of the Marystown (IM/3) and St. Lawrence (IL/14) map areas, Newfoundland. Nfld. Dept. of Mines and Energy, Report 77-8, 81 p.

Strong, D. F. and Minatides, D. G., 1975. Geochemistry of the late Precambrian Holyrood Plutonic Series of eastern Newfoundland. Lithos, v. 8, pp. 283-295.

Strong, D. F., Dickson, W. L., O'Driscoll, C. F., and Kean, B. F., 1974. Geochemistry of eastern Newfoundland granitoid rocks. Nfld. Dept. Mines and Energy, Rept. 74-3.

Taylor, H. P., Jr., 1979. Oxygen and hydrogen isotope relationships in hydrothermal mineral deposits. In: Geochemistry of Hydrothermal Ore Deposits, ed., Barnes, H. L., Wiley, New York, pp. 236-277.

Taylor, S. R., 1965. The application of trace element data to problems in petrology. In "Physics and Chemistry of the Earth." v. 6, eds. Ahrens, L. H., Press, F., Runcorn, S. K., and Urey, H. C., Pergamon Press, Oxford.

Taylor, S. W., O'Brien, S. J. and Swinden, H. S., 1979. Geology and mineral potential of the Avalon Zone and granitoid rocks of eastern Newfoundland. Nfld. Dept. of Mines and Energy, Min. Dev. Div., Report 79-3, 50 p.

Taylor, S. W., 1976. Geology of the Marystown map sheet (E/2), Burin Peninsula, southeastern Newfoundland. M.Sc. thesis, Memorial University of Newfoundland, St. John's, Canada, 164 p.

Teng, H. C. and Strong, D. F., 1976. Geology and geochemistry of the St. Lawrence peralkaline granite and associated fluorite deposits, southeast Newfoundland. Can. J. Earth Sci., v. 13, pp. 1374-1385.

Turner, F. J., 1968. Metamorphic Petrology. New York: NcGraw-Hill, 403 p.

Williams, H., 1984. Miogeoclines and suspect terranes of the Caledonian-Appalachian Orogen: tectonic patterns in the North Atlantic region. Can. J. Earth Sci., v. 21, pp. 887-901.

Williams, H. and Hatcher, R. D., 1983. Appalachian suspect terranes. Geol. Soc. of America, Mem. 158, pp. 33-53.

Williams, H. and Bursnall, J., 1982. Structural map of the Appalachian Orogen in Canada. Memorial University of Nfld., Map No. 4, Scale 1:2,000,000.

Williams, H., 1979. Appalachian orogen in Canada. Can. J. Earth Sci., v. 16, pp. 792-807.

Williams, H. and King, A. F., 1979. Trepassey map area, Newfoundland. Geol. Surv. Can., Mem. 389, 24 p.
Williams, H., (compiler), 1978. Tectonic lithofacies map of the Appalachian orogen: Memorial University of Newfoundland, Map No. 1, scale 1:1,000,000.

Williams, H., 1976. Tectonic-stratigraphic subdivisions of the Appalachian Orogen (abstr.). Geol. Soc. Amer., Prog. with Abstr., v. 8, No. 2, 300 p.

Williams, H., Kennedy, M. J. and Neale, E. R. W., 1974. The northeastern termination of the Appalachian Orogen. In: The Ocean Basins and Margins, eds., Nairn, A. E. M. and Stehli, F. G., Plenum Publishing Corp., New York, pp. 79-123.

Williams, H., Kennedy, M. J. and Neale, E. R. W., 1972. The Appalachian structural province. In: Variations in Tectonic Styles in Canada, eds., Price, R. A. and Douglas, R. J. W., Geol. Assoc. of Can., Spec. Pap. 11, pp. 183-261.

Williams, H., 1969. Pre-Carboniferous development of Newfoundland Appalachians. In: North Atlantic--Geology and Continental Drift, AAPG Memior 12, pp. 32-58.

Williams, H., 1964c. The Appalachians in northeastern Newfoundland - a two sided symmetrical system. Am. J. Sci., v. 262, pp. 1137-1158.

Winkler, H. G. F., 1979. Petrogenesis of Metamorphic Rocks. Fifth Edition, Springer-Verlag, New York.

Zeitz, I., Haworth, R. T., Williams, H., Daniels, D. L., 1980. Magnetic Anomaly Map of the Appalachian Orogen. Memorial University of Newfoundland, Map No. 2.

Appendix A

Vein Orientations

vein	strike	dip
Barite Veins		
BV1	070 Az	vert
BV2	080 Az	vert
BV3	014 Az	90
BV4	012 Az	90
BV6	040 Az	90
BV8	028 Az	90
BV9	100 Az	90
BV11	152 Az	80 W
.	154 Az	90
.	160 Az	70 W
.	167 Az	86 E
overall	165 Az	90
BV11A	148 Az	60 S
BV11B	168 Az	78 E
BV11C	003 Az	76 E
BV15	010 Az	89 E
BV17	022 Az	65 W
BV21	028 Az	70 S
BV22	025 Az	85 W
BV23A	010 Az	70 W
BV23B	015 Az	80 W
BV23C	050 Az	68 W
BV26	025 Az	72 N
BV30	032 Az	75 W
BV38	015 Az	70 W
BV39	158 Az	90
BV40	173 Az	85 S
BV42	166 Az	85 W
BV46	120 Az	90
BV48	161 Az	72 W
BV50	135 Az	90
Quartz Veins		
BV11D	140 Az	80 S
BV14	173 Az	52 E
BV16A	013 Az	64 W
BV16B	104 Az	82 N
BV16C	065 Az	79 N
BV17	120 Az	21 E

vein	strike	dip
Quartz Veins (cont.)		
BV18A	086 Az	54 S
BV18B	064 Az	34 S
BV19	075 Az	87 E
BV20	076 Az	82 S
BV24	060 Az	72 N
BV25	055 Az	90
BV27	065 Az	90
BV29A	130 Az	75 N
BV29B	105 Az	70 N
BV32	105 Az	90
BV33B	068 Az	90
BV34	005 Az	56 E
BV35	064 Az	60 S
BV36	075 Az	42 N
BV37	058 Az	90
BV39	113 Az	90
BV41	135 Az	80 N
BV43	082 Az	68 N
BV48	054 Az	72 N
QVM1	043 Az	84 S
QVM2	052 Az	90
QVM3	056 Az	86 N
QVM4	056 Az	82 N
QVM5	077 Az	86 S
QVM6	058 Az	84 N
QVM7	140 Az	80 S
QVM8	070 Az	90
QVM9	065 Az	78 S
QVM10	070 Az	90
QVM11	065 Az	78 S
QVM12	070 Az	82 S
QVM13	060 Az	82 S
QVM14	064 Az	84 S
QVM15	089 Az	87 S
QVM16	070 Az	90
QVA	061 Az	90
QVB	063 Az	87 N
QVC	057 Az	86 N
QVD	064 Az	90
QVE	060 Az	87 S
QVF	059 Az	90
QVG	055 Az	86 N

Quartz Veins (cont.)			Calcite Veins		
QVH	055 Az	87 S	BV5	086 Az	90
QVI	062 Az	85 S	BV9	120 Az	75 W
QVJ	061 Az	90	BV12	045 Az	to
QVK	060 Az	90	.	070 Az	90
QVL	057 Az	86 S	BV24	015 Az	90
QVM	058 Az	90	BV28	057 Az	82 N
QVN	068 Az	90	BV30	032 Az	75 W
QVO	072 Az	90	BV33A	114 Az	90
QVP	070 Az	90			
QVQ	063 Az	87 N			
QVR	060 Az	90			
QVS	058 Az	90			

Appendix B

Fluid Inclusion Data

Th - Homogenization temperature (°C).
Tm - Temperature of complete melting (°C).
Te - Eutectic temperature (°C), temperature of first observed melt.
HB - Homogenization behaviour - homogenized to a liquid (L), vapour (V), displayed critical (C) homogenization behaviour or inclusion decrepitated (D) before homogenization.

Sample	Th	HB	Tm	Te
Barite				
BV1-H	360	L	+ 0.7	+ 0.6
	153	L	-	-
	427	C	-10	-19
	224	L	- 6.2	-23
	-	D	-	-23
	241	L	+ 0.6	+ 0.4
	-	D	- 0.9	-19
	304	L	-	-
BV7-A	340	L	0.0	- 1.5
	248	L	-10.6	-22
	244	L	+ 0.2	0.0
	359	L	0.0	0.0
	164	L	-23.7	-39.7
	209	L	-	-
	184	L	-	-
	-	D	0.0	0.0
	225	L	-	-
	220	L	-13.0	-22.2
	325	L	+ 0.2	-
	200	L	+ 0.2	-
BV7-B	83.5	L	-25.5	-48
	66.0	L	-25	-48
	137	L	0.0	0.0
BV7-C	161	L	-13.3	-22.6
	315	L	-19	-22.6
	368	L	- 7.0	-20

Fluid Inclusion Data (continued)

Sample	Th	HB	Tm	Te
BV11-C	93	L	-22	-
	-	D	-18	-23
	76	L	-21.5	-
	77	L	-23.0	-25.0
	-	D	-22.0	-23.8
	91	L	-24.6	-24.6
	92	L	-24.6	-24.6
	95	L	-	-
BV11-N	87	L	-	-
	88	L	-23.5	-
	82	L	-20	-41.8
	-	D	-24.3	-44.0
BV30-B	97	L	-19	-21
BV42-A	288	L	- 6.3	-23.0
	238	L	-20.2	-30
	>390	L	-24.9	-40.0
Calcite				
BV11-EX5	85	L	-23	-42
	85	L	-23	-42
	94	L	-23	-42
	88	L	-23	-42
	84	L	-	-
	75	L	-15	-19
BV12-A	85	L	-	-
	73	L	-	-
	85	L	-	-
	79	L	-	-
	79	L	-	-
	65	L	-	-
	66	L	-	-
	75	L	-	-
	60	L	-42	-60
	77	L	-43.9	-60
	80	L	-42.5	-60

Fluid Inclusion Data (continued)

Sample	Th	HB	Tm	Te
BV12-A	74	L	-41.0	-60
(cont)	87	L	-38.6	-51
	74	L	-42.6	-51
	70	L	-23.9	-48
	75	L	-32.4	-
	72	L	-	-
	78	L	-31.9	-44.0
	82	L	-	-
	52	L	-23.9	-51
	-	D	-31.0	-48.0
	-	D	-23.2	-41.0
BV12-C	89	L	-	-
BV12-E	91	L	-	-
	96	L	-22.7	-42.0
	83	L	-23.0	-42.0
BV12-I	71	L	-40.0	-58.0
	71	L	-40.0	-58.0
	-	L	- 6.5	-22
	70	L	-	-
	81	L	-25.8	-48
	79	L	-25.8	-46
	81	L	-26	-46
	74	L	-	-
	76	L	-	-
	68	L	-	-
	67	L	-	-
	86	L	-	-
	86	L	-	-
	79	L	-	-
	74	L	-	-
BV30-A	79	L	-	-
	347	L	-	-
	73	L	-23.0	-49.0
	150	L	-	-
	100	L	-23.0	-40.0
	100	L	-23.4	-47.0

Fluid Inclusion Data (continued)

Sample	Th	HB	Tm	Te
BV30-A (cont)	95	L	-24.0	-47.0
	100	L	-24.0	-47.0
	99	l	-24.4	-
	94	L	-	-
	93	L	-	-
	82	L	-	-
	69	l	-	-
	92	L	-	-
	97	L	-	-
	98	L	-	-
	96	L	-	-
AR1-B2 (Silver Cliff)	197	L	0.0	-
	212	L	-	-
	224	L	-	-
	197	L	0.0	-
	218	L	-	-
	228	L	-	-
	230	L	-	-
	250	L	-	-
	258	L	- 3.0	-
	220	L	-	-
Quartz (Silver Cliff - Ore Veins)				
AR6-B	295	L	-	-
AR6-C	243	L	-	-
	295	L	-	-
	341	L	-	-
	288	L	-	-
	251	L	-	-
	301	L	-	-
	287	L	-	-
	284	L	-	-
	292	L	-	-
	239	L	-	-
AR7-A	307	L	-4.0	-
	271	L	-4.0	-
	280	L	-4.0	-

Fluid Inclusion Data (continued)

Sample	Th	HB	Tm	Te
AR7-A (cont)	284	L	-	-
	285	V	-	-
	340	V	-	-
	277	L	-	-
	291	L	-	-
	275	L	-	-
	265	L	-	-
	300	L	-	-
	255	L	-	-
	440	V	-	-
	276	L	-	-
	284	L	-	-
	325	V	-	-
	270	L	-	-
	272	L	-	-
	271	L	-	-
	275	L	-	-
	270	L	-	-
	329	L	-	-
AR25-A	316	L	-	-
	318	L	-	-
	324	L	-	-
	324	L	-	-
	358	L	-	-
	358	L	-	-
	324	L	-	-
	300	L	-	-
	300	L	-	-
	311	L	-	-
	348	L	-	-
	344	L	-	-
	332	L	-	-
	356	L	-	-
	302	L	-	-
	390	L	-	-
	334	L	-	-
	338	L	-	-
	345	L	-	-
	345	L	-	-
	342	L	-2.0	-

Fluid Inclusion Data (continued)

Sample	Th	HB	Tm	Te
AR25-A (cont)	344	L	-	-
	283	L	-	-
	335	L	-	-
	345	L	-	-
AR25-B	361	L	-	-
	313	L	-3.0	-
	354	L	-	-
	367	L	-	-
	313	L	-2.2	-
	306	L	-2.0	-
AR25-D1	307	L	-	-
	305	L	-	-
	307	L	-	-
	327	L	-	-
	290	L	-	-
	309	L	-	-
	289	L	-	-
	300	L	-	-
	310	L	-	-
	304	L	-	-
	304	L	-1.0	-6.4
	306	L	-1.0	-
	307	L	-1.0	-
	279	L	-	-
	271	L	-	-
	265	L	-	-
	455	V	-	-
	460	V	-	-
	435	V	-	-
	472	V	-	-
	504	V	-	-
	440	V	-	-
	310	L	-	-
	430	V	-	-
	435	V	-	-
	286	L	-	-
	251	L	-	-
	323	L	-	-
	357	L	-	-

Fluid Inclusion Data (continued)

Sample	Th	HB	Tm	Te
AR25-D1 (cont)	334	L	-	-
	365	L	-	-
	347	L	-	-
AR25-D2	460	V	-	-
	485	V	-	-
	495	V	-	-
	495	V	-	-
	480	V	-	-
	441	V	-	-
(Silver Cliff - Barren Veins)				
AR1-B1	285	L	-	-
	290	L	-	-
	290	L	-	-
	290	L	-	-
	330	L	-	-
	276	L	-	-
	300	L	-	-
	255	L	-0.7	-10.9
	255	L	-	-5.0
	270	L	-2.2	-8.0
	278	L	-	-
AR1-B2	235	L	-	-
	253	L	-2.5	-19.0
	235	L	-0.2	-
	235	L	-2.2	-17.0
	239	L	-0.2	-
	245	L	-0.2	-
	239	L	-	-
	247	L	-	-
	260	L	-	-
	276	L	-	-
	285	L	-	-
	300	L	-	-
AR2-A	258	L	-	-
	251	L	-	-
	263	L	-	-

Fluid Inclusion Data (continued)

Sample	Th	HB	Tm	Te
AR2-A (cont)	266	L	-0.1	-7.0
	270	L	-	-
	187	L	-0.1	-7.0
	225	L	-	-
	180	L	-	-
	245	L	-	-
	244	L	-	-
	249	L	-	-
	216	L	-	-
AR20-A	218	L	-	-
	250	L	-	-
	236	L	-	-
	224	L	-	-
	225	L	-	-
	249	L	-	-
	255	L	-	-
	213	L	-	-
	255	L	-	-
	269	L	-	-
(Non Silver Cliff Vein				
BV1-K	220	L	-	-
	185	L	-	-
	217	L	-2.0	-4.0
	190	L	-	-
	222	L	-2.0	-4.7
	170	L	-	-
	175	L	-	-
	186	L	-	-
	195	L	-2.0	-5.0
BV3-C	178	L	-	-
	162	L	-	-
	199	L	-	-
	185	L	-	-

Fluid Inclusion Data (continued)

Sample	Th	HB	Tm	Te
BV3-D	158	L	+0.3	-
	156	L	+0.2	-2.0
	157	L	0.0	-2.0
	159	L	0.0	-2.0
	152	L	-0.2	-
	140	L	0.0	0.0
	152	L	-0.3	-0.9
	148	L	+0.4	-
	152	L	-	-
	160	L	+0.4	+0.2
	166	L	+0.4	+0.2
	155	L	+0.4	+0.2
	140	L	+0.4	+0.2
	164	L	-	-
	167	L	-	-
BV9-D	156	L	-	-
	147	L	-	-
	132	L	-	-
	162	L	-	-
	163	L	-0.6	-4.0
	156	L	-0.9	-3.5
BV24-B	187	L	-	-
	187	L	-	-
	216	L	-	-
	213	L	0.0	-1.0
	200	L	0.0	-1.0
	195	L	0.0	-1.0
	207	L	-	-
	262	L	-	-
	263	L	-	-
	183	L	-	-
	200	L	-	-
BV35-C	430	V	-	-
	460	V	-	-
	460	V	-	-
	450	V	-	-
	460	V	-	-
	464	V	-	-

Fluid Inclusion Data (continued)

Sample	Th	HB	Tm	Te
BV35-C (cont.)	462	V	-	-
	462	V	-	-
	420	V	-	-
	401	L	-	-
	211	L	-	-
	162	L	-	-
	178	L	-	-
	200	L	-	-
	178	L	-	-
	197	L	-	-
	186	L	-	-
	435	V	-	-
	373	L	-	-
	163	L	-	-
	120	L	+1.0	-
	169	L	-	-
	162	L	-	-
	175	L	-	-
	152	L	-	-
	171	L	-	-
	168	L	-	-
	130	L	-	-
	162	L	+0.5	-
	115	L	-	-
	137	L	-	-
	168	L	-	-
	151	L	0.0	-2.7
	141	L	0.0	-1.4
	141	L	0.0	-1.3
	119	L	+0.5	-
	305	L	0.0	-5.0
	116	L	+0.5	-
	136	L	0.0	-
	175	L	-0.5	-
	228	L	-1.0	-
	170	L	-0.5	-
	161	L	-1.2	-9.0
	147	L	-	-
	172	L	-1.1	-7.0
	-	-	0.0	-
	149	L	0.0	-1.0

Fluid Inclusion Data (continued)

Sample	Th	HB	Tm	Te
BV35-C (cont.)	156	L	0.0	-
	150	L	0.0	-0.2
	157	L	0.0	-0.3
	148	L	-	-
	153	L	-	-
	157	L	-	-
	160	L	-	-
	168	L	-	-
	153	L	-	-
	143	L	-	-
	153	L	-	-
	186	L	-0.4	-2.0
	217	L	-	-
	139	L	-	-
	162	L	-	-
	305	L	-	-
	180	L	-	-
	178	L	-	-
	159	L	-	-
	211	L	-	-
BV38-A	190	L	-	-
	181	L	-	-
	201	L	0.0	-0.8
	175	L	+0.2	-1.5
	215	L	0.0	-1.4
	206	L	-	-
	294	L	-	-
	249	L	-	-
BV39-A	174	L	+0.3	-1.8
	173	L	+0.2	-1.5
	180	L	-	-
	196	L	+0.2	-0.3
	151	L	+0.4	-
	168	L	-	-
	178	L	-	-
	163	L	-	-
	175	L	-	-
	171	L	-	-

Fluid Inclusion Data (continued)

Sample	Th	HB	Tm	Te
(Collier Point Veins)				
QV11-A	168	L	-	-
	205	L	-	-
QV11-B	181	L	0.0	0.0
	183	L	0.0	0.0
	175	L	0.0	-
	187	L	0.0	-
	194	L	-	-
	165	L	0.0	-
	161	L	0.0	-
	165	L	0.0	-
	164	L	0.0	-
QV11-L	145	L	-	-
	150	L	-	-
	180	L	-	-
	167	L	-	-
	179	L	-	-
	180	L	-	-
	194	L	-	-
	157	L	-	-
	170	L	-	-
	183	L	-	-
	185	L	-	-
	183	L	-	-
	187	L	-0.9	-3.0
	160	L	-0.9	-2.5
	161	L	-	-
QV11-M	297	L	-	-
	294	L	-	-
	313	L	-	-
	316	L	-	-
	277	L	-	-
	246	L	-0.1	-1.8
	265	L	-0.1	-1.8
	163	L	-	-
	150	L	-	-
	185	L	-	-

Fluid Inclusion Data (continued)

Sample	Th	HB	Tm	Te
QV11-S	175	L	-	-
	161	L	-	-
	159	L	-	-
	189	L	-	-
	180	L	-	-
	250	L	-	-
	160	L	-	-
	270	L	-	-
Sphalerite (Silver Cliff - Ore Veins)				
AR25-A	273	L	-	-
	300	L	-	-
	280	L	-	-

Appendix C

Rare Earth Element Data for Granites and Sedimentary Rocks

	Ce	Nd	Sm	Eu
CP122	44.6	23.2	5.81	1.15
CP123	39.3	61.4	11.9	2.35
CP124	72	39.7	.	1.85
CP126	66.7	34	.	1.39
DA782	96.2	38	7.12	0.59
DA7812	108	40.8	7.60	0.42
FOX-CG	75.3	26.3	4.74	0.61
FOX-FG	58.1	19.9	3.60	0.19
WM78181	55.4	21.7	3.35	0.29
WM78186	53.9	17.2	3.47	0.24

	Gd	Tb	Yb	Lu
CP122	.	0.72	2.99	0.44
CP123	11.1	1.48	4.49	0.63
CP124	6.27	1.24	4.65	0.68
CP126	4.56	0.99	4.05	0.58
DA782	.	0.84	4.60	0.64
DA7812	.	0.90	4.58	0.62
FOX-CG	.	.	4.98	0.69
FOX-FG	.	.	4.27	0.58
WM78181	.	1.17	2.20	0.26
WM78186	.	1.02	2.37	0.28